DEEP-WATER TURBIDITES AND SUBMARINE FANS

HENRY W. POSAMENTIER
Anadarko Petroleum Corporation, 1201 Lake Robbins Drive, The Woodlands, Texas 77380, U.S.A.
e-mail: henry_posamentier@anadarko.com
AND
ROGER G. WALKER
Roger Walker Consulting Inc., 83 Scimitar View NW, Calgary, Alberta T3L 2B4, Canada
e-mail: walkerrg@telus.net

Abstract: Depositional environments of deep-water deposits commonly are complex and consequently do not neatly fit any single facies model. Rather than developing specific models we discuss these deposits within the context of depositional elements and first principles of process sedimentology. Depositional elements are described using 3D seismic as well as outcrop data. Detailed facies descriptions from outcrops are then integrated with these depositional elements. Following the theme of this publication, we emphasize facies and depositional environments rather than the mechanics of turbidity currents and related processes.

The spatial and temporal distribution of depositional elements is determined largely by characteristics of the shelf-edge staging area. Such factors as grain-size distribution, sediment caliber, frequency of flow events, and magnitude of flows are all a function of conditions at the shelf edge and upper slope. Sediments are supplied from the staging area to the slope and basin floor beyond. Turbidity currents traverse the slope through canyons and slope channels. When these flows reach the basin floor they continue to remain confined by levees for a certain distance. This distance is a function of grain-size distribution in the flow, flow magnitude, and flow velocity. Levee height diminishes seaward, and eventually where levees can no longer effectively confine the basal sand-rich part of the flow the leveed channel transitions into a frontal splay or lobe.

Relative sea-level change plays an important role in turbidite deposition, in that sea level is a major factor controlling conditions in the outer shelf and upper slope. During relative sea-level lowstands, shorelines and consequently depocenters tend to be located at the shelf edge. This sets up conditions favorable for delivery of sediments to the slope and basin floor. Conversely, relative sea-level highstands commonly are associated with depocenters at the inner to middle shelf, resulting in a paucity of coarse sediments being actively delivered to the shelf edge and ultimately to the slope and basin floor. Variations in grain size delivered to the shelf edge during a cycle of sea-level change can vary predictably hence the temporal and spatial distribution of depositional elements in linked deep-water environments can likewise be better understood within this context.

INTRODUCTION

The scope of turbidite and submarine-fan facies models is vast, extending from individual beds a few centimeters thick to entire submarine fans with volumes up to a million cubic kilometers or more (for example, Indus fan area 1.1 x 10^6 km^2, thickness 3+ km, hence volume of the order of 3 x 10^6 km^3). The unifying theme is the central role played by individual turbidity currents, where each bed (a turbidite) is the result of a relatively short-lived depositional event. The environment is consistently below storm wave base, such that, once deposited, a turbidite is unlikely to be reworked by other currents aside from the occasional strong contour current. Figure 1 schematically illustrates an idealized shelf to basin-floor physiography displaying most of the key elements of the deep-water depositional environment.

We will briefly examine the history of turbidite and submarine fan models and show that, perhaps more than in any other depositional environment, technology (2-D and 3-D seismic data) has influenced the definition of depositional elements and hence the facies models (e.g., Posamentier and Kolla, 2003a). No single model comes close to embracing the complexity of huge ancient and modern submarine-fan systems, making the depositional elements and their lateral and vertical relationships the basis for interpretation and prediction. Our treatment of facies models will take a first-principles approach that will focus on the linkage between physical processes and associated depositional elements.

Many aspects of turbidity-current generation, movement, and deposition were reviewed by Walker (1992) in the third edition of "Facies Models". This work will be referenced here but not repeated in detail.

HISTORY OF FAN MODELS

The turbidity-current concept was introduced in 1950, in the classic paper "Turbidity currents as a cause of graded bedding" by Kuenen and Migliorini (1950). The paper was based mainly on Kuenen's experimental work both before and after the Second World War. The idea that sand could be transported to great depths in the ocean was very controversial at the time (Walker, 1973), and for many years there was considerable debate about the existence of turbidites and, about their properties. It was understood that modern fans existed, but their internal characteristics were completely unknown—indeed, Kuenen's experiments were much more concerned with the origin of submarine canyons than the transport of sand onto the deep sea floor.

After a dozen years of observations, the first generalization concerning turbidites was published by Bouma, (1962) (Fig. 2)—what is now known as the "Bouma sequence" for the internal structures in individual turbidites. The sequence from Division A (generally structureless) to division B (parallel lamination in sand) and division C (ripple cross-lamination) was compared with flume experiments and interpreted to represent waning flow (Harms and Fahnestock, 1965; Walker, 1965). Division D consists of thin laminae of silt and clay, and Division E is pelitic, probably largely turbidity-current mud with a small proportion of hemipelagic mud

Facies Models Revisited
SEPM Special Publication No. 84, Copyright © 2006
SEPM (Society for Sedimentary Geology), ISBN 1-56576-121-9, p. 397–520.

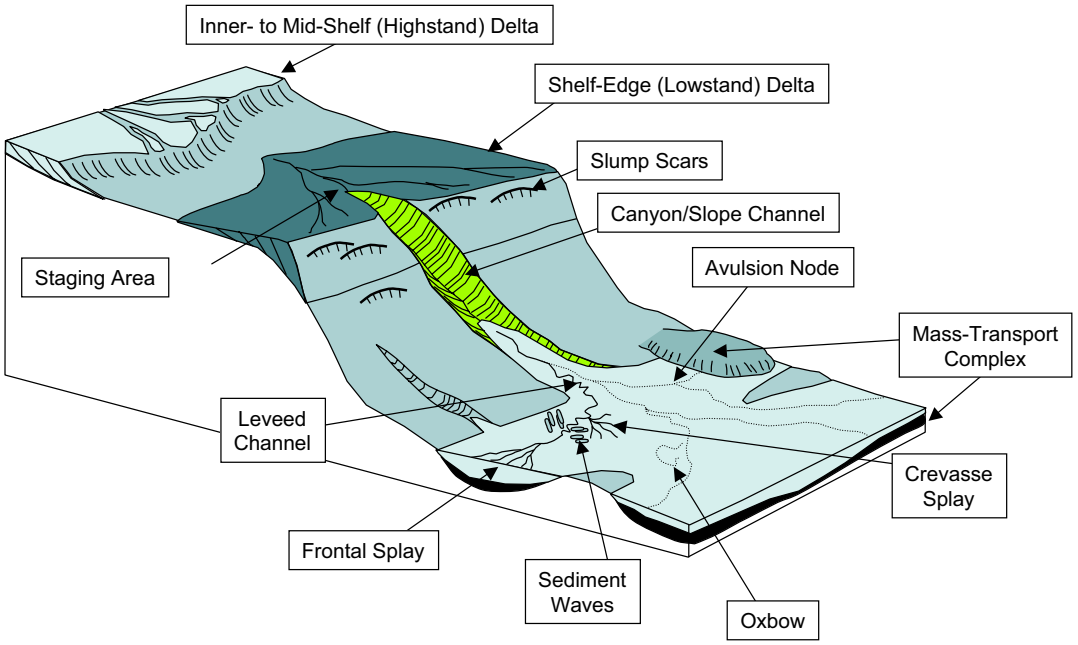

FIG. 1.—Schematic representation of shelf to deep-water physiography. The shelf staging area is connected to the deep-water environment through slope channels and/or canyons. Depositional elements in the deep water include leveed channels, crevasse splays, sediment waves, and frontal splays or lobes. (modified after Posamentier and Kolla, 2003a).

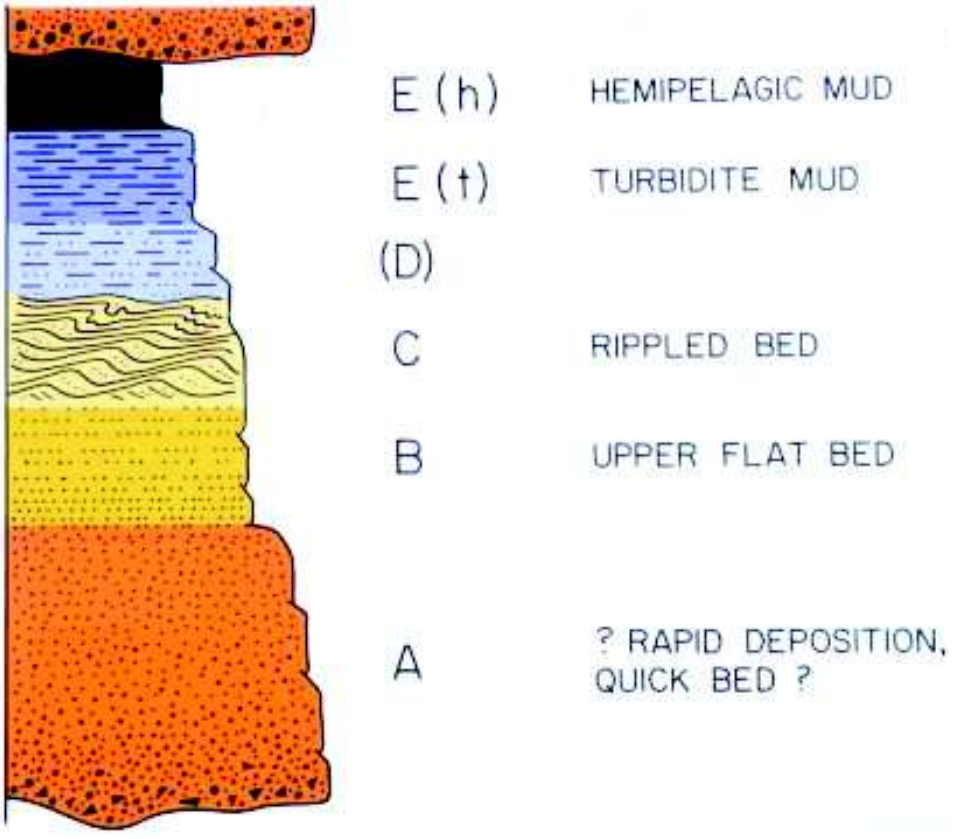

FIG. 2.—The Bouma (1962) sequence for classical turbidites. Division D is placed in brackets because it is difficult to identify in weathered or tectonized outcrops. Division E can be subdivided into two parts: turbidite mud E(t) and hemipelagic mud E(h). In most beds, the turbidite mud predominates.

Gradually, as more information became available on modern fans, the first model was proposed by Normark (1970) in another classic paper—"Growth patterns of deep sea fans". The data base was small, and the paper concentrated on the La Jolla and San Lucas fans. The model showed leveed channels on the upper fan, depositional ("suprafan") lobes on the middle fan, and a smooth surface on the lower fan. This model was based largely on shallow-penetration seismic data.

Shortly afterward, Emiliano Mutti and colleagues proposed fan models based exclusively on observations of ancient rocks. Mutti and Ricci Lucchi (1972) proposed a model with an inner-fan channel that branched into multiple channels on the mid-fan (but without depositional lobes). In the same year, Mutti and Ghibaudo (1972) showed a similar model but with lobes at the ends of the channels. Normark's work was not cited, suggesting that the modern and ancient fan models were derived independently—the proposed models suggested that modern fans and ancient rocks behaved in very similar ways.

The channel-feeding-lobe models dominated turbidite studies for about 10 years (1970–1980). The literature on modern fans and ancient rocks was formally brought together into the model proposed by Walker (1978); the models proved to be popular but also attracted considerable discussion (e.g., Nilsen, 1980). In retrospect, the models clearly had severe limitations—the distribution of sand and mud on the fans was incorrect, and no consideration was given to the influence of grain size or of local and regional tectonics. Perhaps more importantly, the models did not incorporate the influences of relative sea-level fluctuation.

With the advent of sequence stratigraphy, the fan models of the 70s were updated first by Vail et al. (1977) and later by Mutti (1985), Posamentier et al. (1988), and Posamentier et al. (1991), who integrated the effects of relative sea-level fluctuation with the channel-feeding-lobe models. This can be regarded as a period of transition between the older, field-based models and the rapidly evolving seismic-based models—the technology of marine geology was overtaking the efforts of field geologists.

In 1982, the first side-scan sonar images of the Amazon Fan were published by Damuth et al. (1982a), and Damuth et al. (1982b). The presence of long, narrow, and sinuous channels surprised most turbidite workers, as did the scale of the channel–levee complexes, which stood at least 200 m above the adjacent fan surface.

However, 1985 can be considered the year in which the emphasis shifted significantly from ancient rocks to large-scale studies of modern fans. In that year, the first compilation of modern fan studies was published (Bouma et al., 1985), with discussion of the Amazon, Astoria, Bengal, Cap-Ferrat, Crati, Delgada, Ebro, Indus, La Jolla, Laurentian, Magdalena, Mississippi, Monterey, Navy, Rhône, and Wilmington fans. That volume also had a very useful fold-out that tabulated the quantitative descriptors of the fans (channel dimensions and slopes, fan sizes, and fan volumes).

Also that year, Droz and Bellaiche (1985) published a seismic study of the Rhône Fan, showing the existence of meandering channels, channel–levee systems, and the lateral shifting and stacking of these systems to make channel–levee complexes. They also showed large slump masses ("acoustically transparent units") up to 160 milliseconds thick that represented both failure on the slope above the fan and failure of the back of the channel levees.

The studies in the Bouma et al. (1985) compilation essentially changed the direction and style of turbidite research, focusing on modern fans rather than ancient-rock studies. Droz and Bellaiche (1985), without using the term, essentially introduced the idea of depositional elements. This approach was also applied by Weimer (1989) in a classic study of the Mississippi Fan. Weimer (1991) recognized a succession of seismic facies based on reflection patterns (subparallel, wavy, hummocky, divergent, mounded, and convergent) which could be interpreted in terms of mass-transport complexes (hummocky, mounded), channel fill (discontinuous, high amplitude), levee (subparallel to convergent), and basin floor (subparallel to parallel). Work up to 1991 was collected in the volume "Seismic Facies and Sedimentary Processes of Submarine Fans and Turbidite Systems" (Weimer and Link, 1991). The seismic evidence presented was mostly high-quality 2-D data. In that volume, Mutti and Normark (1991) first systematized the depositional-elements approach. They defined depositional elements as the basic mappable components of both modern and ancient turbidite systems and stages that can be recognized in marine, outcrop, and subsurface studies. These features are the building blocks of fan models.

The past ten years have seen an explosion in 3-D seismic studies, with a corresponding better understanding of depositional elements (e.g., Posamentier and Kolla, 2003a). The best sources of this information are in the proceedings volume of a Gulf Coast Section of SEPM research conference ("Deep Water Reservoirs of the World", Weimer et al., 2000) and a thematic compilation of papers on deep-water systems in Marine and Petroleum Geology (Mutti et al., 2003). Various classifications of depositional elements were suggested, but no attempt was made to formulate a general model for submarine fans.

ORIGIN OF TURBIDITY CURRENTS

Density currents flow downslope as gravity acts on the density difference between the flow and the ambient seawater (Fig. 3). The density difference can be due to any or all of the following: the increased salinity of the flow, the cold temperature of the flow, and the suspended sediment within the flow. A turbidity current is a special case of a density flow, where the increased density is due to sediment maintained in turbulent suspension within the flow. The turbulence is maintained by the downslope movement of the flow.

Turbidity currents can originate by two mechanisms: some begin with large sediment slumps that accelerate and become turbulent. Many of these slumps are triggered by earthquakes, the most famous being the Grand Banks (Newfoundland) earthquake, slump, and flow of 1929. The flow broke a series of submarine telegraph cables, and reconstructions of the flow mechanics (Piper et al., 1988) suggest flow velocities up to 20 m/s, flow thicknesses of several hundred meters, and a minimum flow volume of 175 km^3. The flow bypassed the entire Laurentian Submarine Fan, and the deposit, in places over 1 m thick, now covers a large part of the Sohm Abyssal Plain (Walker, 1992).

Similarly, slumps off the delta of the Magdalena River in Colombia have broken telegraph cables up to 100 km from the delta. In the period 1932–1955, there have been 15 cable breaks, averaging one every 1.5 years (Heezen, 1956). The flow of 1935 had an estimated volume of sand of 3×10^8 m^3 (Heezen, 1956). Turbidity currents off the fronts of major deltas may be large and frequent.

In the case of the Congo (Zaire) river, where there is no delta, a submarine canyon has its head within the estuary of the Congo River. At times of peak river discharge in December–January and April–May, and during the years when the river is establishing a new course among the estuarine sand bars (1892–1903 and 1925–1929), submarine cables have been broken seaward of the estuary within the Congo Canyon (Heezen et al., 1964). These cables lay close to the estuary, at the shelf edge, and in water depths as great

FIG. 3.—Experimental turbidity current in a flume. Water depth is 28 cm. Note characteristic shape of the head and eddies behind the head. Sediment is thrown out of the main flow by these eddies, and the body of the flow is about half the height of the head. Experiment conducted by G.V. Middleton at Caltech.

as 2800 m, suggesting that sand swept into the canyon head from the estuary continued down the canyon in flows powerful enough to break cables in abyssal depths. Despite today's relative high stand of sea level, there were 26 cable breaks between 1893 and 1937—an average of one every 1.7 years.

Turbidity currents can also originate with delivery of river flow charged with sediment directly onto the slope. During times of river flood enough sediment can be entrained in the flow in some instances to produce a mix that has greater density than sea water, resulting in hyperpycnal flow down the slope (Mulder and Syvitski, 1995; Mulder et al., 1998). With this mechanism, what begins as inertial flow at the river mouth transforms into density underflow and ultimately turbidity flow on the slope. Such flows generally are of greater duration (i.e., days or weeks) than those that originate from large sediment slumps (i.e., hours).

FAN BYPASSING AND DEPOSITION ON MODERN ABYSSAL PLAINS

Turbidity currents traveling downslope may be moving at several to many meters per second, at which velocities all of the sand and finer sizes are in turbulent suspension. The flows gradually decelerate to velocities of 1–2 m per second, when the coarser sand fraction begins to be deposited from suspension. During this period of deceleration, the flows may largely bypass the slope and move long distances across the basin floor.

There are many studies of abyssal-plain deposition (Pilkey, 1988). The Grand Banks flow bypassed the Laurentian Fan at the base of the slope and deposited a turbidite on the Sohm Abyssal Plain, as discussed above. About 16,000 years ago, an even larger flow bypassed the Hatteras Fan and deposited on the Hatteras Abyssal Plain (western North Atlantic Ocean) (Elmore et al., 1979). Deposition began about 120 km from the end of the Hatteras Canyon system. This "Black Shell turbidite" (named for the distinctive corroded shells contained in the deposit) covers 44,000 km^2 of Hatteras Abyssal Plain in a bed up to 4 m thick, 500 km long, 200 km wide. The volume of the deposit is between 100 and 200 km^3. Characteristics of that deposit (grain size, sorting, mud content, etc.) were discussed in detail by Elmore et al. (1979).

One of the longest documented bypass systems is the Cascadia Deep-Sea Channel (Nelson et al., 2000). The channel originates off the coast of Washington, continues around the outer part of Astoria Fan, cuts through the Blanco Fracture Zone, and ends on the Tufts Abyssal plain. The "turbidity-current pathway [traverses] 1000 km of Cascadia Basin and remained open throughout the late Quaternary … as shown by the presence of the 13 post-MA (Mazama Ash, 7530 YBP) turbidites throughout the pathway in all recent cores we have collected" (Griggs and Kulm, 1968; see also Nelson et al., 2000). Beds within the channel include thick (2 m) Pleistocene graded gravel-to-sand beds over 400 km from the heads of the channel at the Washington coast. These long distances of bypass have significant implications regarding the location of sand deposits in ancient basins, as discussed throughout this review.

Kneller (1995) described the effects of waxing and waning flows within individual events. Waxing flows, commonly at or near the head of a turbulent flow, erode the substrate over which they pass. Significant amounts of sediment can bypass the system during this time. As the flow wanes, coarser sediments tend to come out of suspension and be deposited in the area formerly characterized as a zone of bypass. Consequently, even in slope and proximal basin-floor areas, where sediment bypass and erosion during waxing phase may be common, some sedimentation in the form of lag deposits almost always occurs.

TURBIDITE FACIES—THE BUILDING BLOCKS

There are several schemes for classifying the family of rocks that occur in deep-water settings. The first was proposed by Mutti and Ricchi Lucchi (1972) and was later simplified by Walker in 1978. Subsequent facies classifications have become more complex, including the all-inclusive but unwieldy schemes of Ghibaudo and Vanz (1987) and Pickering et al. (1986).

A detailed subdivision of features within individual beds was proposed by Lowe (1982), based on interpretations of how sedi-

ment was deposited from sandy and gravelly high-density turbidity currents. For sandy flows, division S1 is characterized by traction structures, division S2 contains "thin horizontal layers showing inverse grading and basal shear laminations" and division S3 "may be structureless or normally graded and it commonly contains water escape features". For gravelly flows, division R1 consists of coarse gravel with traction structures, division R2 consists of an inversely graded gravel layer, and division R3 consists of a normally graded gravel layer. Lowe's (1982) scheme is akin to a Bouma sequence (see below) for individual coarse beds, rather than a facies classification of coarse-grained beds. Because it is genetically based, the scheme may change as more is learned about the flow and depositional mechanics of high-density flow events.

In this review, we suggest that deep-water rocks contain a variety of depositional elements (discussed below) and that these elements contain distinctive assemblages of facies. We have chosen to use the simple scheme of Walker (1978), which is descriptive (except for the various deformed facies), and based on grain size. The categories included in this scheme are (1) classical turbidites, (2) structureless sandstones, (3) pebbly sandstones, (4) conglomerates, and (5) various types of deformed rocks. We are more concerned with the descriptive and environmental aspect of the facies than with the mechanics of flow and deposition (which are very difficult to study in flumes a few meters long when in nature flows may change and evolve over distances of hundreds of kilometers).

Classical Turbidites

This category includes all of those rocks originally considered as turbidites in the 1950s and 1960s—the beds that give rise to little or no controversy today. The facies includes thick monotonous successions of alternating sandstones and mudstones (Fig. 4). The sandstones have sharp, flat bases, and the only erosional features are normally on the centimeter scale. They include scour marks (commonly flute casts) and tool marks (commonly groove casts). Channeling on a scale greater than a meter is very uncommon.

Internally, classical turbidites contain some or all of the divisions first proposed by Bouma (1962) (Fig. 2). Division A implies rapid deposition producing structureless sandstone in the absence of any equilibrium bedforms, whereas divisions B and C imply traction of grains on the bed to form parallel lamination and ripple cross lamination, respectively (a waning-flow succession—Harms and Fahnestock, 1965; Walker, 1965). Divisions D and E both imply deposition of fine-grained material from suspension without traction on the bed. Note that Bouma (1962) observed that division D (laminations of silt and mud) was difficult to recognize in "weathered or tectonized

FIG. 4.—Alternating beds of sandstone and mudstone, Devonian, Cape Liptrap, South Australia. Note the monotonous alternation of sandstones and mudstones, and the very parallel nature of the bedding with no evidence of any topography on the sea floor.

outcrops"—consequently it may not be a useful or significant part of the Bouma sequence.

Two sub-categories of classical turbidites have been suggested by several workers: thin-bedded and thick-bedded. It must be emphasized that there is a complete spectrum of bed thicknesses and that their separation is arbitrary. The thick-bedded turbidites (sandstones roughly in the range 10–100 cm in thickness; Fig. 5) tend to be composed of Bouma's division A, with fewer beds also containing divisions B and C (Walker, 1968). Thin-bedded turbidites (Fig. 4) tend to lack Bouma's division A, and the sandstones contain only the B–C or C divisions. The nature of these divisions suggests two distinct types of thin-bedded turbidites.

The simplest type of thin-bedded turbidite contains a single set of ripple cross lamination, with or without division B parallel lamination underneath (Fig. 6). In more complex thin-bedded turbidites, the ripples in division C consist of climbing sets rather than single sets, and the ripple cross lamination (and the parallel lamination beneath) can be convoluted (Fig. 7). These complex thin-bedded turbidites also commonly contain ripped-up mudstone clasts, and they have been termed "CCC turbidites" (Fig. 8A; Walker, 1985); C for climbing, C for convolution and C for clasts.

The presence of convolute lamination implies rapid deposition of sediment and trapping of pore fluid, such that the primary structures are easily deformed. The climbing ripples imply deposition of sediment from suspension while the ripples are moving on the bed. Within the category of thin-bedded turbidites, the simple beds imply traction on the bed and essentially no deposition from suspension, whereas the CCC turbidites suggest high rates of deposition from suspension during formation of the primary bedforms. It has been suggested that thin beds showing high rates of deposition commonly form on levees. The thin beds that show little evidence of rapid deposition from suspension may indicate basin-plain settings, where the turbidity currents have much less sediment left in suspension (Fig. 8B; Walker, 1985). The presence of ripped-up mudstone clasts supports this interpretation—there is more likelihood of erosion associated with confined flows in channels than in unconfined settings on a distal basin plain.

FIG. 5.—Thick-bedded sandstones consisting mainly of Bouma's division A, separated by very thin siltstone partings. Height of cliff about 180 m. Compare with Figure 4. Annot Sandstone (Eocene), southern France.

Structureless Sandstones

There is an association in facies between classical turbidites and structureless sandstones. Individual structureless sandstone beds tend to be thicker (several tens of centimeters to a few meters) than the sandstones in classical turbidites, and mudstone partings between beds tend to be thin (centimeters) or absent (Fig. 5). The deposits of several flows may be amalgamated, the amalgamation planes being denoted by (1) abrupt changes in grain size, (2) layers of ripped-up mudstone clasts, or (3) simply the disappearance of thin mudstone partings (Fig. 9). On a larger scale, scouring on the scale of meters is commonly observed in this facies (Fig. 9). It follows that the monotonous interbedding of sandstones and mudstones, typical of classical turbidites, does not occur in structureless sandstones. Stacks of amalgamated beds without mudstone partings can be as much as 200 m thick, as in the Annot Sandstone (Fig. 5).

Parallel lamination and ripple cross lamination are rare, and the term structureless (now preferred to the older term "massive") denotes this absence of primary sedimentary structures. Graded bedding is present in some beds and not in others; its presence may be largely a function of the range of grain sizes available in the flow.

Although most beds lack primary structures, secondary structures indicating dewatering during compaction of the bed are common (Lowe, 1975). These include vertical or subvertical fluid-escape pipes (Fig. 10), which can become contorted if the bed is sheared by continuing turbidity-current flow during the fluid escape (Fig. 11). If the escaping water encounters a crude, incipient parallel lamination with variations in permeability, the water may be forced to flow horizontally until able to break through the less permeable layers and continue its vertical escape. The curved upward edges of these laminates take the shape of an irregular stack of dishes, hence the term "dish structure" (Figs. 10, 12).

The association of this facies with classical turbidites suggests that individual structureless sandstones are also the deposits of turbidity currents. This interpretation is strengthened by the presence of fluid-escape features, which indicate initial deposition of a fluid-rich sediment–water mixture (rather than a more rigid plug flow with grain-to-grain contacts and much less interstitial water). Despite the thickness of individual beds and the general absence of Bouma sequences, there is no compelling observational or experimental evidence to reject turbidity currents in favor of speculative processes such as fluxoturbidity

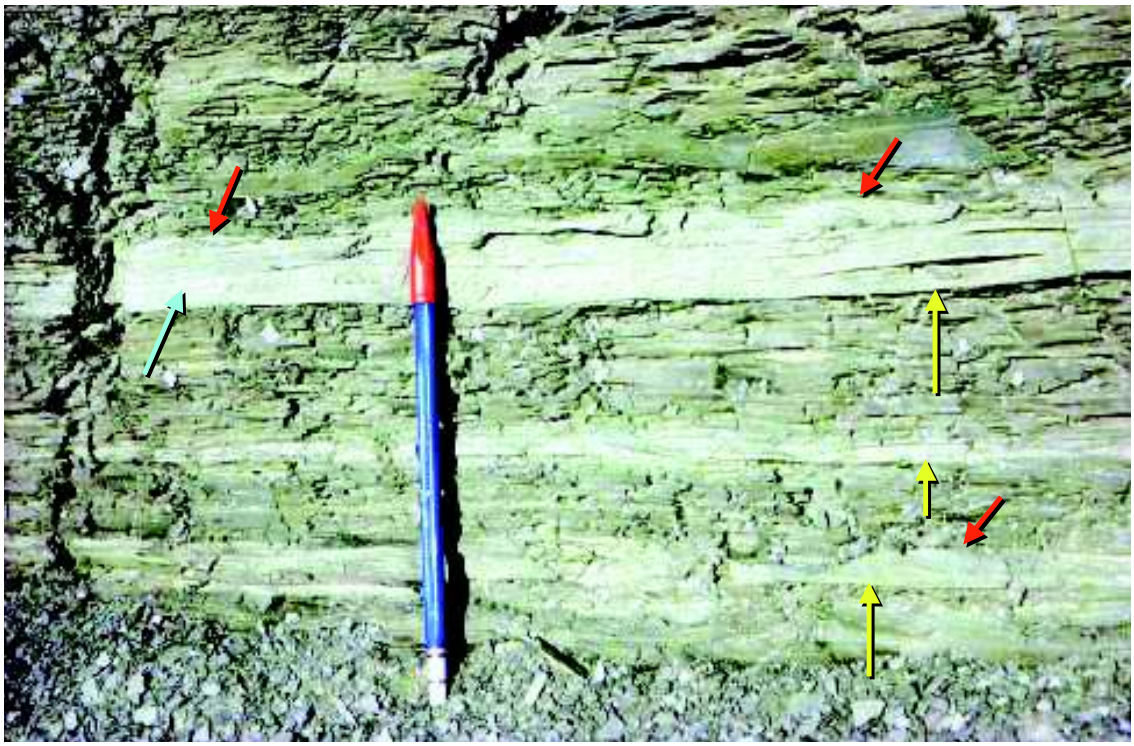

FIG. 6.—Thin-bedded turbidites beginning with Bouma divisions B and C. Sharp bases shown by yellow arrows, parallel lamination by a blue arrow, and ripple cross lamination by red arrows. Note the absence of convolute lamination, climbing ripples, and ripped-up mudstone clasts. Ordovician turbidites at Chutes Montmorency, Quebec.

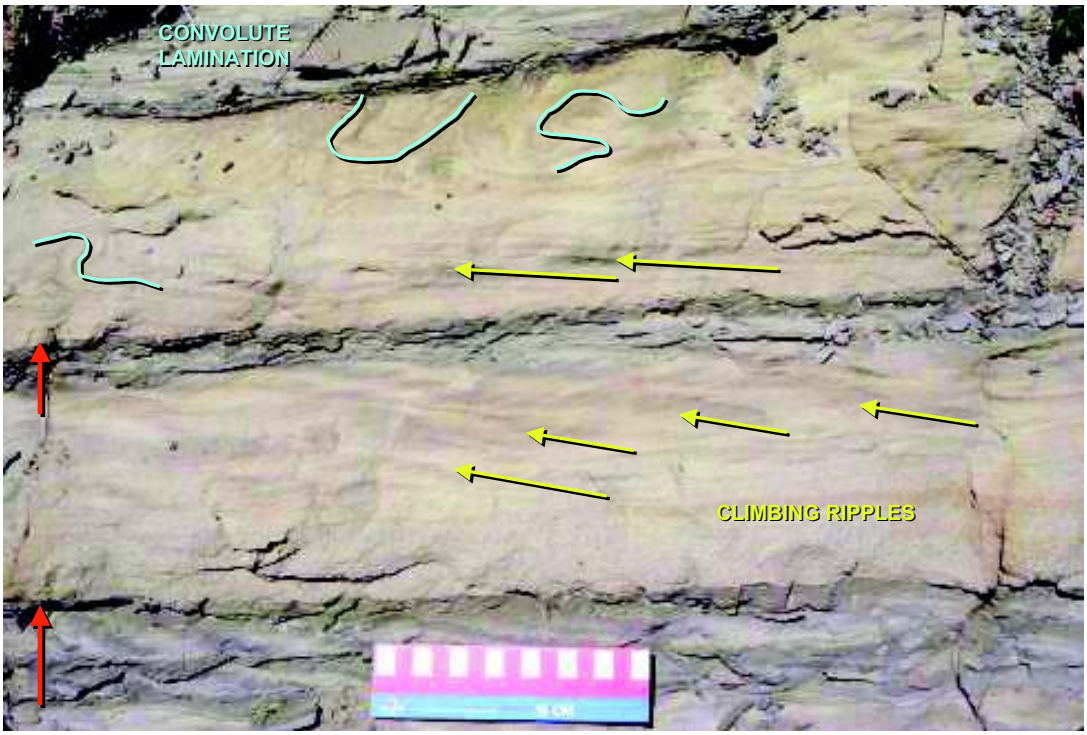

FIG. 7.—Thin-bedded turbidites in the Chatsworth Sandstone (Cretaceous), Chatsworth (Simi Hills), California. Bases shown by red arrows, and climbing ripples shown by yellow arrows. Convolute lamination is outlined in blue. Compare with Figure 6 (where there is no climbing and no convolution).

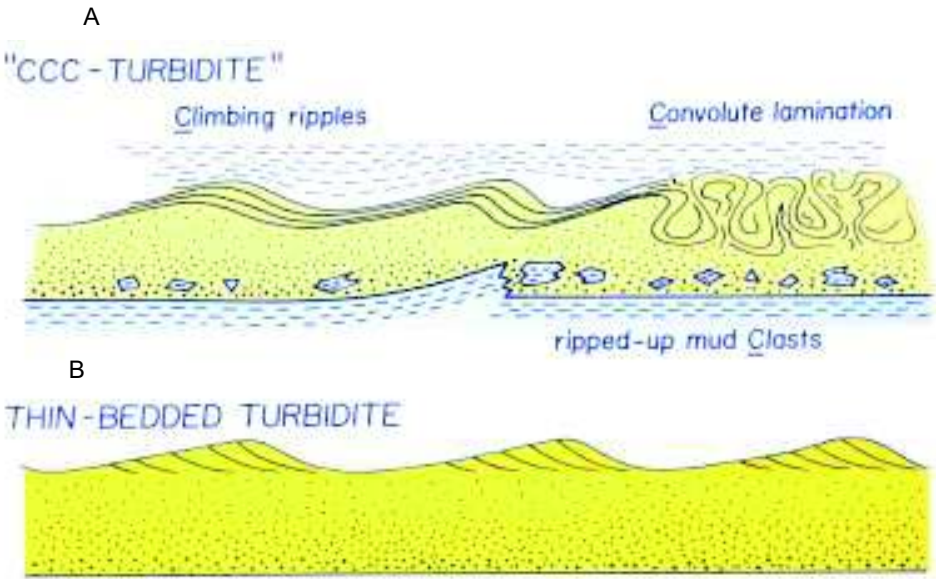

FIG. 8.—Diagram showing two types of thin-bedded turbidites. One is characterized by single rows of ripple cross lamination without climbing, and the other is characterized by climbing ripples, convolute lamination, and ripped-up mudstone clasts **A)**. The "CCC turbidites" are interpreted as levee deposits (see text), and the others as distal basin plain deposits **B)** (From Walker, 1985).

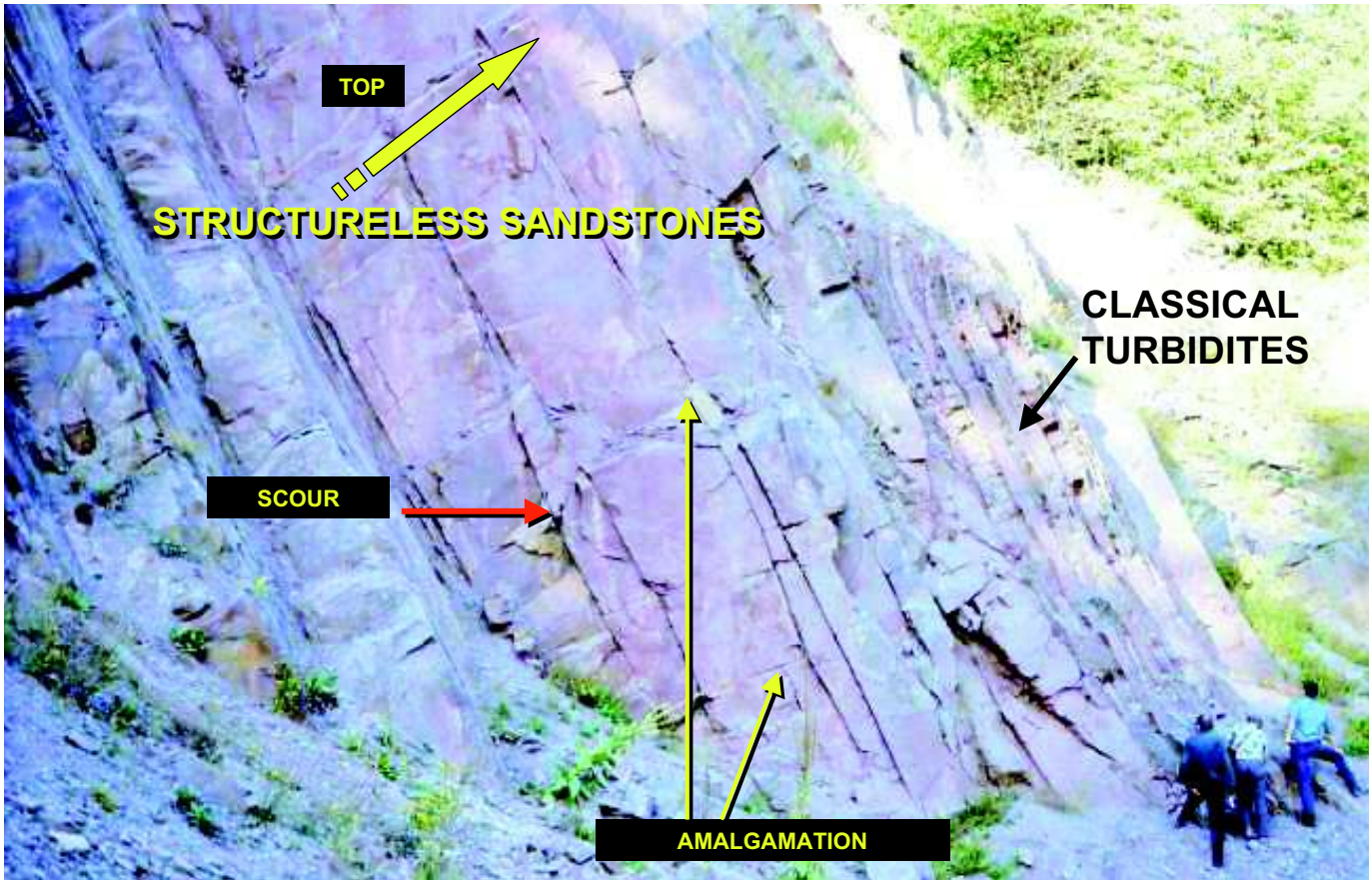

FIG. 9.—Devonian turbidites in Germany. Note the classical turbidites (right) and the underlying thick-bedded structureless sandstones. Yellow arrows show thin mudstone partings that disappear along strike (amalgamation), and the red arrow shows a small scour.

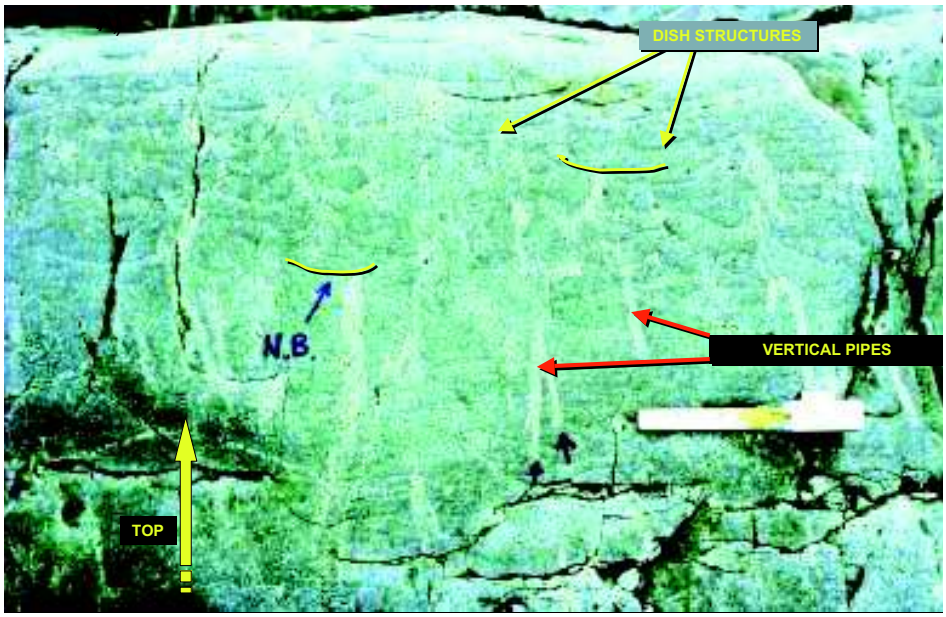

FIG. 10.—Vertical fluid-escape pipes with overlying dish structures (outlined in yellow). Ordovician Cap Enrage Formation, Gaspesie, Quebec.

currents (Dzulynski et al., 1959) or sandy debris flows (Shanmugam et al., 1994; Shanmugam, 1996).

Pebbly Sandstones

As the coarse fraction within flows gradually increases, the structureless sandstone facies grades through granule sandstones into the pebbly sandstone facies. Graded bedding is common (Fig. 13) and readily observed because of the wide range of sizes present. Internally, beds may show a crude horizontal stratification, and, in rare cases, planar tabular and trough cross bedding may be present. In the Cap Enrage Formation (Quebec), the trough sets are up to 50 cm thick, and trough widths seen in plan view are up to at least two meters. Apart from structureless sandstone, the elements of the Bouma sequence do not occur in pebbly sandstones, and hence the Bouma sequence cannot be used as a descriptor in this facies

If blade-shaped or disc-shaped pebbles are present, they are commonly well imbricated (Fig. 14). The features described above—graded bedding, cross bedding, and imbrication—all suggest turbulent flows in which grains are free to move relative to one another, enabling the development of these features.

Making reasonable estimates of the turbulence of the flow and particle settling velocities, it appears that a flow moving at 6 m/s (the Grand Banks flow of 1929 near the toe of Laurentian Fan; Uchupi and Austin, 1979) could suspend by fluid turbulence alone clasts up to 2 or 3 cm in diameter. It therefore appears that pebbles can be transported into deep water by turbidity currents (flow velocities of 6 m/s or greater), and that such flows could deposit graded, imbricated, and/or cross-bedded beds. In these instances, despite the coarse nature of the beds, it is again not necessary to appeal to alternative transport processes such as fluxoturbidity currents and sandy debris flows.

Conglomerates

Conglomerates are not as common as the facies described above, but they do make up an important part of the deep-water sedimentary record. Four distinct facies were recognized by Walker (1975a), but the classification is based on a relatively small sample and does not have the authority of the Bouma sequence for classical turbidites. The features used to define the facies are (1) the style of grading (normal or inverse), (2) the type of stratification, and (3) the fabric. In combination, these features define the four facies.

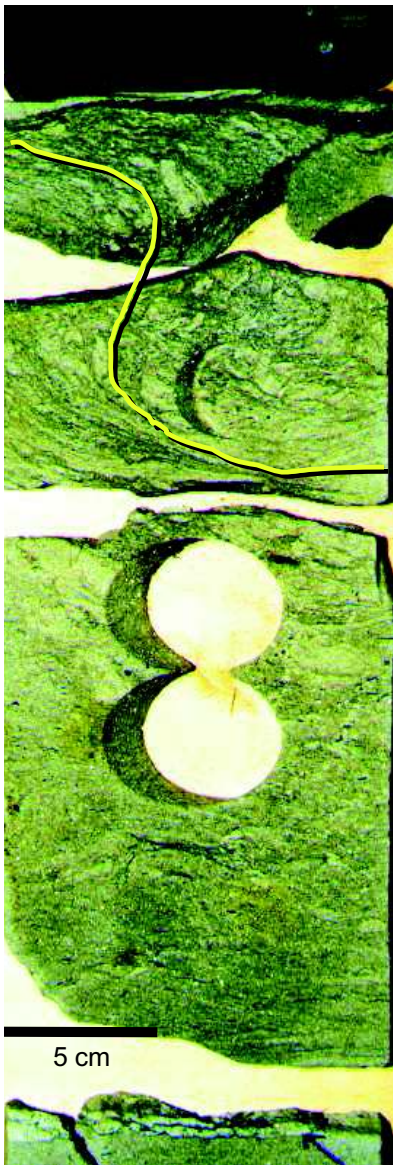

FIG. 11.—Distorted fluid-escape pipes in a core from the Cretaceous Lysing Formation, offshore mid-Norway. Well 6506/12-4, 3240.6 m depth.

The first consists of beds which are normally graded and pass upward into finer-grained stratified pebbly sandstone (Fig. 15). The second consists of beds that show only normal grading (Fig. 16) without a stratified component. The third consists of beds that begin with inverse grading and pass upward into normally graded beds (Fig. 17). Finally, the fourth facies lacks any of these features and is described as disorganized or structureless (Fig. 18).

The first three facies may also display clast imbrication (Figs. 14, 17). In the stratified parts of the graded-stratified facies, clasts lie with their long axes transverse to flow, and the short axis dips upstream. In the graded and inversely graded parts of

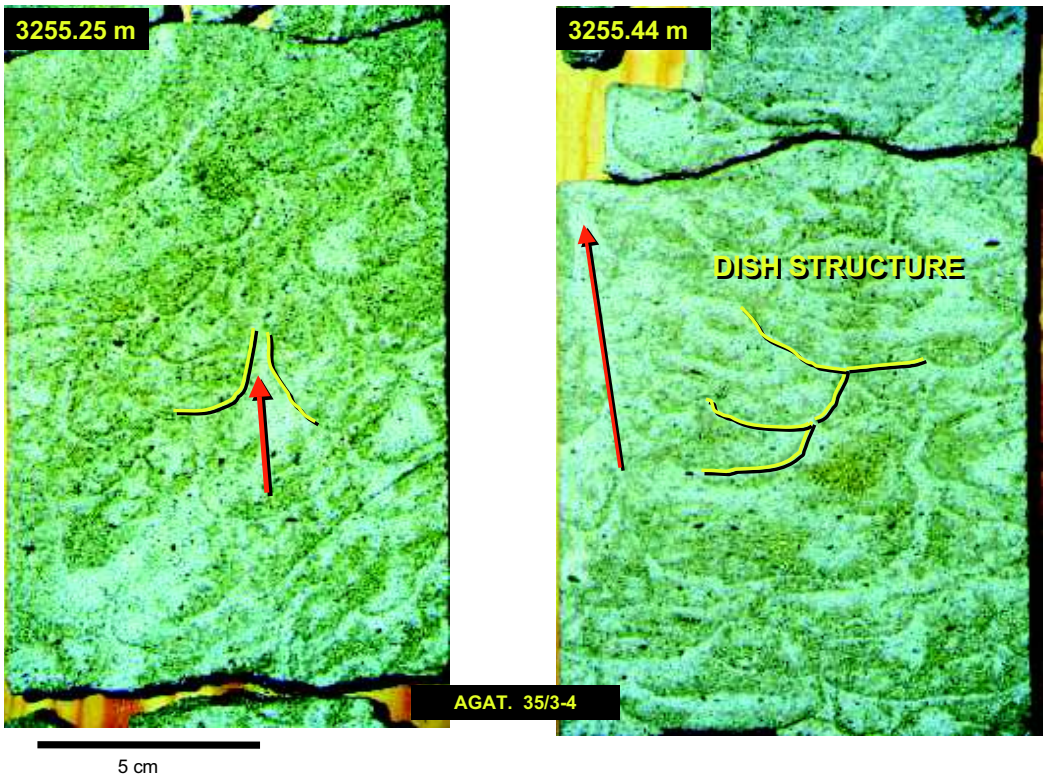

FIG. 12.—Dish structures outlined in yellow from the Agat 35/3-4well, 3255.5 m, offshore Norway. Note darker (less permeable) layer at base of each dish, and a few fluid-escape pipes red arrows) where fluid has broken through vertically.

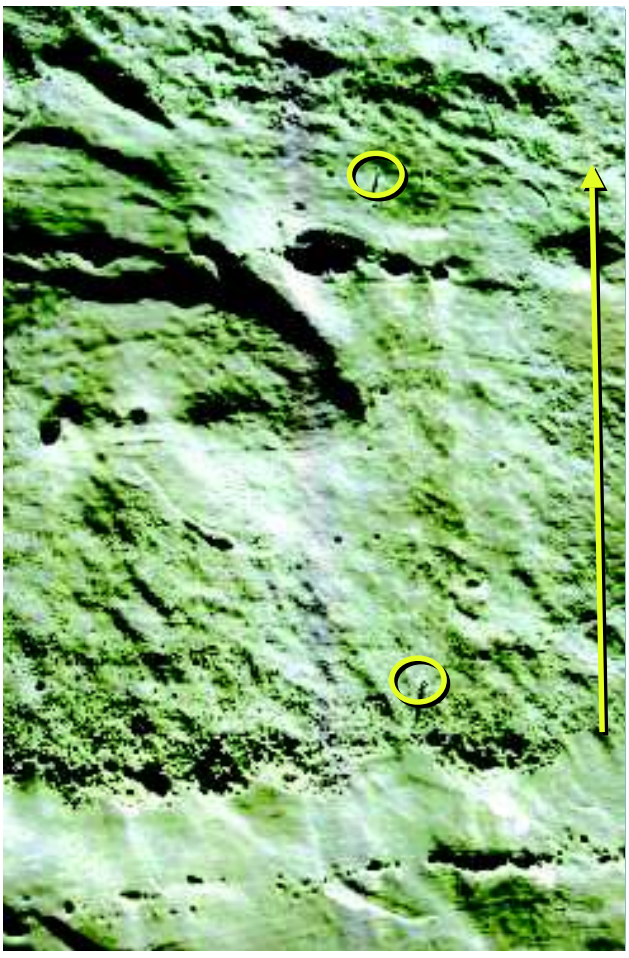

the beds, however, clasts more commonly lie with their long axes parallel to flow, with the long axes dipping upstream. This fabric suggests that the clasts have not been rolling on the bed (if clasts roll, long axes tend to be transverse to flow). A full discussion of conglomerate fabrics has been given by Walker (1975a).

Bed thicknesses in the conglomerate facies are very variable. Individual graded beds can be over 10 m thick (Fig. 16), but alternatively, beds may be only one or two pebble diameters in thickness. The example from Point Lobos, California, in Figure 19, shows several thin conglomerate layers alternating with sandstone layers. The pebbles probably did not constitute the bulk of the flow, because they would not have given a sufficient density contrast with the surrounding fluid to drive the flow. It is more likely that the flows that transported the pebbles were large sandy turbidity currents, and that the thin pebble beds represent lags left behind by the main flows.

Despite the suggestions made above, interpretations of conglomerate facies remain somewhat speculative because of the lack of large-scale experimental work.

EXOTIC FACIES—OTHER TYPES OF DEPOSITS IN DEEP-WATER ENVIRONMENTS

This category contains a variety of facies that do not fit into the four facies described above. They are generally characterized by poor sorting and lack of coherent bedding features. Some of the main types are described below.

←

FIG. 13.—Pebbly sandstone about 1 m thick showing overall graded bedding. Annot Sandstone at Chambre du Roi, southern France. Fixed eyebolts for rock climbers are circled for scale.

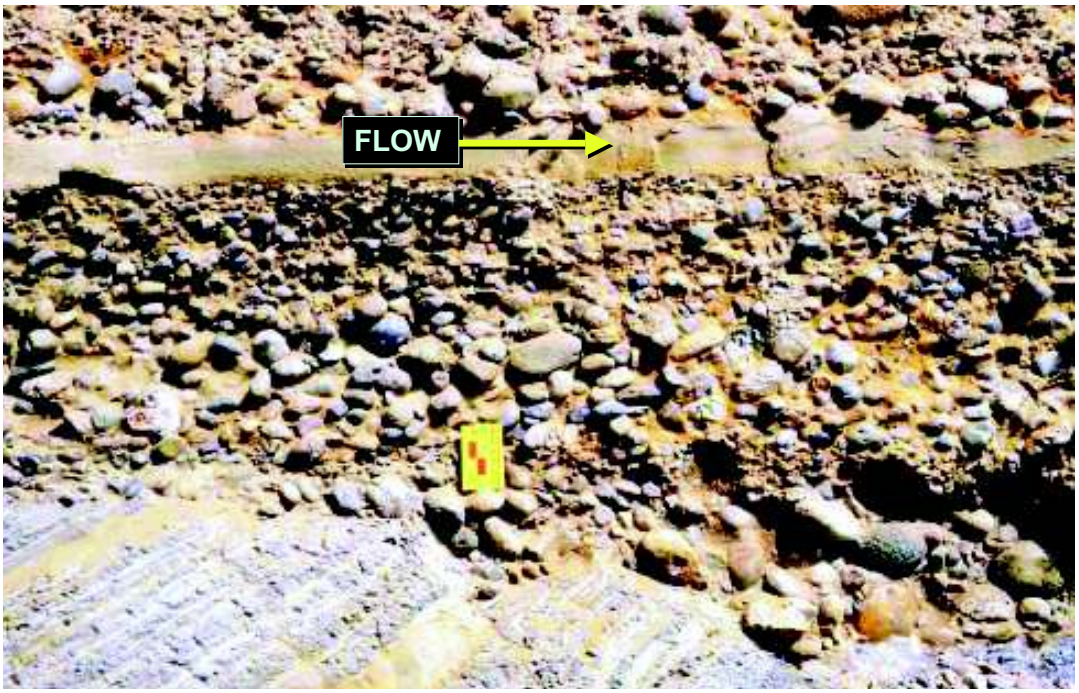

FIG. 14.—Graded conglomerate showing clast imbrication (center of bed above notebook). Bed rests on deformed and slumped mudstones. Tourmaline State Surfing Beach, north of San Diego, California.

Pebbly Mudstones

Pebbly mudstones (Fig. 20) consist of granules and pebbles, commonly along with distorted sandstone clasts, all embedded in a deformed mudstone matrix. The term was introduced by Crowell (1957), who suggested two mechanisms for their origin. The first was emplacement by debris flows, wherein the strength of the muddy matrix prevents the settling of the larger pebbles and clasts during transport. Some debris flows may slide rapidly on a basal layer of lubricating fluid (sea water) (Mohrig et al., 1988), though it is likely that at least part of the moving mass clearly is in contact with and erodes the substrate over which they pass (Fig. 21; Posamentier and Kolla, 2003a) suggesting a more complex rheology. As the flow velocity increases, there is a tendency for sediment to be suspended at the head as well as the upper parts of the flow. Rapidly moving debris flows therefore may tend to transform at least in part into turbidity currents. The transformation may be quite slow for muddy flows, but for sandy debris flows moving at more than 1 to 2 m/s (the velocity at which sand is carried in suspension) the transformation into a turbulent turbidity current may be rapid, and take place over a short distance.

A second mechanism for depositing pebbly mudstones (Crowell, 1957) involves the passage of a sandy/pebbly turbidity current over a bed of fluid-saturated, uncompacted mud. The coarser material from the flow may be deposited on the muddy surface and then quickly sinks into the uncompacted mud. The pebble–sand–mud mixture may then flow for a short distance as it dewaters, mixing the various grain sizes and then depositing an ungraded, poorly sorted pebbly mudstone.

→

FIG. 15.—Graded conglomerate in the Cap Enrage Formation, Ordovician, Quebec. Note the large carbonate blocks in the base of the bed, and the gradation into structureless pebbly sandstone, stratified pebbly sandstone, and finally structureless sandstone. Bed is at least 8 m thick.

FIG. 16.—Graded conglomerate about 14 m thick, Eocene of Oregon. Close field examination showed a progressive decrease in maximum and estimated mean grain size throughout the bed, and no internal planes or grain size changes that might suggest an amalgamated bed.

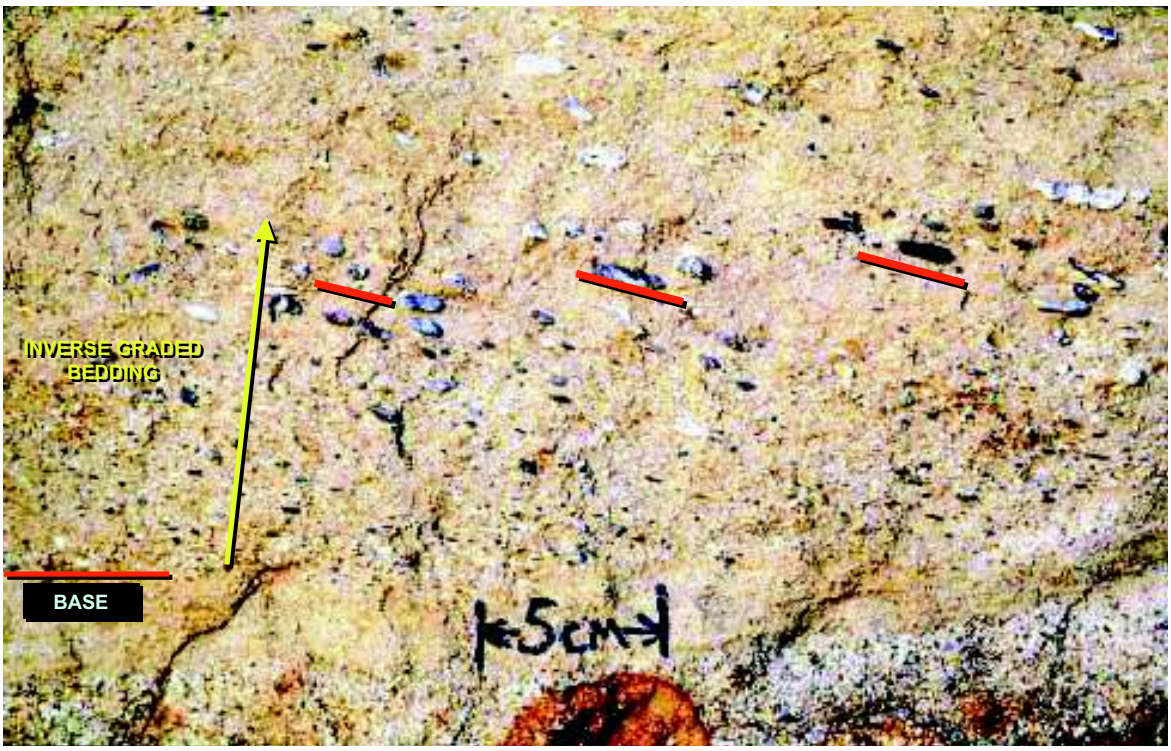

FIG. 17.—Inversely to normally graded conglomerate, Cretaceous La Jolla Formation, California. Note also the well developed imbrication with clasts dipping upstream (to the right).

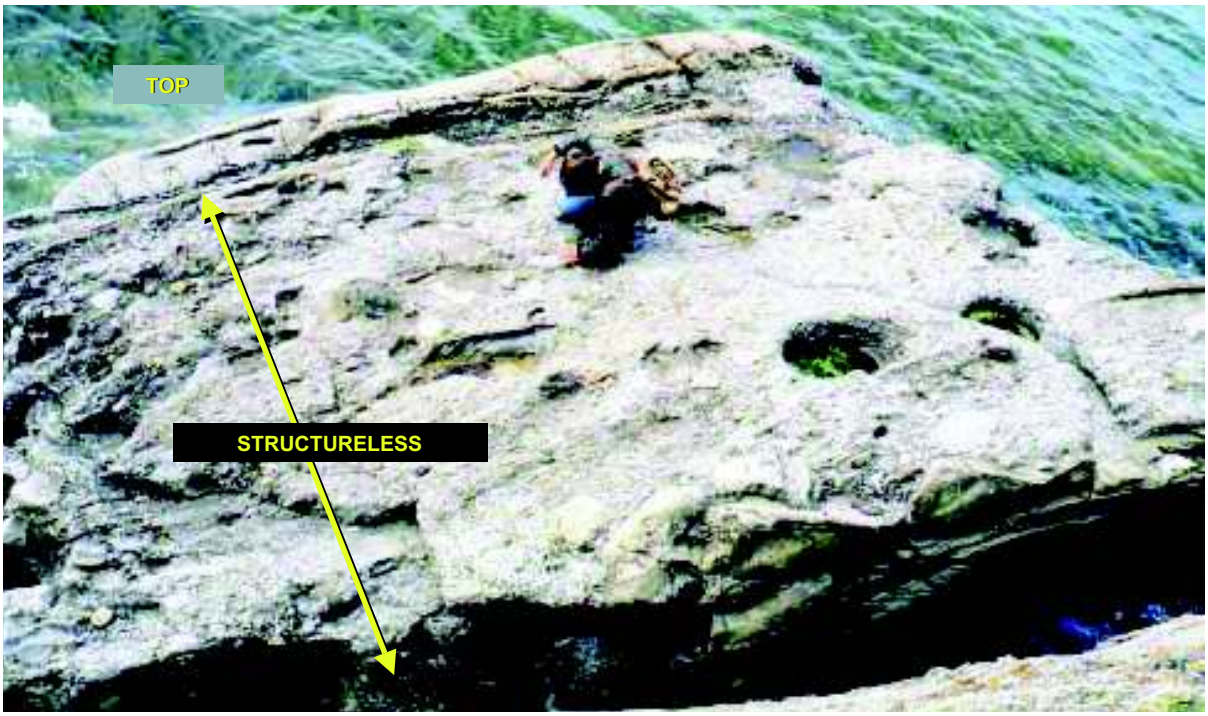

FIG. 18.—Conglomerate in the Ordovician Cap Enrage Formation, Quebec, showing no grading and no imbrication. The bed is described as disorganized or structureless.

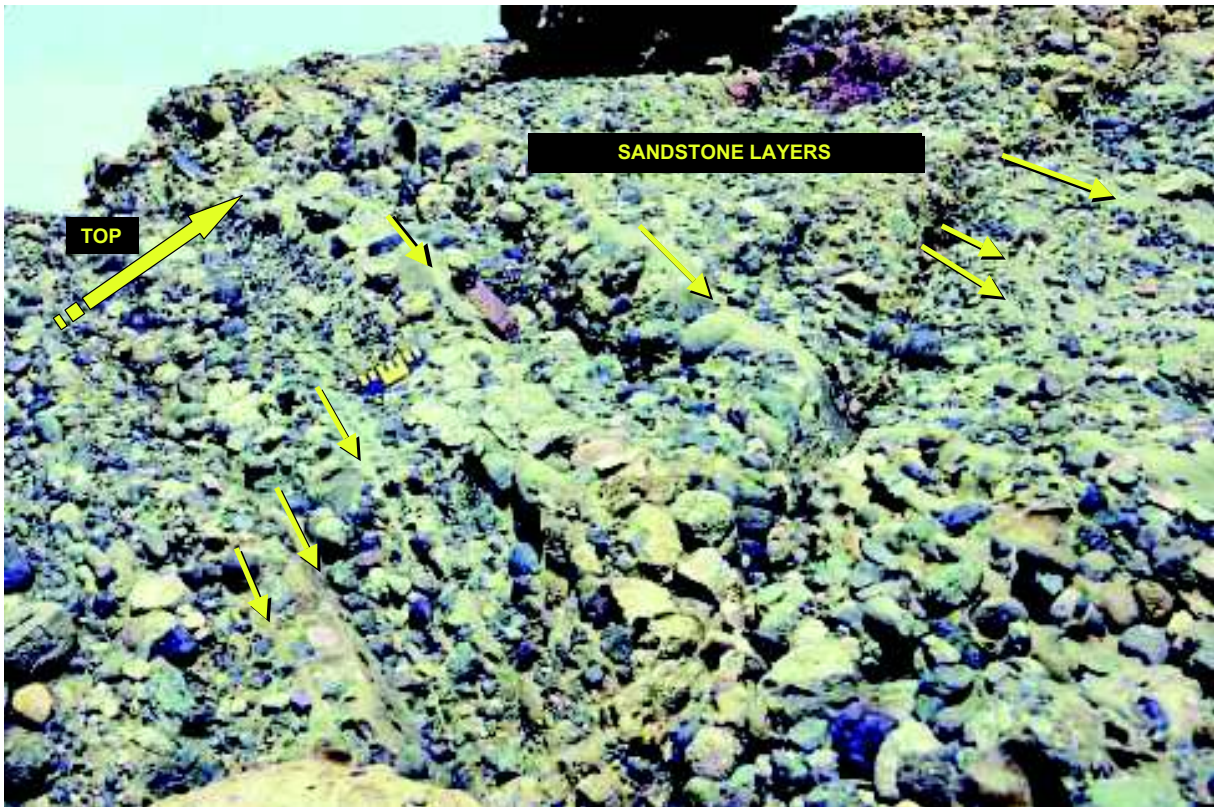

FIG. 19.—Thin conglomerate horizons separated by sandstone layers (shown by yellow arrows). Cretaceous, Point Lobos, California.

FIG. 20.—Pebbly mudstones from Pigeon Point, California. This is the classic location where Crowell (1957) first discussed the origin of pebbly mudstones. Note clasts scattered throughout the muddy matrix, along with rolled-up sandstone beds (above notebook).

Slumps

Slumps (Figs. 22, 23) comprise a large category of variously deformed sediments. The term in its most general sense describes chaotic unbedded units meters to tens of meters in thickness. The lithology may consist only of mudstone (Fig. 22), or it may involve pulled-apart or rolled-up sandstone beds in a matrix of mudstone. In all cases, deposition was probably fairly rapid, and mudstones form an important part of the facies. Transport distances vary from a few meters (e.g., collapse of channel walls) to hundreds of kilometers across basin floors. Original depositional conditions may have involved rapid deposition of sandstone with trapped pore water, followed by mudstone deposition and sealing of the pore fluid. With continued deposition, the lithostatic load would increase, but, if the pore fluid could not escape, the fluid pressure would also increase. Slumping would be initiated if beds fail along a weak layer with high pore pressure. The sediment may move a few meters during dewatering and deposit a unit that consequently would be identified as a slump. Alternatively, if the sediment moved a greater distance the resulting deposit may be identified as a debris flow. Some slumps may move fast enough so that much of the sediment is taken into suspension with turbulence characterizing the flow, transforming the mass into a turbidity current.

Slumps with Stratified Blocks

Slumps with stratified blocks (Fig. 24) are not uncommon. The stratified blocks may be meters in diameter, and they consist of interbedded layers of sandstone and mudstone (perhaps originally classical turbidites). In most cases the blocks were probably not lithified, so that transport in a turbulent medium would probably result in splitting of the blocks along the cohesionless sandstone layers. This would destroy the stratified blocks and probably would give rise to large mudstone clasts. One suggestion is that the blocks were derived from an undermined, collapsed channel wall, where the blocks subsequently were buried by turbidity-current sediment before they could be transported downchannel. Later in this paper, examples will be shown of large blocks that have been rafted on top of mass-transport complexes. Such flows are not turbulent, and the rafted blocks may retain some stratification.

Slumps involving only one or two beds (Fig. 25) are fairly common. The deposit is characterized by undeformed bedding below and above the slumped horizon, and coherent but rolled-up beds within the slump. The beds are commonly thin (a few tens of centimeters maximum), and are associated with other thin beds and with "CCC" turbidites (Walker, 1985) interpreted as levee deposits. Thus the slumps may indicate rapid deposition of beds on the levee (either the side facing the channel, though more

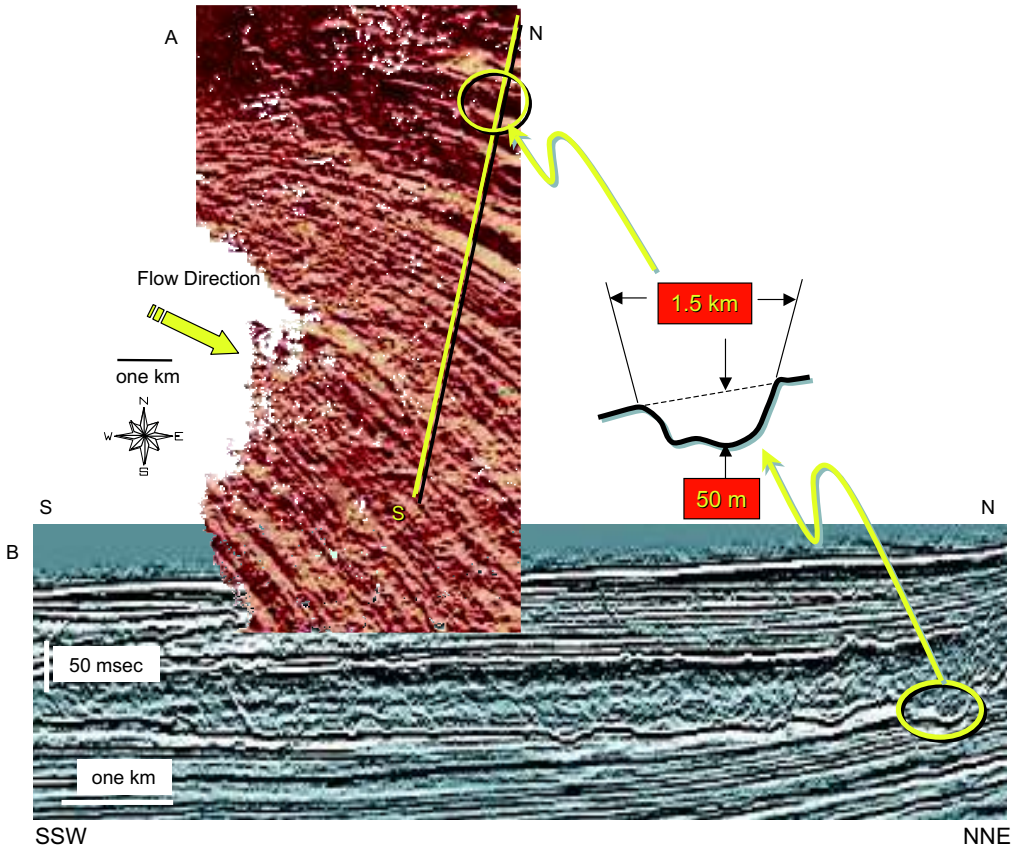

FIG. 21.—**A)** Plan view of the erosional base of a mass-transport complex in the ultra-deep environment of the Makassar Strait, Indonesia. Parallel to divergent erosional grooves are observed. **B)** Section-view image of mass-transport complex. The mass-transport complex is characterized by chaotic seismic reflection character, with erosional scour in excess of 50 m locally, and up to 1.5 km wide (modified from Posamentier et al., 2000). Seismic data courtesy of WesternGeco.

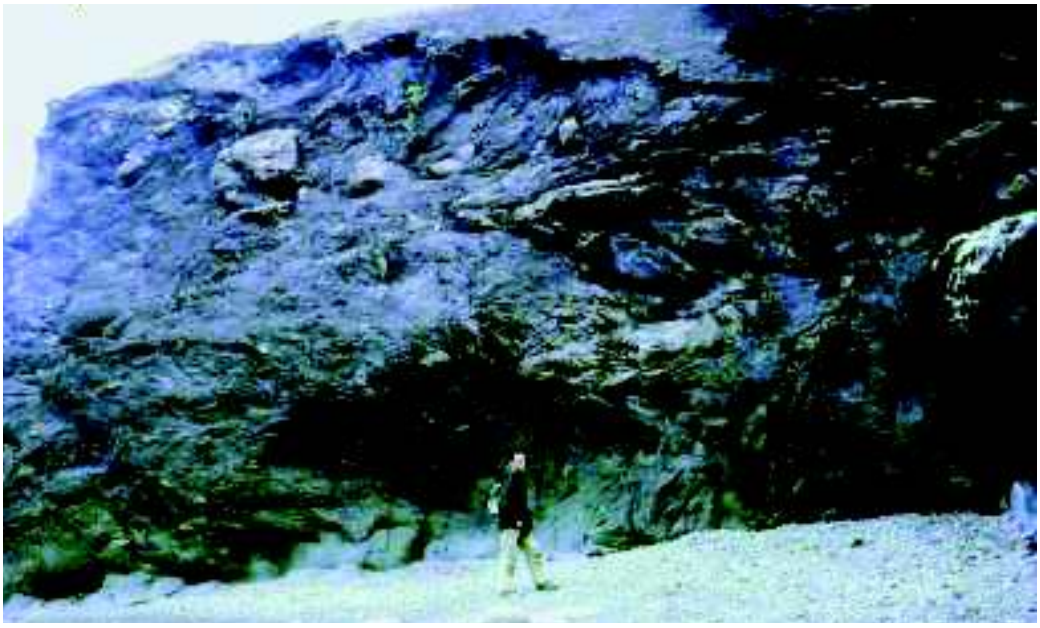

FIG. 22.—Large slump resulting in almost complete disruption of bedding, Carboniferous Bude Sandstones at Efford, southwest England.

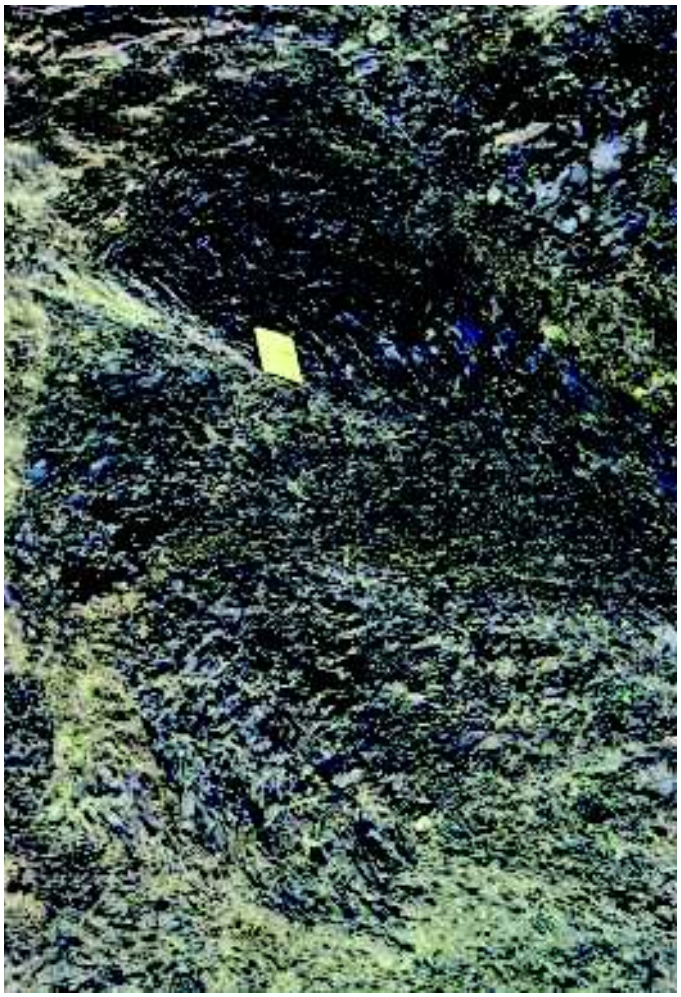

commonly on the back side of the levee), perhaps with trapped pore fluid within the sandstones. The slopes associated with the levee must have been sufficient to allow gentle sliding of just one or two beds, without large-scale deformation of the underlying sediment

CONTROLLING FACTORS ON DEEP-WATER SYSTEMS

Here, we discuss some of the principles relevant to the deposition of turbidites and the depositional elements within which they occur. We will "set the stage" with regard to the context within which deep-water depositional elements are deposited. A sound understanding of process is key to the construction of robust depositional models, enabling geoscientists to construct models that will be applicable to their unique set of environmental circumstances. Such models can then be a useful predictor of

←

FIG. 23.—Slump folds in Eocene slope mudstones of the Cozy Dell Formation, Highway 33 north of Wheeler Gorge, California. Scale shown by notebook.

FIG. 24 (below).—Slump involving large stratified blocks in the Upper Cretaceous Great Valley Sequence, Lake Berryessa, California. The two heavy black lines show bedding (top to the left)—the bedding is parallel but the lines converge because the camera is pointed steeply up the cliff. The matrix is a silty mudstone with a large variety of pebbles and cobbles. The stratified blocks consist of layers of sandstone and mudstone. It is argued that these would easily be disintegrated along the unconsolidated sandstone layers if there had been significant transport. It follows that they may have collapsed from a nearby channel wall and were buried before they could break up. Slumped bed is about 7 m thick.

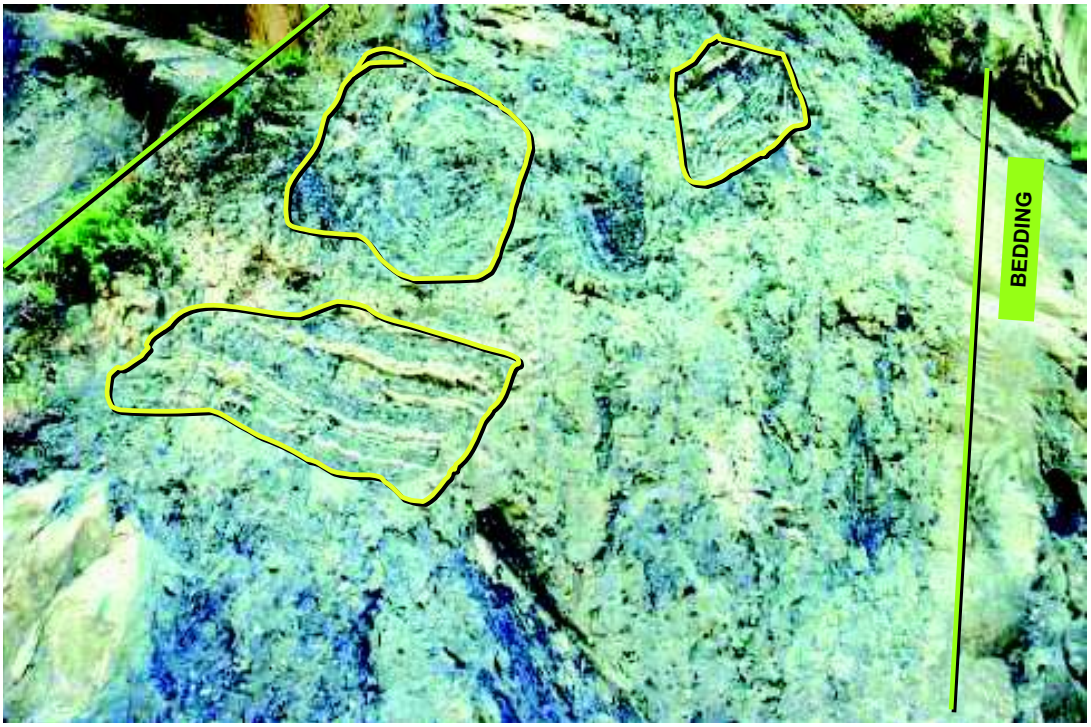

FIG. 25.—Small-scale slump involving only two beds within otherwise flat-bedded succession, Eocene, Waitemata Group, New Zealand.

spatial and temporal lithofacies distribution. A typical deep-water depositional environment with associated depositional elements is illustrated in Figure 1.

Sediment Staging Areas

The staging area can be defined as the shelf and/or upper-slope location where turbulent flows originate (Fig. 1). This staging area and the characteristics of the sediments delivered to that area are all-important in dictating the nature of turbidity currents and subsequently their deposits farther down-system. In particular, the sand-to-mud ratio that characterizes these sediments plays an important role in determining whether long leveed channels will develop down-system or whether short leveed channels feeding frontal splays or lobes will characterize downslope areas instead. The sediments that ultimately get incorporated into flows can be delivered to the staging area by fluvial, eolian, or longshore-drift processes. Subsequent turbidity currents originate as sediment failures, associated with seismicity and slope instability. Alternatively, if rivers deliver sediment directly to canyon heads, high-density flows within rivers can continue directly into the deeper basin by density underflow (i.e., hyperpycnal flow). Such density underflows can transform into true gravity flows farther down the slope.

The Significance of Sand-to-Mud Ratio within Flows

The initial sand-to-mud ratio within flows is dictated largely by conditions in the staging area. The grain-size distribution in these shelf-edge depocenters ultimately plays a critical role in the style of turbidite deposition downslope, a relationship described by Reading and Richards (1994). Posamentier and Kolla (2003a) discuss how grain-size distribution exerts this control on the style of turbidite deposition, and is schematically illustrated in Figure 26. This figure illustrates the relationship between total flow height, the height of the high-density part of the flow, and levee height, and the resulting transition between leveed channel and frontal splay in the absence of a change in the gradient of the slope.

As flows travel down-system, they progressively become better organized, with finer sediments concentrating in the upper part of the flow and coarser sediments concentrating in the lower part of the flow. The result is that the upper part of the flow tends to have a lower density and concentration than the lower part of the flow. The tops of many turbulent flows are higher than the associated levee crests (Fig. 27), the result of which is that the lower part of the flow, where much of the sand-size sediment is concentrated, is fully confined by the channel walls. In contrast, the upper part of the flow, which rides well above the levee crests, is largely unconfined by channel walls and hence is free to expand laterally beyond the levee crests and onto the overbank. This process of flow spillover results in the deposition of thin, fine-grained turbidites (commonly CCC turbidites; Figs. 7, 8) on the crests and backs of the levees, and it also results in progressive impoverishment of mud within the total flow. In addition to mud being lost from the flow by spillover, some sand may also be lost from the flow because of sedimentation at the flow base and by mixing with the remaining upper, lower-density part of the flow. However, the amount of sand lost from the flow is volumetrically significantly less than the amount of mud lost from the flow by

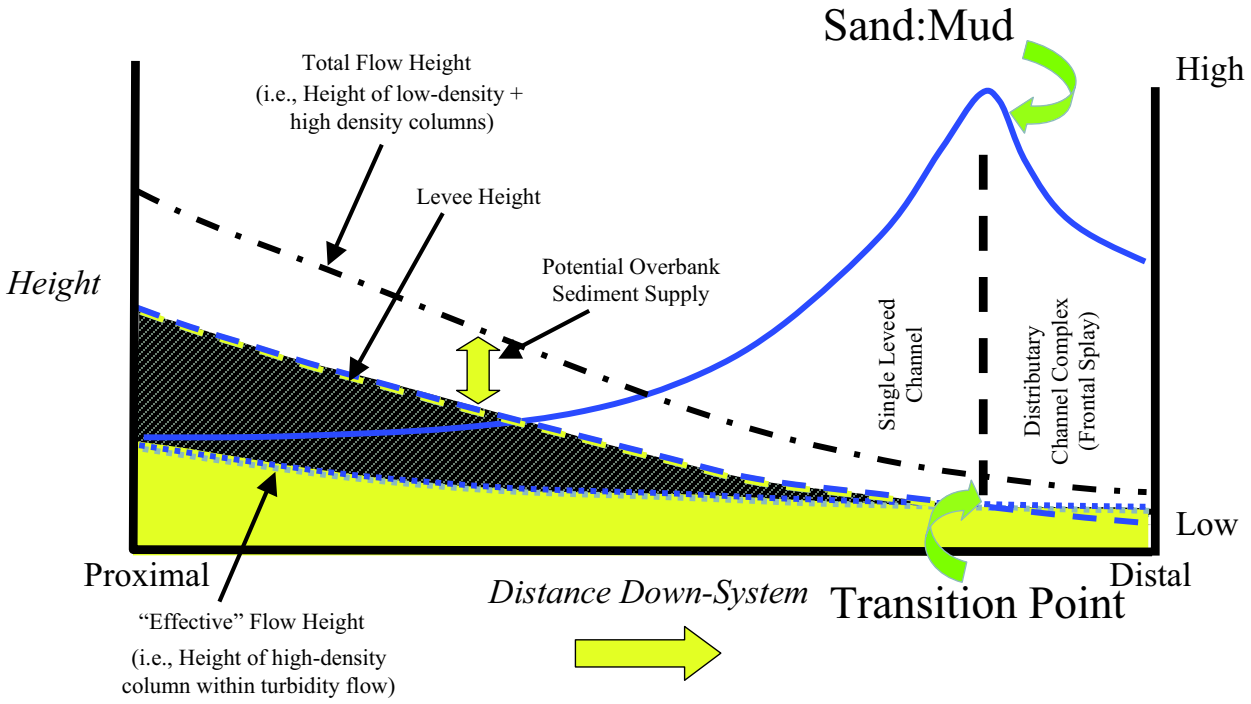

FIG. 26.—Schematic depiction of the interplay between sediment gravity flows, net sand, and levee height with distance down-system. Note that the high-density part of the gravity flow is located progressively more closely to the levee crest with distance seaward. A transition from leveed channel to frontal splay / lobe occurs when the high-density part of the flow (i.e., the sand-rich part of the flow) reaches bankfull stage. Note also that the highest sand-to-mud ratio occurs there as well (modified from Posamentier and Kolla, 2003a).

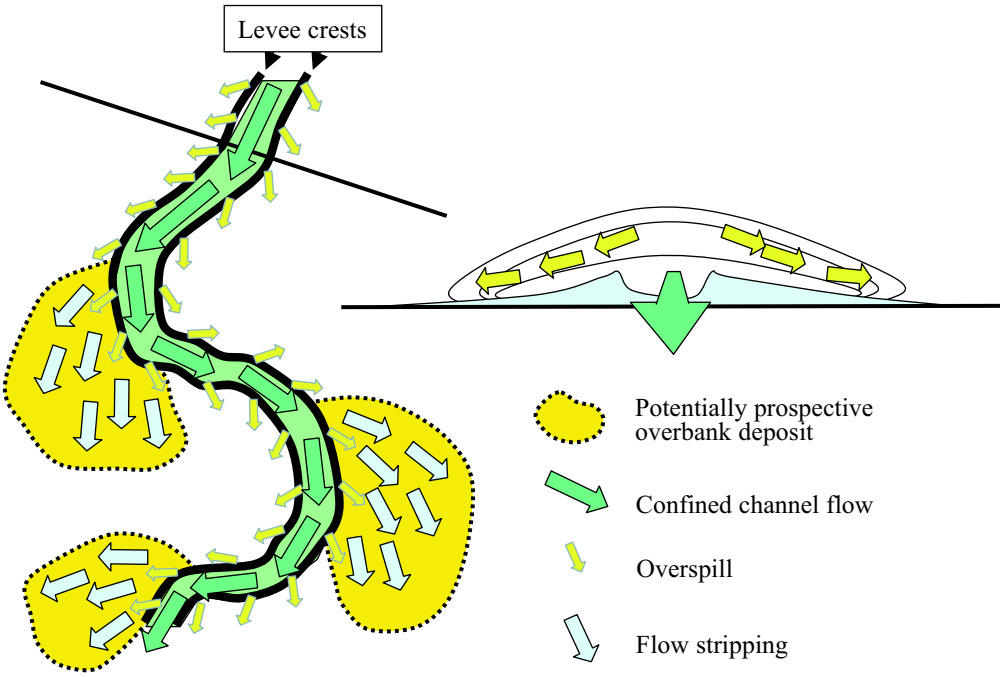

FIG. 27.—Schematic illustration of sediment gravity flow through a leveed channel (compare with Fig. 77). The cross-sectional view illustrates that the flow top lies well above the levee crest. The part of the flow between the flow top and levee crest is unconfined and systematically spills out of the channel. Enhanced spillover occurs at outer bends (by the process of flowstripping). These locations constitute areas of preferred sand deposition in the levee environment.

spillover. Thus the channel floor tends to aggrade somewhat more slowly than the levee crests.

Also, somewhat counterintuitively, flows tend to become sandier down-system (i.e., flows have a progressively higher sand-to-mud ratio down-system) as a result of continual preferential shedding of muddier sediment due to spillover. Kolla and Coumes (1987), Pirmez and Flood (1997), and Hiscott et al. (1997) have observed that with increased distance down-system there is a gradual increase of net sand deposited on levees, consistent with a progressive impoverishment of mud within flows in the down-system direction. The progressive loss of the upper or mud-rich part of the flow results in a progressive decrease in levee height down-system (Fig. 28). At some point down-system, the high-concentration or sand-rich part of the flow reaches the levee crests (bankfull stage). This is a critical location because down-system from this point spillover is no longer associated mainly with the muddy part of the flow; rather, sand-rich flows are now directed across the overbank. Geomorphologically this is expressed as a transition from a single leveed channel to a distributary channel complex or frontal splay (Posamentier and Kolla, 2003a). This location, referred to as the *transition point*, also marks the location where the sand-to-mud ratio within the flow is greatest. Downslope of this location the rate of sand being lost from the flow exceeds the rate of mud being lost from the flow, largely because the sand-rich part of the flow is now largely unconfined. The increased cross-sectional area of the floor results in decreased flow velocity and sand deposition.

The sand-to-mud ratio in the flow is critical to this analysis insofar as changing this flow characteristic changes the location of the transition point (Figs. 29, 30). Thus, if a succession of sand-rich flows is followed by a succession of mud-rich flows, the transition point shifts seaward and the result is the superposition of a single leveed channel across an older frontal splay (Fig. 31). Under certain circumstances, where later flows are more sand rich, the reverse can occur as well. As previously discussed, such changes in sand-to-mud ratio commonly originate in the staging area, and are manifestations of changing proportions and rates of delivery by rivers and shelf processes, of different sediment sizes.

Slope and Basin Physiography

The morphology of the slope and basin floor influences the deposition of turbidites in a variety of ways. Physiographic factors include (1) sea-floor rugosity on a large scale such as fault scarps and intraslope basins associated with salt tectonics or toe-of-slope thrust faults, (2) small-scale sea-floor rugosity comprising sea-floor irregularities associated with earlier depositional events such as slides or debris flows, (3) the height of the available relief from shelf edge to basin floor, (4) the gradient of the slope, (5) the presence of significant breaks in slope such as those that can occur where the slope meets the basin floor, and 6) the rate of change of the slope.

Perhaps the most well documented example of the effect of sea-floor rugosity on turbidite systems is the fill-and-spill model of turbidite systems that characterizes salt-supported intraslope basins (Prather et al., 1998). They described a scenario whereby a string of intraslope basins would fill progressively from the

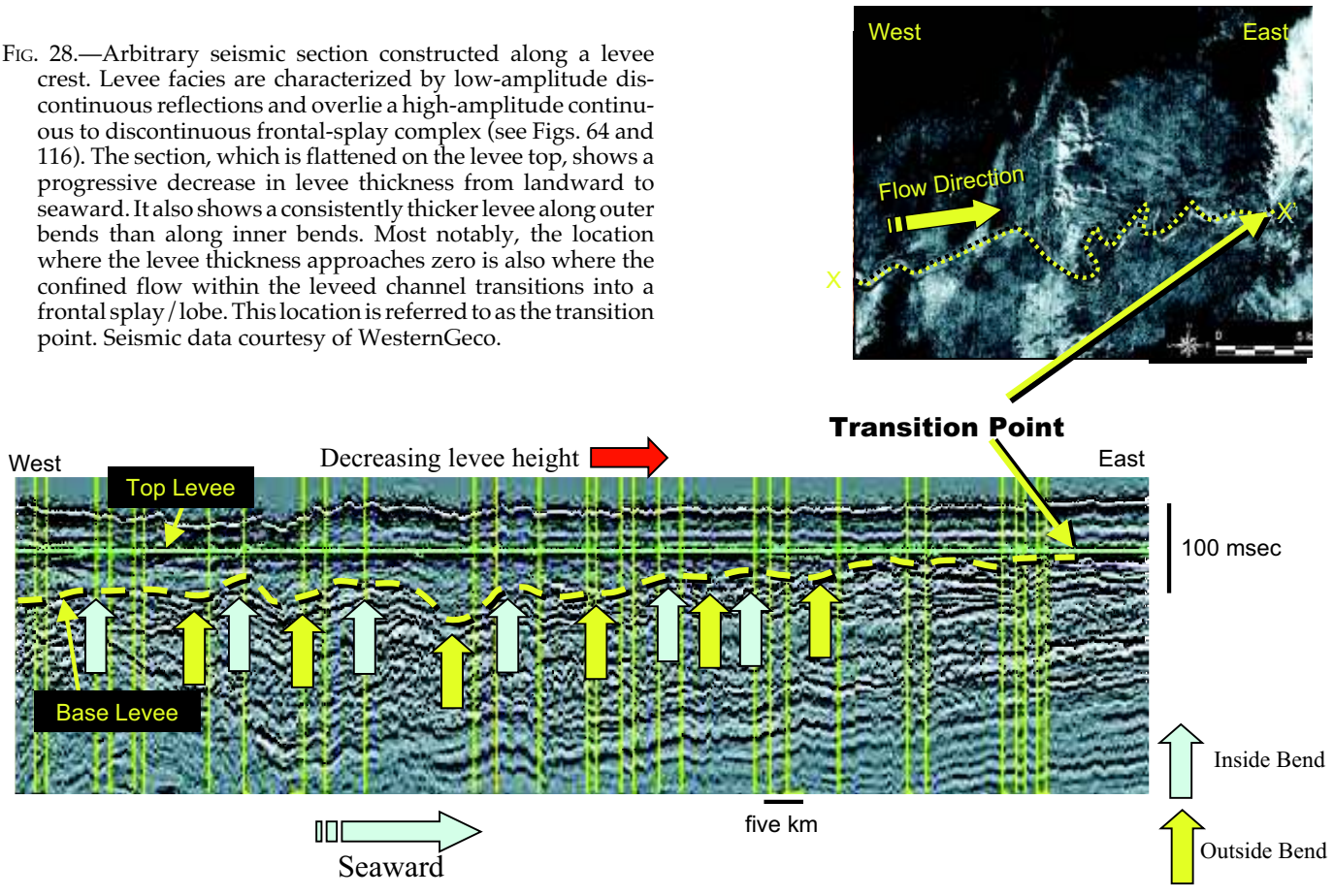

FIG. 28.—Arbitrary seismic section constructed along a levee crest. Levee facies are characterized by low-amplitude discontinuous reflections and overlie a high-amplitude continuous to discontinuous frontal-splay complex (see Figs. 64 and 116). The section, which is flattened on the levee top, shows a progressive decrease in levee thickness from landward to seaward. It also shows a consistently thicker levee along outer bends than along inner bends. Most notably, the location where the levee thickness approaches zero is also where the confined flow within the leveed channel transitions into a frontal splay / lobe. This location is referred to as the transition point. Seismic data courtesy of WesternGeco.

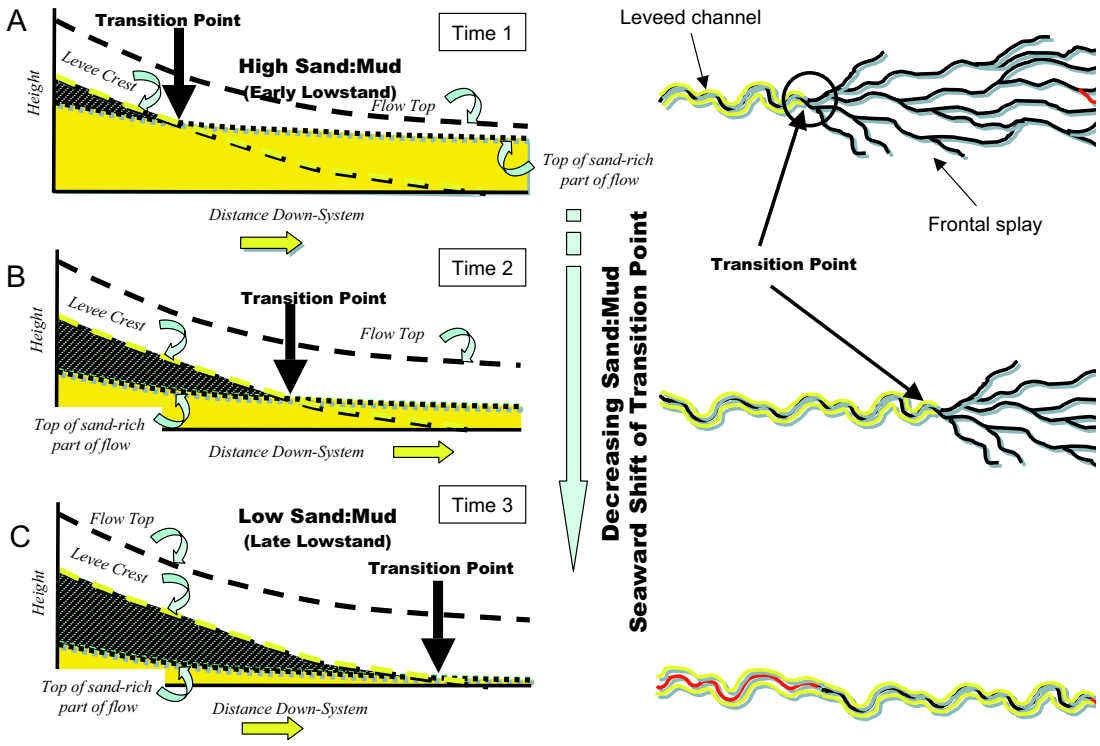

FIG. 29.—Shift of the transition point in response to differences in sand-to-mud ratio with sediment gravity flows. **A)** A high sand-to-mud ratio is associated with a transition point that is significantly farther landward than is the case with a lower sand-to-mud ratio **B, C)**.

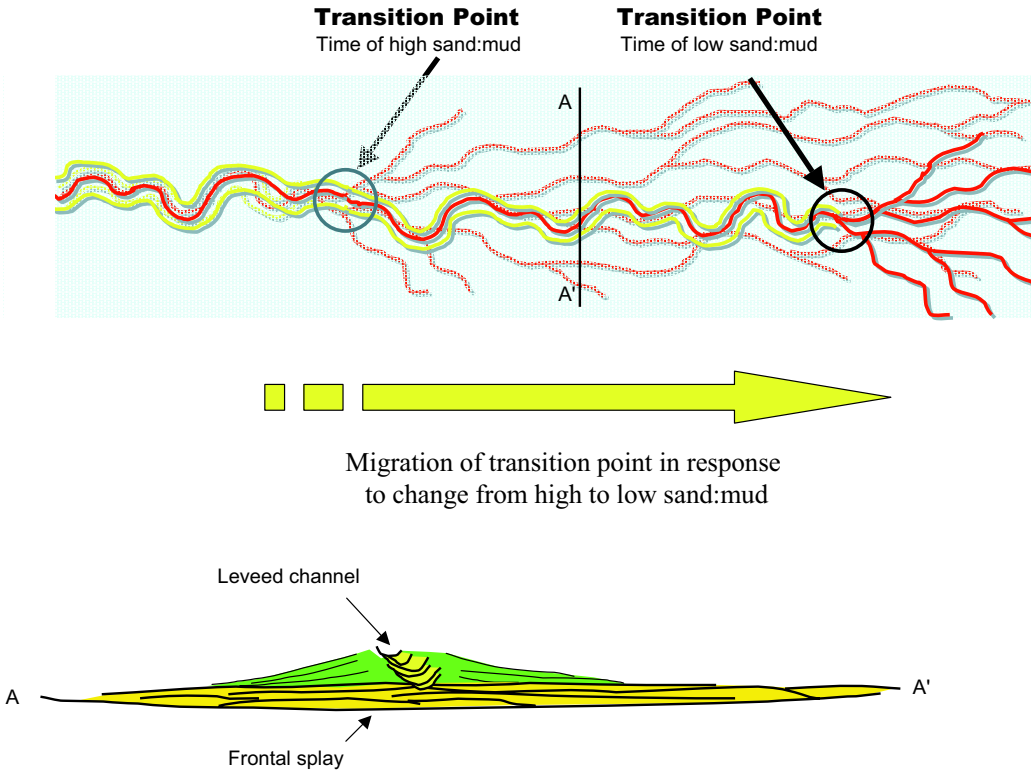

FIG. 30.—Superposition of leveed-channel system over a frontal splay/lobe, which would accompany a progressive muddying-up of successive sediment gravity flows (compare with Figs. 31, 74, 116, and 163).

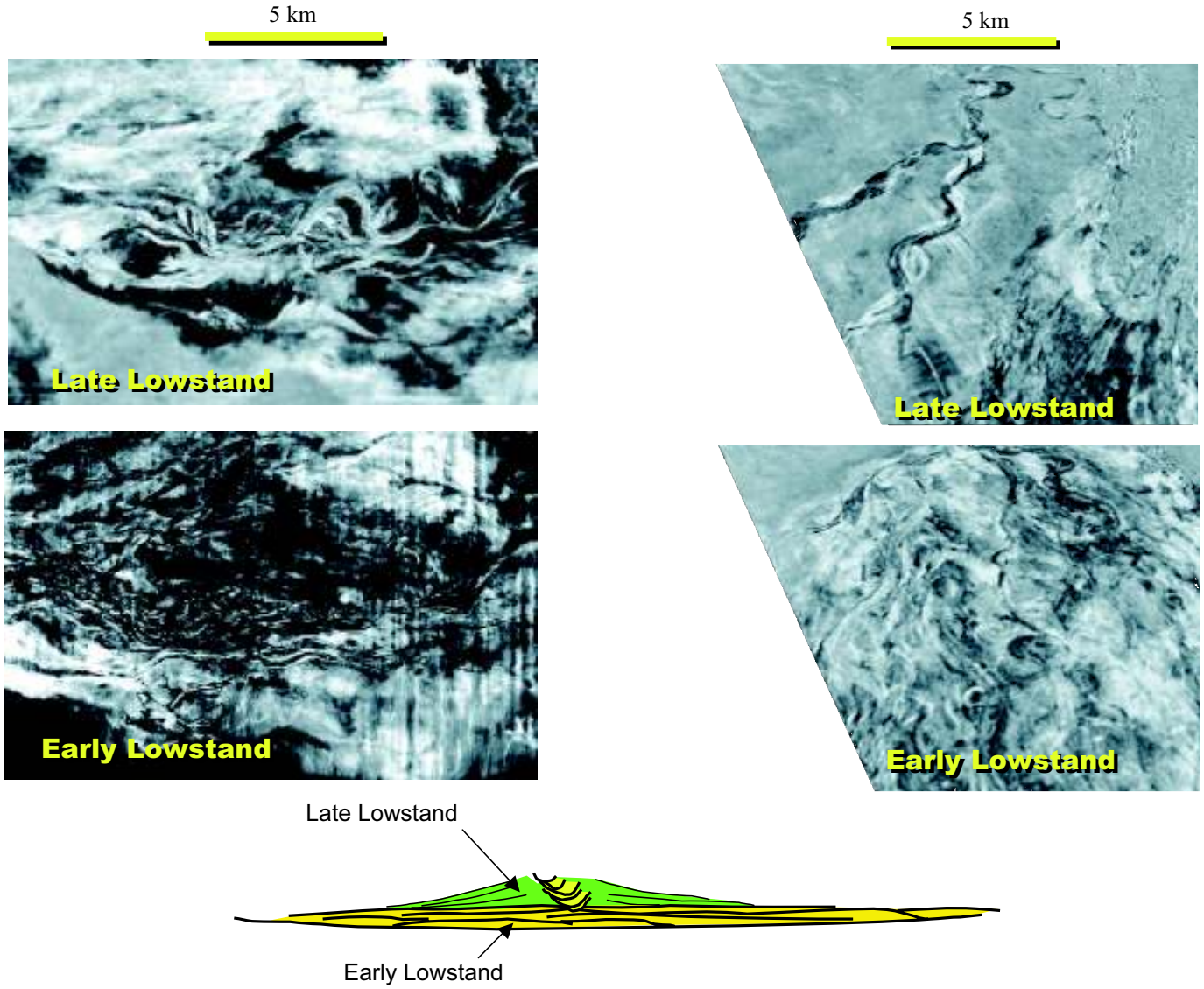

FIG. 31.—Two examples of the superposition of late lowstand leveed-channel deposits over early lowstand frontal-splay deposits (compare with Fig. 30). Seismic data courtesy of WesternGeco.

proximal basin to ever more distal basins through time. Within each intraslope basin, turbidite deposition comprises a succession from sheet-bedded deposits at the base to leveed-channel deposits near the top. Flows entering an intraslope basin would initially encounter markedly concave-up topography. This concave-up morphology results in a rapid deceleration of flow, which in turn favors deposition of sheet-like frontal splay deposits (Posamentier and Kolla, 2003a). As the basin gradually fills, the topography progressively becomes less concave up. The response is an upward transition from frontal splays to leveed channels. As a result, leveed-channel deposits tend to dominate the upper part of intraslope basin fill. This basin-fill evolution from frontal-splay dominated to leveed-channel dominated is an autocyclic phenomenon occurring in response to the evolution of local topography. Posamentier and Kolla (2003a) describe a matrix of possible outcomes associated with varying slope concavity and varying sand-to-mud ratio (Fig. 32A).

The effect of a slope to intraslope-basin transition is shown in Figure 32B and C. Flow vectors on the slope are directed primarily downslope parallel to flow. Upon encountering an intraslope basin, laterally directed flow vectors are significantly enhanced. This increases the likelihood of levee breaching and a resultant distributive channel pattern and deposition of a frontal splay.

Sea-floor rugosity associated with fault scarps or other abrupt changes in slope gradient can also have profound influence on turbidite deposition. In general, the farther a flow travels without any significant breaks in slope the more the sand grains tend to become concentrated towards the base of the flow and mud tends to concentrate towards the top. Thus grain-size sorting or segregation within the flow progressively improves down-system—the flow becomes better organized. The presence of an abrupt slope change in the path of the flow results in a perturbation (i.e., a hydraulic jump; Komar, 1971) within the flow and a consequent tendency for abrupt increased flow disorganization. This pertur-

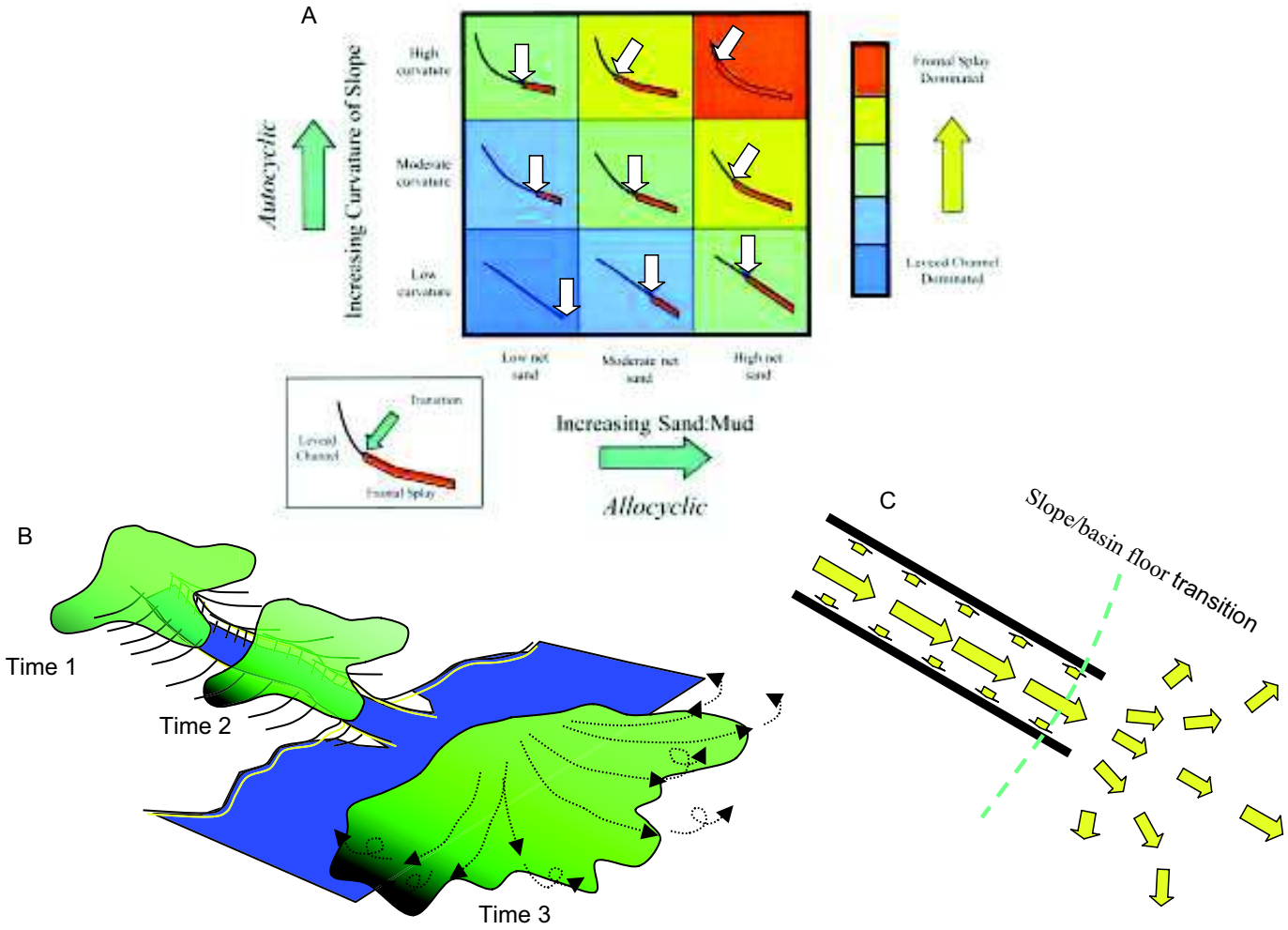

FIG. 32.—**A)** Matrix of possible responses of location of transition point to varying sand-to-mud ratio and varying slope curvature. Increased slope curvature, a local or autocyclic parameter, results in a landward shift of the transition point. Increased sand-to-mud ratio, an external or allocyclic parameter, has a similar effect (after Posamentier and Kolla, 2003a). **B)** Turbidity flow through a leveed channel onto a basin floor. **C)** Upon encountering the basin floor, laterally directed flow vectors are significantly and abruptly increased. This can result in deposition of a frontal splay on the basin floor. The degree to which a frontal splay forms at the transition from slope to basin floor is a function of the abruptness of the slope change at this location.

bation results in poorer grain-size sorting within the body of the flow down-system of the abrupt slope change. Consequently, settings such as the base of a fault scarp or an abrupt slope-to-basin transition can cause significant reorganization of flow. The result of this reorganization is the tendency for the system to change from relatively confined leveed channels to relatively unconfined frontal splays (Posamentier and Kolla, 2003a) as illustrated in Figure 33. The available relief from point of flow origin to the basin floor can also play an important role in determining the style of turbidite deposition. Assuming constant slope gradient, the greater the relief from shelf edge to basin floor, the longer the run of the turbidity flow, and therefore the greater the tendency for concentration of sand towards the flow base. This allows greater efficiency of levee construction and a greater likelihood for levees to extend across the basin floor. All else being equal, two flows of identical grain-size composition flowing down two slopes with different length (each characterized by the same gradient), one with relief of a few hundred meters and the other with relief of a few thousand meters, can be associated with a very different set of turbidite depositional elements on the associated basin floor. As illustrated in Figure 34A the flow that has reached the basin floor early in its run has not had the chance to become organized from a grain-size distribution perspective, hence the transition point is located significantly farther landward. The basin floor in this instance is characterized by a minimal leveed channel and a relatively widespread frontal splay or lobe. Where the flow has had a long run before reaching the basin floor (Fig. 34B) the flow is much better organized and the transition point lies farther across the basin floor.

DEPOSITIONAL ELEMENTS

The integration of facies description and process sedimentology leads to the identification of larger-scale depositional or architectural elements and their linkage into depositional systems and ultimately depositional sequences. Depositional elements in deep-water systems are of the order of ten to a few tens of meters in thickness, and may extend laterally for tens of meters

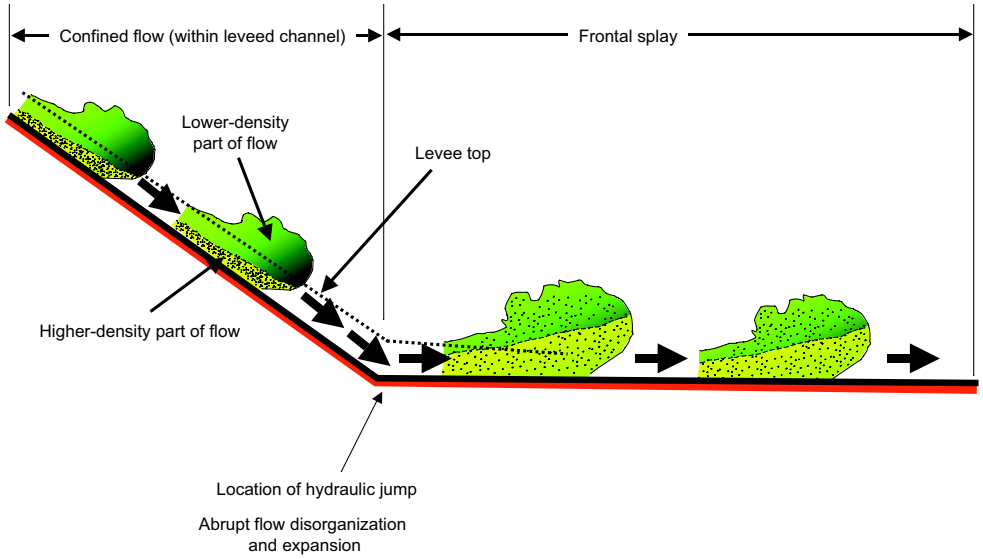

FIG. 33.—Schematic depiction of flow expansion that occurs at the base of slope where the change of gradient is abrupt. Flow on the slope is sufficiently well organized so that coarser-grained sediments are entrained in the flow base and are fully confined by levees. Once the flow strikes the abrupt change in gradient that is located at the base of slope, the flow abruptly becomes disorganized as it experiences a hydraulic jump. This abrupt increased disorganization causes a sudden increase in sand content within the upper part of the flow and results in a situation where the higher-density part of the flow lies above the levee crests and avulsions are likely to occur at this location. At this abrupt base-of-slope location, transition from leveed channel to frontal splay is likely (compare with Fig. 32B, C).

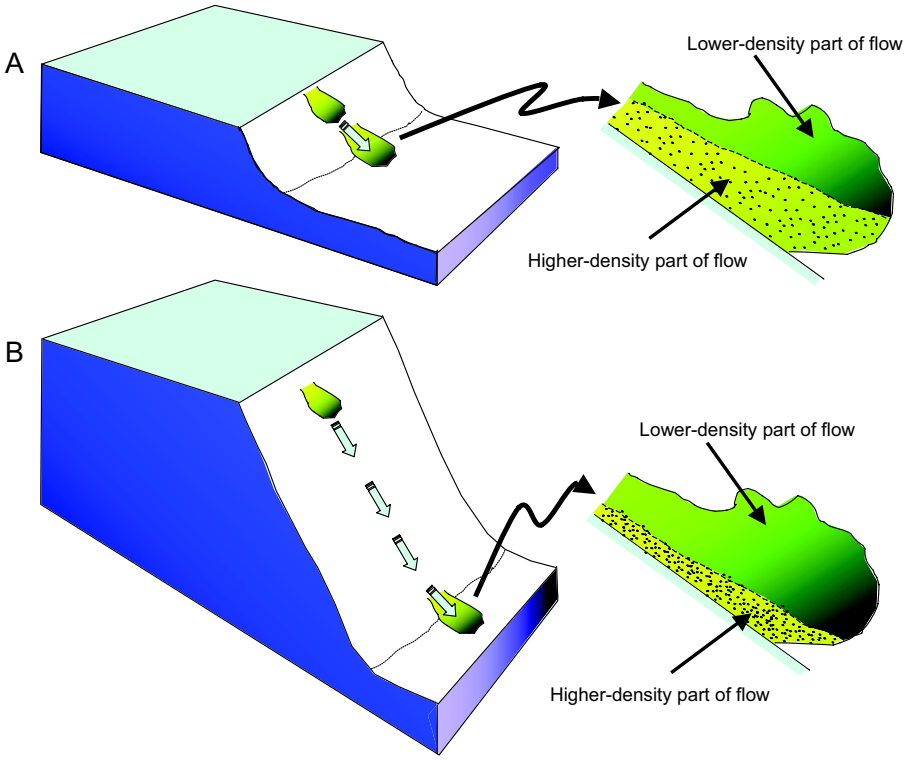

FIG. 34.—Schematic depiction of two similar sediment gravity flows at the point of initiation (i.e., similar sand-to-mud ratio, volume, etc.), but facing slopes of the same grade but significantly different length. The sediment gravity flow that faces the short slope **A)** has less distance available to it for sorting to occur than does the sediment gravity flow facing a long slope **B)**. The result is that, when the flow finally reaches the basin floor, the flow down the long slope is significantly better sorted, with coarser sediment more concentrated near the flow base, than the flow down the short slope, where poorer sorting results in sands much higher up in the flow.

up to tens of kilometers. The elements are defined by (1) their external geometries and (2) the internal facies within the elements. Our approach will follow that of Mutti and Normark (1991), and our analysis of depositional elements will integrate stratigraphic, geomorphologic, and facies observations, based on seismic, outcrop, and borehole data. Moreover, the relationships between depositional elements in time and space will be within the framework of process sedimentology. We will start with depositional elements that are observed in proximal settings—slope channels and canyons—and then move progressively farther seaward down the slope and across the basin floor, where we will examine leveed channels, overbank deposits (including sediment waves, crevasse splays, and planar levee deposits), frontal splays (i.e., lobes or distributary channel complexes), and debris-flow deposits (including debris-flow lobes, channels, and sheets). In each instance we will suggest, based on process sedimentology, what facies would be encountered in association with specific depositional elements.

Canyons and Slope Channels

Canyons and slope channels are the primary conduits for sediments to travel from the shelf-edge staging area, across the slope, and onto the basin floor. They can range in scale from a few meters in depth and width (these would be referred to as slope gullies) to ten or more kilometers wide and over a kilometer deep (submarine canyons). They tend to be largely erosional with significant incision into the substrate. In the context of this discussion, the distinction we draw between canyons and slope channels is that canyons consistently fully confine the flows that pass through them, whereas slope channels only partially confine the flows that pass through them (Fig. 35). The effect of partial confinement is that some spillover from the tops of the flows passing through slope channels occurs, resulting in the construction of levees on the flanks of the channel. Levee construction does not occur when the flows are fully confined, as they are with canyons (though some canyons contain smaller leveed channels within the confines of the canyon walls). Another distinction between canyons and slope channels is that, whereas both can be deepened by the passage of turbidity currents, canyons are more likely to widen by mass wasting on the canyon walls than are slope channels. In the distal reaches of canyons, as channel-wall relief diminishes, turbidity current height eventually exceeds the height of the canyon walls, and levees develop.

Canyons.—

An example of a canyon is shown in Figure 36. There is no evidence of levee construction on the flanks of the canyons, suggesting that flows were fully confined within this feature. The presence of sand within this canyon is largely at the base (Figs. 37–39), expressed as moderate- to high-sinuosity channel threads. These channel deposits can be fully to partially preserved, the latter illustrated by the segment of high-sinuosity channel deposits observed in the canyon terrace perched above the canyon floor (Fig. 37). The canyon fill is inferred to be overwhelmingly mud dominated, as evidenced by the seismic reflection character observed within the confines of the canyon Figs. 37, 40). The seismic reflection pattern of canyon fill commonly is characterized by moderate- to low-amplitude, discontinuous chaotic-contorted seismic reflections. This seismic reflection character commonly has been associated with mass-transport deposits such as associated with slides and debris flows (Posamentier and Kolla, 2003a). The morphology of the top of the canyon fill is characterized by linear flow lines (Fig. 36A, C), further evidence for the absence of turbulence in the flows responsible for at least the most recent phase of canyon fill (Posamentier and Kolla, 2003a). However, there can exist isolated threads of channel sands, characterized by high-amplitude, continuous to discontinuous seismic reflections at the canyon base or embedded within the canyon fill near the canyon base.

The fill of many canyons is commonly fine grained, and it is deposited after the canyon or channel has been abandoned. If abandonment is due to cutoff of sediment supply during relative sea-level rise, the fill may consist largely of slump and slide material from the canyon or slope channel walls with additional contribution of hemipelagic mud and silt that gradually settles over the area of the slope and in the canyon. The present-day Mississippi Canyon appears to have filled in this way (Goodwin and Prior, 1989). Consequently, it is likely that the preponderance of canyon filling occurs only after the axial turbidity-

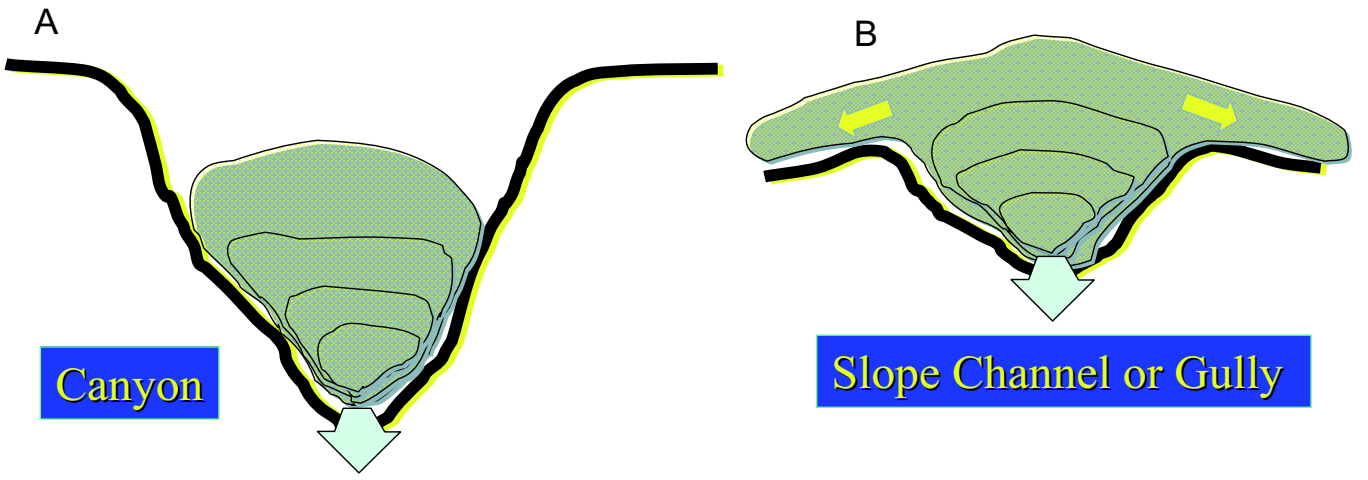

FIG. 35.—Schematic illustration showing section views across a canyon **A)** and slope channel or gully **B)**. Sediment gravity flows within canyons are fully confined by canyon walls. Consequently no levee deposits are observed outside the canyon. In contrast, sediment gravity flows within slope channels or gullies are not fully confined by channel walls so that levee deposits are observed outside the channels or gullies.

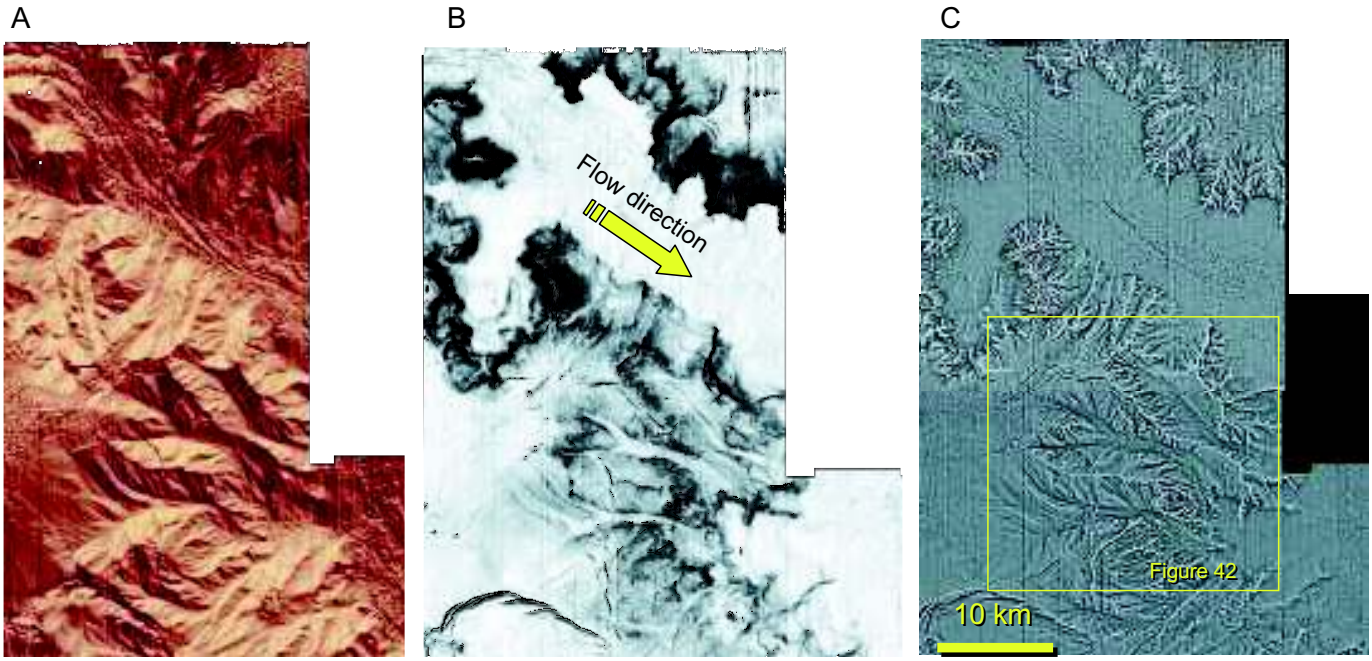

FIG. 36.—Seismic attributes of the modern sea floor in the vicinity of Mississippi Canyon, Gulf of Mexico; seaward is from upper left to lower right. **A)** seismic dip azimuth map—this map highlights the principal canyon as well as smaller tributary channels. The canyon floor is characterized by long linear grooves. The walls of the canyon are characterized by delicate tributary networks of small gullies. **B)** seismic dip magnitude—this attribute highlights the edges of the canyon floor as well as the edges of the tributary channels. **C)** seismic reflection curvature—this attribute highlights the drainage networks and drainage divides; it also clearly shows the arcuate nature of the canyon walls in places (compare with Fig. 42). Seismic data proprietary to PGS Marine Geophysical NSA.

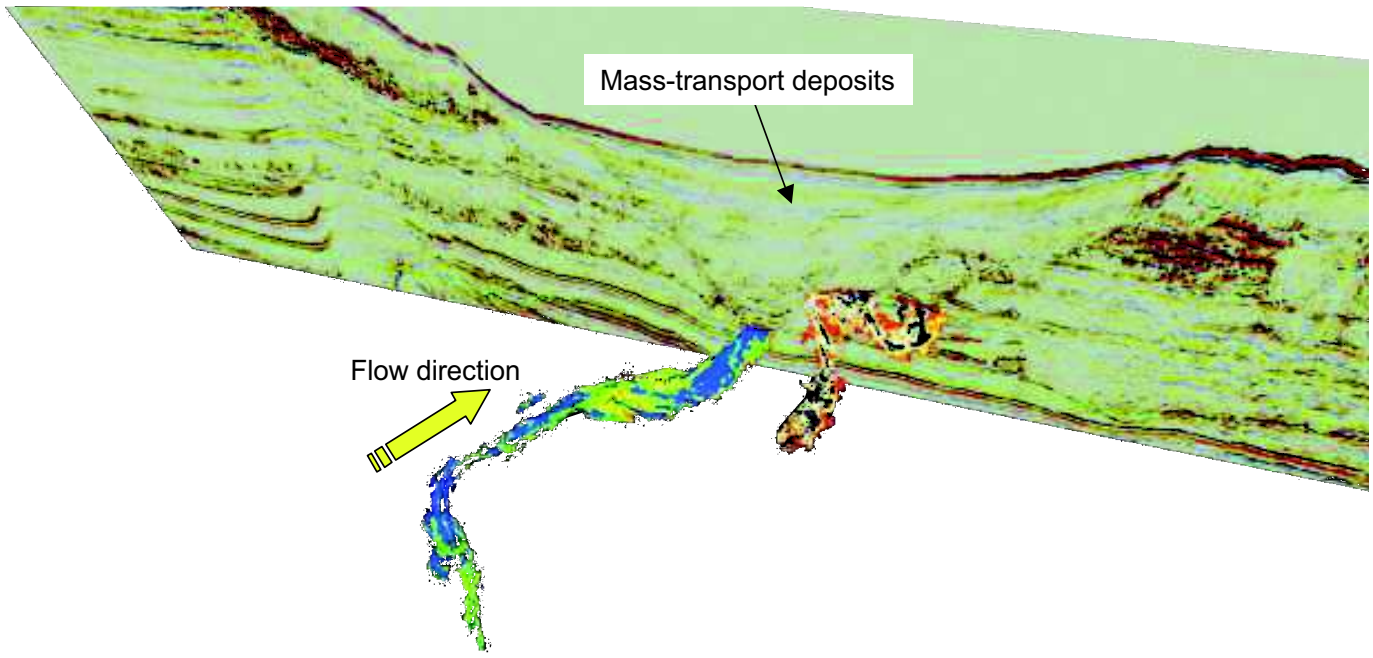

FIG. 37.—Seismic cross section through Mississippi canyon, with low-sinuosity to moderate-sinuosity turbidite channels at the canyon base. Note that the bulk of the canyon fill comprises mass-transport deposits. The axial channel shown here corresponds to the channel segment shown in Figure 38A. The sinuous channel on the flank of the canyon fill is only partially preserved. Seismic data proprietary to PGS Marine Geophysical NSA.

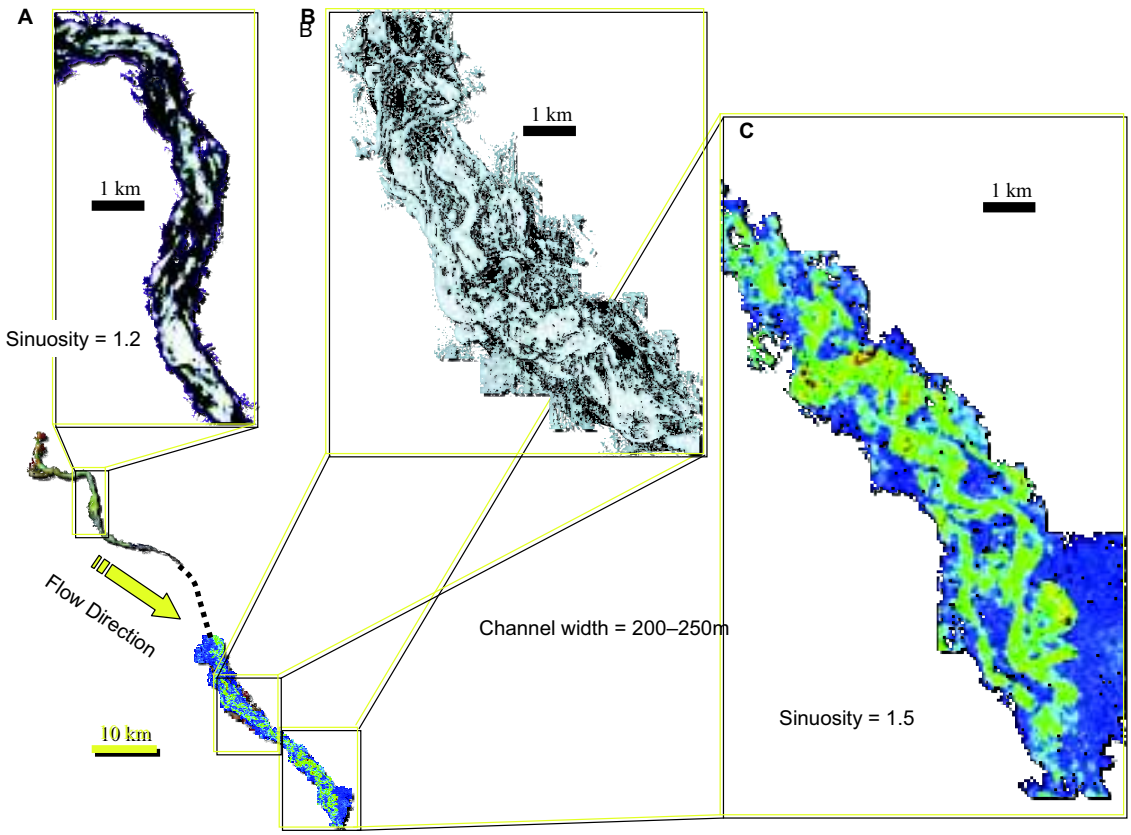

FIG. 38.—Seismic reflection amplitude images of the channel at the base of Mississippi canyon (compare with Figs. 37 and 39). Sinuosity ranges from 1.2 proximally to 1.5 distally. Seismic data proprietary to PGS Marine Geophysical NSA.

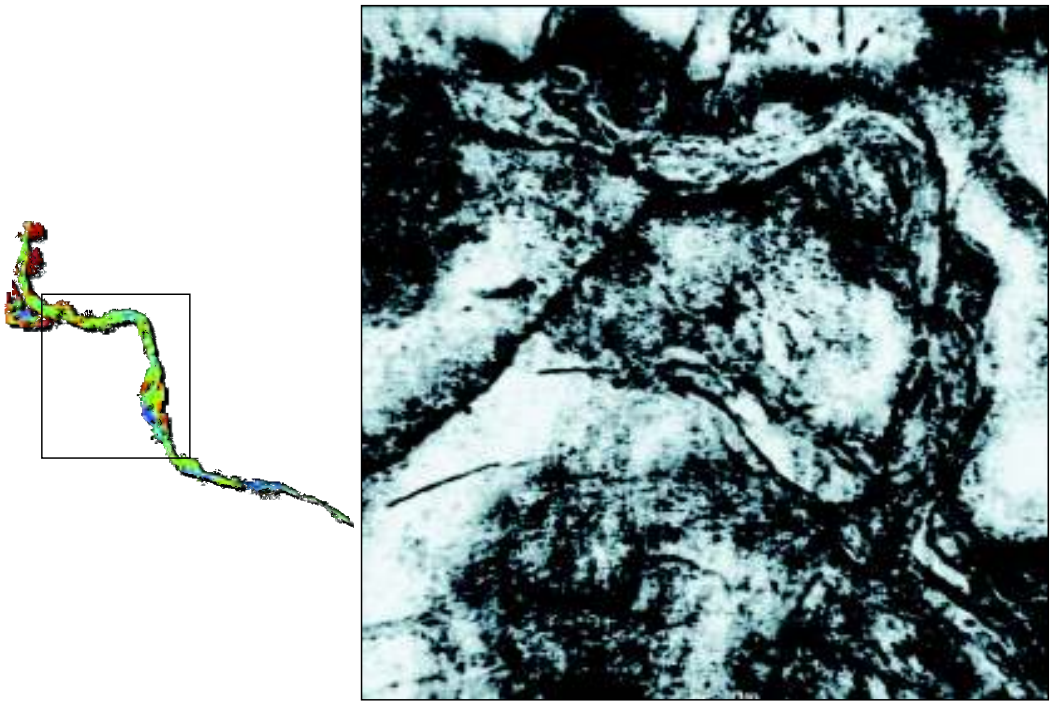

FIG. 39.—Coherence image of proximal Mississippi canyon channel. Note the discrete channel threads indicate meander loop expansion (i.e., swing) and down-system migration (i.e., sweep). Seismic data proprietary to PGS Marine Geophysical NSA.

current channels shut down. Once these "conveyer belts" cease to be active, any sloughing off the canyon walls remains within the confines of the canyon. Extensive slumping commonly characterizes the canyon walls (Figs. 40, 41). Thus, the bulk of canyon filling likely occurs as a result of mass wasting during rapid sea-level rises and subsequent highstands, thus making the fill predominantly part of the transgressive and highstand systems tracts.

Some canyon systems characterized by supply of very coarse-grained sediment can have extensive coarse-grained sediments deposited within canyons (e.g., Pigeon Point Formation, Lowe, 1979; Carmelo Formation, Clifton, 1981, 1984). This is most common in active continental-margin settings where deep-water turbidite systems are linked to short and steep fluvial drainage systems.

The facies that would most likely characterize the bulk of the canyon fill is that of a debrite, that is, a mud-dominated deposit with minimal internal organization. Convolute bedding associated with isolated cohesive blocks can be present in some instances. The isolated channel deposits (e.g., Fig. 37) observed within the canyon would be characterized by true turbidite facies, likely dominated by Bouma A and B units, with Bouma C, D, and E units commonly lacking preservation potential because of erosion by successive turbidity currents through the channel. These channels commonly are not associated with constructional levees, inasmuch as the canyon walls serve the purpose of confining the flows in their entirety, thus precluding the possibility of flow spillover and levee construction. In isolated instances, small channels within the middle to upper part of the canyon fill can have associated levees, all deposited within the confines of the canyon walls. This situation can develop when a turbidity flow travels across the relatively flat floor of a partially filled canyon. Essentially, this constitutes an underfit situation; the flows coming through the channel no longer "feel" the canyon walls, hence they form their own confining levees.

Some canyons can be completely mud filled and contain channels that have no associated sand deposits. This commonly occurs within tributary arms of larger canyon systems. Such tributaries may have formed as a result of retrogressive slumping on the canyon margin. The heads of these tributary systems do not apparently link up with shelfal fluvial systems; hence there is no significant sand input. These tributary systems commonly are characterized by small slope gullies or rills, feeding larger, commonly straight axial channels. A tributary arm of Mississippi Canyon, shown in Figure 42, is characterized by channels at the base but notably no associated high-amplitude seismic reflections, suggesting a complete absence of sand in the channels. Such features are thought to have formed by low-density, slow-moving turbidity currents originating along the crests of steep drainage divides.

Slope Channels.—

Sand-prone slope channels such as that shown in Figure 43 have been described in some detail by Hackbarth et al. (1994), Mayall and Stewart (2000), Kolla et al. (2001), and Posamentier (2003a). In contrast with the canyon previously discussed, this type of sediment conduit is associated with levee construction. Such levees can be observed high up on the slope at least to within 8 km of the shelf-edge staging area (Posamentier, 2003a). The channel thread at the base of the slope channel illustrated by Posamentier (2003a) is characterized by high-amplitude seismic reflections and a moderate- to high-sinuosity channel pattern that persists landward nearly to the toe of slope of a small shelf-edge delta, which itself is laterally confined to the head of the slope channel (Fig. 44). The presence of channel sinuosity nearly to the slope channel head suggests the presence of turbulent flow at least this high up on the slope, if not all the way to the shelf–slope break. Further, a time slice through the upper slope and outer shelf reveals a protuberance of the shelf edge precisely where the slope channel is located (Fig. 45). The associa-

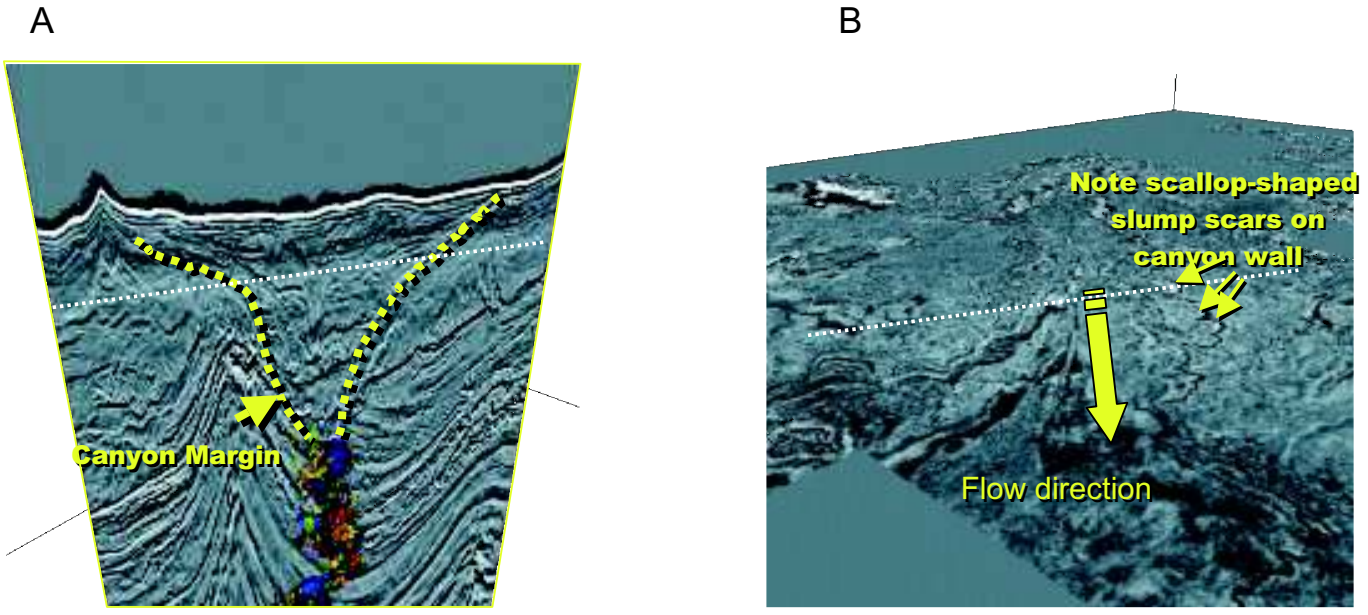

FIG. 40.—**A)** Transverse profile through Mississippi Canyon illustrating canyon cut as well as sand-prone channel fill at base of canyon. Dotted line indicates location of time slice shown in B. **B)** Time slice through Mississippi Canyon illustrating arcuate walls indicative of extensive slumping along canyon walls. Dotted line indicates location of time slice shown in A. Data proprietary to PGS Marine Geophysical NSA.

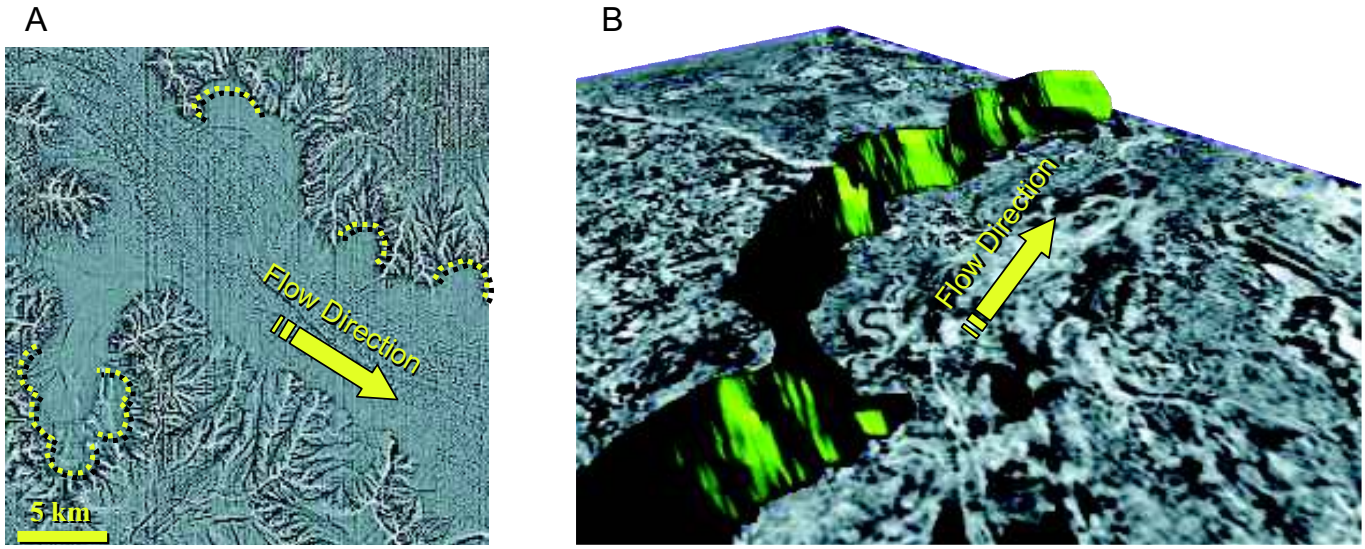

FIG. 41.—**A)** Curvature map of modern sea floor over Mississippi Canyon characterized by arcuate walls indicative of extensive slumping. **B)** Time slice across Mississippi Canyon and 3D perspective view of interpreted arcuate wall of the canyon. Data proprietary to PGS Marine Geophysical NSA

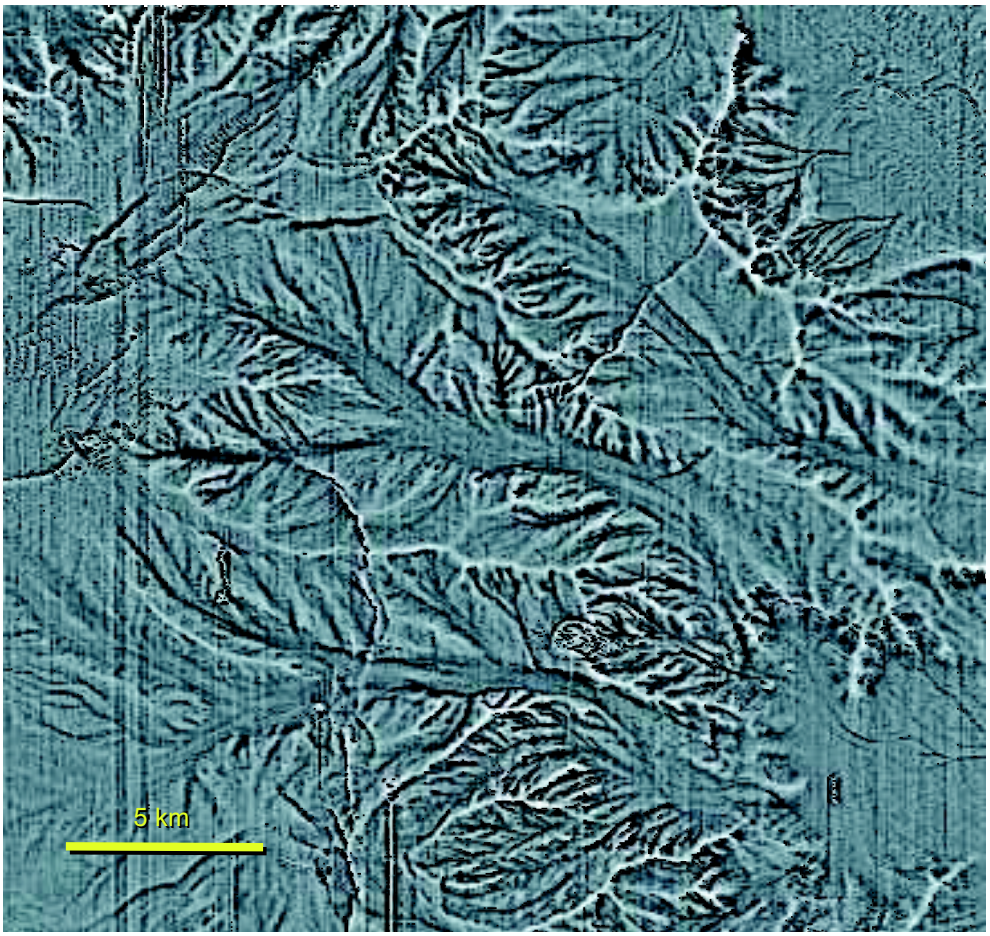

FIG. 42.—Seismic reflection curvature of the sea floor along southwestern side of Mississippi Canyon, Gulf of Mexico (detail of Fig. 36). Three larger channels up to one kilometer wide, as well as numerous smaller gullies and rills, are shown. Note that many of the smaller gullies and rills originate along knife-edge drainage divides. Seismic data proprietary to PGS Marine Geophysical NSA.

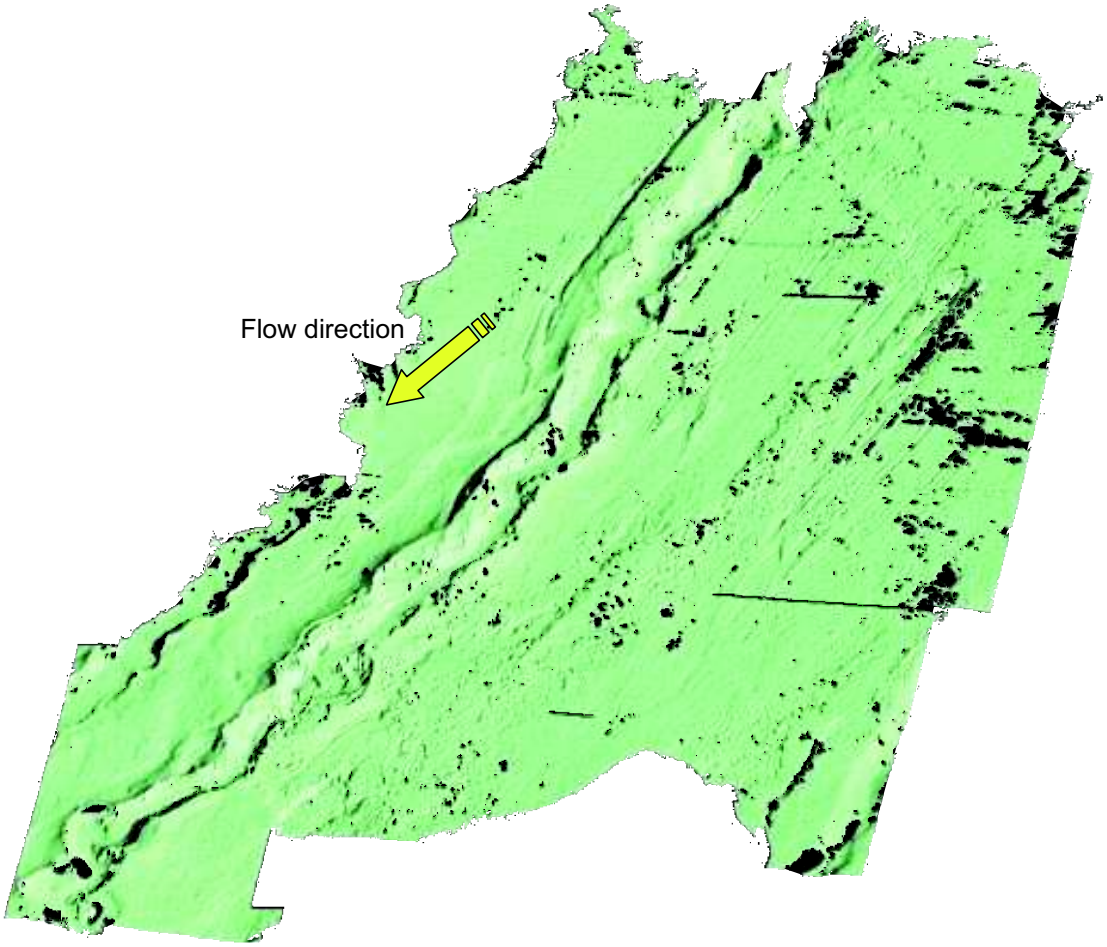

FIG. 43.—3D perspective illumination of the Einstein Channel on the upper slope of the Desoto Canyon area, eastern Gulf of Mexico. Note the presence of levees external to this channel as well as the sinuous nature of the channel pattern. The channel is approximately 1.5 km wide, from levee crest to levee crest. Seismic data courtesy of VeritasDGC.

tion of a shelf-edge protuberance or delta with the slope channel suggests a genetic link between shelf fluvial and distributary-channel sediment delivery systems and the presence of turbidite deposits on the slope. One can infer from this close connection between the fluvial distributary channels and the meandering threads within the slope channel that the turbidity currents which came through the slope channel may have originated as density underflows (i.e., hyperpycnal flows) sourced by river-borne sediments. Such processes likely would have been active for days or weeks at a time, while the river was in flood. Direct links between fluvial distributary channels and canyon systems is also common. Most well-developed canyons are associated with major river systems on the shelf (e.g., the Hudson canyon, the Congo canyon, and the Mississippi canyon) (Posamentier and Allen, 1999).

Slope channels commonly contain sand-prone facies at or near the base of the conduit. Mayall and Stewart (2000) document examples and propose a model for slope channel fill that contains debris-flow deposits at the base overlain by amalgamated turbidites. The fill culminates with late-stage, isolated underfit leveed channels associated with diminishing flow discharge, located within the master slope-channel walls. Other examples of complex slope channel fill are documented in Kolla et al. (2001), Sikkima and Wojcik (2000), and Abreu et al. (2003). The amalgamated sandy facies are characterized predominantly by Bouma A and B turbidites, whereas the underfit late-stage channels are characterized by Bouma A to D turbidites. Climbing current ripples can be observed most commonly within the levees associated with the late-stage underfit channels.

Examples of Coarse-Grained Canyon Fills.—

In unusual cases, the upper parts of large canyons may contain significant quantities of sand. Two examples have been reported from the Atlantic margin of Brazil, in studies based on closely spaced log and core control. The sand-prone fill of a large slope channel (canyon?) has been documented in the Carapeba–Pargo system on the Atlantic margin offshore Brazil (Fig. 46; Bruhn and Walker, 1995), where a large slope channel can be traced for at least 150 km. Turbidites have been studied in the Carapeba and Pargo oilfields, which lie about 90 km down-canyon from the updip erosional edge of Cretaceous rocks. The slope-channel width is of the order of a few kilometers, the precise width of the channel being hard to determine because younger turbidites spread more and more widely over the upper parts of the slope-channel margins. The thickness of the fill is

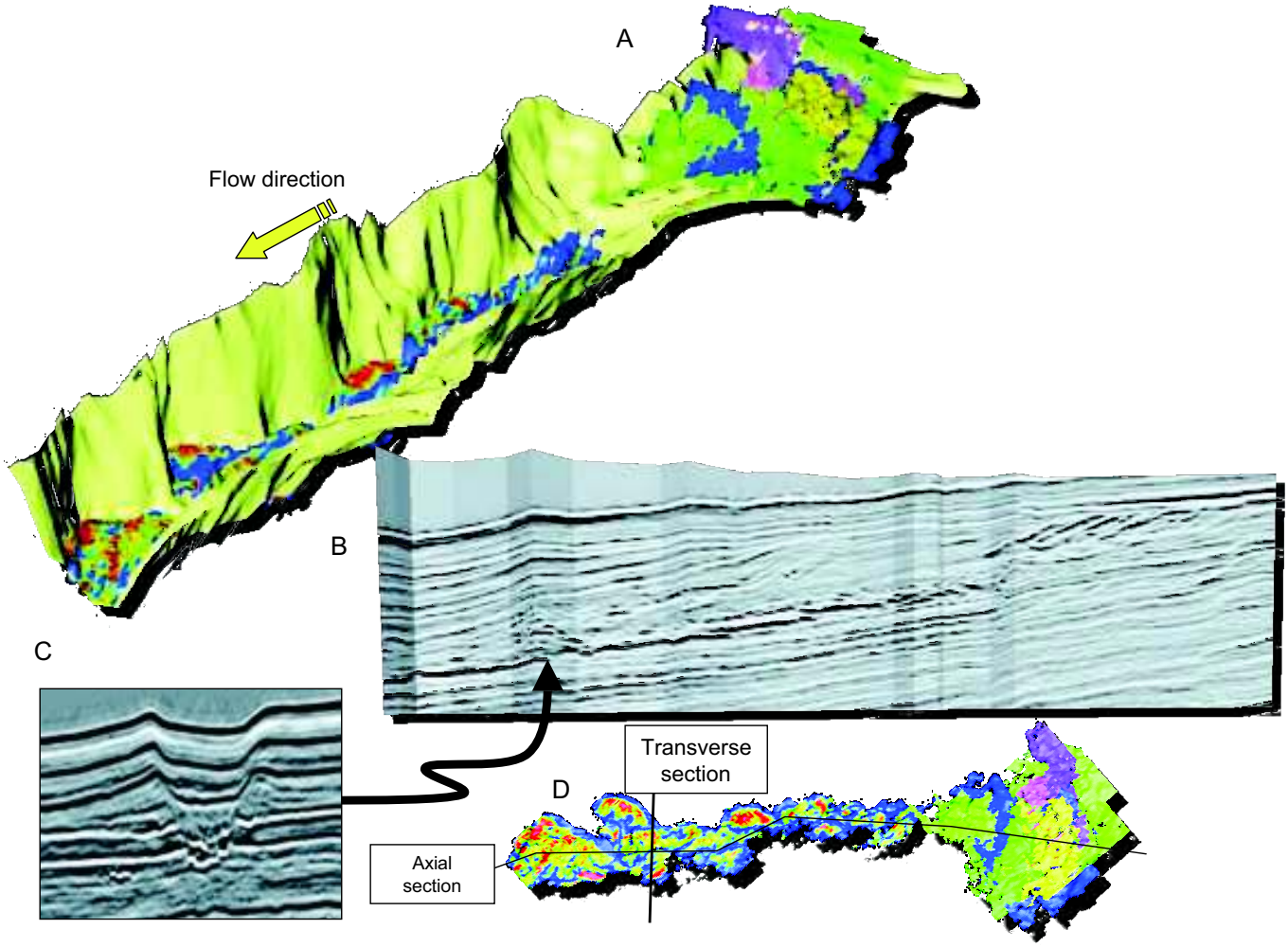

FIG. 44.—**A)** 3D perspective view of the Einstein channel (approximately 2 km wide) with associated sand-prone channel fill at the base and shelf-edge delta at the slope-channel head. Each delta-front shingle is shown in a different color. **B)** Axial section through the Einstein slope channel illustrating the shingled nature of the slope-channel-head delta as well as the high reflection amplitude of both the delta as well as the channel fill at the base of the slope channel. **C)** Transverse section through the Einstein channel illustrating high-amplitude sand-prone deposits at base of channel. **D)** Seismic reflection amplitude of the deposits at the base of the slope channel illustrating the presence of sinuous narrow channel threads, characterized by down-system migration of meander loops. Seismic data courtesy of VeritasDGC.

about 260 m (Turonian) plus 24 m (Maastrichtian). The turbidites within the slope channel form eight thinning- and fining-upward successions. Individual beds at the bases of the successions can be up to 12 m thick and consist of granule sandstones with scattered pebbles (Fig. 47; the pebbly sandstone facies described earlier in this paper). The successions are 27 to 140 m thick and can be mapped as tabular or linguoid sandbodies 1 to 12 km wide in which the younger turbidites become finer grained, thinner bedded, and more discontinuous upsection and downcanyon. The successions are stacked in an overall retrogradational back-stepping pattern for at least 20 km, recording the fill of the slope channel.

The slope-channel morphology can be traced at least 60 km downslope from Carapeba (Fig. 46), thus defining the depositional site at Carapeba and Pargo as within the slope channel. The depositional elements consist of the thinning- and fining-upward successions, which appear to spread with a sheet-like geometry from wall to wall (Bruhn and Walker, 1995, their Figs. 5 and 6). A hypothetical continuous outcrop of this canyon fill, 200 m thick and covering one km^2, would be almost impossible to interpret as a canyon fill—the only suggestion of channelization might be the very thick beds and the coarse grain sizes.

The second example of canyon filling is also from the Atlantic margin of Brazil, in Regencia Canyon (Bruhn and Walker, 1997). The canyon can be mapped near the mouth of the Doce River (Fig. 48) and is up to 6 km wide. It can be mapped for at least 15 km, and the fill is up to 1 km thick. Lagoa Parda field is about 2.8 km long and 2.5 km wide, and it has 70 wells with an average spacing of 200–250 m. Seven wells are cored, with a total of 324 m of core. Because of this unusually good control, individual beds can be traced from well to well; where beds or groups of beds can no longer be correlated, channel margins can be defined (detailed correlations are shown by Bruhn and Walker, 1997, their fig. 13, and a schematic correlation diagram is shown here in Fig. 49). The thirty-eight channels so defined are 210 to more than 1050 m wide and over 1 km long. The channel fills range in thickness from 9 m to more than

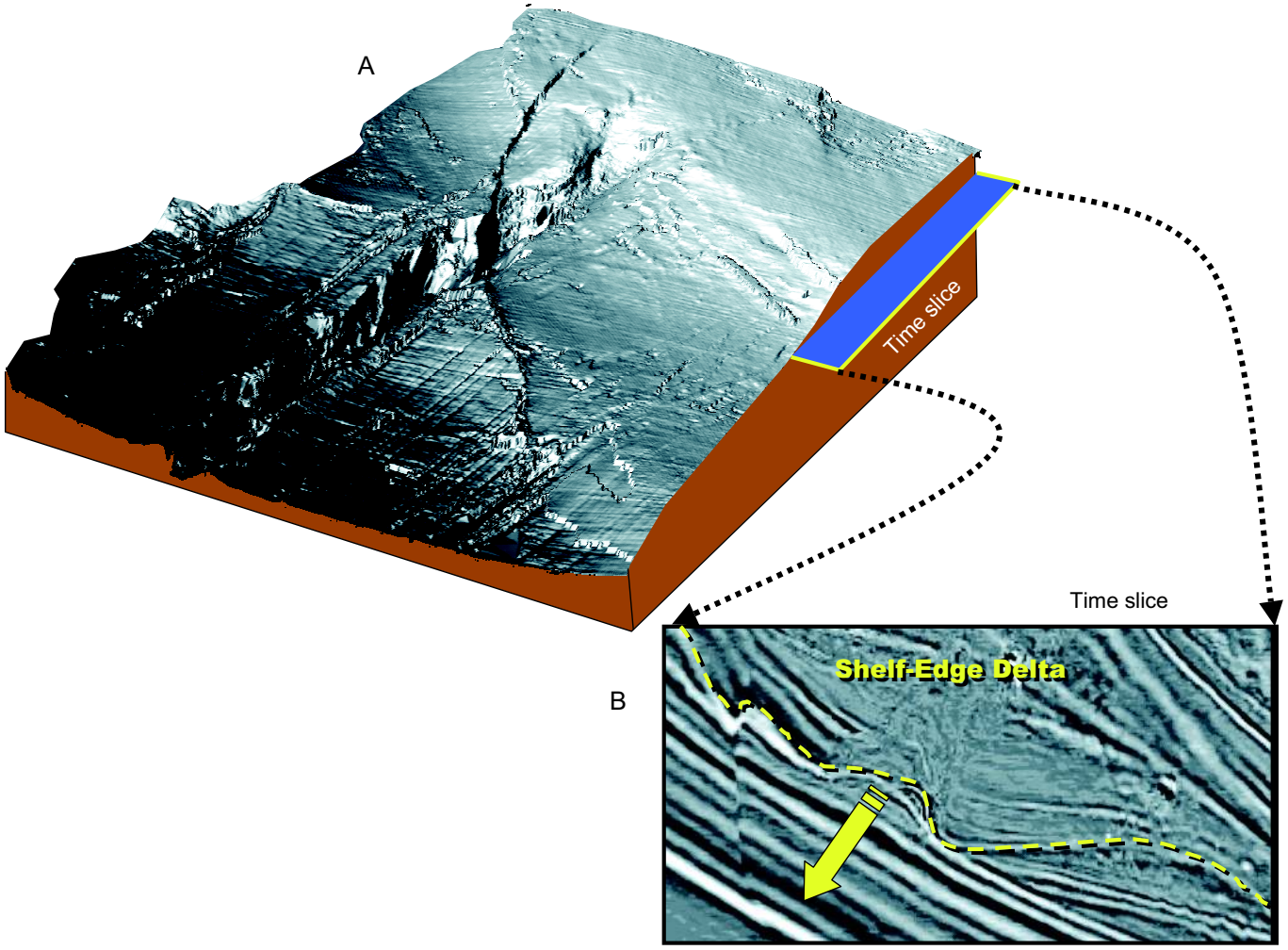

FIG. 45.—**A)** Perspective view of Einstein channel and associated shelf edge, Gulf of Mexico, from 3D seismic data. The surface shown lies at the base of the channel levees and is Late Pleistocene in age. **B)** Time slice through the upper part of the section reveals a protuberance of the shelf edge corresponding to a shelf-edge delta (compare with Fig. 57). Note that this protuberance corresponds precisely to the location of the Einstein slope channel. Seismic data courtesy of VeritasDGC.

50 m. Relationships of channels and their stacking patterns are shown in Bruhn and Walker (1997, their figs. 14, 15, and 16).

Channel fills comprise bouldery to pebbly conglomerates in normally graded beds up to 6.4 m thick, along with graded sandstone beds up to 3.8 m thick. Finer-grained facies include bioturbated mudstones and thin-bedded sandstones, and monotonous dark gray mudstones. Detailed correlations show that these finer-grained facies are deposited as the levees of channels filled with the coarser facies.

The channels can be grouped into three channel complexes (CC), colored orange (channels 1–11), yellow (13–35), and red (36–38) in Figure 49. Overall, the channel fills become narrower, thinner, and finer grained from CC 1 (orange) to CC 3 (red). Channel complexes 1 and 2 are deeply incised. Channel orientations in CC1 suggest flows from smaller tributaries along the northwest margin of Regencia Canyon (Fig. 48), and there are no levee facies associated with the CC1 channels. Orientations in CC2 suggest flows generally from west to east along the axis of the canyon. Levees are associated with channels 19–35 (Fig. 48). Slopes on the levees are up to 10 degrees, with slopes facing the channels generally being steeper than slopes facing away from the channels. Levees are also steeper on the left sides of the levees (Coriolis effect in the southern hemisphere). In CC3, channel orientations again suggest flow from the northwest margin of Regencia Canyon, and asymmetrical levee growth appears to have influenced channel switching (details in Bruhn and Walker, 1997). Channels are only 230–280 m wide, with fills 13–15 m thick.

Two main points emerge from this study. First, it is clear that turbidity currents can deposit coarse sediment within canyon heads, where the distance between flow initiation and sediment deposition is only a few kilometers. Deposition may be strongly influenced by the abrupt flattening of the gradient from canyon margin to canyon floor, particularly in CC1 and CC3. Second, it is clear that small (10–20 m deep, 200–300 m wide) leveed channels can develop within canyon heads—this makes the interpretation of some limited outcrops very difficult. Specifically, the channels at San Clemente, California (described below), have coarse fills, muddy channel walls, and multiple incisions. They have previously been described as mid-fan channels (Walker (1975b), but this interpretation is revised below, partly in the light

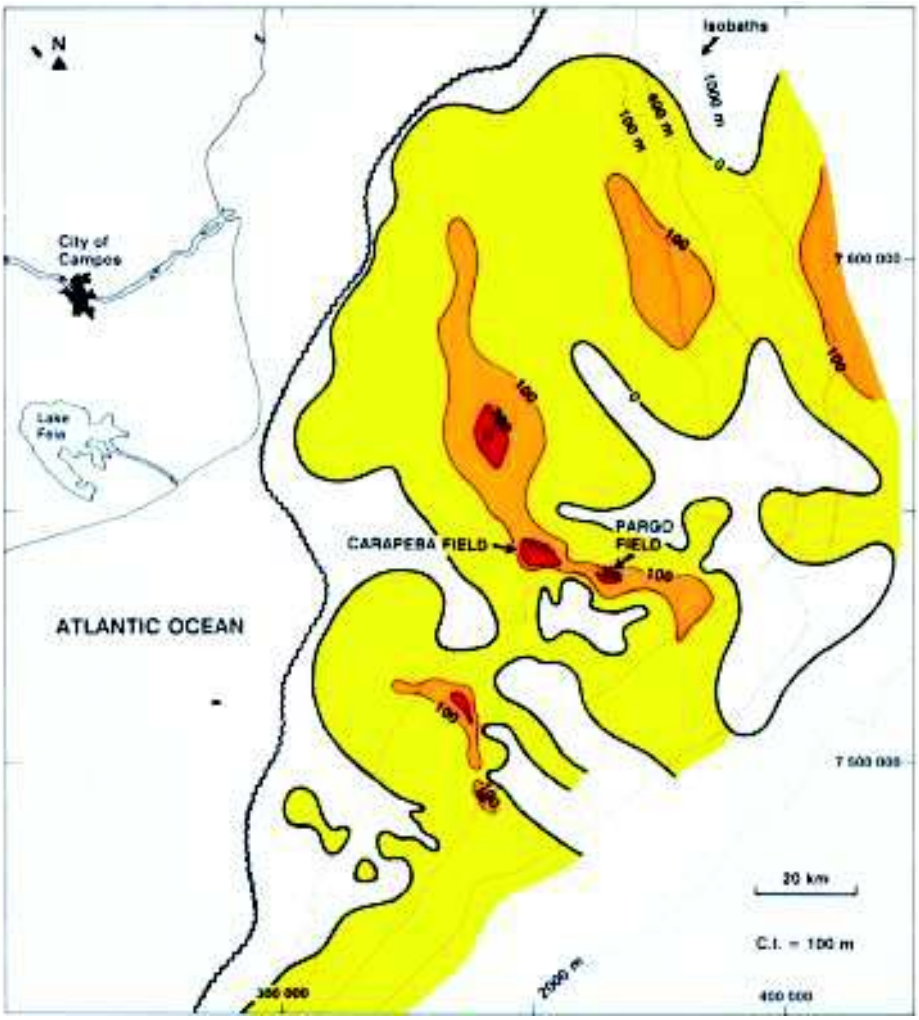

FIG. 46.—Location map of Carapeba and Pargo fields, offshore Brazil. Note Brazilian coastline and city of Campos. Long serrated line shows limit of occurrence of Upper Cretaceous rocks (after Bruhn and Walker, 1995).

of a resemblance between the San Clemente channels and the CC3 channels of Lagoa Parda. The general point to emphasize is that, unless an ancient example can be fairly positively identified, it cannot be used to construct general facies models—using the data from San Clemente without being sure of its setting (canyon head or basin floor) could lead to distorted syntheses of data during modern–ancient comparisons and facies modeling.

Example of Slope-Channel Fill, San Clemente, California.—

A candidate for a slope-channel fill is observed in the Capistrano Formation (Upper Miocene) at San Clemente, California (Fig. 50; Walker, 1975b; Campion et al., 2000; Camacho et al., 2002). The channel complex cuts into mudstones containing some beds of chert (similar to beds in the Monterey Chert). Bedding is generally horizontal in these mudstones, but some beds are broken by small soft-sediment faults suggesting movement on a slope—thus the beds outside the channel may be slope deposits.

Within the channel complex, beds are very well exposed. They are also horizontal, and the channel complex can be traced for over 500 m (Fig. 51). The Upper Miocene part of the cliff is 20 m thick, with indications that the nested channels may be as much as 40 m thick (Walker, 1975b). In addition to horizontal beds, there are eight prominent inclined surfaces, seven of which are draped with mudstone (Fig. 51). The surfaces have dips ranging from 5 to 18 degrees, and the mudstone drapes vary from 30 cm to 2 m in thickness.

The interpretation of the San Clemente section is that it comprises a series of nested channels, separated by dipping mud-draped surfaces. There were no outcrop indications that the channels might be sinuous, although excavations of channel walls suggested that the strikes of the walls varied from 230 to 300 degrees (Walker, 1975b).

The fill of the channels consists of interbedded sandstones and mudstones. The grain size is up to coarse sand, with many beds containing scattered granules and pebbles. Sandstone bed thickness is variable; in some of the channels it is typically a few tens of centimeters (Fig. 52), whereas in other channels beds can be almost 1 m or thicker (Fig. 53). The thicker beds tend to be amalgamated, without mudstone layers (Fig. 54). Amalgamation surfaces are characterized by grain-size changes and bedding irregularities that suggest loading of the upper sandstone into the lower one (Fig. 54).

FIG. 47.—Core photo of pebbly sandstone, Carapeba Field. Core sleeves are 1 m long, top to left. The core shows one pebbly sandstone bed, with prominent fluid-escape features in the uppermost two core sleeves.

The finer layers between the sandstones consist of gray siltstones and mudstones with abundant bioturbation. On the inclined mudstone drapes, gray silty mudstones are irregularly interbedded with very fine-grained brown claystones (Fig. 55). The different fine-grained facies were not examined micropaleontologically, but commonly in Tertiary turbidites in California the gray silty mudstones contain transported shallow-water foraminifera whereas the brown claystones contain deeper-water benthonic foraminifera. It therefore is assumed that the inclined mudstone drapes consist of silt and mud introduced by turbidity currents (the gray layers), as well as hemipelagic brown claystones deposited between turbidity currents.

These relationships are particularly well displayed in channel 6 (Fig. 56). The lower three beds pinch out rapidly toward the channel margin. In the case of the lower two beds, thin sandy layers a few millimeters thick continue up the channel margin and eventually disappear. It appears that the turbidity currents transported sand close to the bed, and that silt and mud (with very thin sand layers) was draped higher up over the channel margin. Note also that potential reservoir rocks in the channel pinch out laterally against the channel margin within a few meters.

The suggestion of soft-sediment disturbance in the beds outside the channel complex, and the proven occurrence of small leveed channels within larger incisions (Lagoa Parda, Brazil; Bruhn and Walker, 1997), suggests that the Capistrano Formation at San Clemente can be interpreted as a slope-channel fill.

3D Seismic Examples.—

In contrast with outcrop data, good-quality 3D seismic data can afford a comprehensive view of depositional elements and their relationship to each other, though, of course, ground-truth calibration may be lacking. In a well-documented example from the eastern Gulf of Mexico, Posamentier (2003a) illustrates the evolution of a linked shelf-edge delta and slope channel. The shelf and slope environment became an active depocenter likely in response to sea-level lowering and associated forced regression resulting in a seaward shift of the depocenter across the shelf and to the shelf edge. Once the depocenter reached the shelf edge a lowstand shelf-edge delta formed. This lowstand delta, shown in axial view in Figure 57, is characterized first by successive downstepping of the delta plain, likely associated with falling sea level (i.e., the early lowstand systems tract of Posamentier and Allen, 1999, or the falling stage systems tract of Plint and Nummedal, 1998), and later aggradation of the delta plain, likely associated with rising relative sea level (i.e., the late lowstand systems tract of Posamentier and Allen, 1999, or simply the lowstand systems tract of Plint and Nummedal, 1998). Numerous small slope channels or gullies are observed on the surface that marks the base of this lowstand delta complex (Posamentier, 2003a) (Fig. 58). These slope gullies are not uniformly distributed along the entire breadth of the slope shown, but rather tend to cluster in one area. The area where the gullies are clustered directly coincides with the location of the shelf-edge protuberance, suggesting a genetic link between deltaic distributary channels and downdip slope gullies (Posamentier, 2003a). These slope gullies are observed only at the base of the lowstand delta complex; within and to the top of the delta a single larger slope channel can be observed (Figs. 43, 44). This larger slope channel seems to have captured most of the flow from the shelf systems at the expense of the numerous smaller slope gullies that originally were present and seems to represent the culmination of an evolution from many slope gullies to a single slope channel within a single depositional sequence.

Basin-Floor Leveed Channels

Basin-floor leveed channels commonly are genetically linked with canyons or slope channels. Examples of basin-floor leveed channels are illustrated in Figures 59 and 60 and are described by Posamentier et al. (2000), Peakall et al. (2000), and Posamentier (2003b). Aggradation of channel-fill deposits can occur both on the basin floor (Fig. 61) and on the slope. The Joshua channel, described by Posamentier (2003b), built a channel ridge that stands c. 65 m above the adjacent basin floor. Likewise, the channel shown in Figure 61 stands c. 90 m above its adjacent basin floor. Sinuosity can be variable, from segments that are nearly straight to segments that can display sinuosity of up to 3.0.

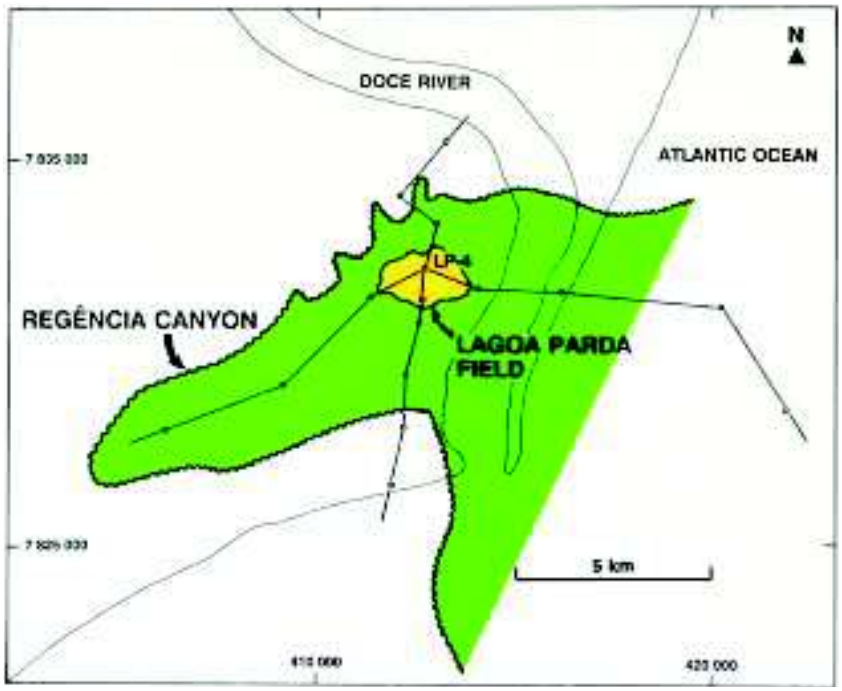

FIG. 48.—Location map of Regencia Canyon, State of Espirito Santo, Brazil. The canyon head is just onshore, close to the present day Doce River mouth, 550 km northeast of Rio de Janeiro.

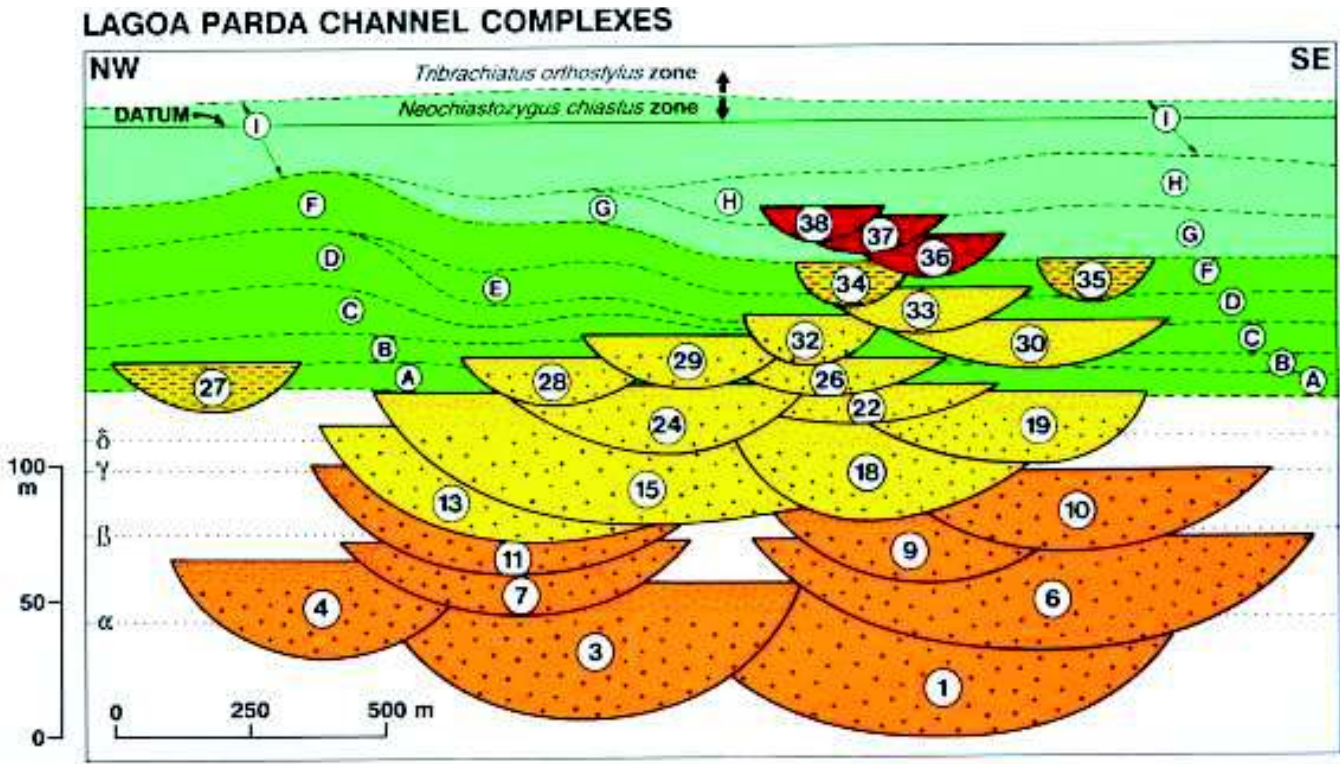

FIG. 49.—Diagram of channels within the Lagoa Parda field, Regencia canyon head. Orange—channel fills of unstratified bouldery to pebbly conglomerate and very coarse-grained sandstone. Yellow and red—unstratified coarse-grained sandstone and parallel stratified medium-grained sandstone. Green—interbedded bioturbated mudstones and thin-bedded sandstones, interpreted as levee facies. Note decrease in channel size and grain size upward. Lower channels do not have levees, but channel horizons 26 and higher have associated levees.

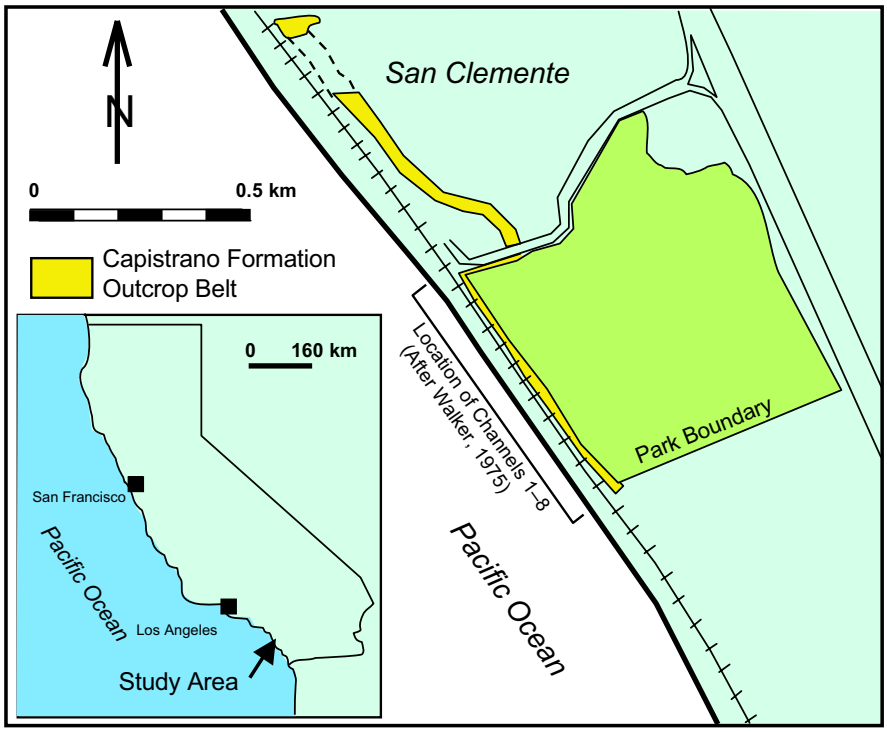

FIG. 50.—Location of the outcrop at San Clemente, California, south of the parking lot (from Campion et al., 2000).

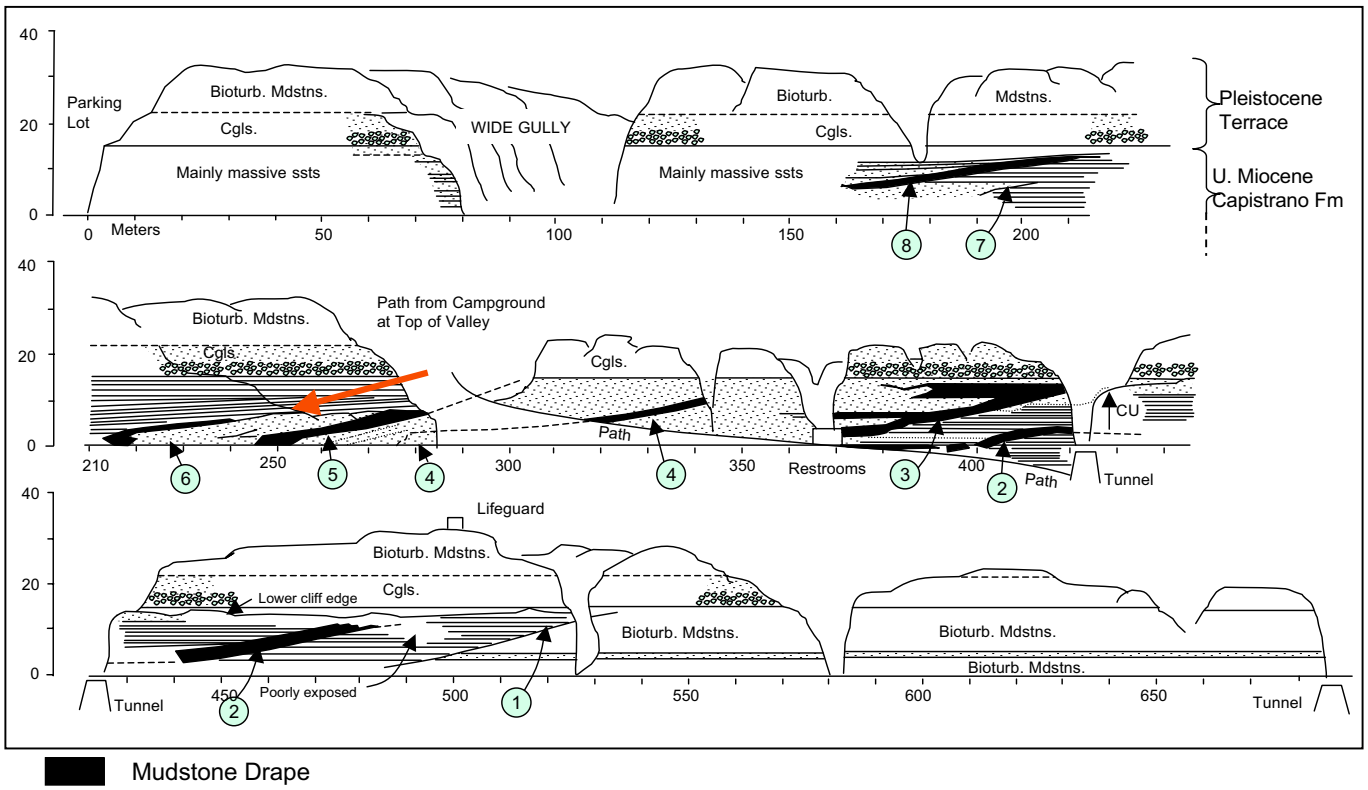

FIG. 51.—Measured section of the cliff at San Clemente. Distances are in meters south of the parking lot. Regional bedding is horizontal, and heavy dipping black lines indicate mudstone drapes on channel walls (numbered 2 through 7). Channel 6 is shown with red arrow and is discussed in the text. From Walker (1975b).

FIG. 52 (above).—Four thin but coarse-grained sandstone layers separated by gray (turbidite) mudstones. Part of the fill of channel 7, San Clemente.

Meander-loop migration is a common attribute of deep-water channels, with both meander swing and sweep being common features (Fig. 62). This can be observed both in section as well as in map view (Figs. 62–64). In many instances, the seismic expression of meander loops in plan view can be characterized by a series of scrolls (Fig. 62). Somewhat less common are meander-loop cutoffs with associated oxbows (Fig. 65). Internal scour at successive channel bases within an overall aggradational amalgamated channel package is very common. The base of basin-floor channel complexes is erosional with at least some incision into the substrate (Fig. 64).

In association with meander-loop channel migration, lateral-accretion deposits can be observed on seismic sections (Figs. 66–69). Abreu et al. (2003) present a well-illustrated example of lateral-accretion sets in a deep-water meandering channel offshore west Africa. Such features are similar in stratigraphic architecture to fluvial point bars (Fig. 70), though the formation process can be quite different. Nonetheless stratigraphic compartmentalization from a petroleum flow-unit perspective is quite similar.

Lateral-accretion surfaces have been observed in outcrop as well, as in the Ross Sandstone and overlying Gull Island Formation of western Ireland (Lien et al., 2003). Figure 71 shows a cliff outcrop with prominent lateral-accretion surfaces characterized by alternating layers of sandstone and mudstone. These lateral-accretion surfaces have a vertical relief of about 5 m. In the Gull Island Formation, lateral-accretion surfaces can be seen in a continuously sandy succession (Fig. 72).

Lateral accretion commonly can be seen in 3-D seismic images (Figs. 66–69). In Figure 62 the "point bars" show a series of scrolls

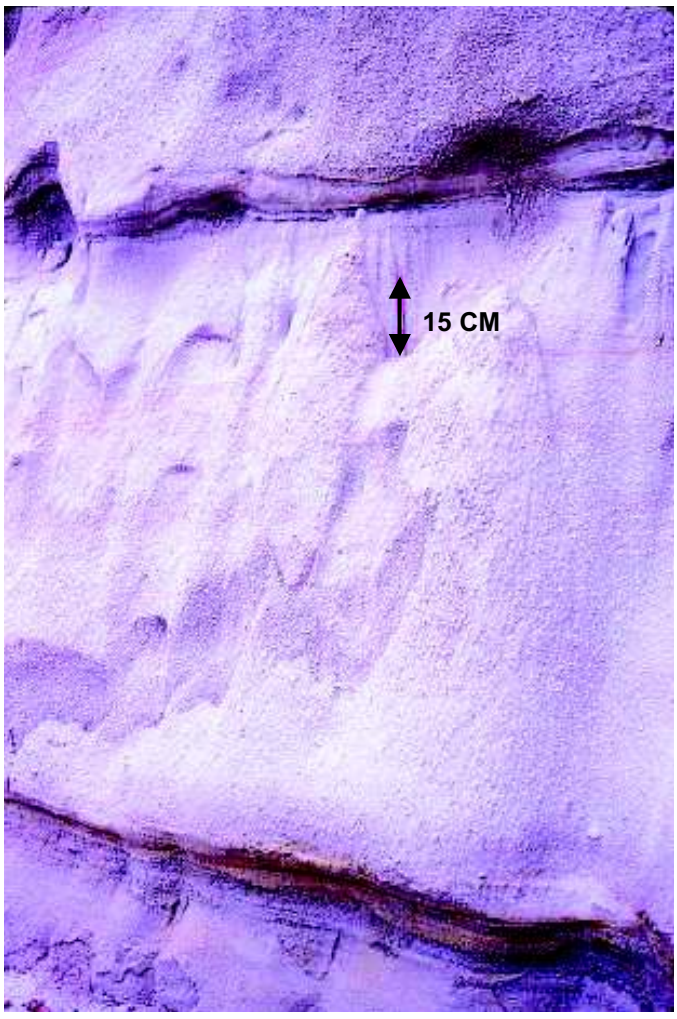

→

FIG. 53.—Graded coarse sandstone at San Clemente, part of the fill of channel 8.

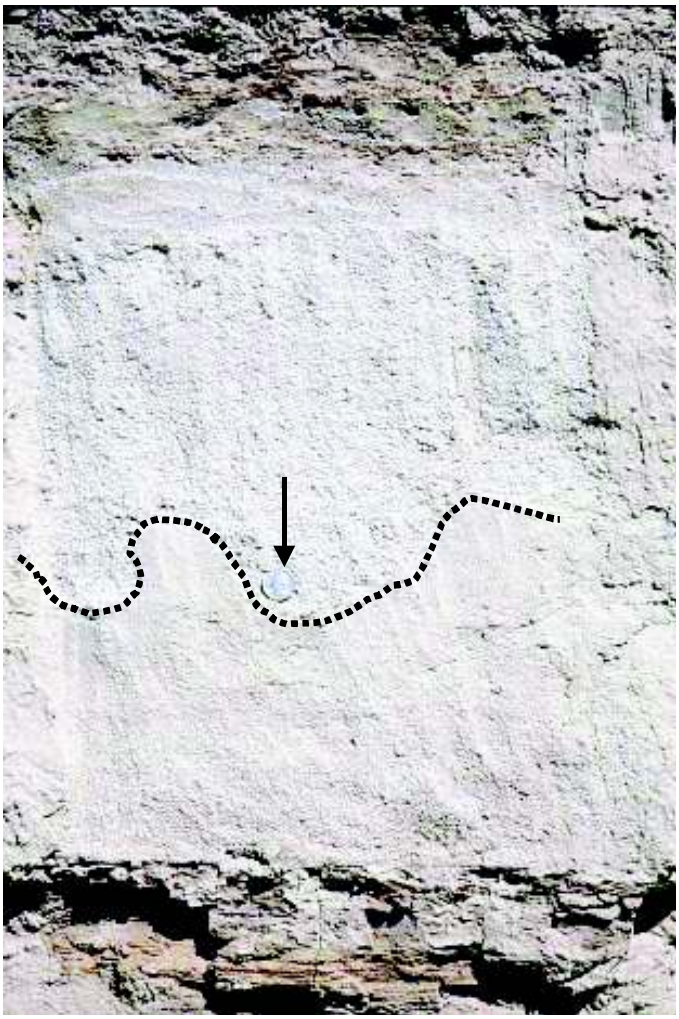

←

FIG. 54.—Two coarse sandstone beds amalgamated along a loaded contact (black line). Quarter for scale. Note gray (turbidite) mudstones above and below.

that may be comparable to the mudstone-draped lateral-accretion surfaces of the Ross Formation or to the channel-wall drapes from San Clemente (Fig. 51).

In both the San Clemente and the Ross examples, the lateral-accretion surfaces contain prominent mudstone layers. These could form vertical and/or lateral baffles to fluid flow in a reservoir situation. Meander-loop ("point bar") settings in the subsurface (Fig. 62) may therefore present engineering problems with respect to fluid flow within the meander loops.

The process responsible for meander-loop migration may involve a single flow event with lateral accretion developing in a way similar to point-bar development in fluvial systems. That is, a prolonged flow event would produce an undercut bank along outer bends of a meandering channel, and at the same time accretes sediment on inner bends, forming lateral-accretion sets such as shown in Figures 71 and 72. An alternative explanation for how deep-water meander loops migrate down system is shown in Figure 73. This process involves a succession of discrete flows, so that, with each flow event, cutting or erosion accompanies the passage of the head and body of the turbidity flow, and fill accompanies the tail. Each flow event would preferentially erode outer bends more deeply, thus resulting in lateral shift of channel axis (i.e., meander swing). Moreover, because the thalweg would exercise maximum erosive force on the outer bend just down system of the channel bend itself, the meander loop

FIG. 55 (below).—Part of the drape on the wall of channel 2. The gray layers are silty and easily disaggregated, and represent mud introduced by the turbidity currents. The brown layers are clay and contain a benthonic fauna. They represent hemipelagic deposition between turbidity currents. Arrows indicate truncation surface of the margin of channel 2 (see Fig. 51).

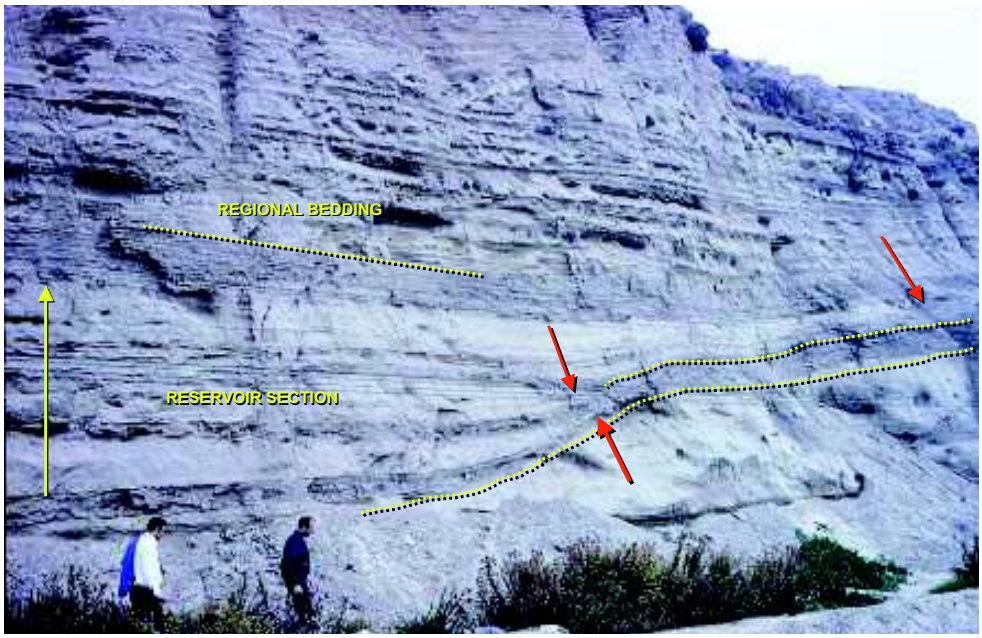

FIG. 56.—Channel 6 at San Clemente, California. Note the lateral pinchout of the lower three beds against the channel margin (red arrows). In detail, the beds can be traced part way up the wall, where they are represented by very thin (< 1 cm) sandy layers. The yellow dotted lines mark the mudstone drape on the channel wall—note that the lower two sandstones pinch out into the drape. In the subsurface, the thick turbidites in the channel fill might make up a reservoir section—but note how rapidly this section would disappear along strike.

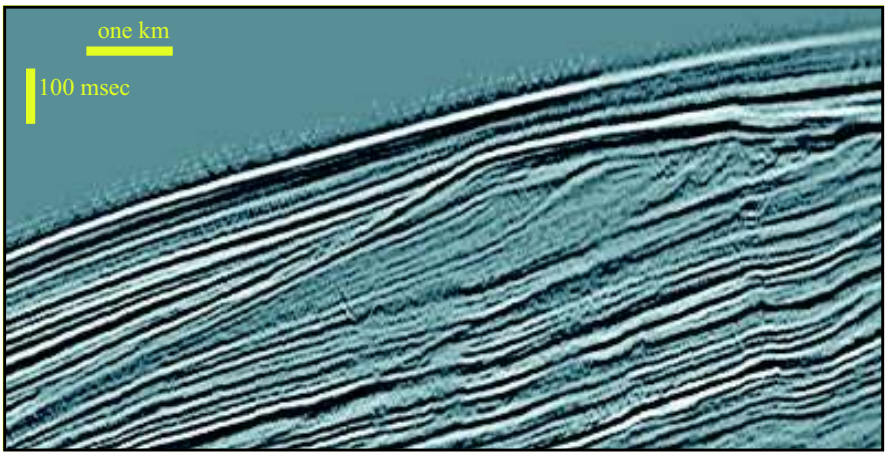

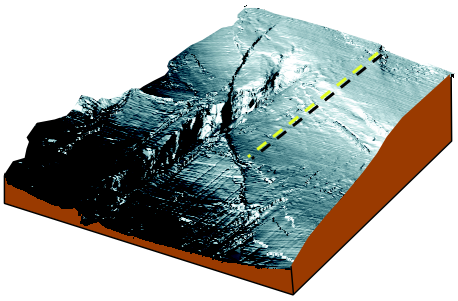

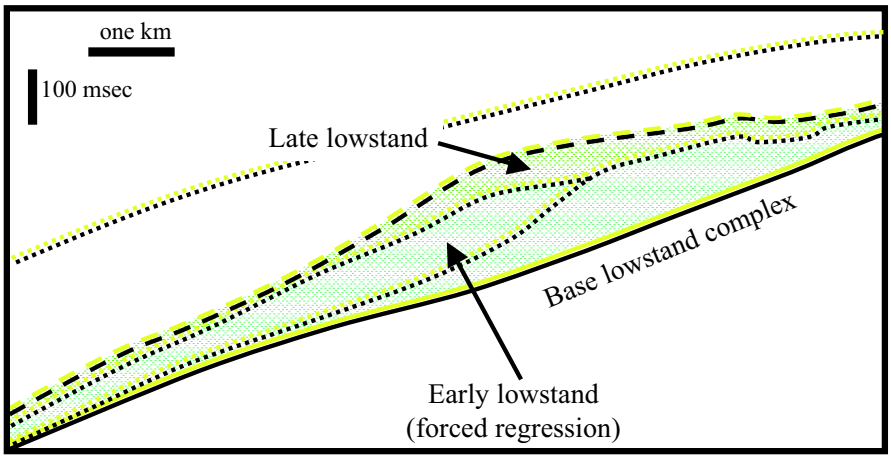

FIG. 57.—Shelf-edge delta in close proximity to Einstein Channel. Note the successive downsteps of the delta top, indicating that the delta prograded under the influence of falling sea level. This is an excellent example of deposits associated with forced regression. The slightly progradational to aggradational section that caps the delta represents deposition during the latter phases of a sea-level lowstand, when sea level is slowly rising. Seismic data courtesy of VeritasDGC.

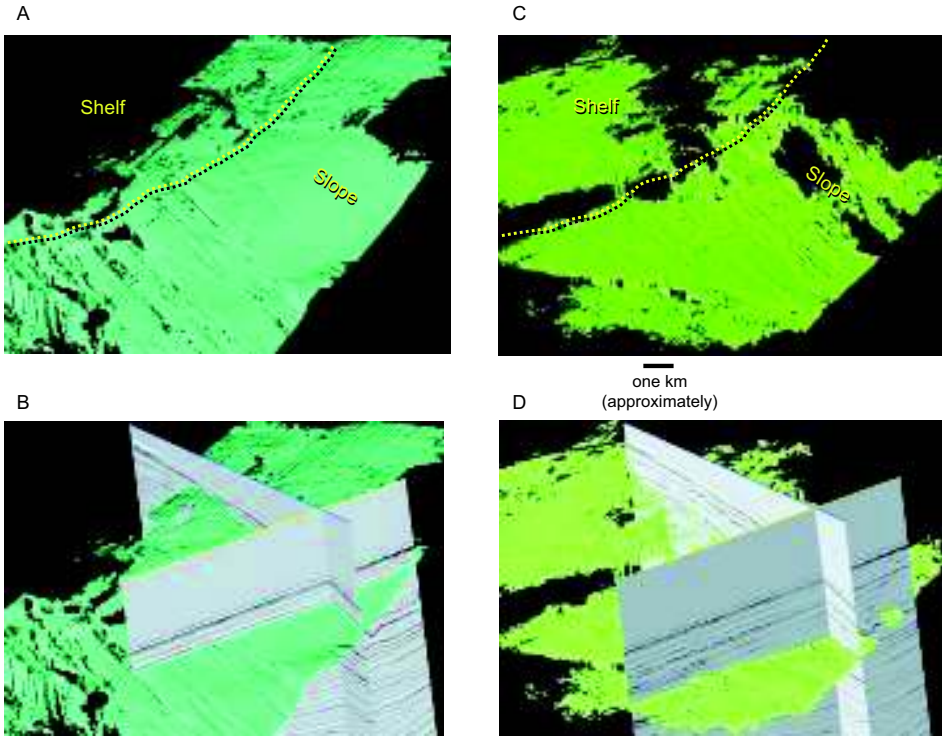

FIG. 58.—**A, C)** Clustering of slope gullies on two late Pleistocene surfaces in the area of the Einstein Channel, Gulf of Mexico, derived from 3D seismic data. In each instance the gully clustering is at the base of a lowstand slope succession, and in each instance the top of the lowstand slope succession is characterized by a single, larger slope channel, not coincidentally where gully clustering at the base was greatest. **B, D)** illustrate seismic reflection profiles parallel to and transverse to the slope gullies. The relief of these gullies commonly is less than 20 m. Seismic data proprietary to PGS Marine Geophysical NSA.

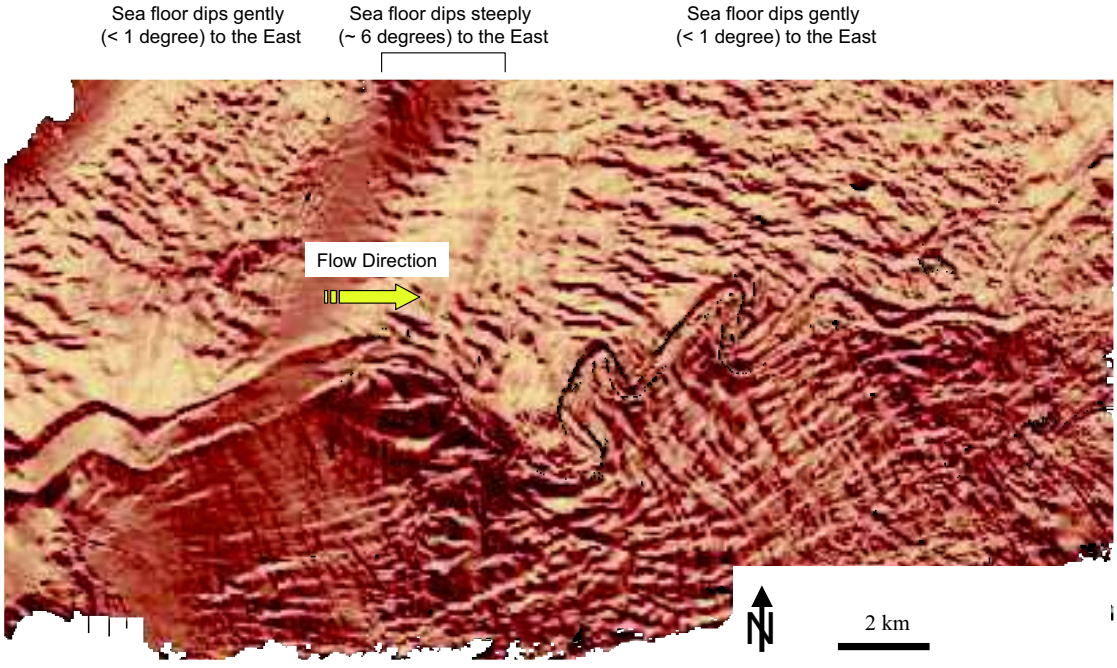

FIG. 59.—Seismic reflection dip-azimuth map of deep-water leveed channel system in the Makassar Strait, Indonesia. The sea floor dips to the right at a very low angle (less than 1 degree) with the exception of a seaward-dipping segment as indicated. This steep dip is associated with the surface expression of a syndepositional base-of-slope toe thrust. Note the abrupt increase in channel sinuosity and decrease of channel width seaward of this toe thrust. Note also the extensive sediment waves on both sides of the leveed channel (compare with Fig. 77) (after Posamentier et al., 2000). Seismic data courtesy of WesternGeco.

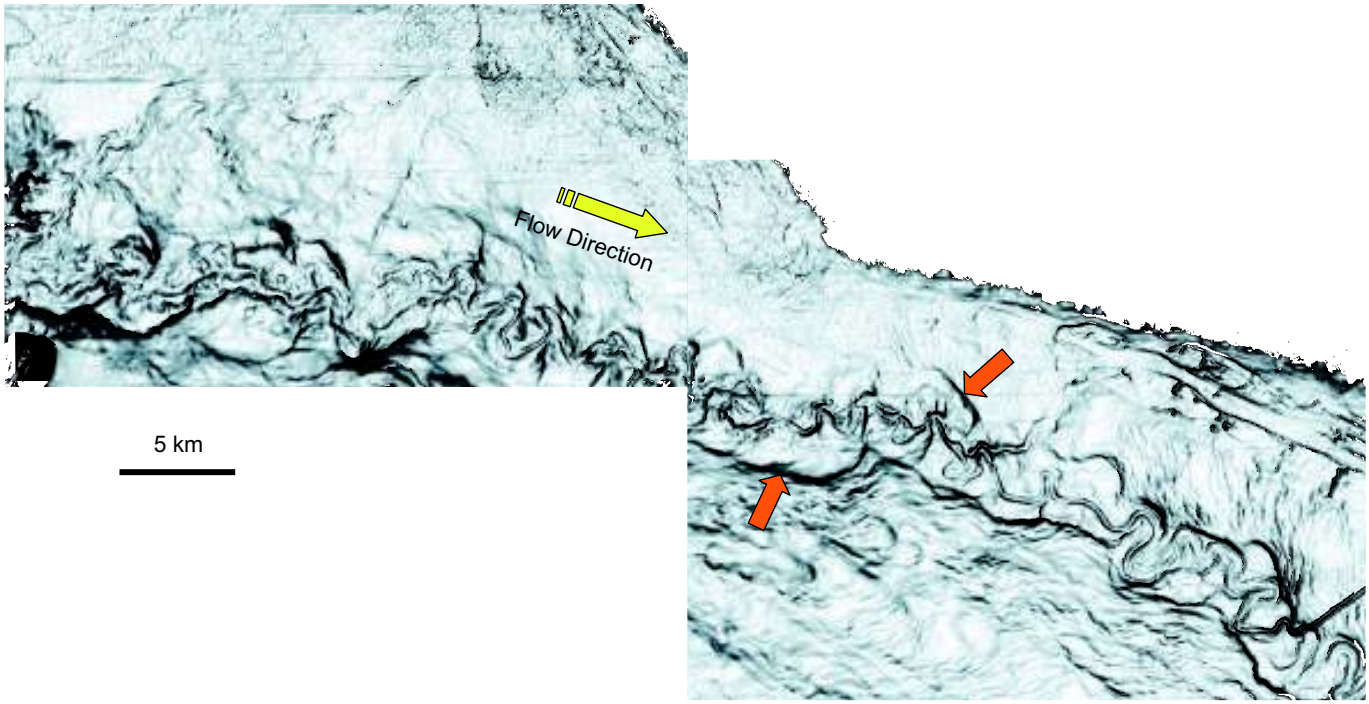

FIG. 60.—Seismic reflection dip-magnitude map of Joshua channel. The channel itself is part of a channel belt that lies within a larger leveed channel (shown by red arrows). (Posamentier, 2003b). Seismic data courtesy of WesternGeco.

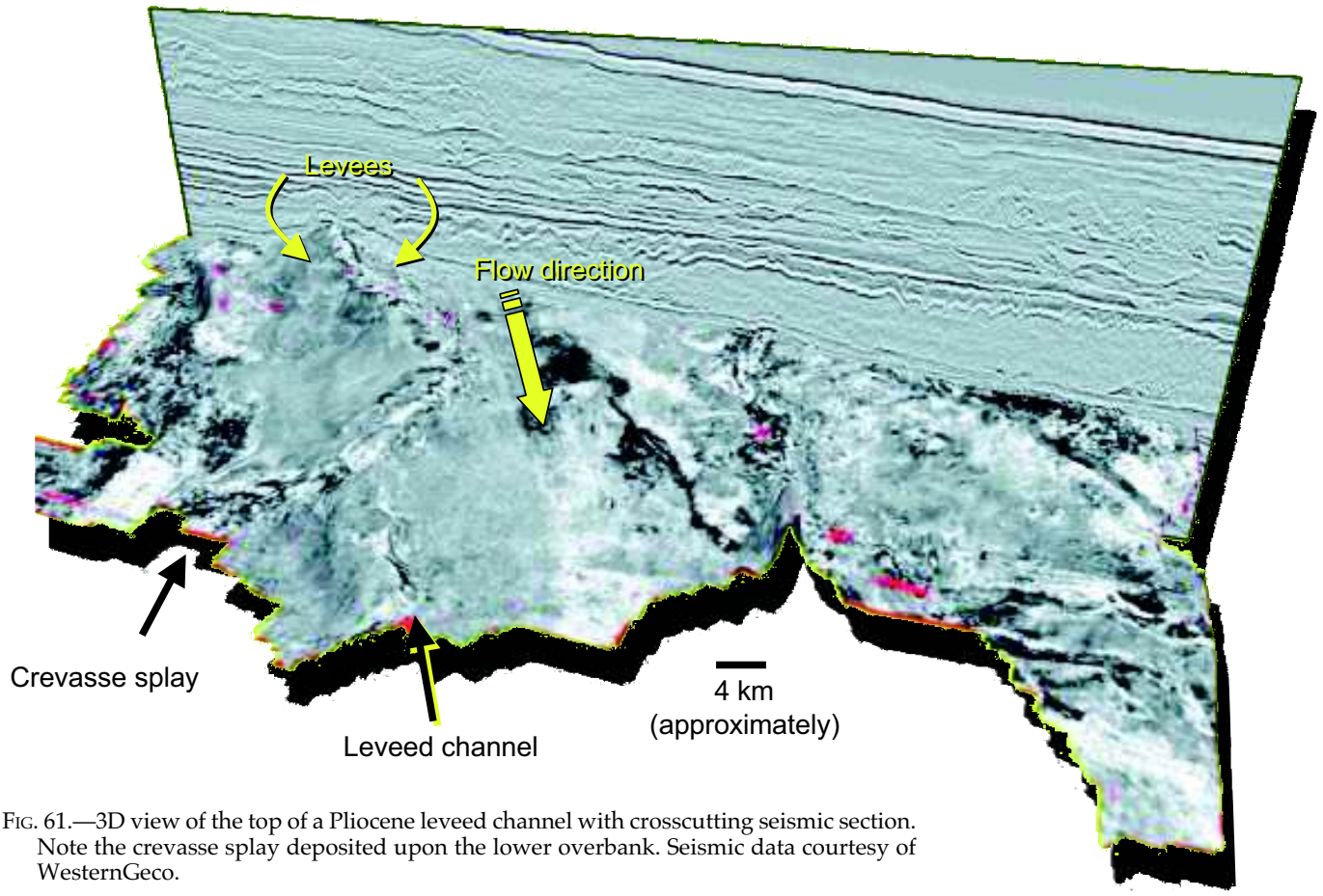

FIG. 61.—3D view of the top of a Pliocene leveed channel with crosscutting seismic section. Note the crevasse splay deposited upon the lower overbank. Seismic data courtesy of WesternGeco.

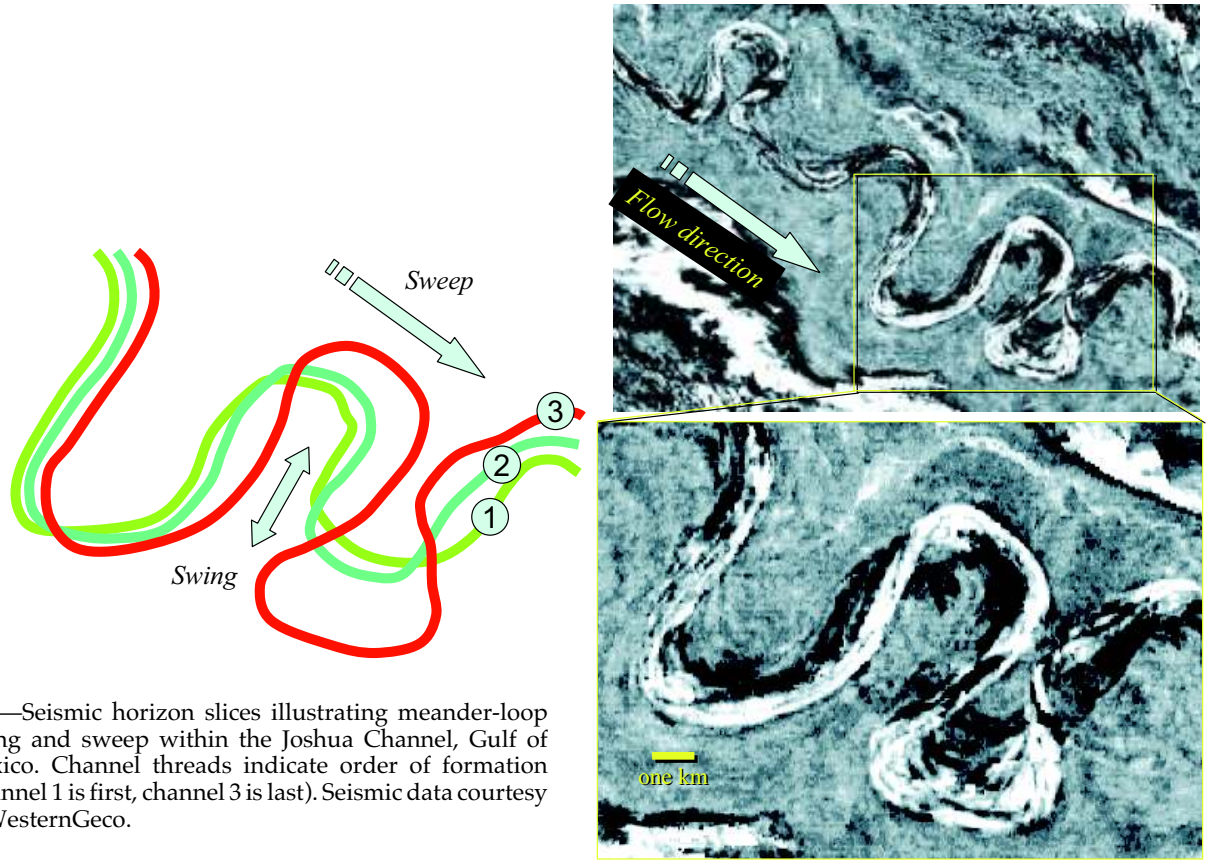

FIG. 62.—Seismic horizon slices illustrating meander-loop swing and sweep within the Joshua Channel, Gulf of Mexico. Channel threads indicate order of formation (channel 1 is first, channel 3 is last). Seismic data courtesy of WesternGeco.

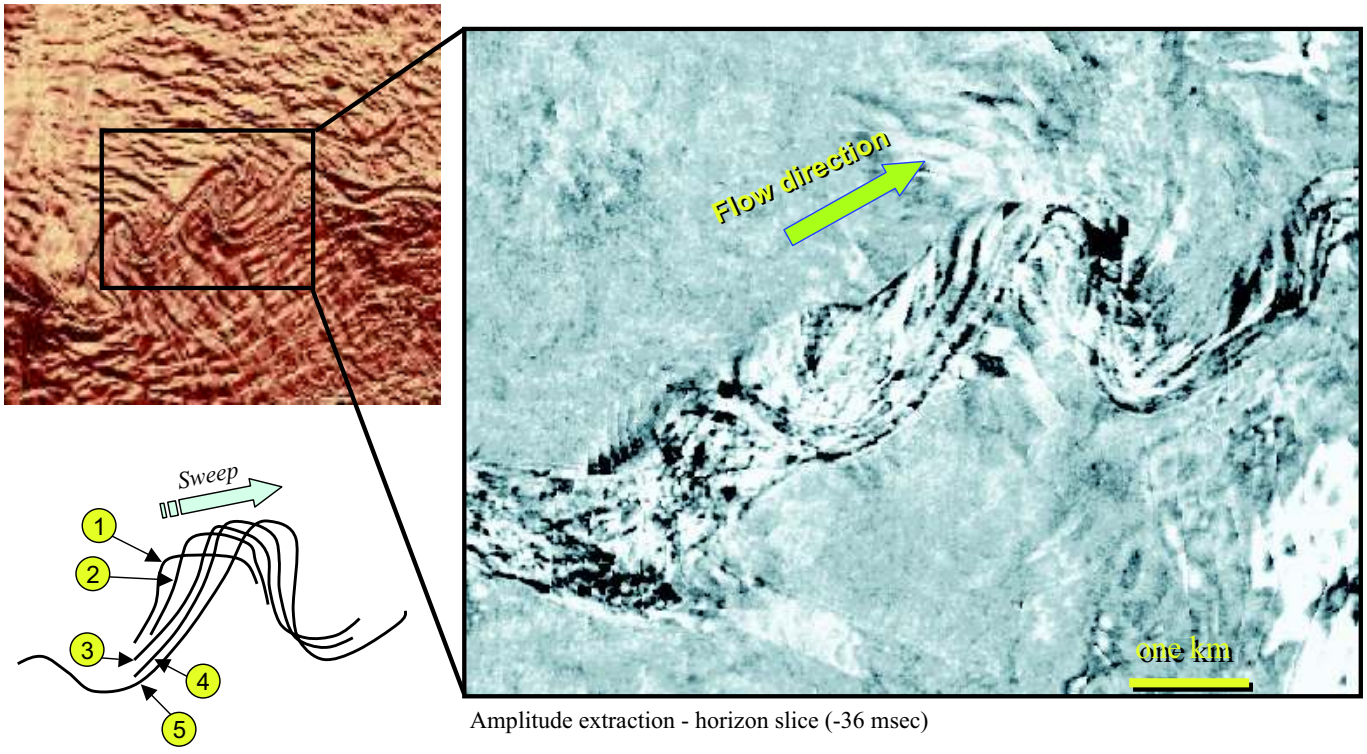

FIG. 63.—Seismic horizon slice through the deep-water leveed-channel system shown in Figure 59, in the Makassar Strait, Indonesia section. Down-system migration of meander loop is well expressed. Channel threads indicate order of formation (channel 1 first, channel 5 last) illustrating channel sweep. Seismic data courtesy of WesternGeco.

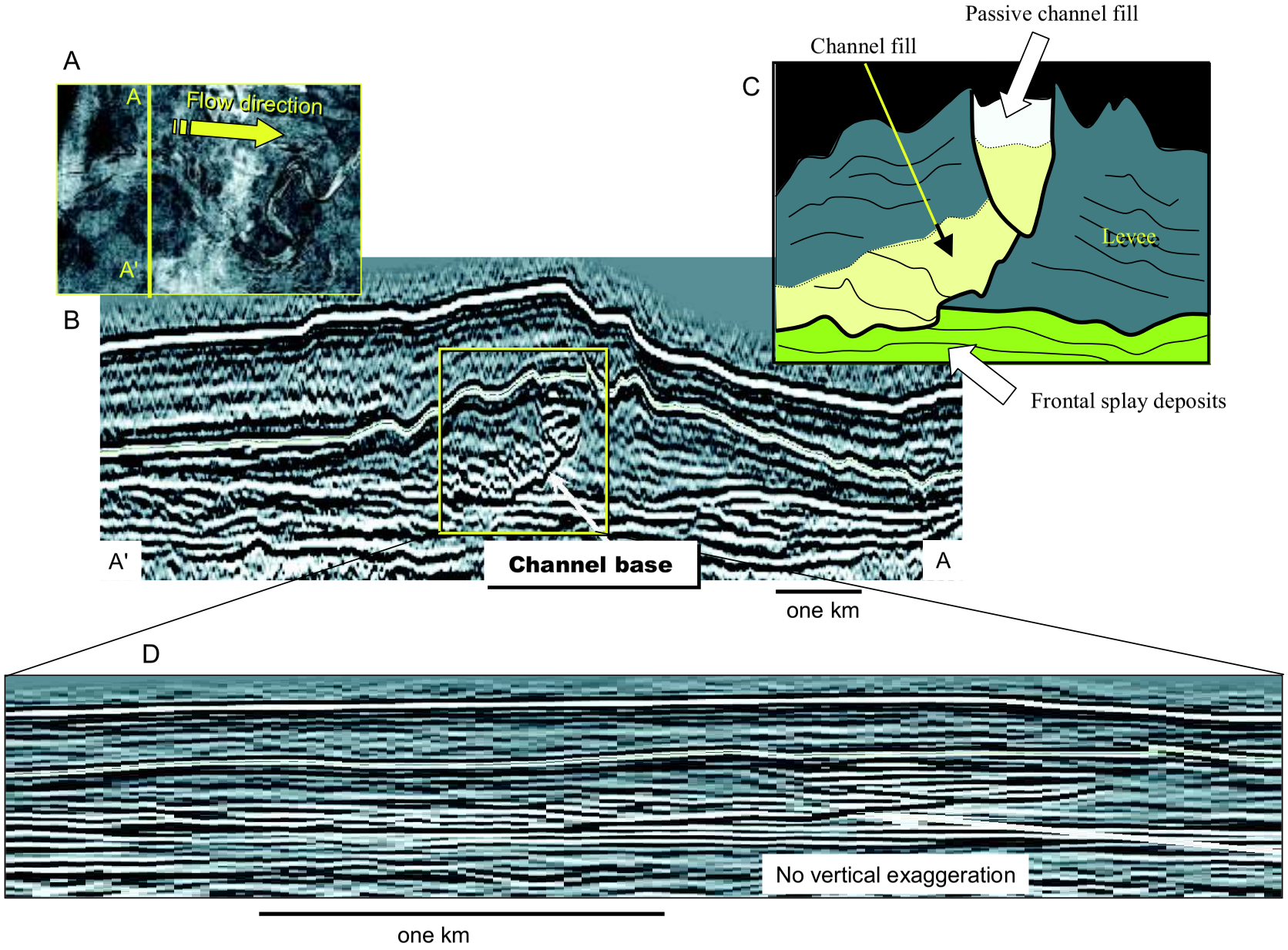

FIG. 64.—Seismic reflection profiles across the channel–levee system shown in Figures 59 and 63 (illustrated in plan view in **A)** and section view in **B– D)**. This section shows the channel fill to be characterized by high-amplitude reflections, inferred to be sand-prone (C). The transverse profile also is shown without vertical exaggeration to reinforce the observation that interpretation of the architecture of these types of deposits can be greatly facilitated by "squashing" the profile. Seismic data courtesy of WesternGeco.

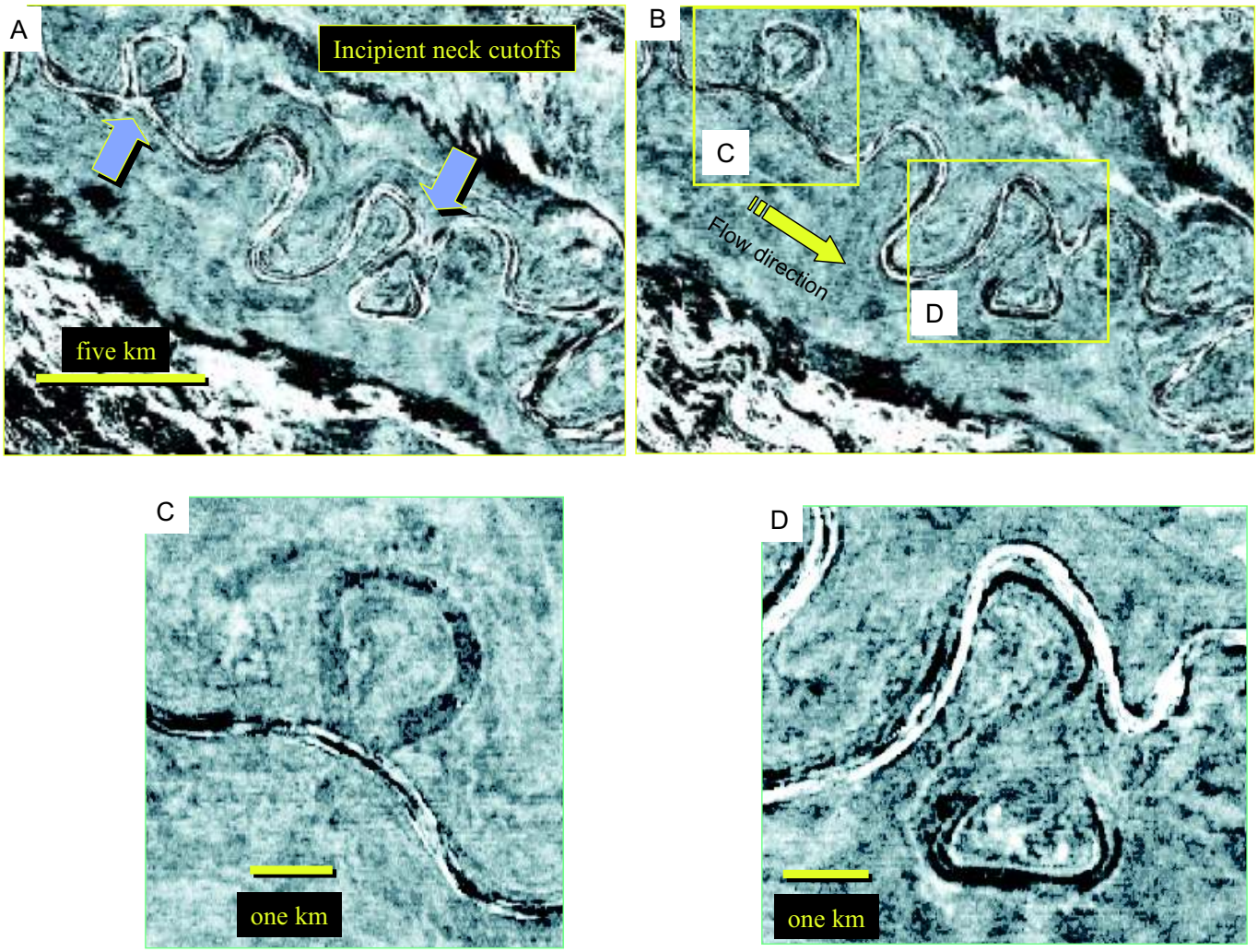

FIG. 65.—Meander-loop development within the Joshua channel, eastern Gulf of Mexico, as observed on seismic reflection horizon slices (compare with Fig. 62). **A)** Time slice that illustrates two incipient cutoffs of meander-loop necks. **B)** Slightly higher (approximately 12 m) time slice that illustrates cutoff of meander-loop necks. **C, D)** Time-slice details of the neck cutoffs and resulting oxbows shown in Parts A and B. Seismic data courtesy of WesternGeco.

would therefore display down-system migration (i.e., meander sweep). Figure 73 illustrates how flow velocity vectors tend to be greater along outer bends especially just down-system from each meander bend, thus tending to cause a down-system shift of successive channel axes (i.e., meander sweep). The resulting architecture of cut and fill can readily appear as lateral-accretion architecture on seismic data, whereas the outcrop expression would be one of cut and fill accompanying a progressive shift of channel axes. Within each cut and fill, it is possible that smaller-scale true lateral accretion such as shown in Figures 71 and 72 can be present.

Avulsion events in deep-water channels have been documented using 3D seismic data (Posamentier and Kolla, 2003b). Figure 74B, C illustrates a late lowstand leveed channel that underwent an avulsion event. Avulsion events tend to be associated most commonly with levee breaches or crevasses on outer channel bends (Figs. 61, 75), though in isolated instances, because of flow perturbations, crevasses can form on inner bends as well.

Channel-fill lithofacies in these basin-plain leveed channels would be similar to that which is encountered within slope channels. Those basin-floor channels characterized by more significant aggradation would allow greater preservation of waning-phase turbidites, so that Bouma A to C units would be most common.

Levee and Overbank Deposits

Channel levees commonly are deposits with concave-up, gull-winged shapes. In general, the facies common to this depositional element include CCC turbidites, lenticular bedding and small-scale erosion, slumping involving one or two beds, and large-scale chaotic failures. Seismically, levees tend to be characterized by low-amplitude continuous to discontinuous reflections (Figs. 64, 67, 69, 74).

Because the tops of turbidity currents associated with channels commonly ride higher than the channel walls, there is continual spillover onto surrounding areas (Fig. 27). When this occurs, flows abruptly become less confined, and in response to this flow expan-

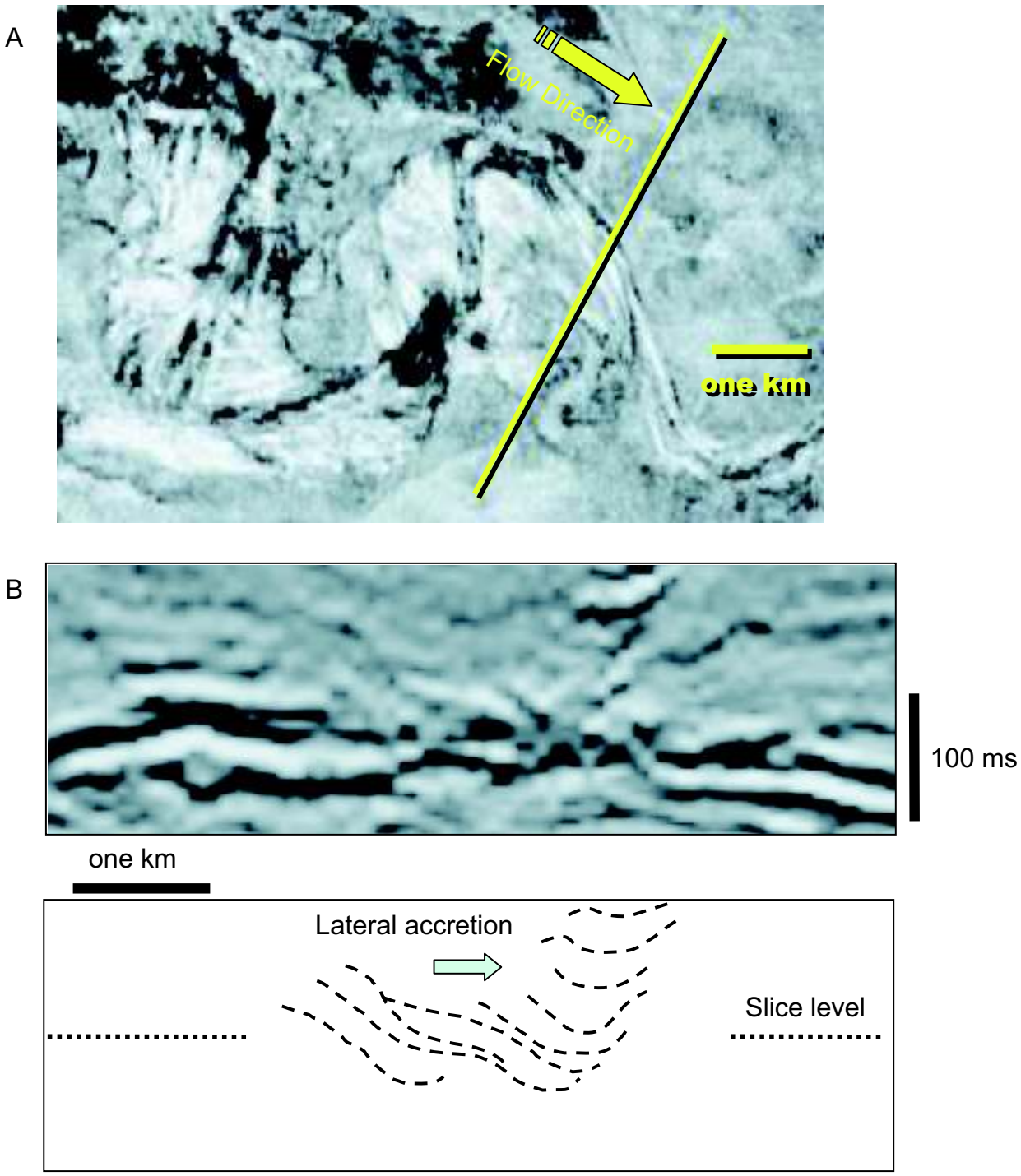

FIG. 66.—Seismic reflection horizon slice illustrating **A)** plan view and **B)** section view across a high-sinuosity deep-water leveed channel, Gulf of Mexico. Down-system migration of meander loops (A) and lateral-accretion deposits (B) are clearly shown. Seismic data courtesy of WesternGeco.

sion (i.e., increase in cross-sectional area), flow velocity abruptly decreases. Lowered flow velocity results in decreased sediment-carrying capacity; that is, the flow is less capable to transport sediment, and rapid sedimentation out of suspension takes place. As noted before, thin-bedded turbidites in levees commonly contain climbing current ripples (Bouma C facies), convolute lamination, and ripped-up mud clasts (CCC turbidites). These sedimentary structures are more common in proximal overbank/levee settings than in any other turbidite environment of deposition.

Enhanced spillover occurs at outer bends of channels as the upper parts of flows tend to continue in a straight-line trajectory whereas the lower parts of flows tend to follow the curving

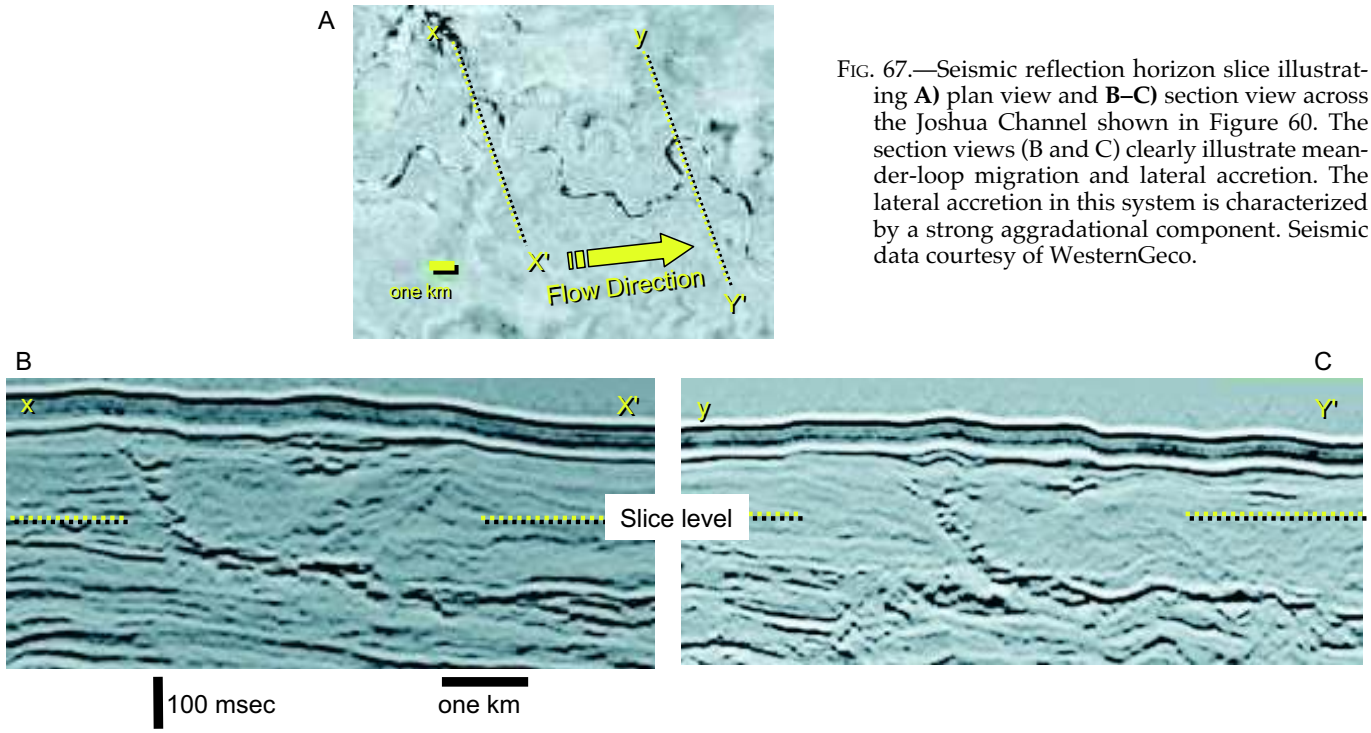

FIG. 67.—Seismic reflection horizon slice illustrating **A)** plan view and **B–C)** section view across the Joshua Channel shown in Figure 60. The section views (B and C) clearly illustrate meander-loop migration and lateral accretion. The lateral accretion in this system is characterized by a strong aggradational component. Seismic data courtesy of WesternGeco.

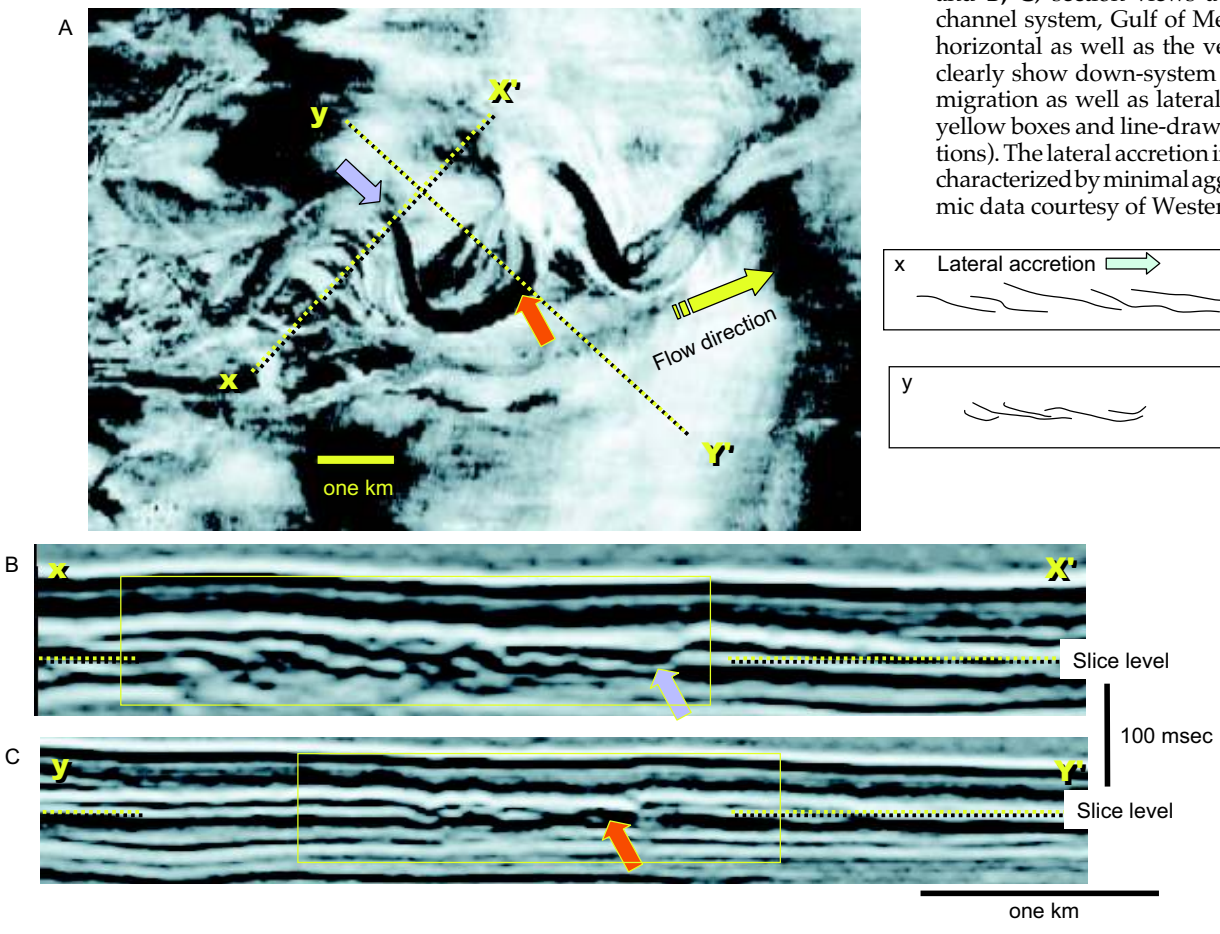

FIG. 68.—**A)** Seismic reflection horizon slice and **B, C)** section views across a leveed channel system, Gulf of Mexico. Both the horizontal as well as the vertical sections clearly show down-system meander-loop migration as well as lateral accretion (see yellow boxes and line-drawing interpretations). The lateral accretion in this system is characterized by minimal aggradation. Seismic data courtesy of WesternGeco.

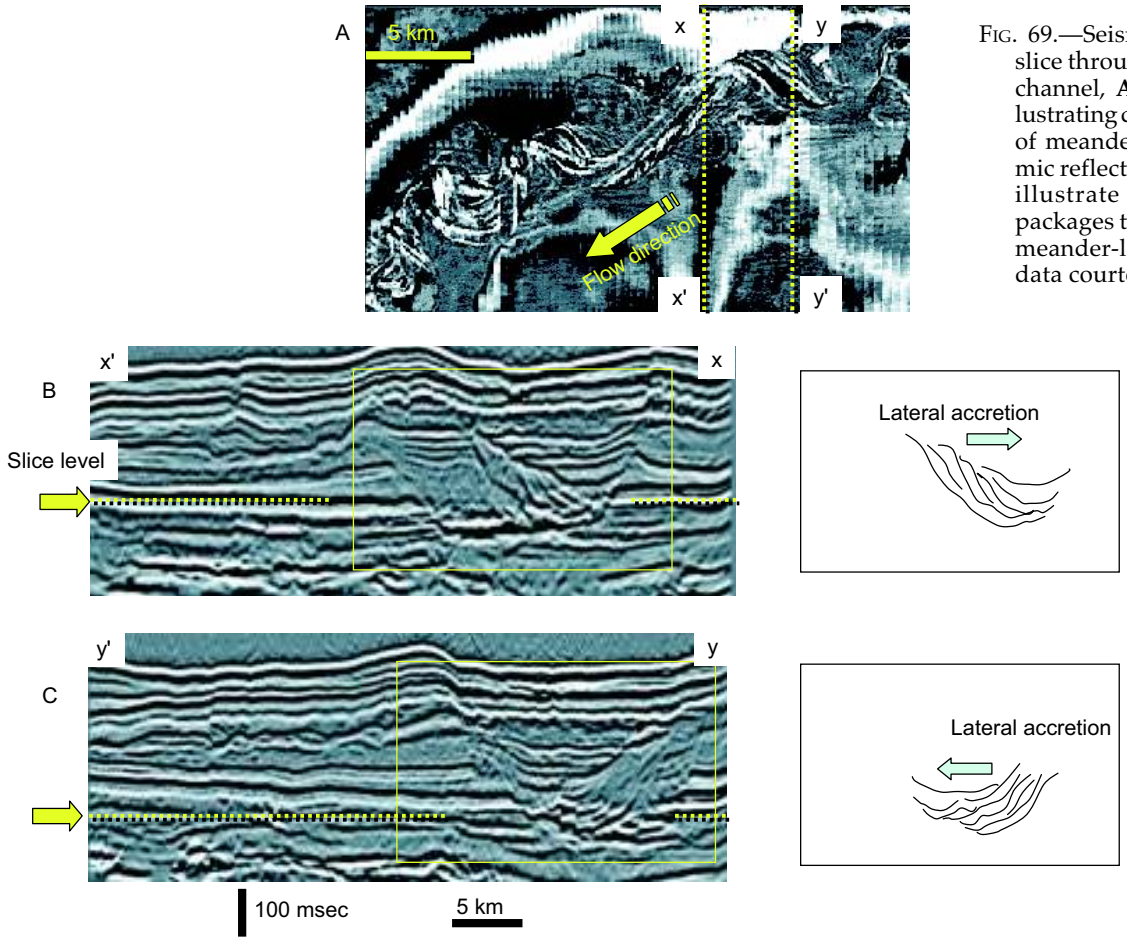

FIG. 69.—Seismic reflection horizon slice through a meandering slope channel, **A)** offshore Nigeria, illustrating down-system migration of meander loops. The two seismic reflection cross sections **B, C)** illustrate the lateral-accretion packages that are associated with meander-loop evolution. Seismic data courtesy of VeritasDGC.

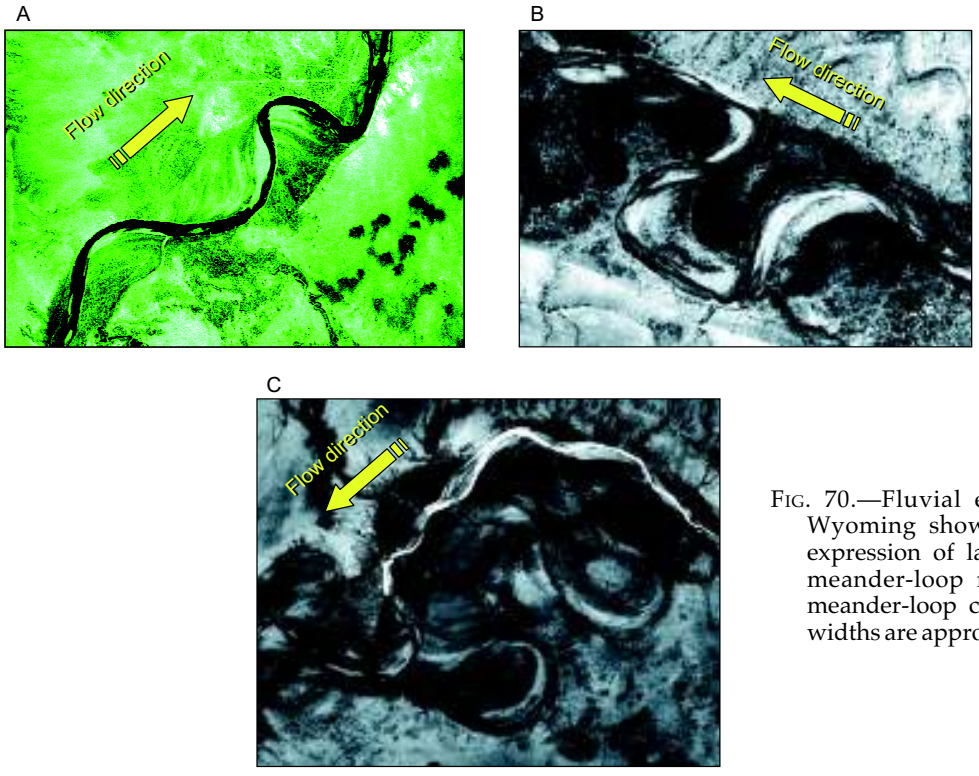

FIG. 70.—Fluvial examples from Wyoming showing plan-view expression of lateral accretion, meander-loop migration, and meander-loop cutoffs. Channel widths are approximately 500 m.

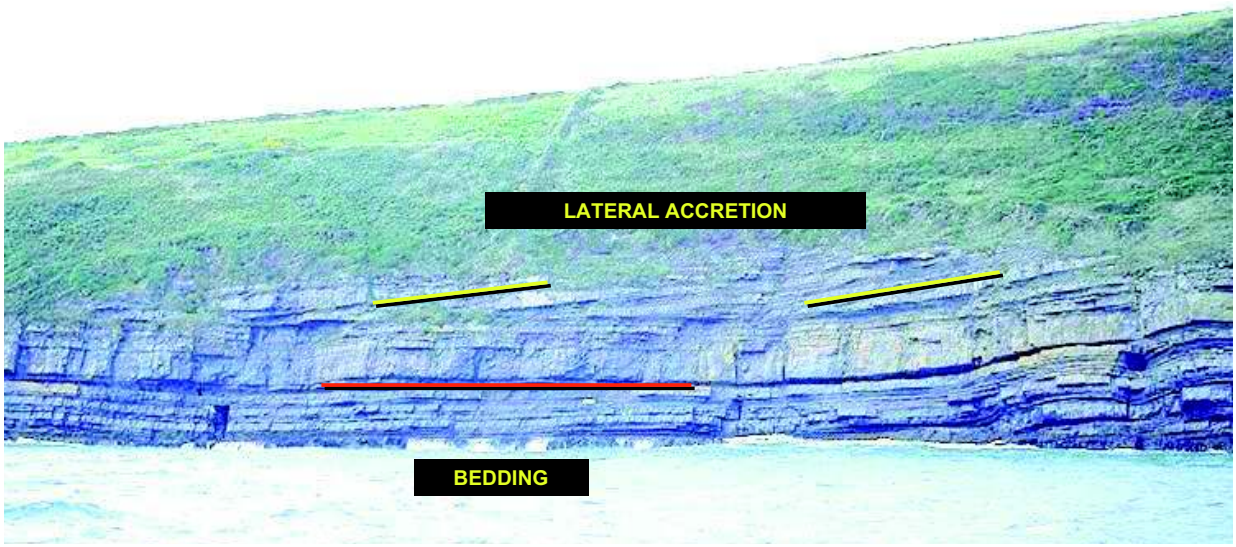

FIG. 71.—The Ross Sandstone in Rehy Cliff, Shannon Estuary, western Ireland. Regional bedding here is horizontal, and the dips in the sandstone and mudstone layers in the upper part of the cliff are interpreted to represent lateral accretion on a "point bar"-like feature in a submarine channel. Vertical relief of the lateral accretion surfaces is about 5 m.

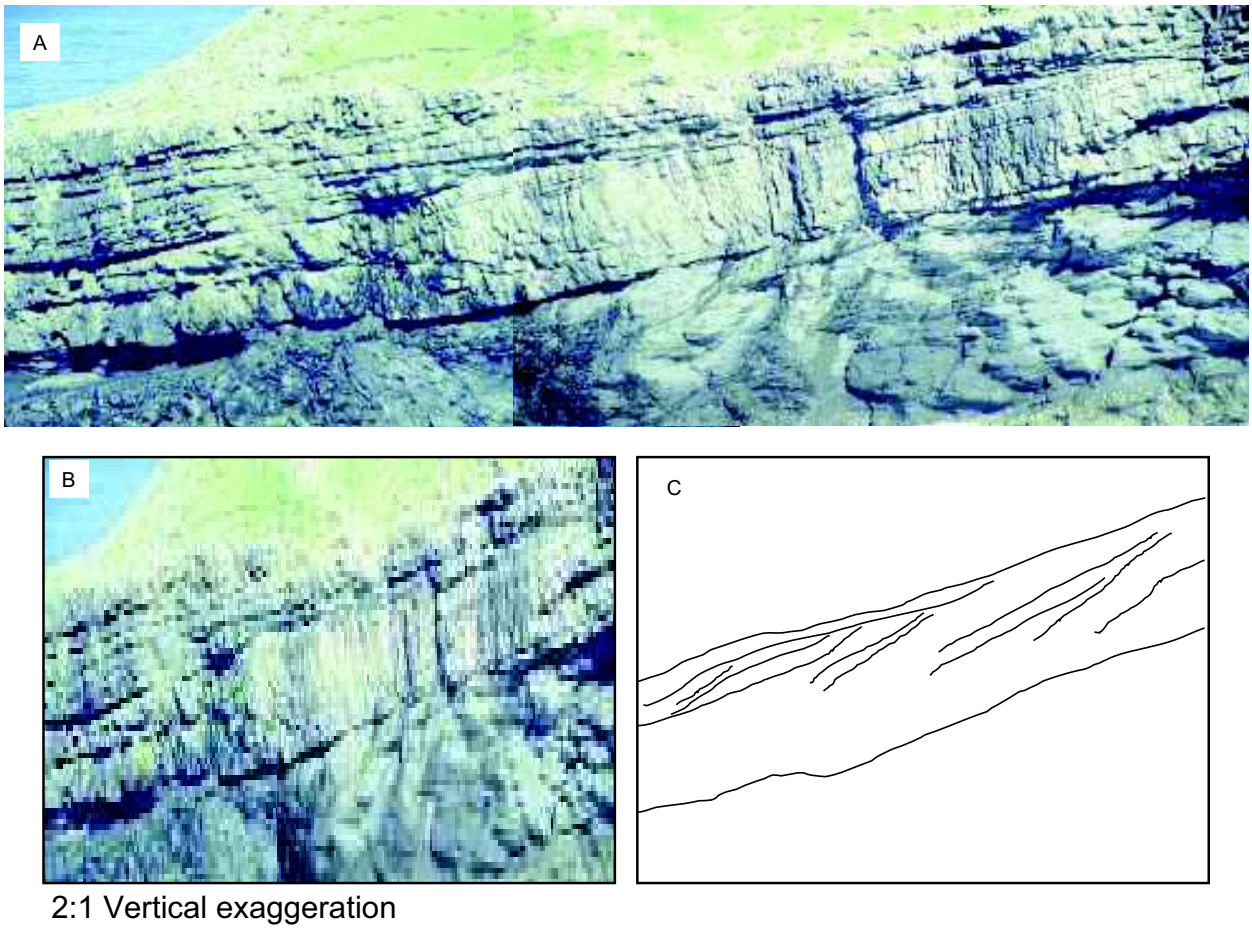

FIG. 72.—**A)** Lateral-accretion surfaces in a sandstone from the Gull Island Formation (immediately above the Ross Formation) of western Ireland. Thickness of sand body about 20 m. **B)** Two-to-one vertical exaggeration of outcrop photo with line-drawing interpretation **C)**.

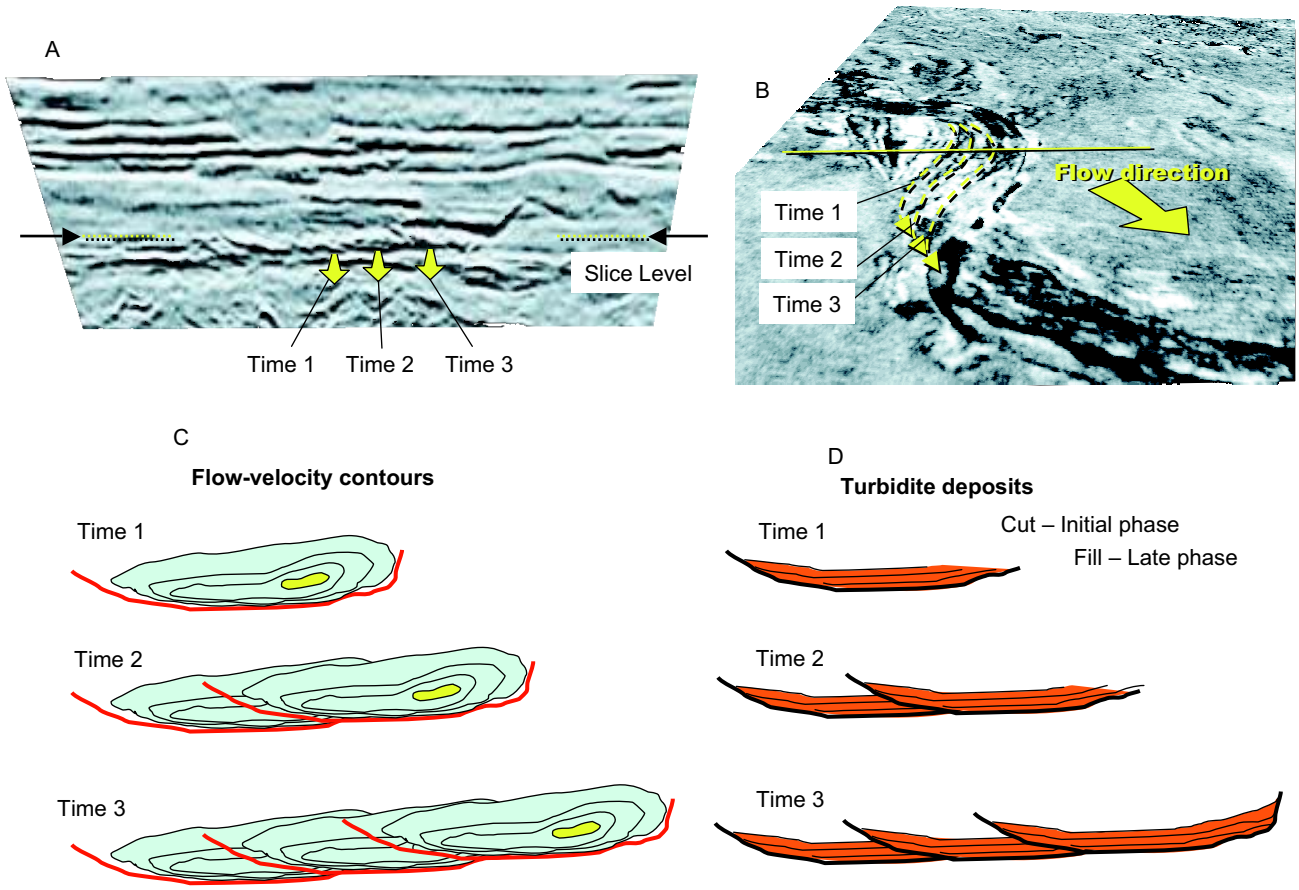

FIG. 73.—Moderately sinuous deep-water channel, eastern Gulf of Mexico. Cross section view shows apparent lateral accretion **A)**. Seismic time slice shows meander loop expansion (i.e., swing) as well as down-system meander-loop migration (i.e., sweep) **B)**. Schematic cross section illustrates flow velocity contours with highest velocity shown in yellow. Note the progressive lateral shift of channel axis through time in response to highest flow velocity occurring on the right side of each channel **C)**. Schematic depiction of successive turbidite channel fills. Note that with the progressive lateral shift of the channel axis through time, only the left side of each channel (with the exception of the final channel position) is preserved **D)**. Seismic data courtesy of WesternGeco.

channel path. This process of enhanced spillover by which the upper part of the flow tends to shear off and decouple from the lower part of the flow has been referred to as flow stripping (Piper and Normark, 1983). One result of flow stripping is that levee crests on outer channel bends are consistently higher than those on inner channel bends (Fig. 76). Flow-stripping deposits in certain instances can take the form of transverse sediment waves (Fig. 77–80). These sediment waves consistently appear to be thicker on their proximal flanks, suggesting up-system migration of wave crests (Fig. 78). The sedimentology of some sediment waves has been documented by Migeon et al. (2000) in the Var fan-channel turbidite system (Fig. 79). These waves also are characterized by up-system wave-crest migration and have formed transverse to flow direction. Cores taken from the updip, crestal, and downdip limb of one of the Var sediment waves reveal significantly greater amounts of sand present in the updip limb of the sediment wave and the least amount in the downdip limb (Fig. 79). Grain sizes up to medium sand were observed in the updip limb. Other sediment waves observed in mid- to upper-slope settings, which are not associated with turbidity-flow channels but rather with oceanic currents such as loop currents, likely are not sand prone (Fig. 81).

Outcrop Example—Simi Hills, California.—

An excellent example of levee deposits in outcrop is the Cretaceous Chatsworth Formation, Simi Hills, California, which has been described by Link et al. (1984). Several hundred meters of the Chatsworth Formation can be viewed along the north side of the freeway (Highway 118) that traverses the Santa Susana Pass (Fig. 82). Thick-bedded, channelized turbidites can be examined in Chatsworth State Park, with channel–levee facies exposed just to the south.

The levee facies is characterized by interbedded sandstones and mudstones in beds up to a few tens of centimeters thick. Sandstone grain size is up to medium sand. Beds in the basal parts of thinning-upward successions tend to be structureless and amalgamated (Fig. 83), but the thinner beds at the tops of successions are commonly lenticular (Fig. 84) and are characterized by CCC turbidites (Fig. 8). Climbing ripples, and climbing ripples that become convoluted, are well displayed in Figure 7. A scour with ripped-up mudstone clasts is shown in Figure 85. The combination of these features suggests an environment in which minor erosion is common, yet individual beds are fairly coarse though relatively thin. Also, the

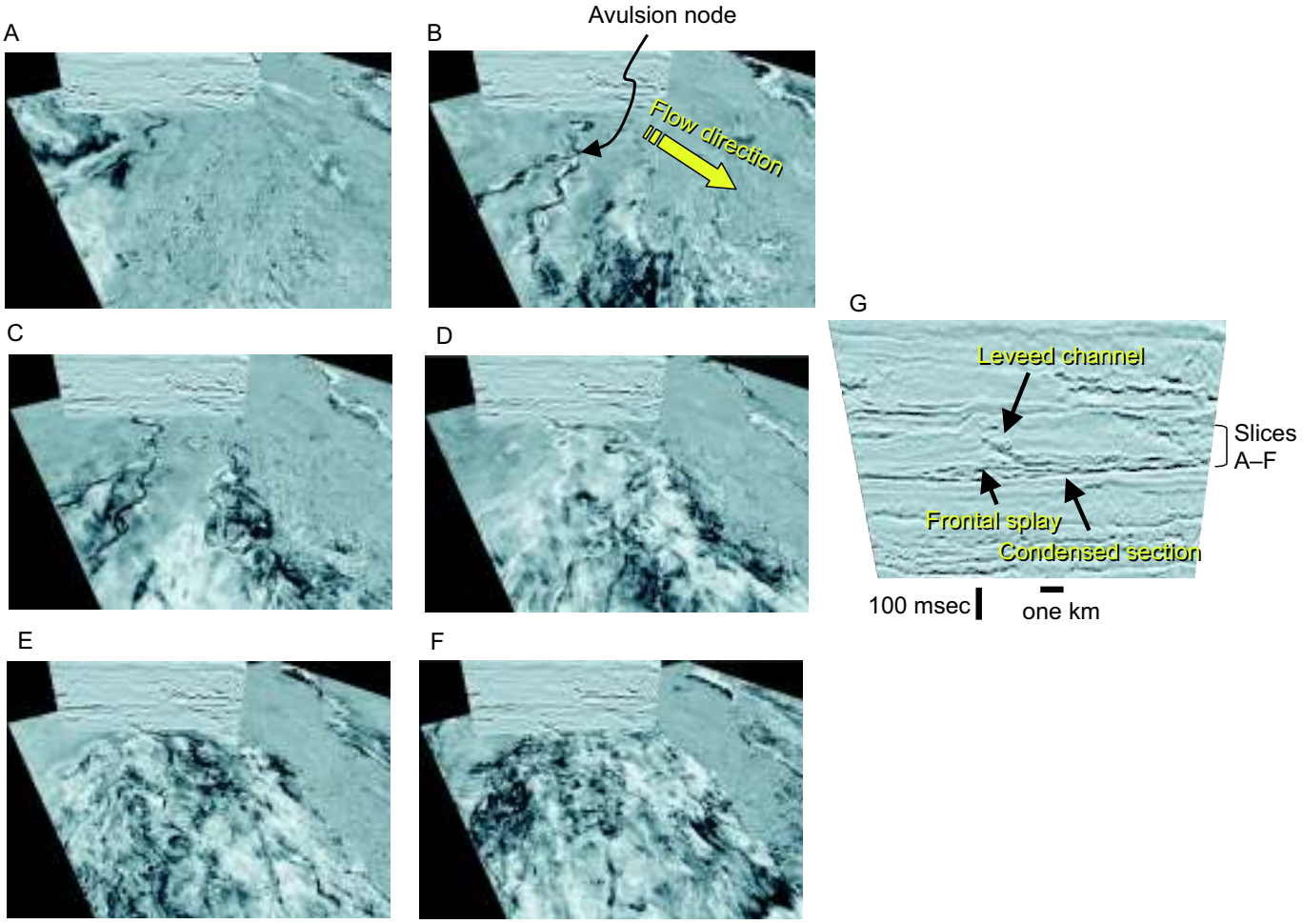

FIG. 74.—Succession of horizon slices through a deep-water turbidite system, eastern Gulf of Mexico. **A–F)** Horizon slices illustrate the evolution of this system from an initial frontal splay (F), eventually evolving into an isolated leveed channel (A). The cross-section view (G) illustrates this evolution as well. Seismic data courtesy of WesternGeco.

climbing ripples and convolute lamination suggest rapid deposition from suspension. The combination of features described suggests rapid deposition of relatively coarse sand, yet in a setting in which the beds are consistently relatively thin—that is, high on a channel margin, or on the back side of a levee. In this setting, turbidity currents may in places be erosive (Fig. 85), and the bedding lenticularity may be a function of deposition in minor erosional scours and hollows (Fig. 84), or due to the pinching of beds against a depositional topography (the channel margin or levee).

Evidence for local slope instability within the levee deposits is in the form of slump deposits involving a few beds, with undeformed beds above and below. Such slumps are commonly associated with CCC turbidites, and in this context probably represent the local sliding of one or two beds, either on the back of the levee away from the channel or down the channel wall toward the channel. In many instances these slumps are subseismic in scale. However, a seismic-scale example of slumps into a channel is illustrated in Figures 76 and 80, and slumps on the distal side of a levee in Figure 86.

The important architectural elements in these settings consist of CCC turbidites, lenticular bedding styles, and slumps involving just one or two beds. Singly or in combination, these elements combine to characterize the upper parts of channel margins, or the backs of levees. These two settings can best be distinguished by their context, as shown in the next example.

Outcrop Example—Wheeler Gorge, California.—

An outcrop example of distal thin-bedded turbidites overlain by a channel–levee complex is observed in the Cretaceous Wheeler Gorge channel systems north of Ojai, California (Rust, 1966; Walker, 1975b). The beds are vertical and are preserved as a sliver along the Santa Ynez Fault of the Transverse Ranges. They occur as an isolated outcrop, and cannot be related to other Cretaceous deposits in southern California. This example emphasizes the importance of the vertical relationships of depositional elements in establishing an overall interpretation of the depositional setting. Once the overall setting has been established, individual depositional elements can be reexamined in the light of the overall setting.

The section can be subdivided into three parts (Walker, 1975b): (1) a lower section of "zebra-striped" mudstones with 1-cm-scale graded siltstones (about 250 m thick; Fig. 87); (2) a central section that consists of three conglomerate-to-sandstone packages (105 m thick; Fig. 88); and (3) an upper section of interbedded sand-

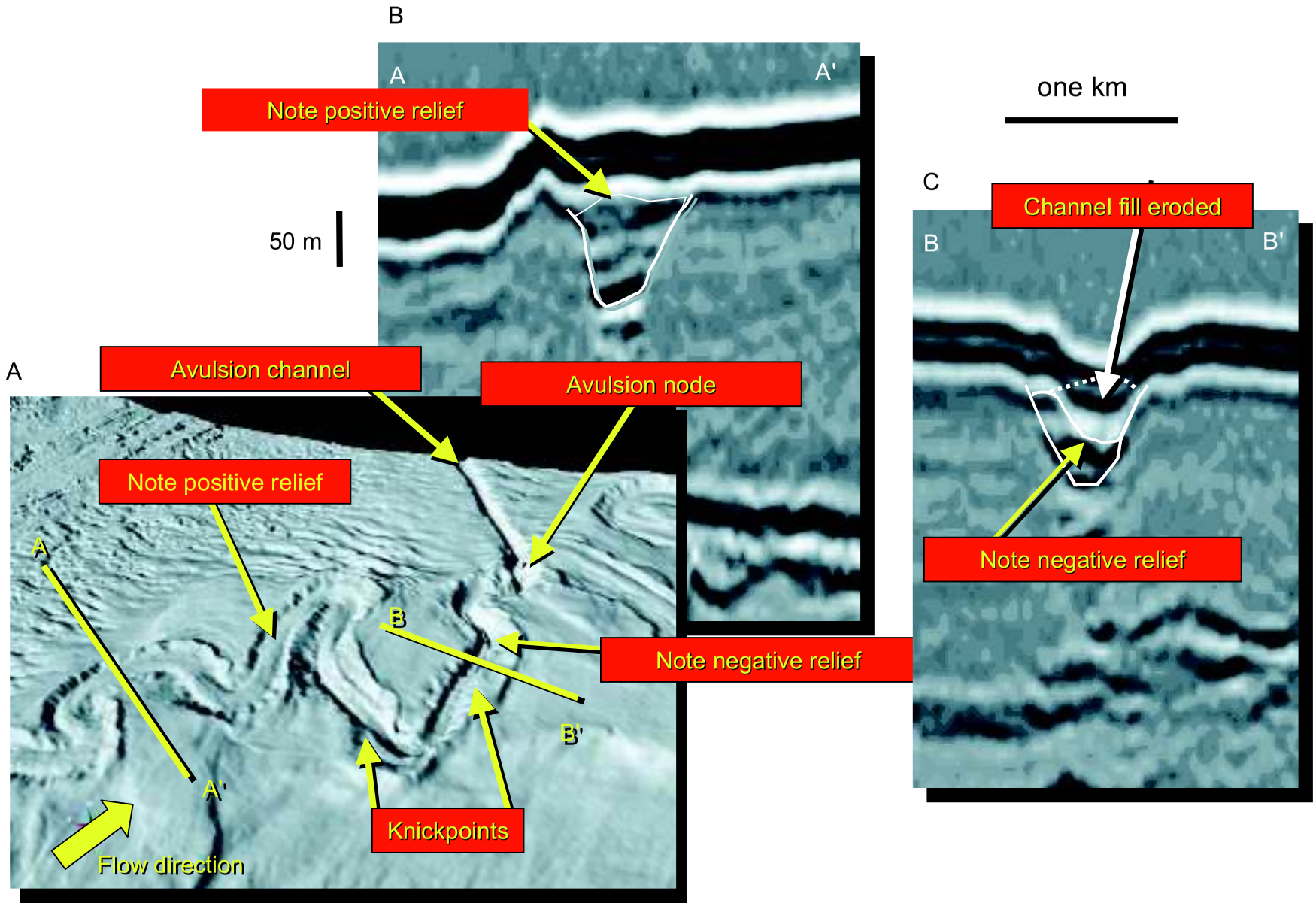

FIG. 75.—**A)** Shaded oblique perspective view of channel shown in Figure 76. Two knickpoints are shown in association with an avulsion channel. The channel downsystem of the kickpoints remains unfilled and is characterized by a concave-up profile **C)**. Upstream of the knickpoints the channel is filled with sand as indicated by the convex-up profile **B)**. Seismic data courtesy of WesternGeco.

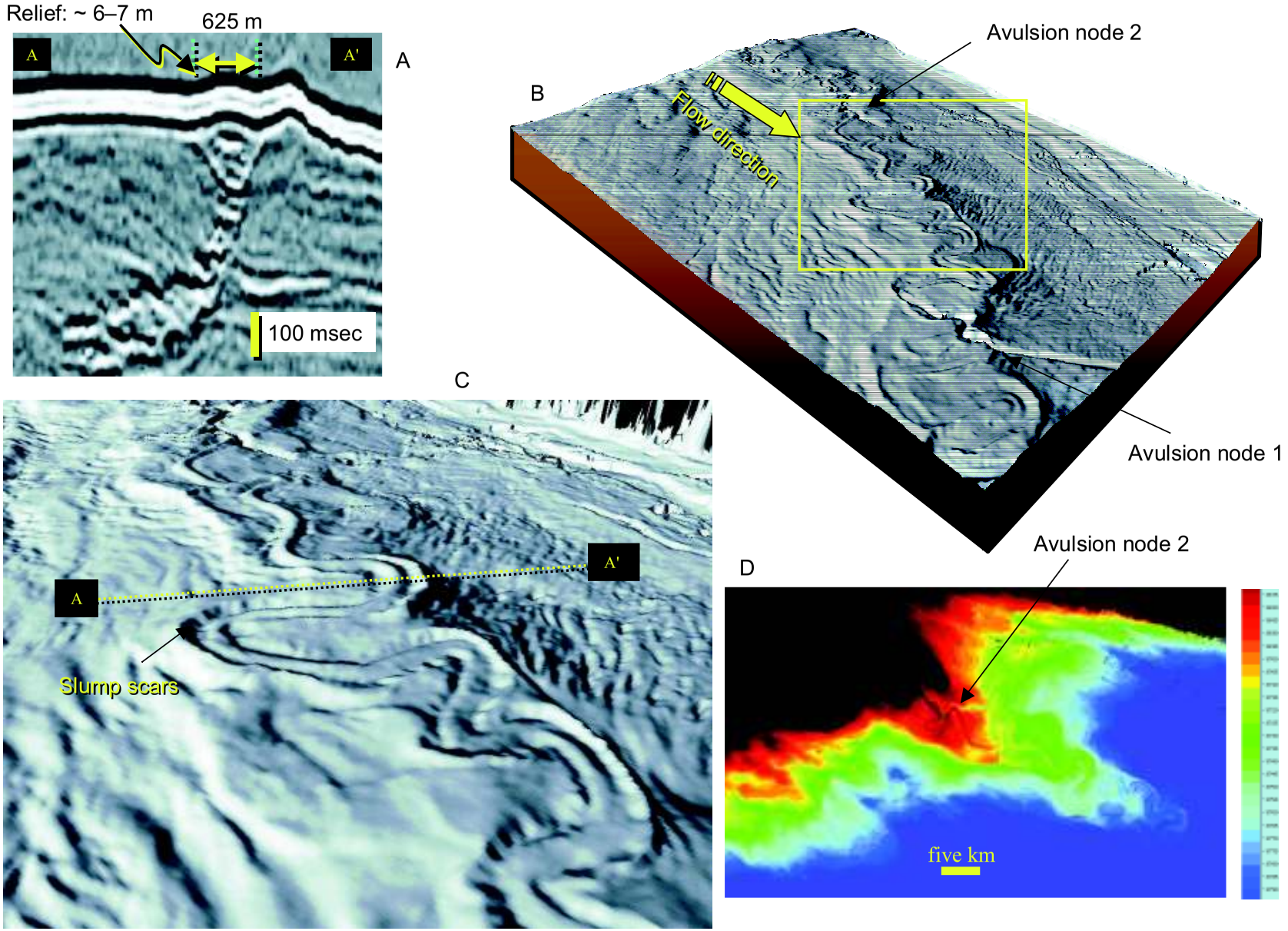

FIG. 76.—Images of Pleistocene Joshua channel, eastern Gulf of Mexico (Posamentier, 2003b). The perspective view **B)** and detail **C)** reveal the elevated nature of the channel fill, suggesting a differential compaction effect associated with predominant sand fill of the channel. Note that levees are highest on outer bends. Note also the small slump scars that characterize the inner levee slope. The channel is part of a channel belt that has accreted to a level 65 m above the adjacent basin plain **D)**. Internally, the channel is characterized by lateral accretion coupled with vertical aggradation **A)**. Seismic data courtesy of WesternGeco.

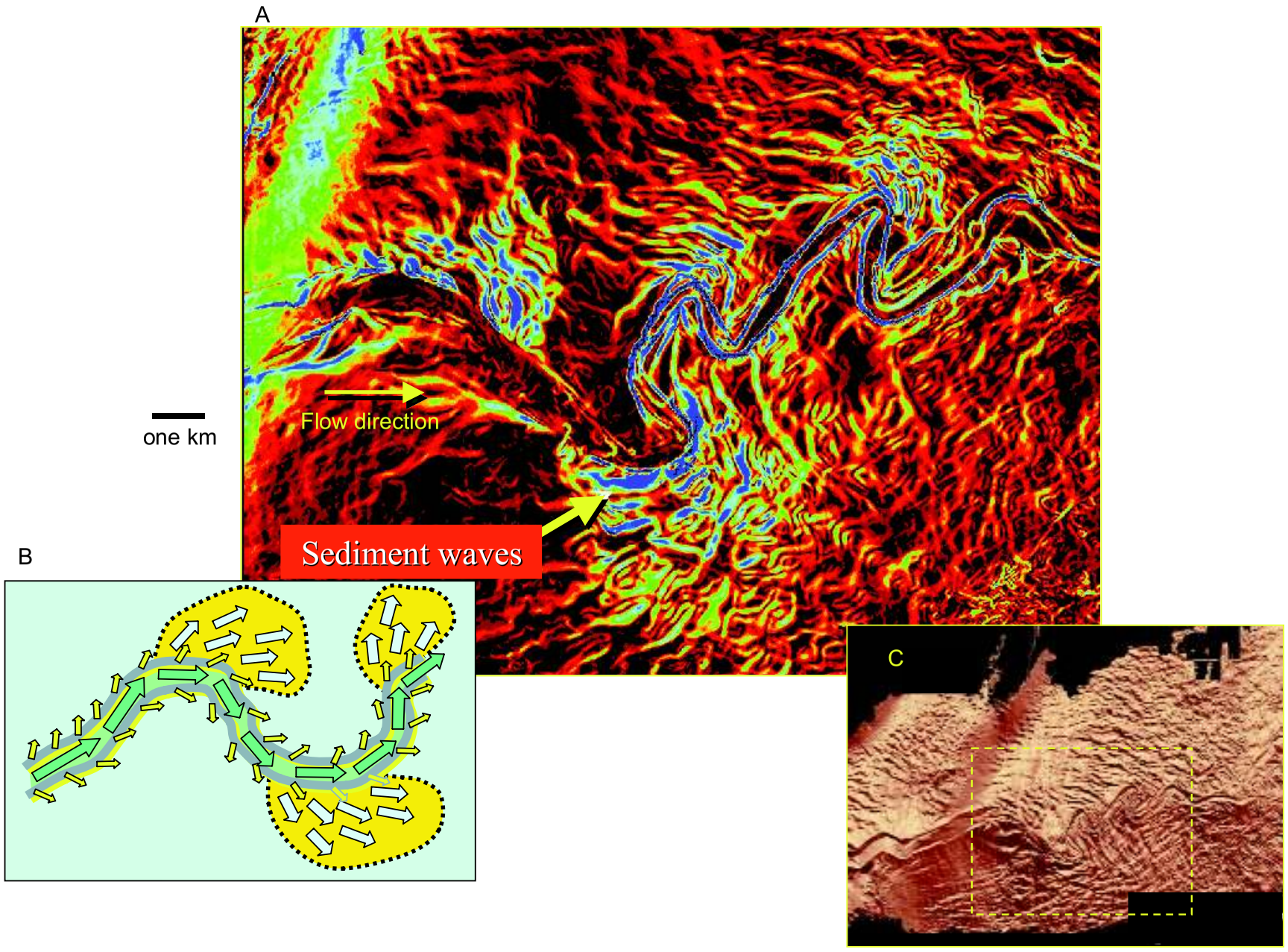

FIG. 77.—Leveed channel on the basin floor of the Makassar Strait, Indonesia **C)**, characterized by overbank sediment waves illustrated on the associated dip magnitude map **A)**. Sediment waves are best developed on outer bends of the channel. Compare with the schematic illustration **B)**. Seismic data courtesy of WesternGeco.

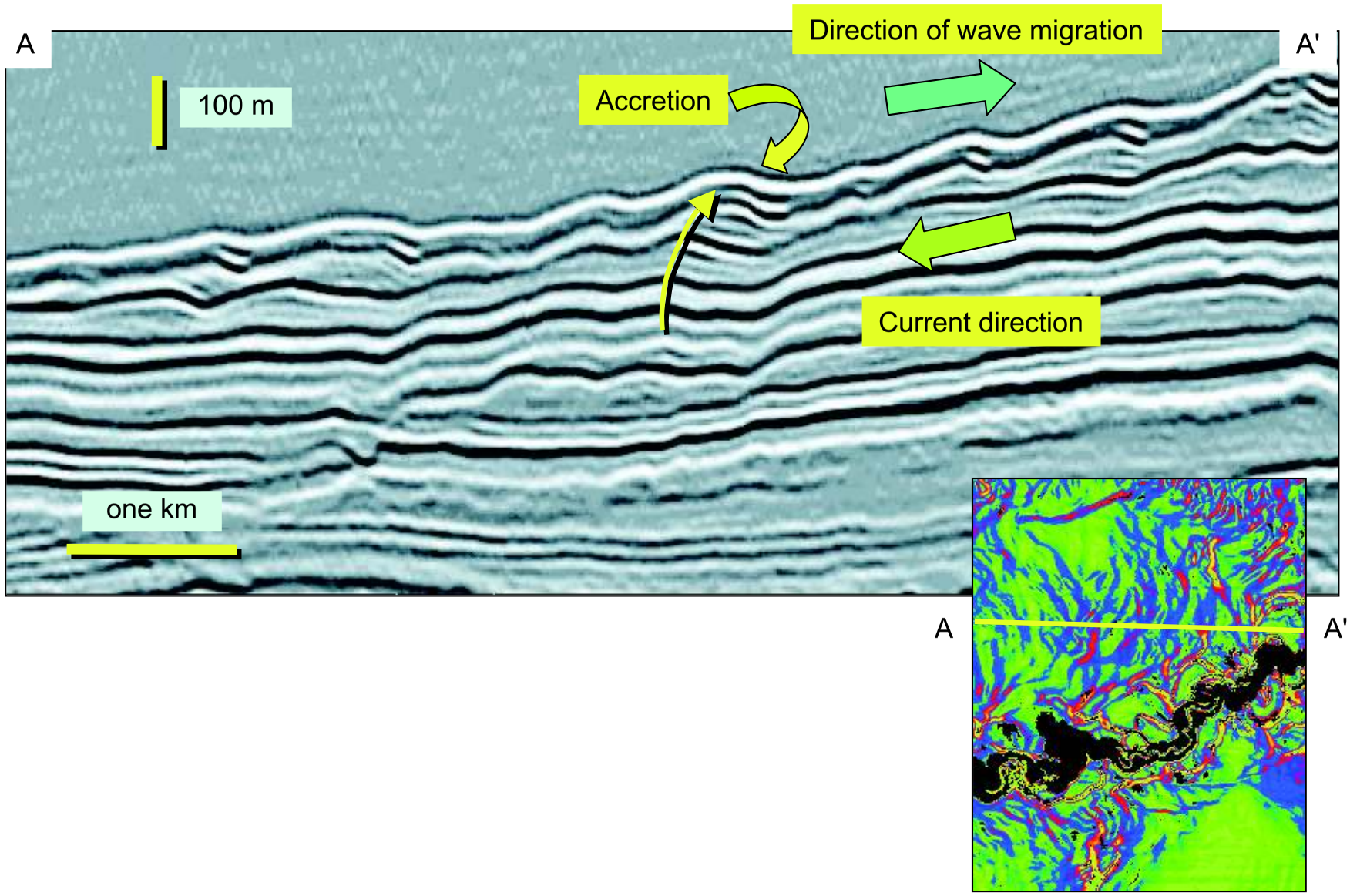

FIG. 78.—Sediment waves associated with slope channels offshore Nigeria. Note that the levee crests migrate progressively up-system, suggesting landward migration of these sediment waves. Seismic data courtesy of VeritasDGC.

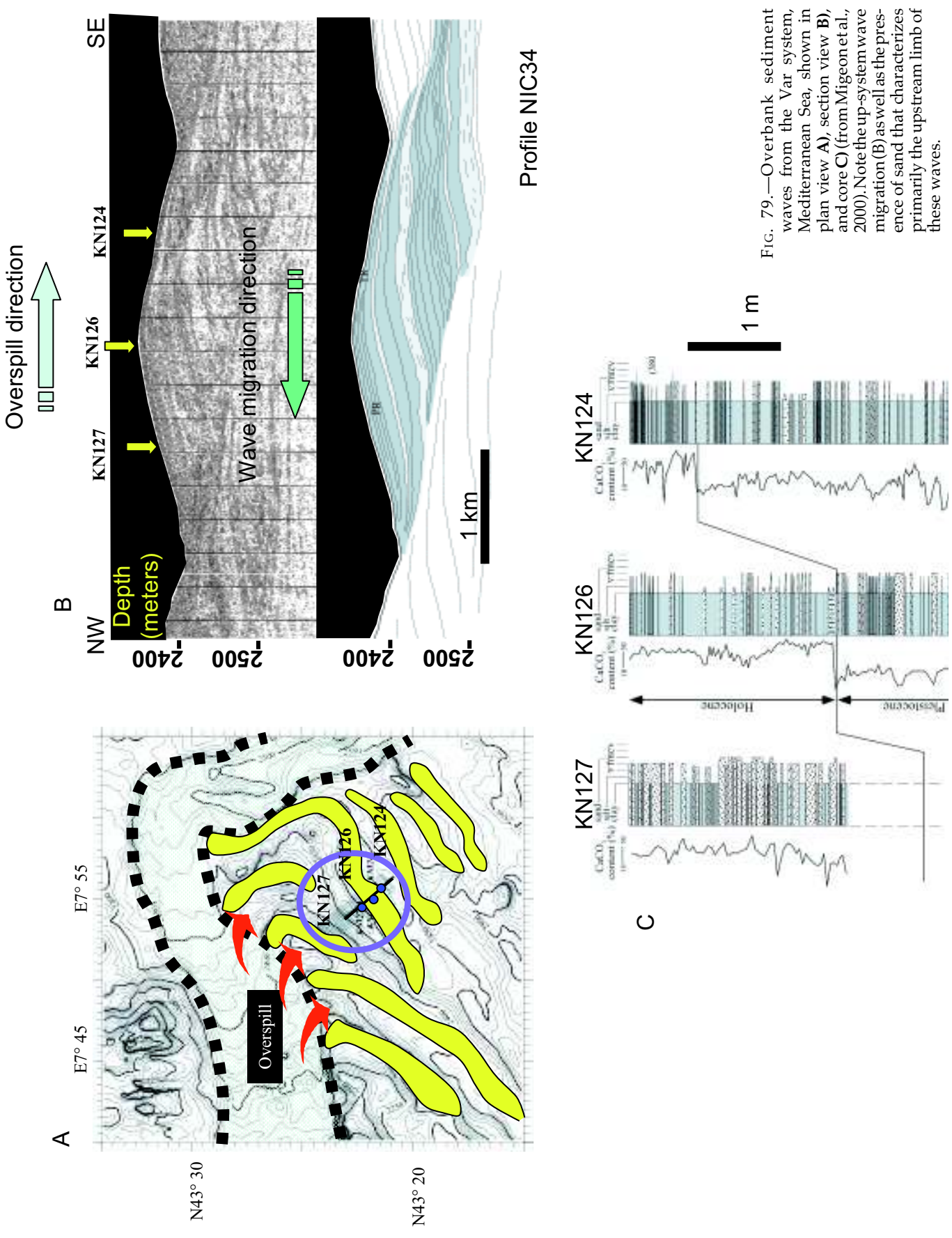

FIG. 79.—Overbank sediment waves from the Var system, Mediterranean Sea, shown in plan view **A)**, section view **B)**, and core **C)** (from Migeon et al., 2000). Note the up-system wave migration (B) as well as the presence of sand that characterizes primarily the upstream limb of these waves.

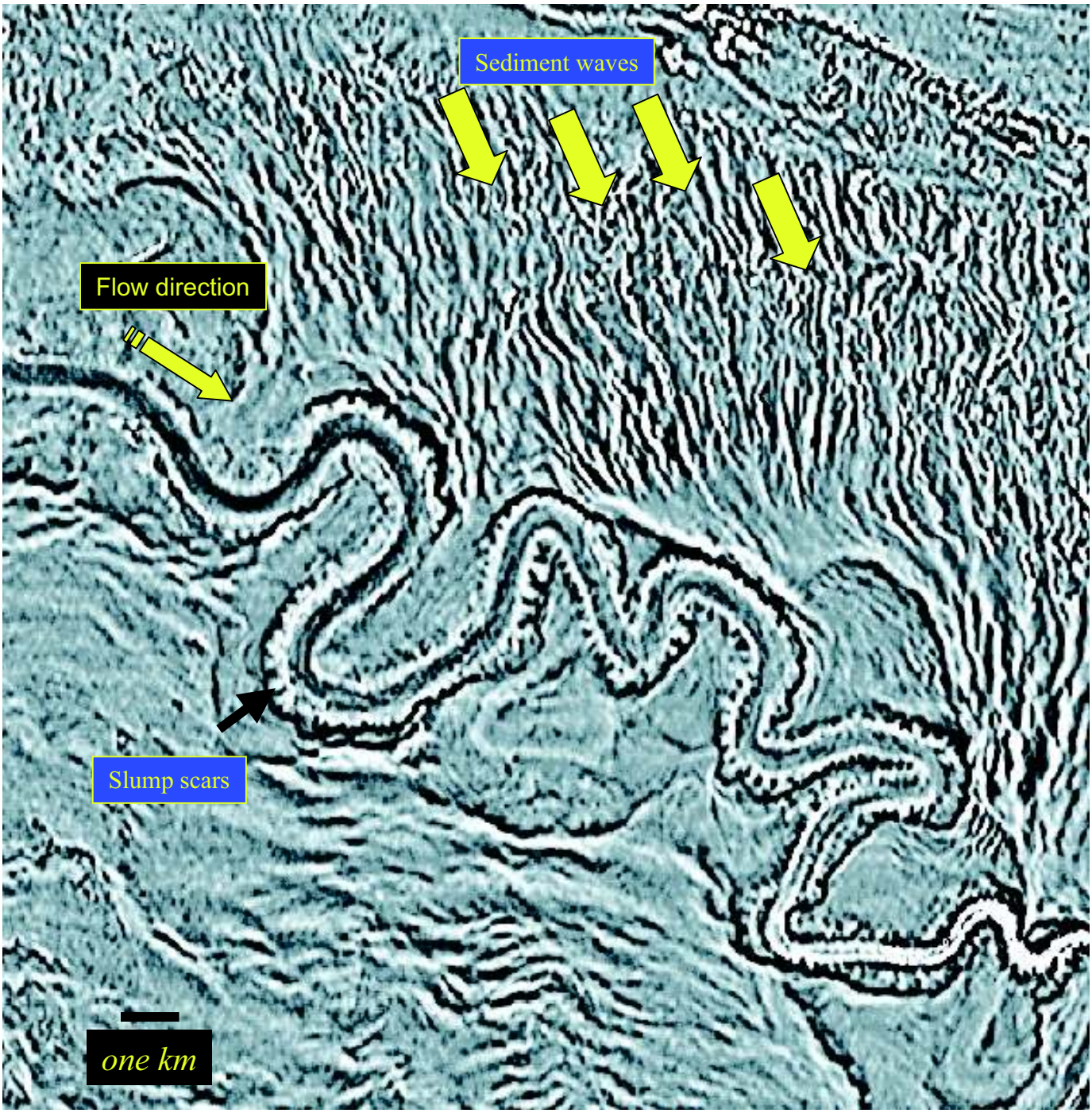

FIG. 80.—Sediment waves in the overbank of the Joshua channel, eastern Gulf of Mexico, shown on a curvature map extracted from the upper bounding surface of the channel–levee complex. Note also the small-scale slump scars on the inner levee. Seismic data courtesy of WesternGeco.

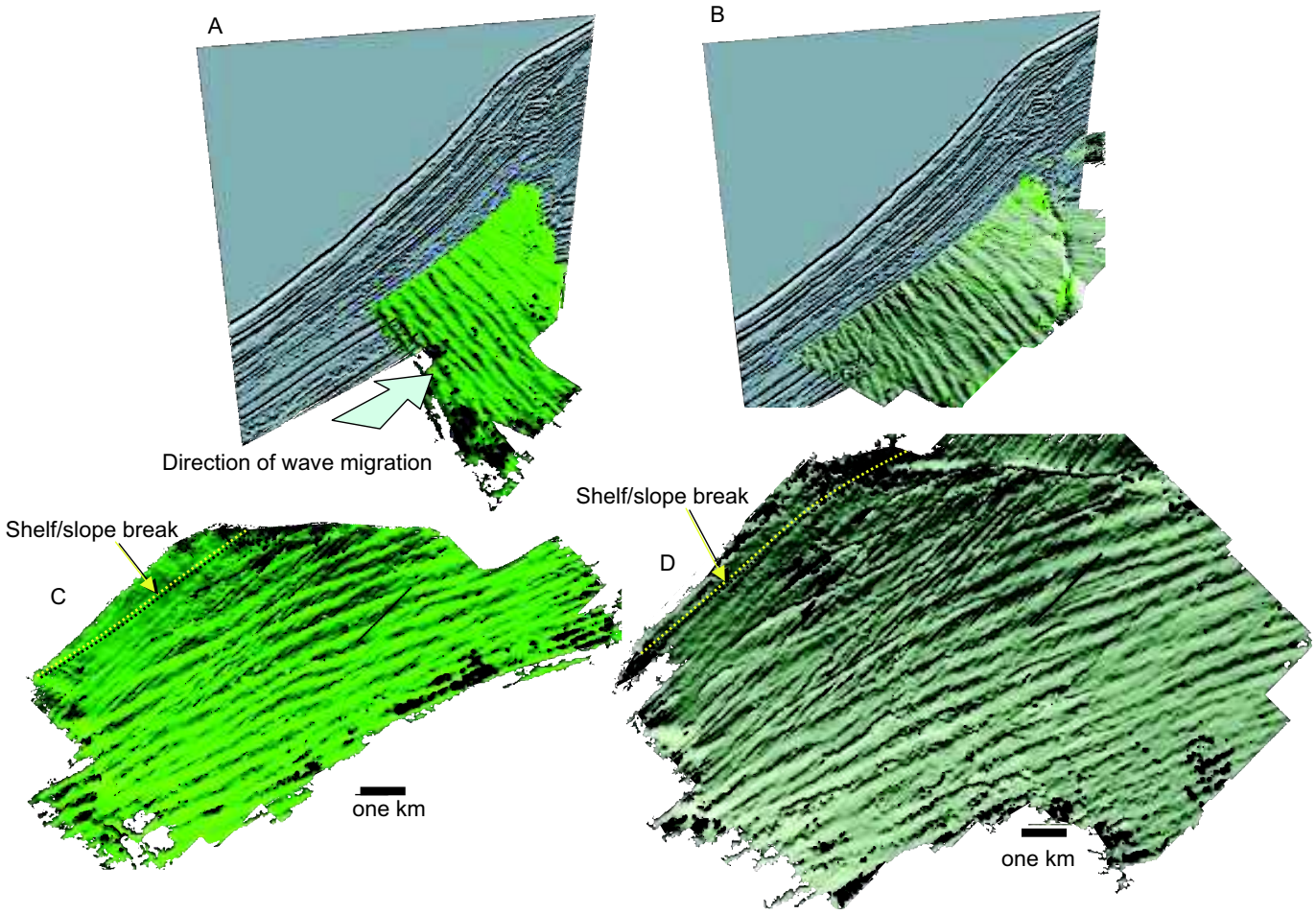

FIG. 81.—Sediment waves on the middle to upper slope of the eastern Gulf of Mexico. These waves appear to be migrating obliquely upslope. They are not associated with any nearby channel or canyon. Wavelength ranges from 400 to 600 m and wave amplitude ranges from 5 to 10 m. Seismic data courtesy of VeritasDGC.

FIG. 82.—Outcrop of Cretaceous Chatsworth Sandstone on north side of Highway 118, Santa Susana Pass, California. Note subtle changes in bed thickness and sand/shale ratio from highway to skyline.

FIG. 83.—Sharp-based (yellow arrow), thick-bedded sandstones, with one prominent amalgamation surface (red arrow). The irregular horizontal marks were made by an excavator! Total thickness of structureless sandstone about 3 m. This photograph was taken about 20 years ago at the back of a trailer park—it is unlikely that the outcrop still exists; if it does it is probably overgrown. Chatsworth Sandstone near Chatsworth, California.

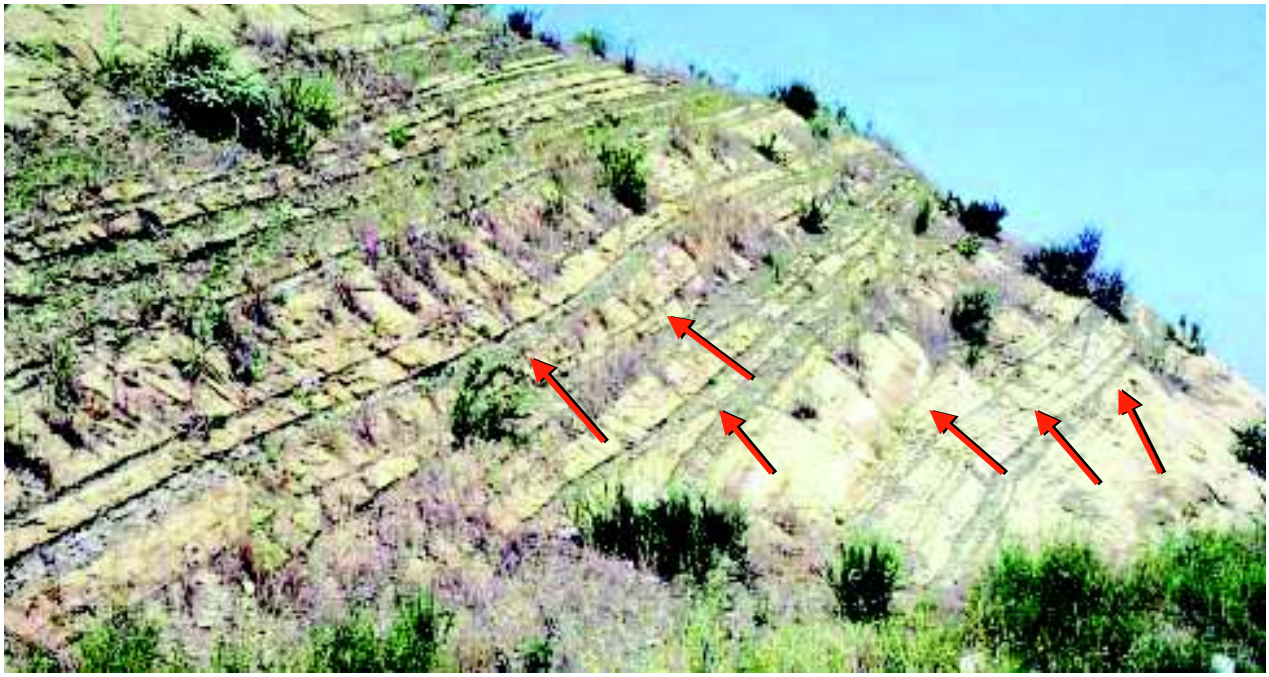

FIG. 84.—Interbedded sandstones and mudstones in the Chatsworth Sandstone, stratigraphically a few meters above the structureless sandstones of Figure 83. Note the lenticularity of many of the beds (arrows). Thickness of section about 5 m.

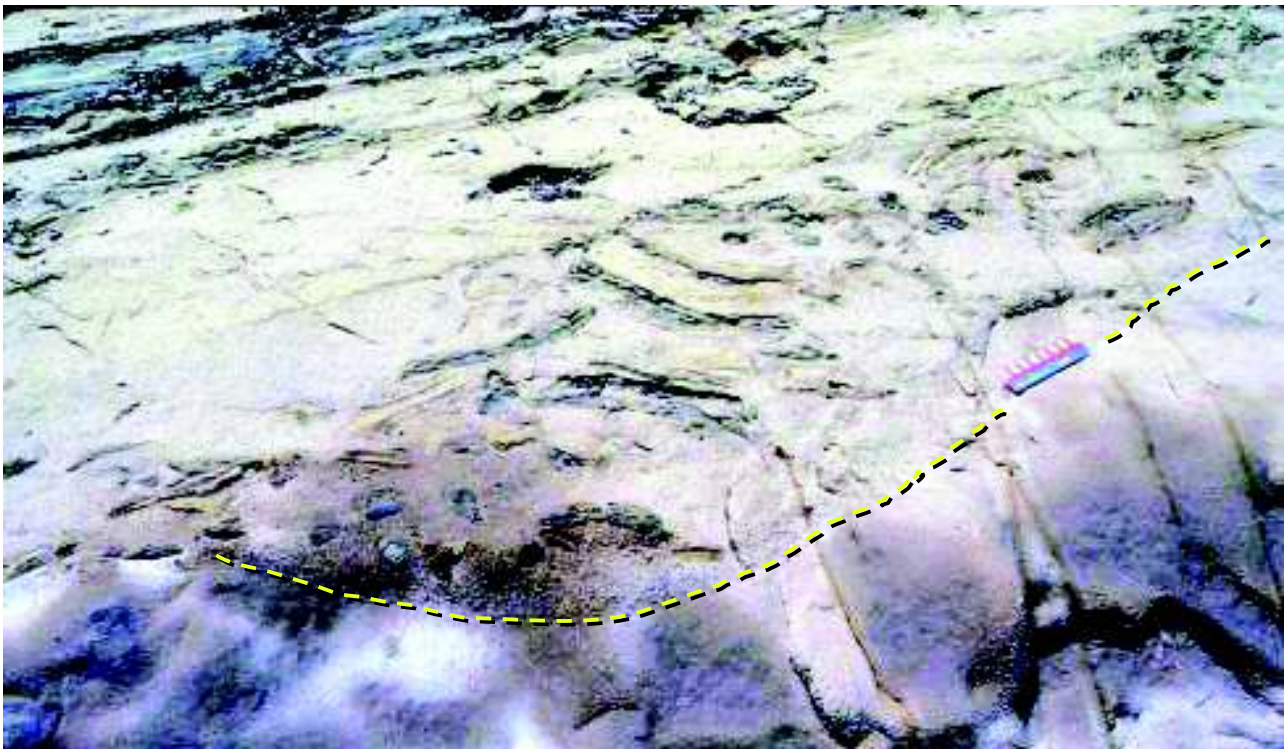

FIG. 85 (above).—Scour outlined in yellow, with coarser-grained structureless sandstone fill and abundant ripped-up mudstones clasts. Chatsworth Sandstone near Chatsworth, California.

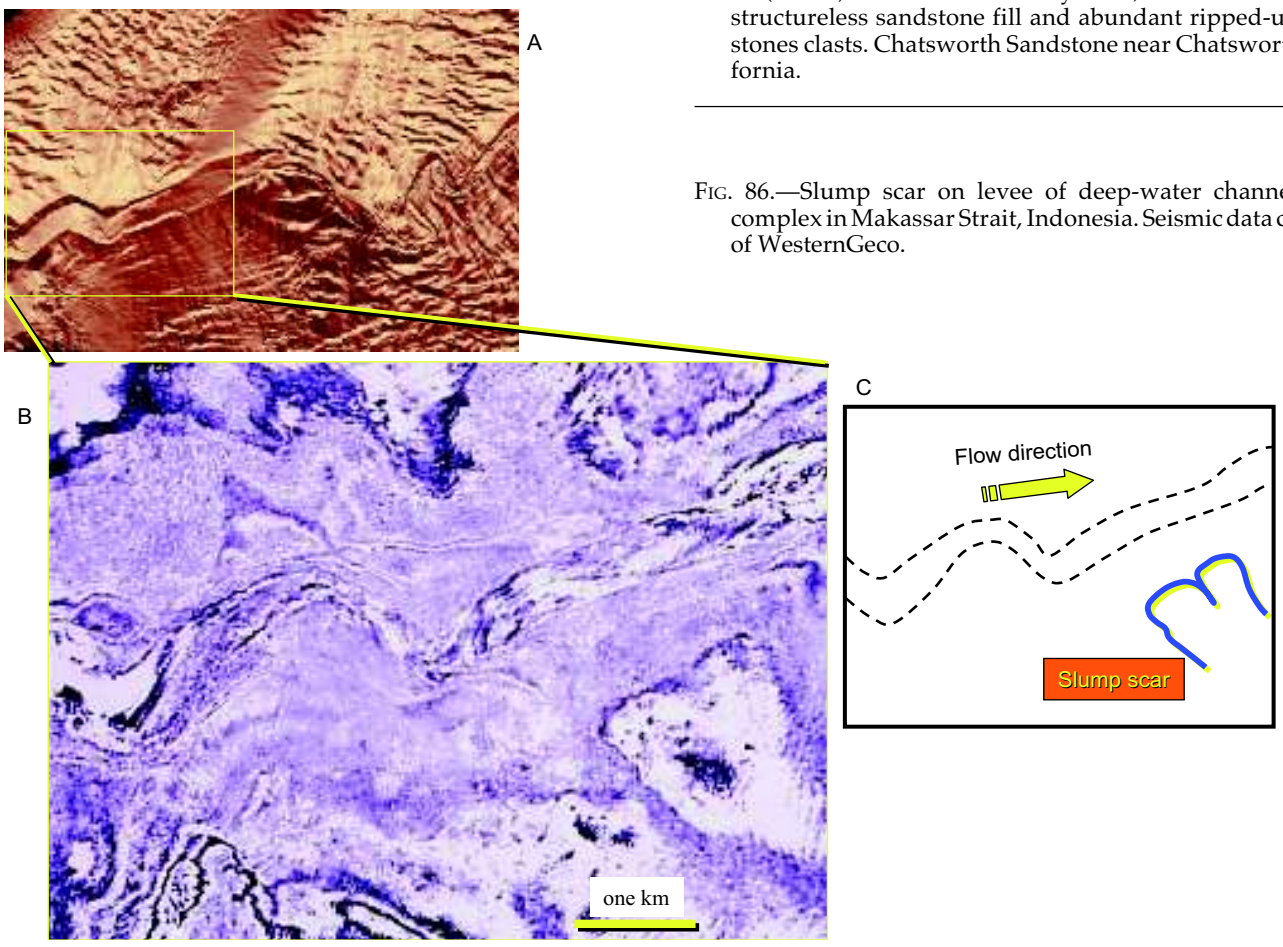

FIG. 86.—Slump scar on levee of deep-water channel–levee complex in Makassar Strait, Indonesia. Seismic data courtesy of WesternGeco.

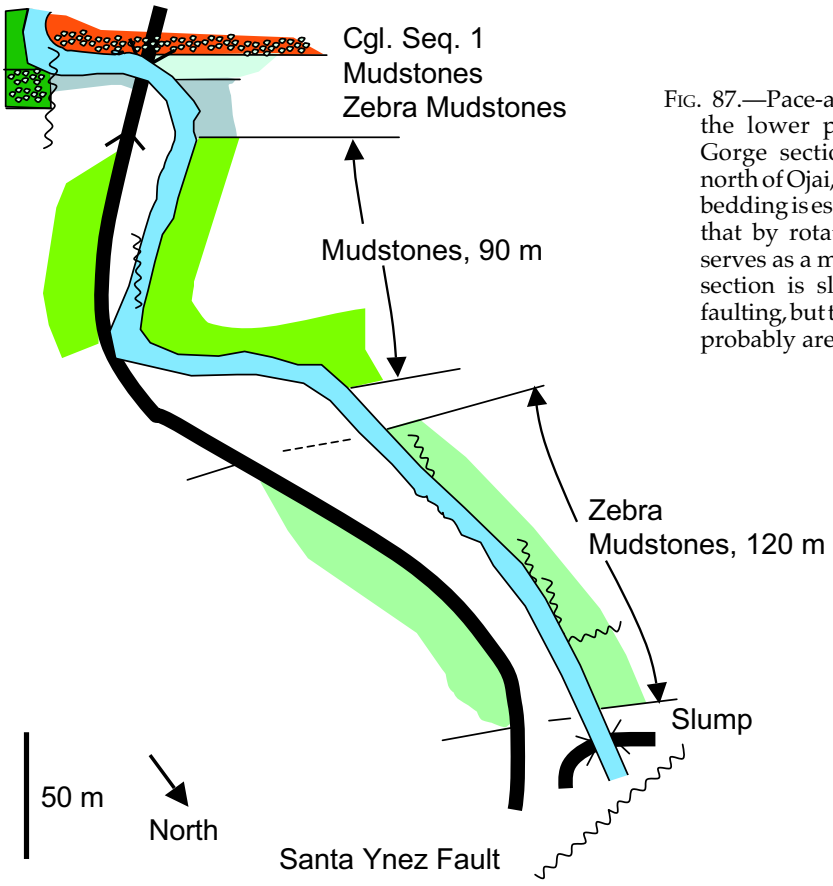

FIG. 87.—Pace-and-compass map of the lower part of the Wheeler Gorge section on Highway 33, north of Ojai, California. Note that bedding is essentially vertical, and that by rotating the map it also serves as a measured section. The section is slightly disrupted by faulting, but the thicknesses shown probably are fairly close.

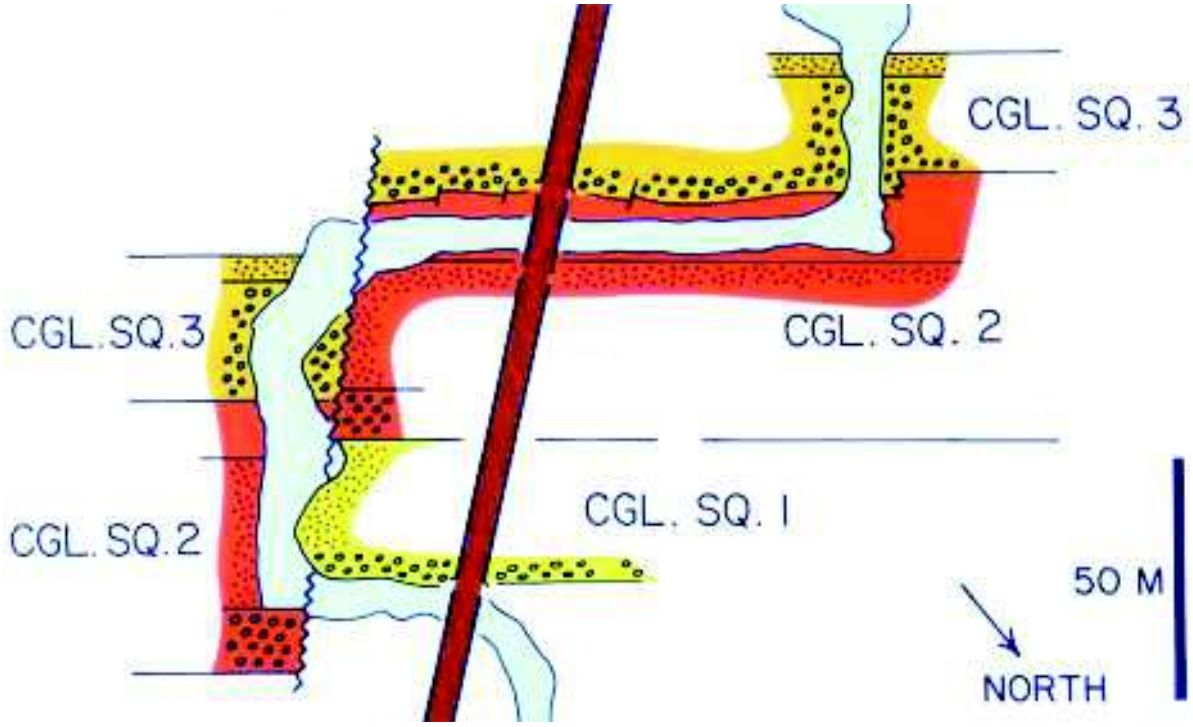

FIG. 88.—Pace-and-compass map of the central channel complex at Wheeler Gorge, California. The channel complex can be divided into three separate conglomerate sequences, interpreted as one channel fill.

stones and mudstones with abundant soft-sediment deformation (more than 120 m thick; Fig. 89).

The zebra-striped mudstones consist almost entirely of color-graded siltstones 1 to 2 cm thick alternating with mudstones (Fig. 90). Right at the base, these beds are slumped in a section some 5 meters thick. The entire package is faulted, but it is estimated that there are about 5500 of the graded siltstone beds. None of the characteristics of levee deposits is present (i.e., no climbing current ripples, no mud rip-up clasts, etc.); the depositional environment is postulated to be very distal—either at a fan fringe or lateral but very distal to a channel.

The central section comprises three stacked conglomerate-to-sandstone packages. The base of the first sharply overlies the zebra-striped mudstones and is characterized by large flute casts (Fig. 91) and associated groove casts, some of which retain pebbles at the ends of the grooves. There are also abundant ripped-up clasts of the zebra mudstones within the basal channel fill (Fig. 92). This lowest package is about 25 m thick, and it consists of conglomerates and interbedded structureless sandstones and is interpreted as channel fill. The conglomerates are characterized by abundant mudstone clasts, probably derived from adjacent channel walls. The second package is approximately 50 m thick. There is a basal conglomerate, but the bulk of the succession consists of graded conglomerate–sandstone beds (Fig. 93) and graded pebbly sandstones (Fig. 94). The uppermost part of this package overlies these channel-fill deposits and comprises a 15-m-thick succession of thin-bedded turbidites and mudstones. Convolute lamination (Fig. 95), bedding lenticularity (Fig. 96), and minor erosion surfaces (Fig. 96) with small ripped-up mudstone clasts suggest that this is a channel-margin or back-of-levee facies.

As mentioned above, context is one of the most important characteristics that allow architectural elements to be assigned to depositional environments. The interbedded sandstones and mudstones directly overlie the graded coarser facies of the channel fill. If the channel had migrated laterally, shifting the main coarse-sand depocenter elsewhere, the channel margin could migrate over the channel fill. A seismic example of this relationship is shown in Figure 64B.

The third conglomerate-to-sandstone package is about 30 m thick, and consists of conglomerates (25 m) that grade into structureless sandstones (5 m) (Fig. 97). These are in turn overlain by thin-bedded classical turbidites (Fig. 97). The base of this package is spectacular, and erodes about 5 m into the underlying beds. Large stratified sandstone–mudstone clasts have been ripped from the channel wall and deposited in the channel, with a sand and conglomerate matrix (Fig. 98). Conversely, coarse sand from the channel has been injected into the beds of the channel wall as sills (Fig. 99)—the sill in this photograph terminates abruptly, but smaller sills splay from the top and bottom of the main sill. In places, the sills feed dikes, clearly showing that these coarse deposits are not original beds in the channel wall. Well developed sills and dikes have also been documented in the subsurface (the Tertiary Alba Field in the North Sea; Hurst et al., 2005) as well as in outcrop (Surlyk and Noe-Nygaard, 2003; Hurst et al., 2005).

The uppermost part of the section exposed in Wheeler Gorge consists of about 120 m of interbedded sandstones and mudstones. The lower 80 m consists of classical turbidites, with beds averaging about 10 cm in thickness. Overall, there is a thinning-upward succession. Individual beds have small ripped-up mudstone clasts, and convolute lamination is common. There is no soft-sediment deformation. The upper 40 m contains similar

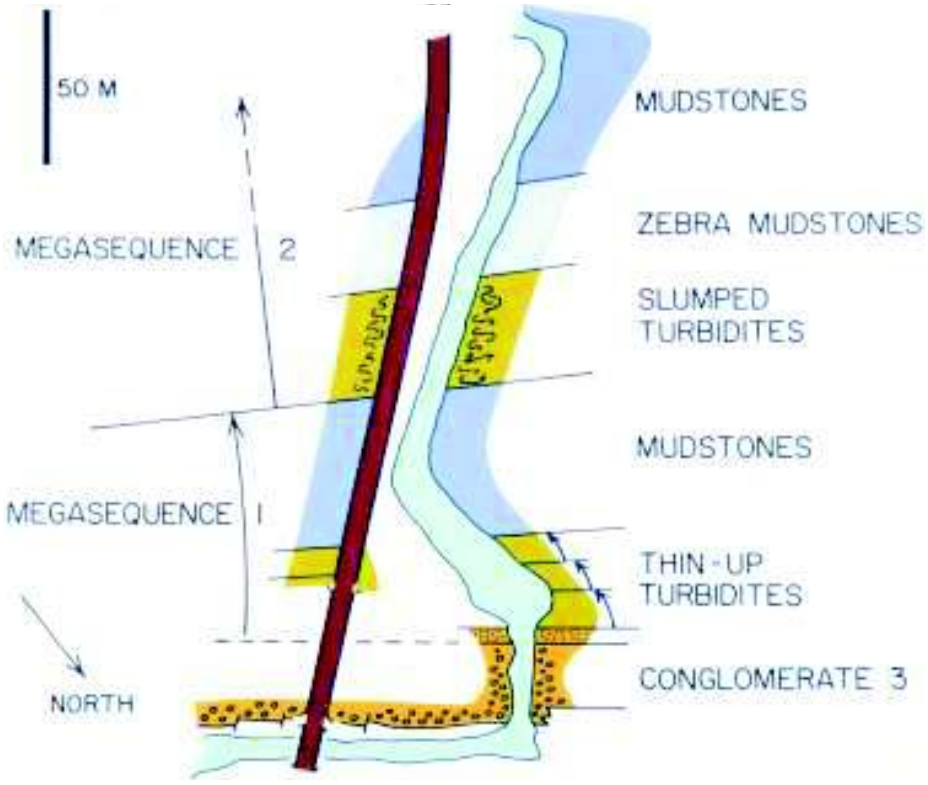

FIG. 89.—Pace-and-compass map of the section above the channel complex at Wheeler Gorge, California. Two separate levee complexes have been identified (both within the slumped turbidites).

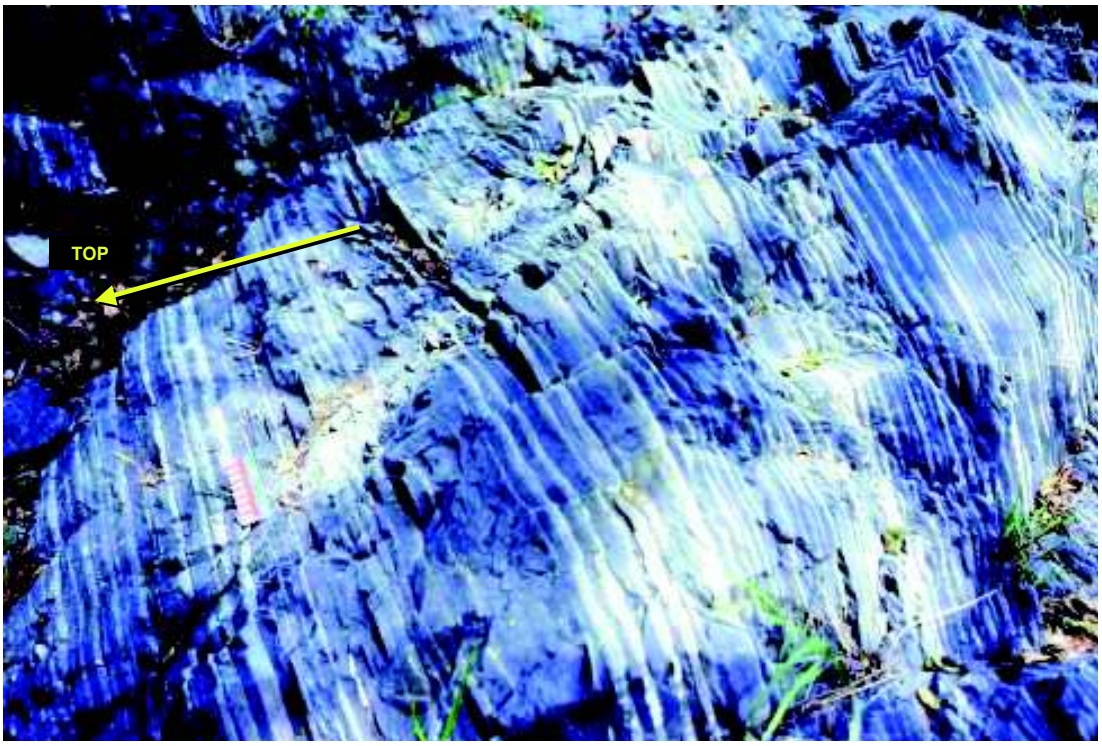

FIG. 90 (above).—Very thin-bedded "zebra-striped" mudstones below the main channel complex (Fig. 87) at Wheeler Gorge, California. The striped appearance is the result of the stacking of a large number of thin graded siltstone (pale) to mudstone (dark) beds. Flat lamination and ripple cross lamination are rare.

classical turbidites, but soft-sediment deformation is abundant. A few beds a meter or so in thickness are completely disrupted, but more commonly the deformation is restricted to a few beds that show distinct soft-sediment folds (Figs. 100, 101). Convolute lamination is also present, and in places there are distinct trends in bed thickness—two thinning-upward successions, one thickening-upward succession, and one thickening-to-thinning upward succession.

The sedimentary folds involving one or two beds, and the presence of convolute lamination, suggest that these thin-bedded turbidites are channel-margin or levee deposits. Unlike the channel-margin deposits described above, these thin-bedded turbidites are not closely associated with thick, coarse-grained channelized deposits. They are interpreted to represent back-of-levee deposits associated with a channel system different from that described above—a channel that is not exposed at Wheeler Gorge (Fig. 102).

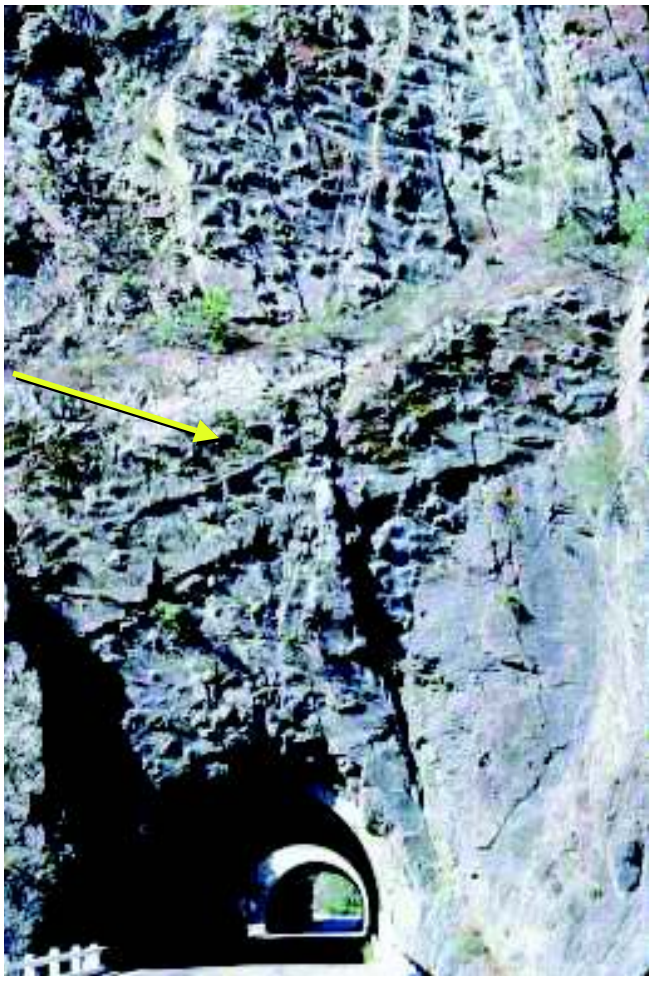

→

FIG. 91.—Large flute casts on the base of the lowest conglomerate sequence (Fig. 87), Wheeler Gorge, California. The bed is vertical, flow direction is shown by the yellow arrow, and the highway tunnel gives the scale.

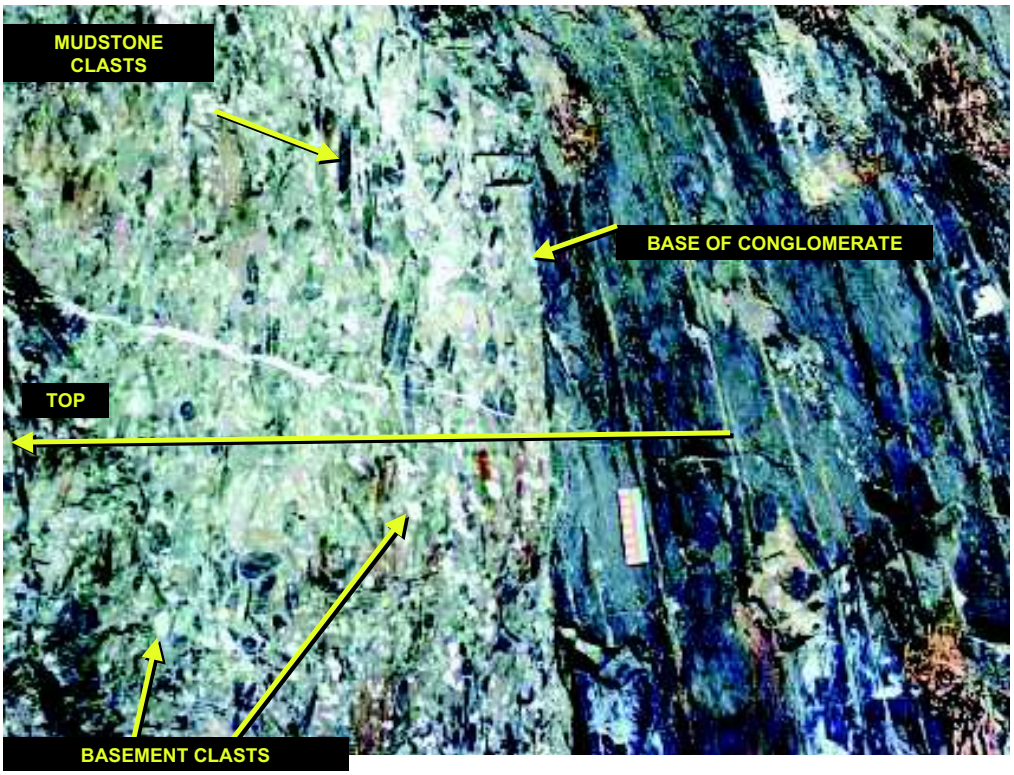

FIG. 92.—Very sharp base of conglomerate sequence 1 on the underlying zebra-striped mudstones. Note pale-colored basement clasts and abundant ripped-up mudstone clasts.

FIG. 93.—Graded conglomerate-to-sandstone bed, as part of the fill of conglomerate sequence 2 (Fig. 88), Wheeler Gorge, California.

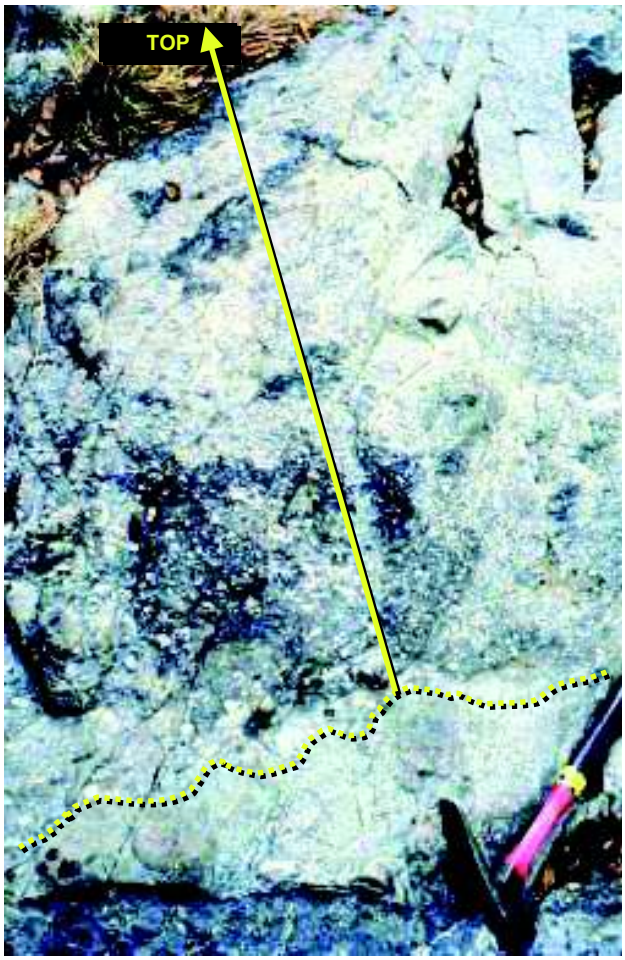

←

FIG. 94.—Graded pebbly sandstone, part of conglomerate sequence 2 (Fig. 88). Irregular base shown by yellow dotted line. Wheeler Gorge, California.

Outcrop Example of Levee Failure—New Zealand.—

Probably the best example of levee failure and collapse is in the Waitemata Group (Eocene, New Zealand; Ballance, 1964). The large-scale soft-sediment deformations have been described by Gregory (1966). The best outcrop is on Whangaparaoa Head, where there is about 4 km of continuous coastal exposure in high cliffs. The facies consists dominantly of thin-bedded classical turbidites, with soft-sediment folding occurring on many different scales. Some of the deformation consists of stacked disharmonic folds that can be seen in the cliff (Fig. 103) and on the wave-cut platform (Fig. 104). In other places, entire sections of turbidites appear to have been rotated, as in Figure 105, where the regional dip of the Waitemata Group is only 20 degrees. The beds in this rotated section contain CCC turbidites (Fig. 106) and slumps involving one or two beds (Figs. 25, 107); both of these features strongly suggest a levee origin for the thin-bedded turbidites, and hence a levee-failure origin for the disharmonic folding and rotation. Locally, sections of thick-bedded turbidites suggest associated channel fills (Figs. 108, 109).

FIG. 95 (below).—Convolute lamination in the uppermost part of the fill of conglomerate sequence 2 (Fig. 88), Wheeler Gorge, California.

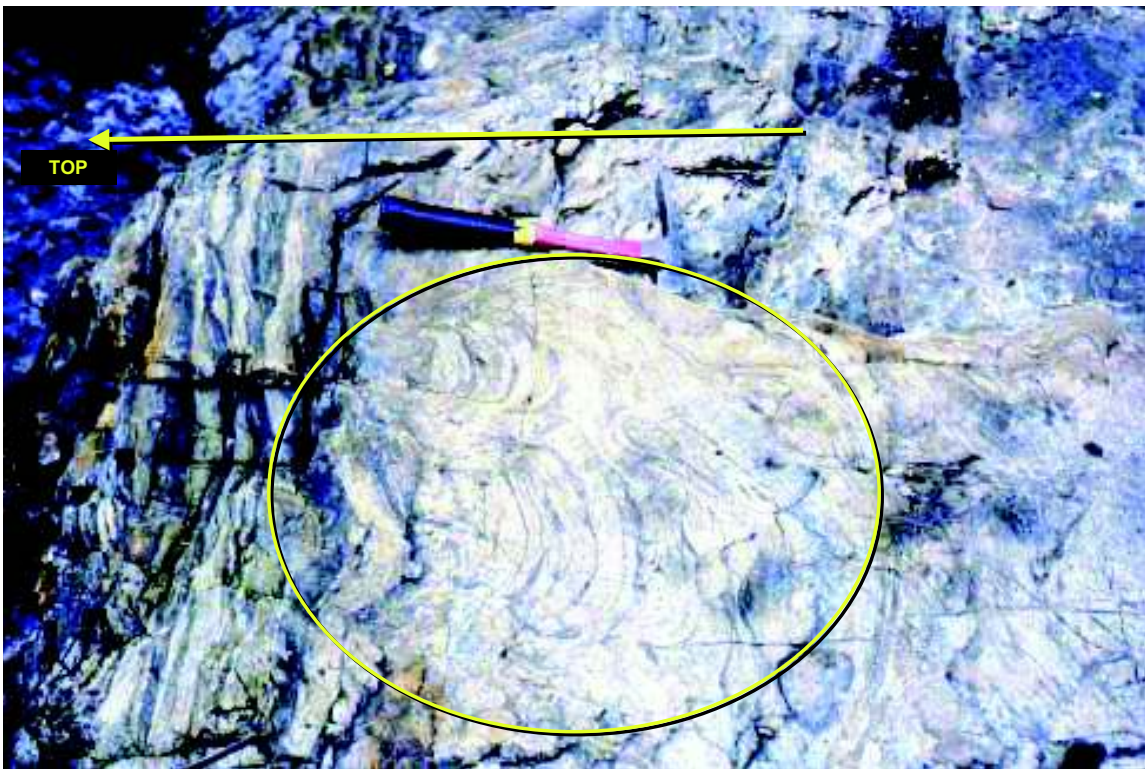

FIG. 96.—Bedding lenticularity (red arrow) in the interbedded sandstones and mudstones, uppermost part of conglomerate sequence 2 (Fig. 88). Yellow dotted line shows scouring and more bed lenticularity. Wheeler Gorge, California.

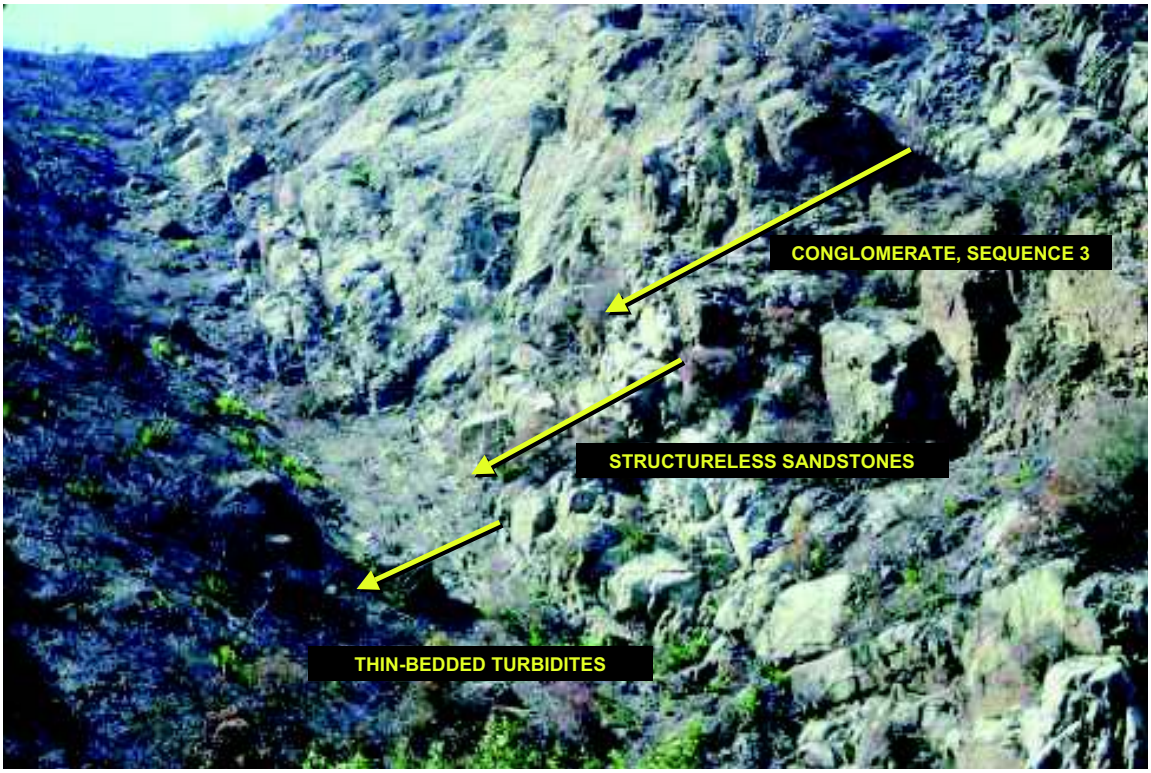

FIG. 97.—Overview of conglomerate sequence 3 (Fig. 88) after a forest fire. Note overall change from conglomerate, via structureless sandstone, into classical turbidites. Section is about 30 m thick. Wheeler Gorge, California.

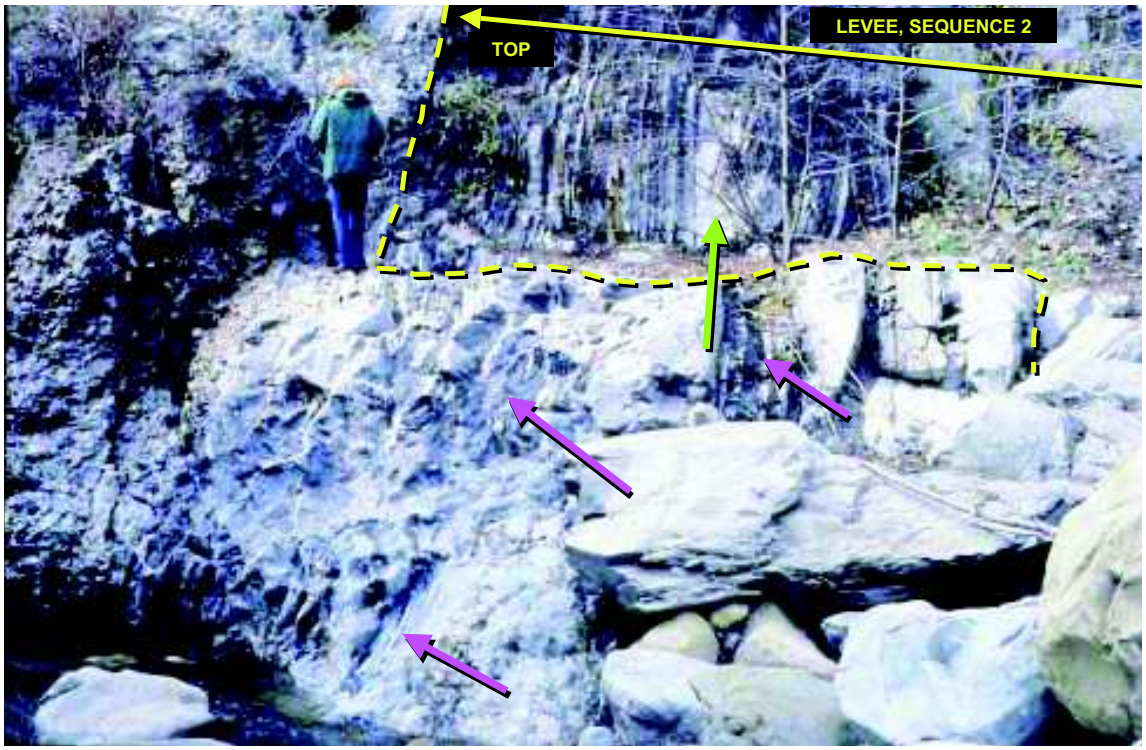

FIG. 98 (above).—Base of conglomerate sequence 3 (Fig. 88), shown by yellow dotted line. Conglomerate cuts into levee deposits of sequence 2 (yellow arrow). Channel fill consists of basement clasts, as well as stratified clasts plucked from the channel wall (pink arrows). Green arrow shows a sill of coarse sandstone injected into the fine-grained levee deposits. Wheeler Gorge, California.

Crevasse Splays

Another form of overbank deposit is the crevasse splay. In contrast with sediment waves, which are associated with flow *over* the levee crest and onto the overbank, the crevasse splay is associated with flow *through* the levee and into the overbank environment. Because the crevasse splay involves flow through the levee, this flow taps deeper into the main flow than simple spillover flow, which taps only into the upper part of the flow. As a result, flow through a breach in the levee is sourced by the more sand-prone part of the main flow.

A typical crevasse splay is characterized by a short channel leading away from the main channel and feeding a smaller distributary channel system (Figs. 61, 110–112). Note the plan-view similarities between deep-water turbiditic and shallow-water, continental-shelf deltaic crevasse splays (Fig. 113). A crevasse splay can be considered a failed avulsion channel. The distinction is that, in the case of an avulsion channel, flow is permanently diverted through the crevasse and associated chan-

→

FIG. 99.—Sill of coarse sand and granules (see Fig. 98) injected into interbedded sandstones and mudstones of the wall of channel 3. Note very abrupt termination of the sill. Wheeler Gorge, California.

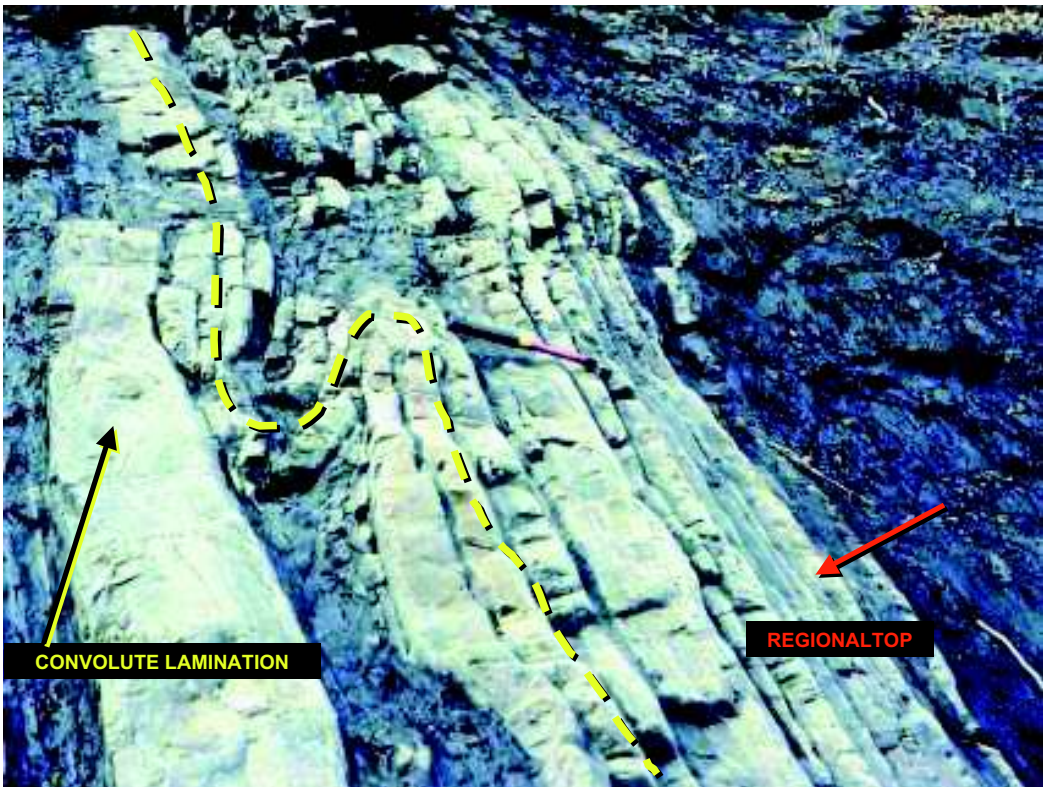

FIG. 100.—Distinct soft-sediment folds involving two beds, with undisturbed bedding above and below. Note convolute lamination in the uppermost bed of this small thickening-upward succession. Levee facies (Fig. 89) above the channel complex in Wheeler Gorge.

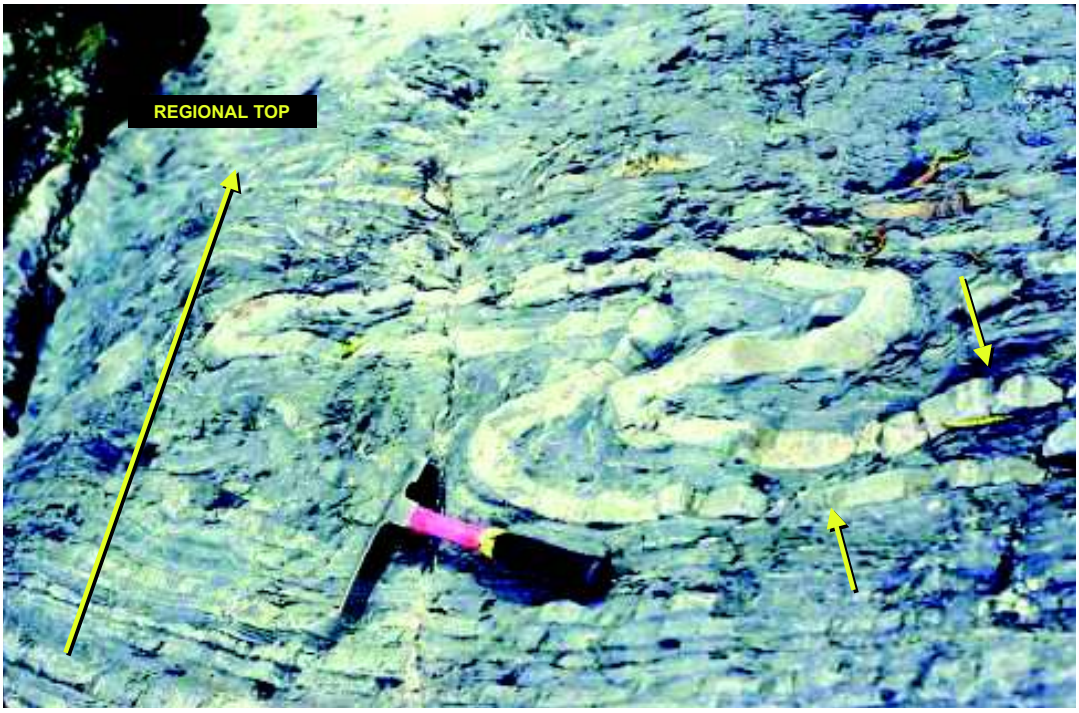

FIG. 101.—Re-folded fold involving one bed in an otherwise well-stratified succession. Regional top shown by yellow arrow, and way-up of the folded bed is shown by yellow arrows. Levee facies (Fig. 89), Wheeler Gorge, California.

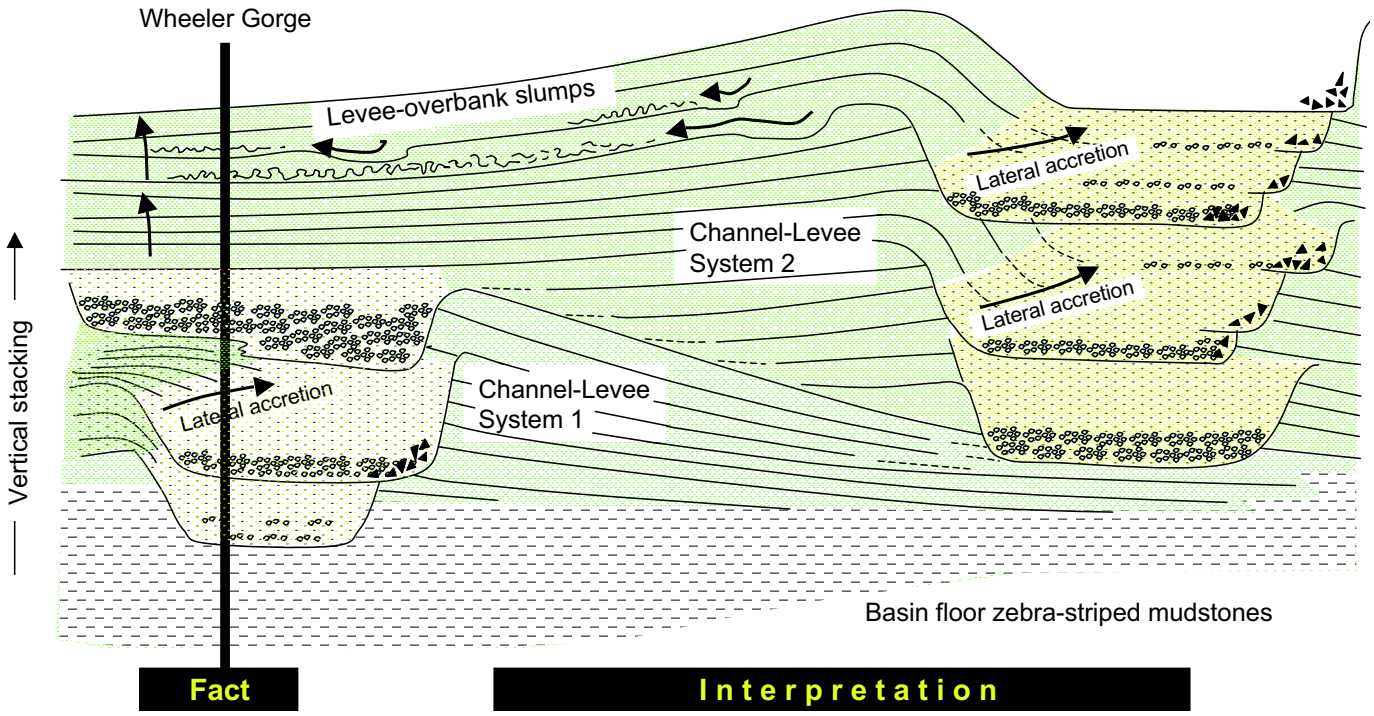

FIG. 102.—Interpretation of the Wheeler Gorge section. The vertical line ("fact") shows the location of the Wheeler Gorge section—the rest of the diagram is a reconstruction based on Wheeler Gorge data plus models derived from channel shingling patterns in fans such as the Amazon and the Rhone.

FIG. 103.—Large scale, disharmonically stacked soft-sediment folds in the Eocene Waitemata Group, Whangaparaoa Head, New Zealand. Cliff is about 30 m high.

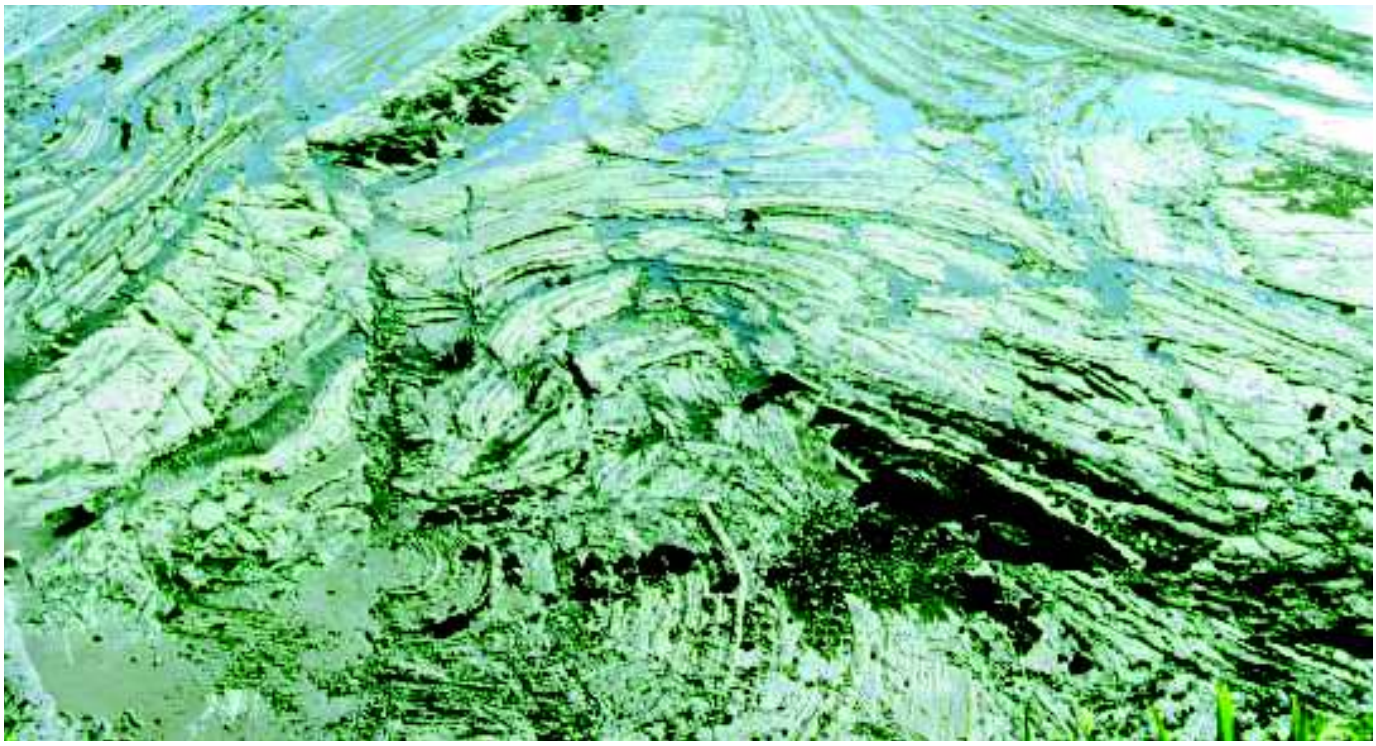

FIG. 104.—View from cliff down onto the wave-cut platform, showing disharmonic soft-sediment folding. Width of section at base of photo about 60 m.

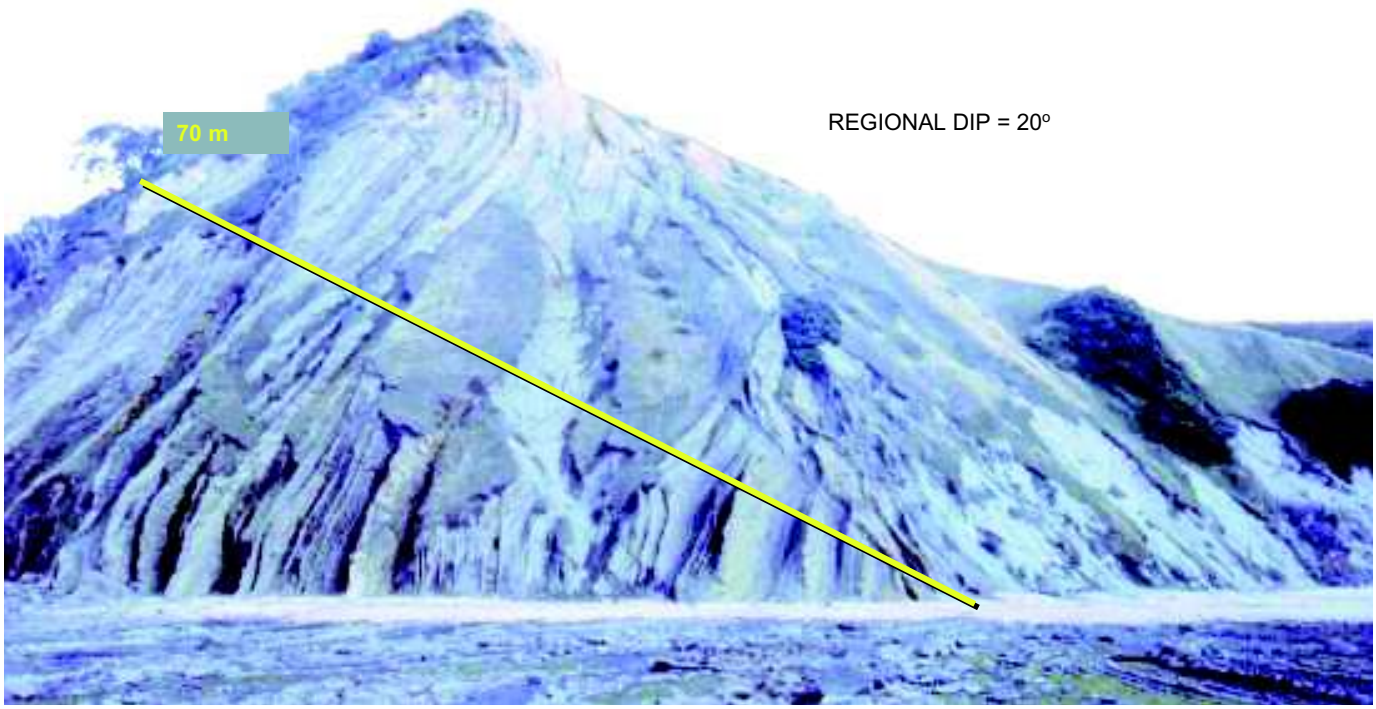

FIG. 105.—The Eocene Waitemata Group has a regional dip of about 20 degrees—this photograph shows a section some 70 m thick rotated by slumping to an angle of about 70 degrees. It lies just north of the disharmonic folds of Figure 101. The nature of the thin-bedded turbidites in this outcrop is shown in Figures 106 and 107.

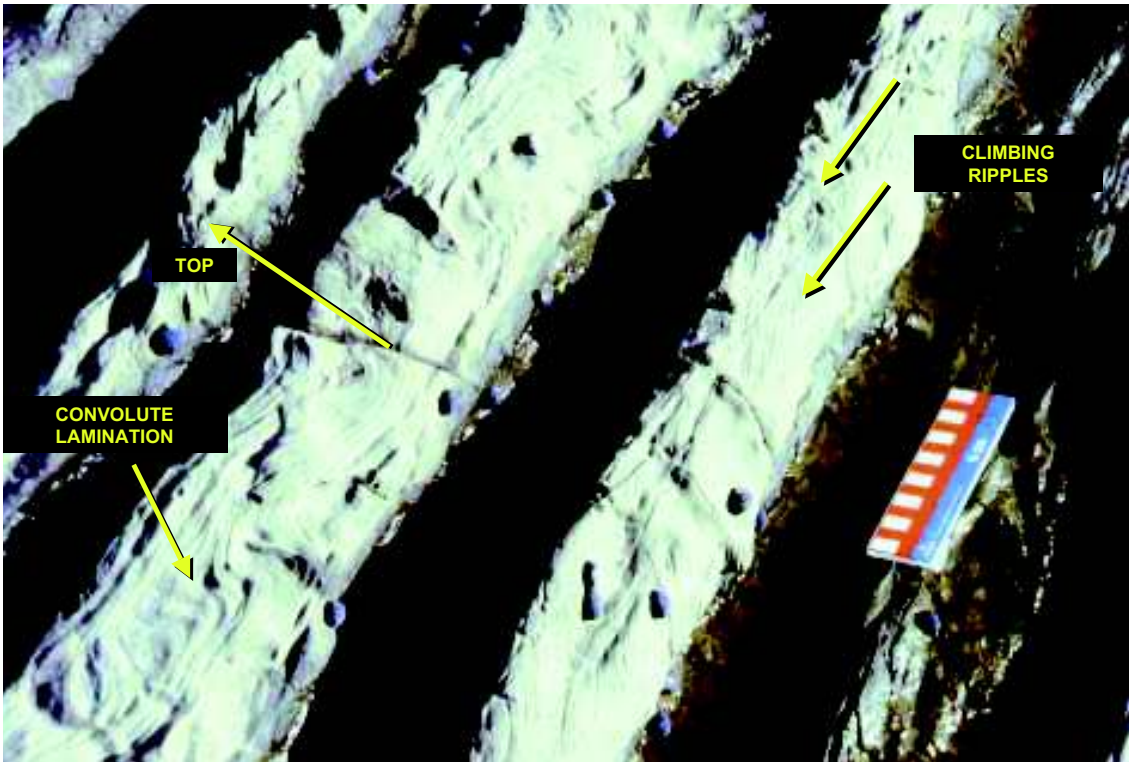

FIG. 106.—Thin-bedded turbidites with convolute lamination and climbing ripples, exposed on the wave-cut platform as part of the 70 m thick rotated section shown in Figure 105. Whangaparaoa Head, New Zealand.

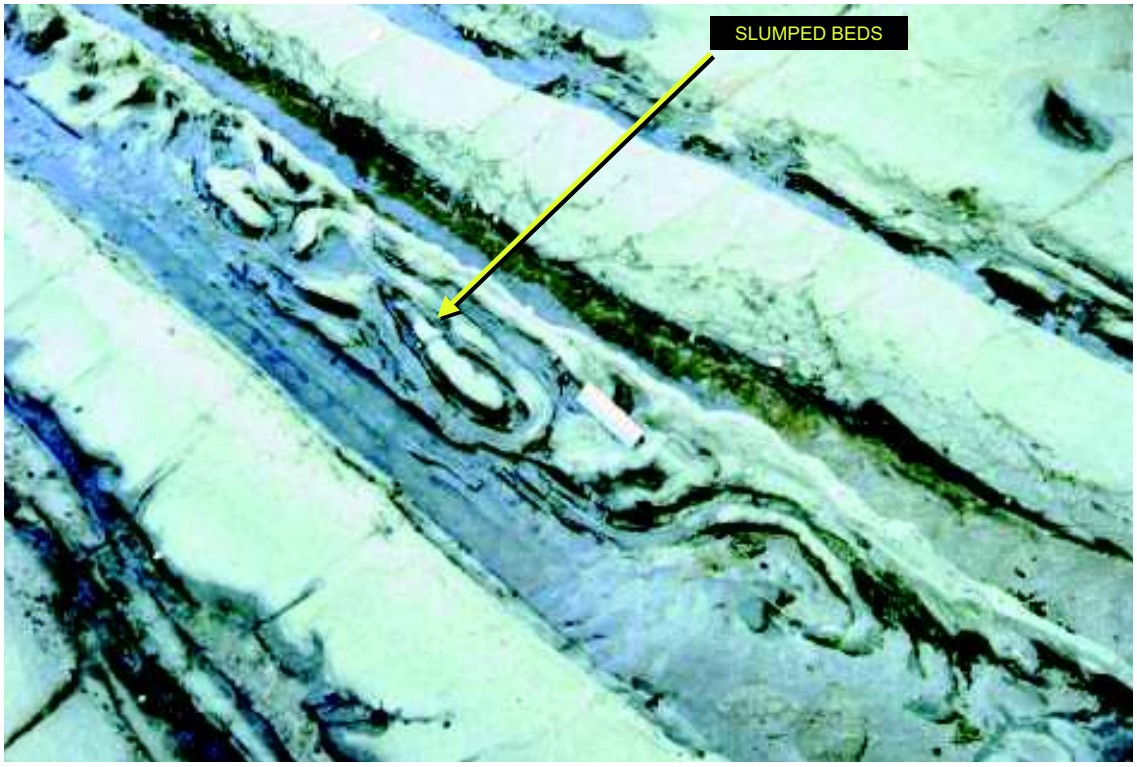

FIG. 107.—Thin-bedded turbidites, with one deformed horizon involving about 2 thin beds in a soft-sediment fold. Same location as Figure 105.

←

FIG. 108.—Thick-bedded turbidites in the Eocene Waitemata Group at Whangaparaoa Head, New Zealand. 15 cm scale is circled.

nel, whereas with the crevasse splay the flow diversion is temporary and relatively short-lived. In some instances, as revealed by 3D seismic data, the early stage of a crevasse splay is characterized by a levee breach that feeds a field of transverse sediment waves (Fig. 114). As the system becomes progressively better organized, the sediment waves are overlain by a gradually expanding distributary channel network (Posamentier and Kolla, 2003b; Van Wagoner et al., 2003). Channels within this distributary network are associated with low-relief, probably sand-prone levees.

The most distinctive sedimentary structure associated with crevasse-splay deposits is climbing current ripples. As with overbank sediment waves, flow expansion, which occurs when the confined flow within the main channel cuts through the levee and becomes unconfined within the overbank environment, results in rapid sedimentation from suspension. In addition, because of erosion through the levee, locally derived mud rip-up clasts can be common. The stratigraphic architecture of crevasse-splay deposits is characterized by amalgamated turbidites near the apex of the splay, becoming less amalgamated with distance away from the splay apex.

In general, crevasse splays are far more common in basin-floor environments than in slope environments. On the slope, gravity-flow vectors tend to be directed parallel to flow, down the

FIG. 109 (below).—Thick-bedded turbidites, with a suggestion of a thinning-upward succession, in the Eocene Waitemata Group, Whangaparaoa Head, New Zealand.

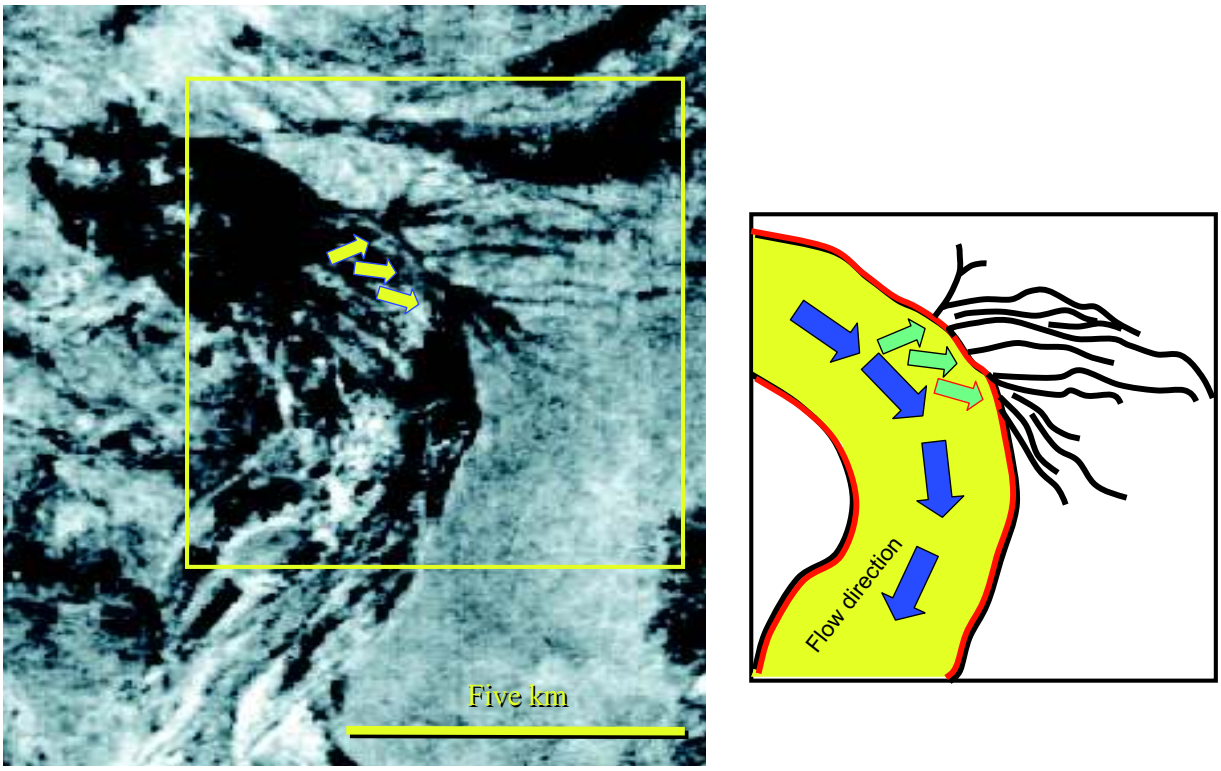

FIG. 110.—Seismic reflection horizon slice illustrating a crevasse splay associated with a channel–levee complex on the basin floor of the Gulf of Mexico. Note that several crevasses seem to have formed along this outer channel bend, feeding multiple small channels characterized by bifurcation. Seismic data courtesy of WesternGeco.

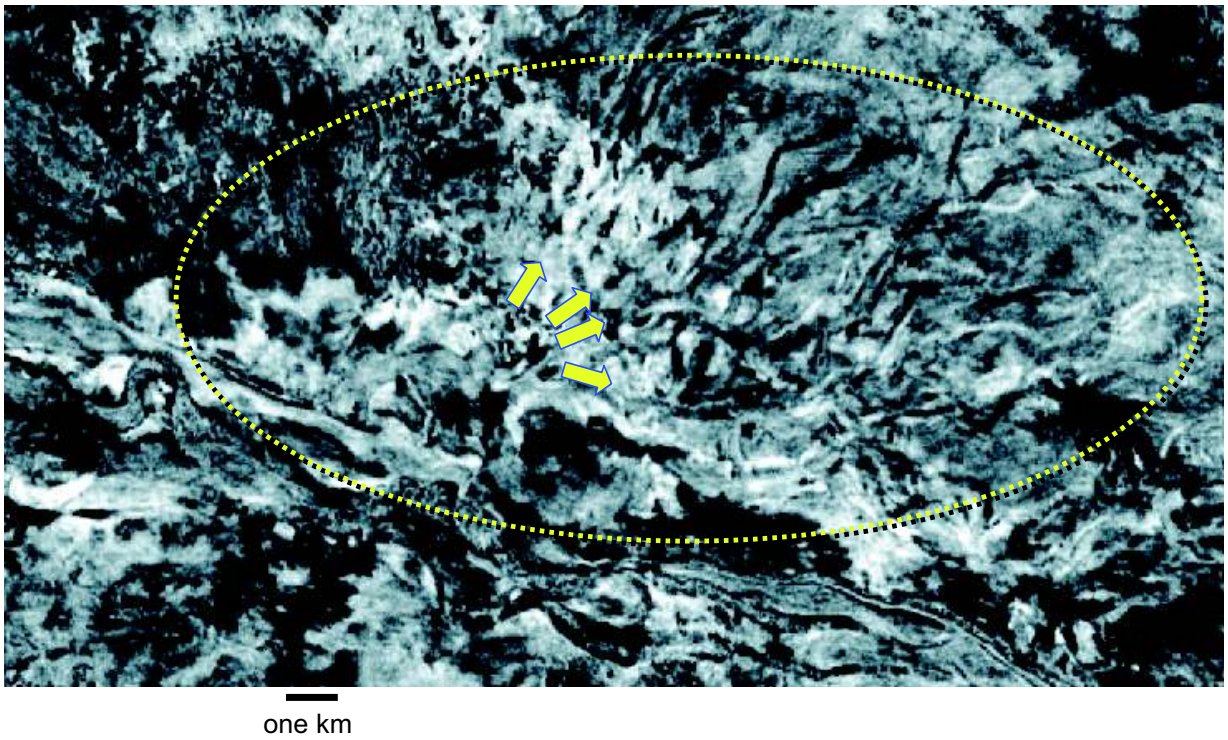

FIG. 111.—Seismic reflection horizon slice illustrating a crevasse splay associated with a channel–levee complex on the basin floor of the Gulf of Mexico. Seismic data courtesy of WesternGeco.

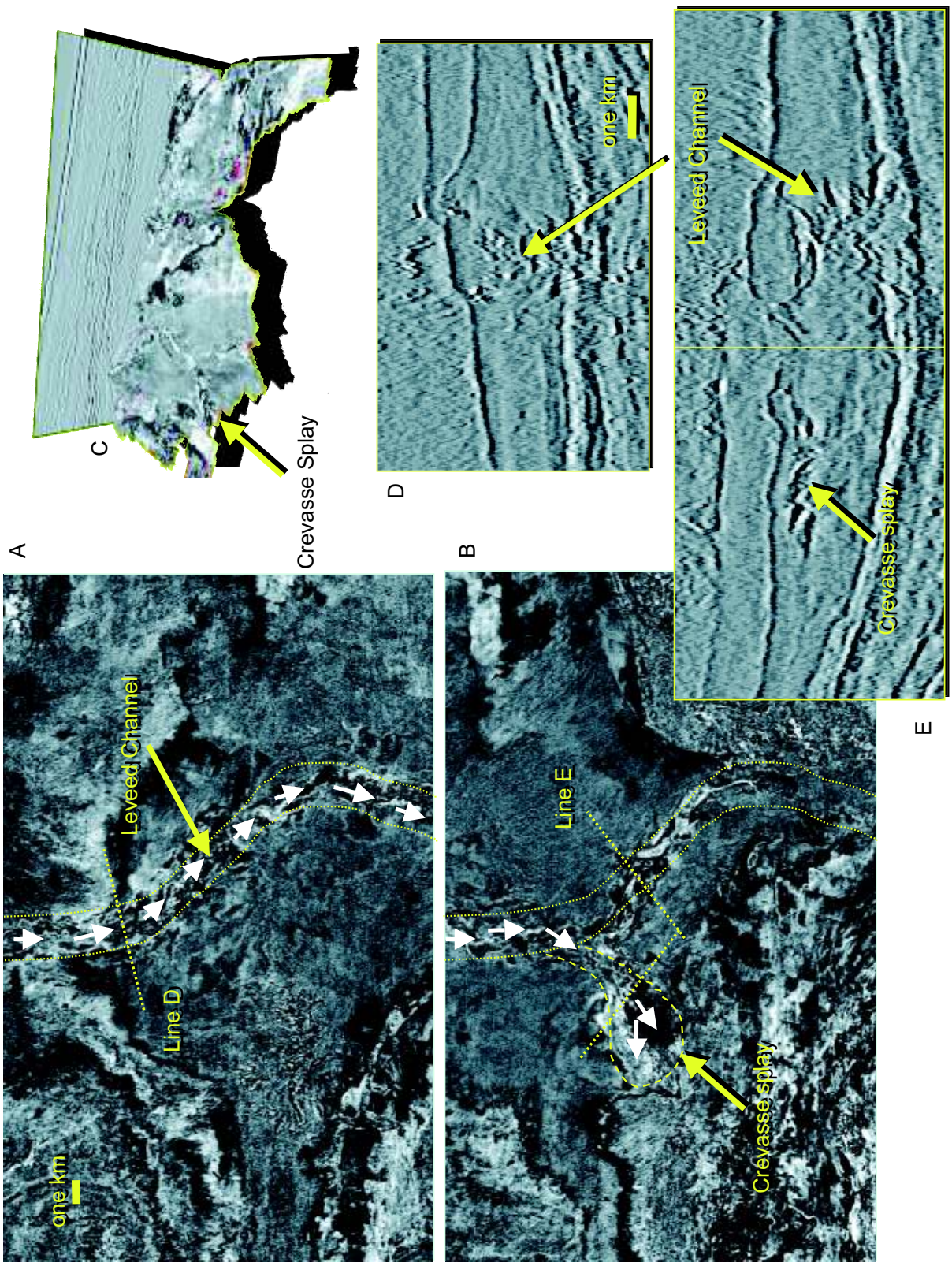

FIG. 112.—Crevasse splay associated with a basin-floor channel/levee complex, Gulf of Mexico. Seismic reflection horizon slices **A, B)** illustrate deeper and shallower slices through this system respectively. The crevasse splay is illustrated in perspective view in Part **C)** (see Fig. 61). Cross-section views through the principal channel **D)** and the crevasse splay **E)** illustrate the high-amplitude character of these depositional elements. The high-amplitude character suggests the presence of sand in these deposits. Seismic data courtesy of WesternGeco.

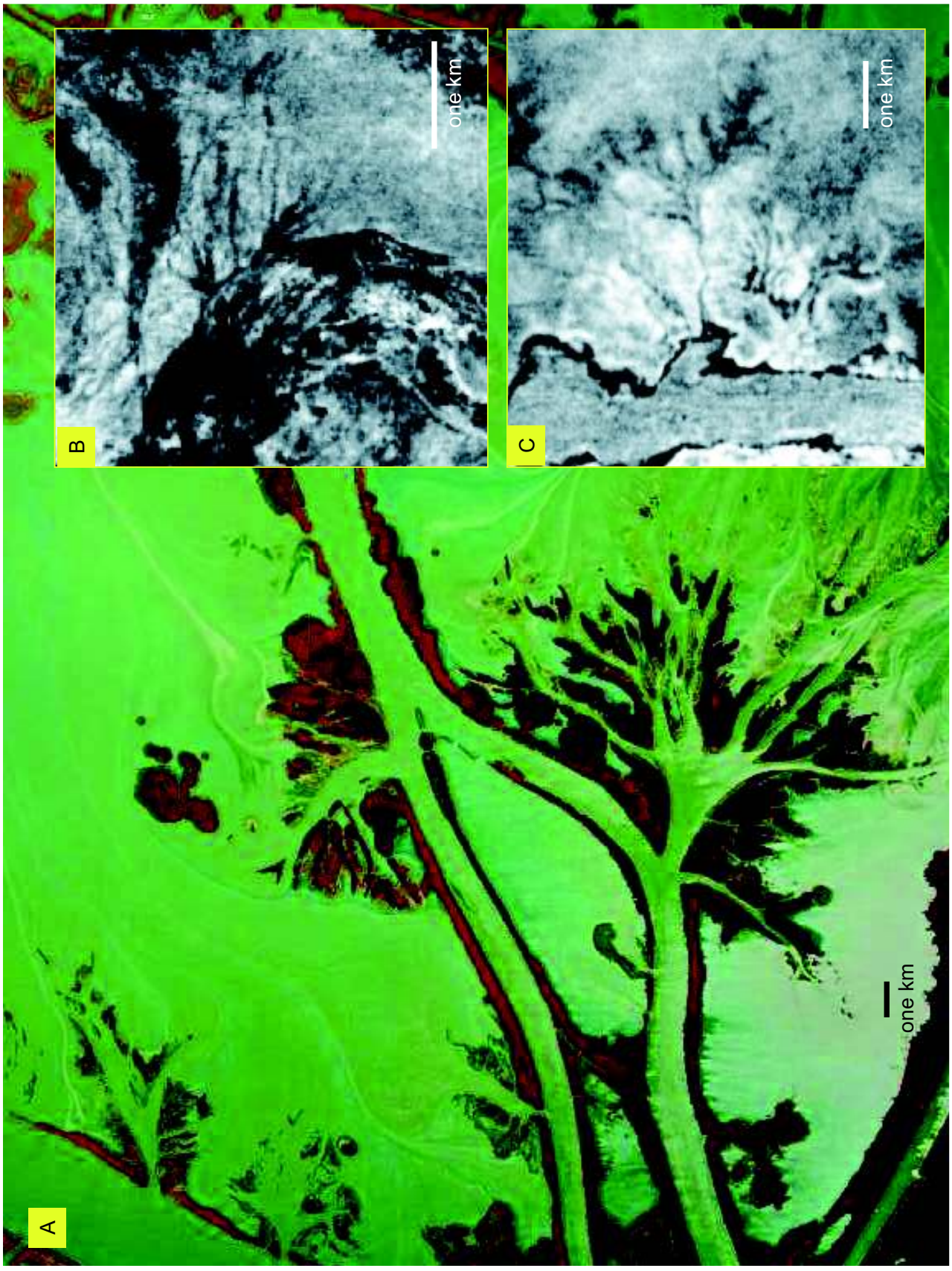

FIG. 113.—Comparison between **A)** a shallow-water deltaic crevasse splay (from the Mississippi River delta) and **B, C)** two deep-water crevasse splays (Figs. 110 and 114) suggesting a strikingly similar morphology and likely similar depositional processes. Seismic data courtesy of WesternGeco.

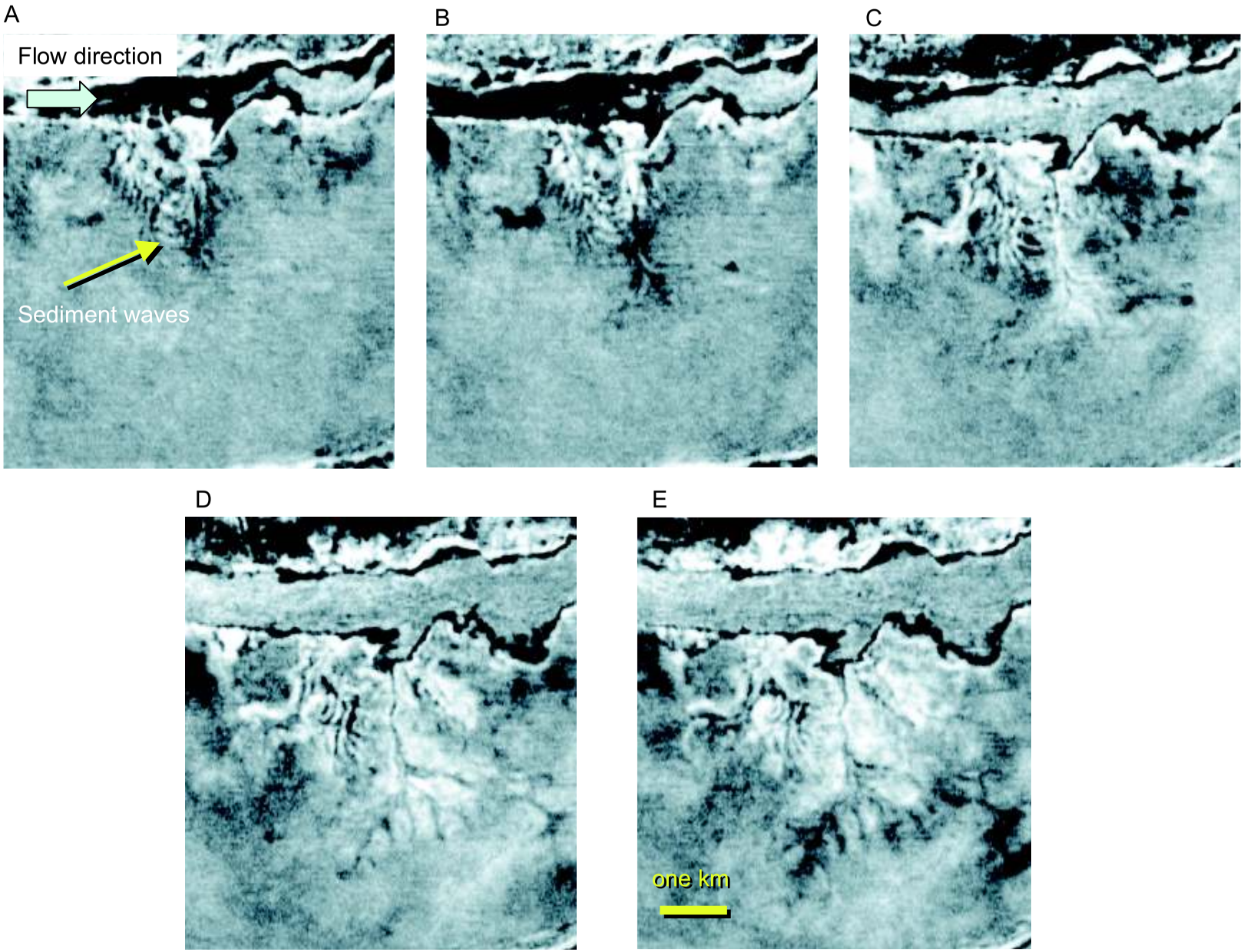

FIG. 114.—Seismic reflection horizon slices from base **A to top E)** showing the morphological evolution of a leveed-channel crevasse splay. Note that the early morphology appears to be characterized by transverse sediment waves as indicated by arrow (A). As the system evolves it appears to become better organized, developing a distributary pattern (B through E). Seismic data courtesy of WesternGeco.

relatively steep slope (i.e., slope angle commonly from 2 to 4 degrees), rather than normal to flow parallel to contour, thereby diminishing the likelihood that sufficient force is exerted on channel walls (i.e., levees) to form crevasses and hence crevasse splays. Consequently the crevasse-splay sand habitat is an uncommon element in slope settings.

Frontal Splays (i.e., Lobes)

Leveed channels commonly are associated with terminal lobes, or frontal splays (Figs. 115–120). The terms frontal splay, distributary channel complex, and lobe or lobeform can be used somewhat interchangeably. Each term describes a depositional element that lies at the end of a leveed channel and tends to be fan or lobe shaped in plan view. Each term implies a different perspective on this feature: (1) frontal splay has process significance, wherein a flow spreads out or expands, (2) distributary channel complex has map-pattern significance, wherein successive channel bifurcation results in a distributive channel network, and (3) lobe or lobeform has morphologic significance wherein the deposit has a fan-shaped or lobate planform.

As discussed above, frontal splays form at the *transition point*, the location where levee height is no longer capable of fully confining the sand-prone or high-concentration part of the turbidity flow. At that location the sand-prone part of the flow readily flows over the levee and establishes new courses on the associated overbank. Also at this location, the down-system trend towards increasing sand-to-mud ratio in the flow changes to a decreasing sand-to-mud ratio, as shown schematically in Figure 26. Up-system of the transition point mud is preferentially lost from the flow by overbank spillover, whereas down-system of the transition point sand is lost more rapidly from the flow by sedimentation in the overbank and within distributary channels.

Frontal splays have much in common with crevasse splays both sedimentologically and architecturally. Both are distinguished by relatively common current ripples and sheet-like bedding geometry with shallow channels and sand-prone, low-relief levees. Both tend to be more amalgamated near the splay apex and less so distally. Preservation of interbedded mudstones becomes progressively more common with increasing distance away from the transition point, which corresponds to the frontal

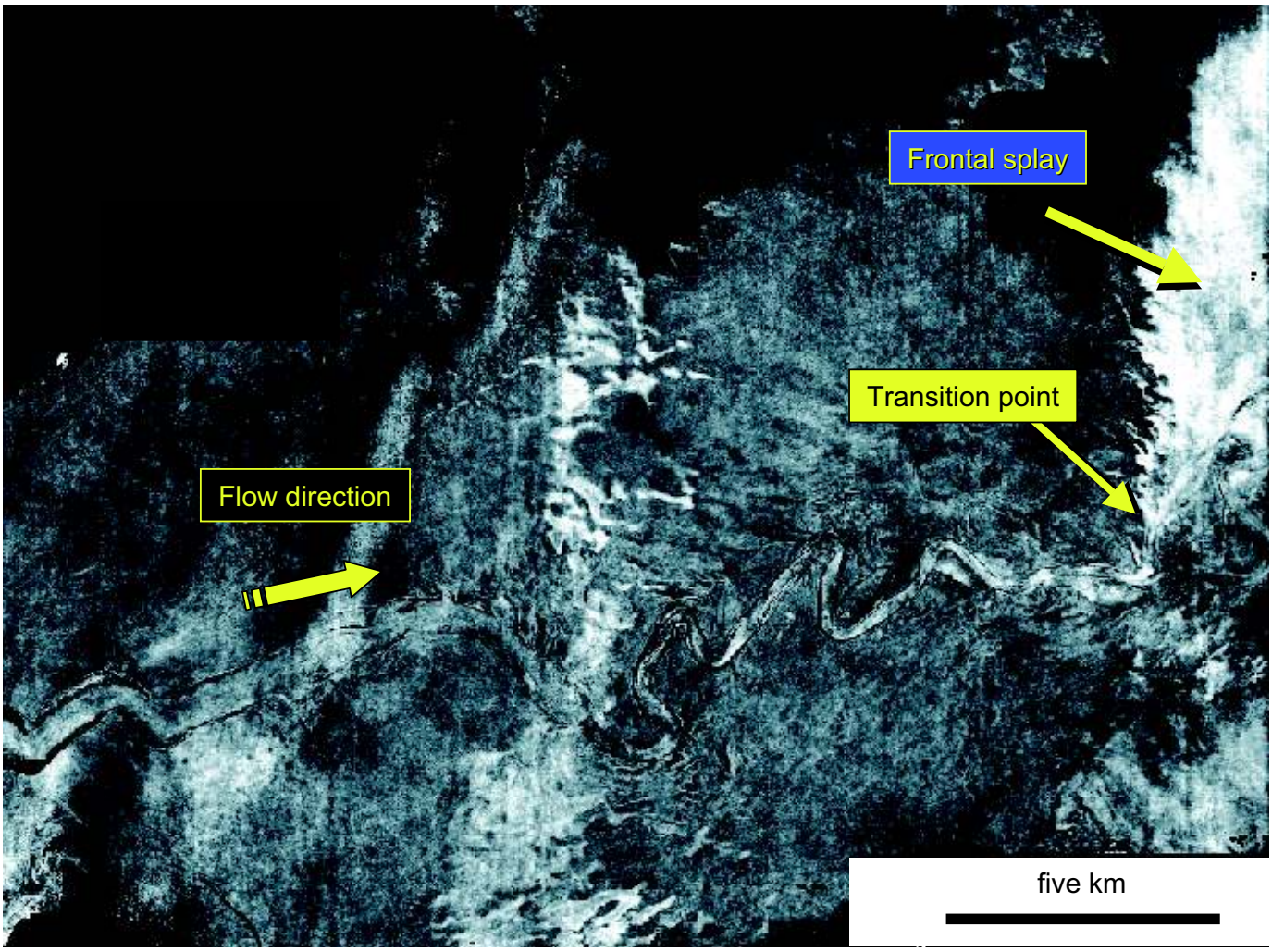

FIG. 115.—Frontal splay at the end of a leveed channel system on the basin floor of the Makassar Strait, Indonesia. The transition point between leveed channel and frontal splay is located where levee height has diminished to below seismic resolution (compare with Fig. 28). Seismic data courtesy of WesternGeco.

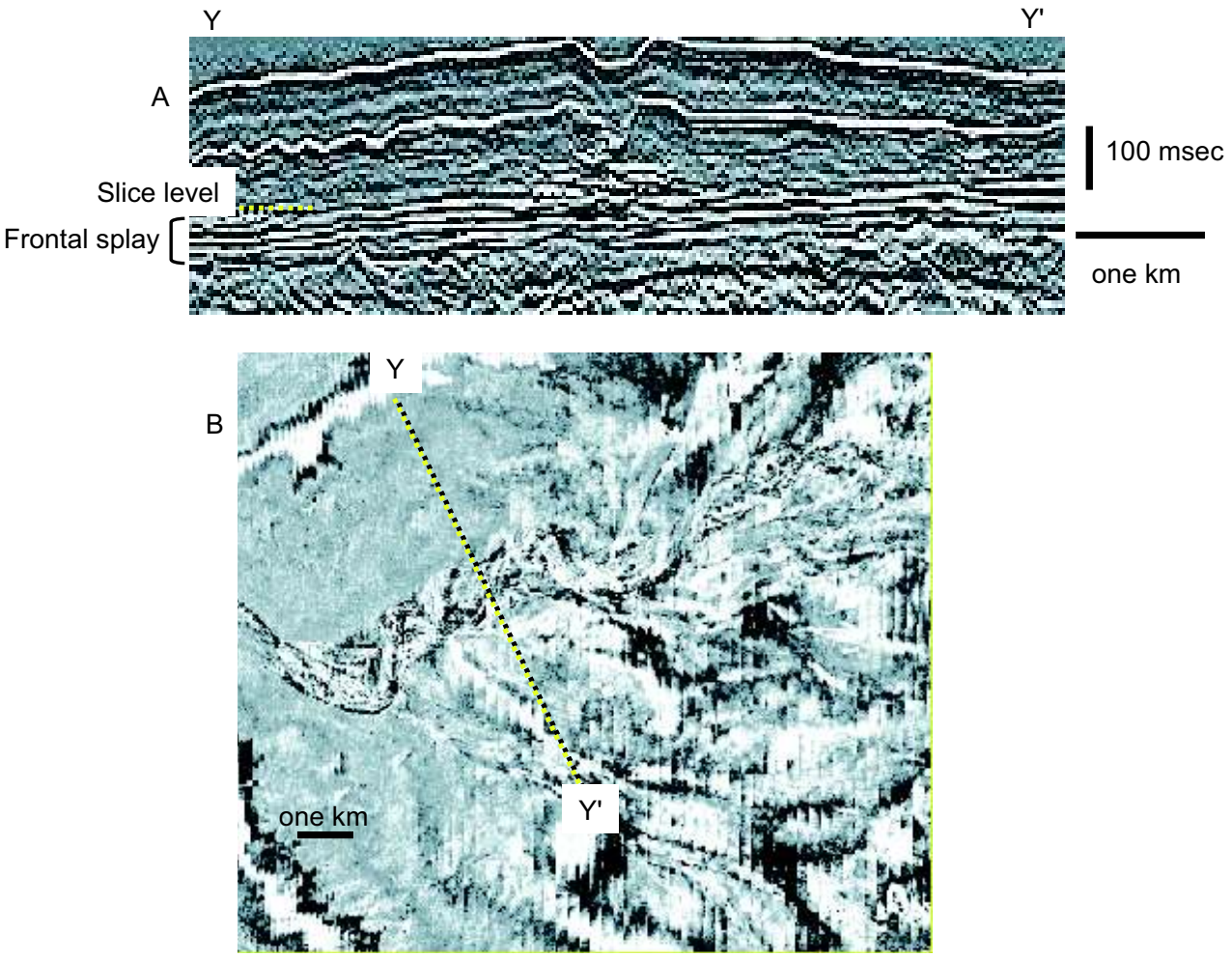

FIG. 116.—Frontal splay at base of channel–levee complex, Makassar Strait, Indonesia. This splay complex is characterized in section view by continuous to discontinuous high-amplitude seismic reflections and in plan view by extensive bifurcation. Note that, as with the channel-levee complex illustrated in Figure 117, the frontal splay immediately underlies a moderate- to high-sinuosity solitary leveed channel. Seismic data courtesy of WesternGeco.

splay apex. However, several characteristics distinguish frontal splays from crevasse splays: (1) Frontal splays tend to be larger, insofar as they involve the entire flow discharge in contrast with only part of the flow discharge (i.e., that part of the flow that is temporarily diverted through the crevasse) associated with crevasse splay. (2) Crevasse splays commonly tend to be associated with levee-derived rip-up clasts. These clasts tend to be mud prone. (3) Crevasse splays lie in close proximity to channel levees, where the flows have passed through a breach. (4) Slope instability with resulting bed convolution and slumping is more common in crevasse-splay settings, insofar as they are deposited on potentially steeper slopes of the overbank environment.

Most commonly, frontal splays are deposited on basin floors or on the floors of intraslope basins, with leveed channels and channel complexes being the more common form of turbidite element encountered in slope environments. In some instances, however, frontal splays can be observed on slopes as well, especially in intraslope basins (Prather et al., 1998), but also in some instances on open slopes as well (Fig. 121).

The splays shown in this paper are mostly channelized, with channel widths from about 100 m to smaller than can be imaged. The channels appear to be multiple (possibly "braided"), although it is not clear if more than one channel is occupied and active during any single turbidity current. Other images show that in more distal settings, the top of the frontal splay may be essentially smooth—any topography is too small to be imaged.

Outcrop Example—County Clare, Ireland.—

The outcrop example of a frontal splay discussed here is from the Carboniferous Ross Sandstone of western Ireland (Figs. 122, 123; Martinsen et al., 2000; Lien et al., 2003). The Ross is about 460 m thick, and details of the regional geology, stratigraphy, and paleotectonic setting are given by Lien et al. (2003). It can be informally divided into lower and upper parts, 170 m and 290 m thick, respectively.

Frontal splays are best seen in the lower Ross—the base is gradational from the underlying Clare Shale. Initial turbidites are very thin and widely spaced stratigraphically, but overall, throughout the 170 m thickness, the beds tend to thicken upward (Lien et al., 2003). In detail, however, there are no systematic thickening-upward or thinning-upward trends (on the scale of ten meters, or

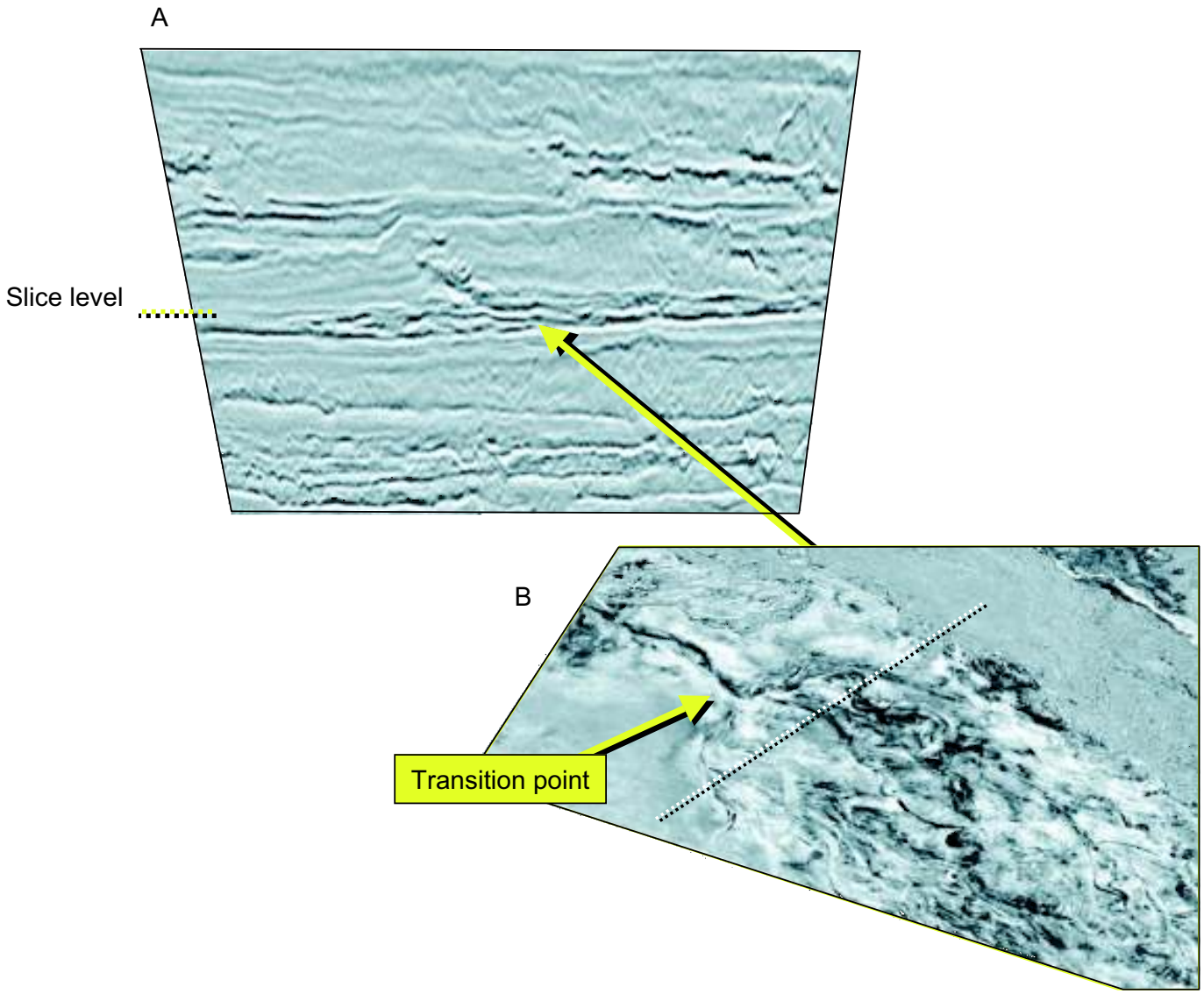

FIG. 117.—Cross section **A)** and horizon slice **B)** views of a deep-water leveed channel feeding a frontal splay, Gulf of Mexico. Note the clear location of the transition point where the leveed channel transitions into a frontal splay. The frontal splay is characterized by continuous to discontinuous high-amplitude seismic reflections in section view, and by extensive bifurcation and braiding (?), forming a complex distributive network in plan view. Seismic data courtesy of WesternGeco.

a few tens of meters), and no readily recognizable channels. Beds appear to be continuous for at least 200 m and of constant thickness as far as they can be traced in the cliffs (Fig. 124). These characteristics suggest that deposition was from unconfined turbidity currents that could spread on the sea floor with no apparent topographic obstructions—characteristic of the distal parts of frontal splays. The absence of bed-thickness trends suggests that each turbidity current was unrelated to the previous ones, with the deposits of larger and smaller flows interbedded. The overall upward bed thickening suggests seaward stepping of the frontal splay over a long period of time.

The upper Ross is characterized by thickening-upward packages, channel fills, slump–slide horizons, and turbidites with no bed-thickness trends. Lien et al. (2003) showed that the thickening-upward packages (Figs. 125, 126) represented aggrading spillover lobes developed during the lateral migration of channels. The top surfaces of many of the packages show giant erosional features resembling flutes (Fig. 127). The packages are superficially very similar to the thickening-upward sequences first described by Mutti and colleagues (Mutti and Ricci Lucchi, 1972) and interpreted to result from the progradation of depositional lobes. However, in the case of the Ross thickening-upward packages, the intimate relationship with channel fills suggests that they are spillover (sediment waves?) rather than frontal lobes.

The channels in the upper Ross vary from about 10 to over 25 m and consist dominantly of amalgamated thick-bedded turbidites. No consistent patterns of bed-thickness change were observed. Two areas define the relationships of channels to packages best—Kilbaha Bay and Cloonconeen.

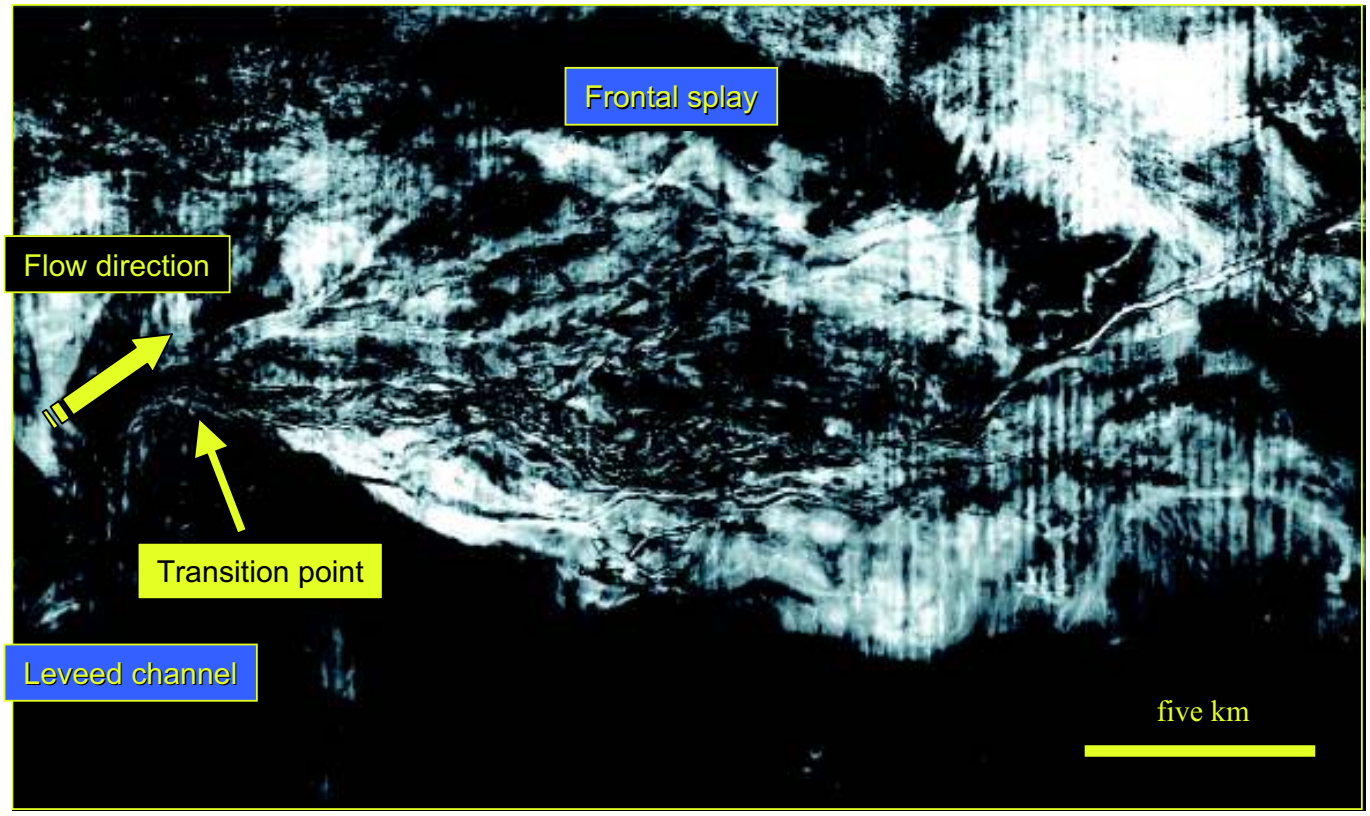

FIG. 118.—Horizon slice view of a deep-water frontal splay, Gulf of Mexico. The transition point is located where the levees associated with the up-system leveed channel have diminished in height to below seismic resolution. The frontal splay is characterized by extensive bifurcation, forming a complex distributive network. Seismic data courtesy of VeritasDGC.

At Kilbaha Bay (Fig. 123) almost horizontally dipping beds are exposed for 1.5 km along the cliff, with a composite stratigraphic thickness of about 40 m. There are 20 thickening-upward packages (Fig. 128). In several locations the thick-bedded portions of the packages can be traced laterally and seen to split into non-amalgamated, thin-bedded turbidites with mudstone partings between beds. The Kilbaha Bay channel (Fig. 128) has a visible depth of incision of about 3 m, with a fill of at least 6 m. The base is characterized by a layer of mudstone clasts, with at least two stratified sandstone blocks up to 3.5 m long and 35 cm thick; these are interpreted to represent channel-wall collapse, as described above from Wheeler Gorge. Most importantly, on the eastern side of the channel fill, thick-bedded amalgamated channel-fill sandstones split into thinner beds and grade laterally into adjacent packages (Fig. 128). This relationship suggests that the packages are in some way related to channel filling (and not lobe progradation)—the relationships are seen even better at Cloonconeen Point.

The channel at Cloonconeen Point (Figs. 129, 130) has a minimum fill thickness of 15 m. There appear to be at least three separate incisions, and the fill consists of separate thick-bedded turbidites close to the margin but an almost completely amalgamated succession closer to the channel center. The uppermost part of the fill consists of about 3 m of amalgamated sandstones, but these beds can be walked out laterally for about 100 m (Fig. 130), where they split progressively and pass into thin-bedded turbidites separated by mudstone partings. These thin-bedded turbidites are organized into a thickening-upward package identical to the packages outside the channel. This relationship strongly suggests that the thickening-upward packages represent aggradation of spillover lobes rather than frontal splays developed downstream from channel mouths. Both the Kilbaha and the Cloonconeen channels suggest that the thickening-upward packages are closely related to channel filling. Lien et al. (2003) also illustrate lateral-accretion surfaces, suggesting that the channels can migrate laterally (Figs. 71–73).

These relationships between architectural elements suggest the following interpretation. Where the channel is far from a particular depositional site, the only overbank deposits to reach that site consist of mudstones (Fig. 131). During lateral channel movement toward the site, overbank deposition may consist of thin-bedded turbidites. The closer the channel approaches, the thicker and more amalgamated the overbank succession become. Closest to the channel, turbidity currents may be scouring (forming the giant flutes) and bypassing without depositing.

The detailed relationships between all of the architectural elements are shown in Figure 131. In phase 1 the channel is active and is migrating laterally, forming lateral-accretions deposits on one side and eroding a cut bank on the other side. In phase 2 during channel filling, note the lateral shift of the cut bank, resulting in thicker and thicker overbank deposits.

Integrated Interpretation of the Ross Sandstone

Lien et al. (2003) suggested that the upper Ross consists mainly of sinuous channels stacked into sinuous channel belts.

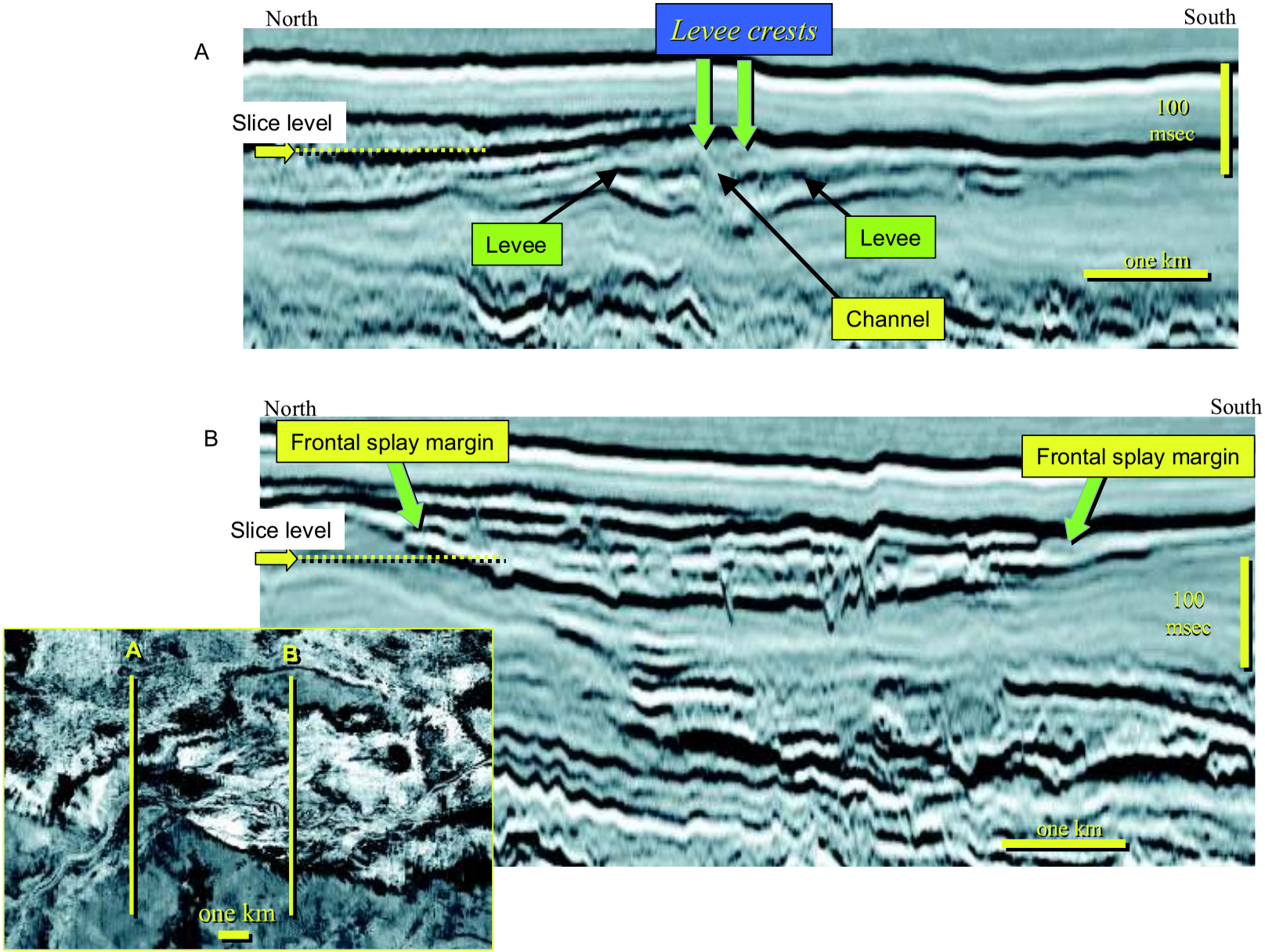

FIG. 119.—Seismic reflection cross-section views through the frontal splay **B)** and the feeder leveed channel **A)** associated with the system shown in Figure 118. Note the single leveed channel clearly shown in section view (A), contrasted with the high-amplitude continuous to discontinuous seismic reflection character of the frontal splay. The section view through the frontal splay also shows that this system is characterized by numerous small channels that seem to coalesce into a sheet-like morphology. Seismic data courtesy of VeritasDGC.

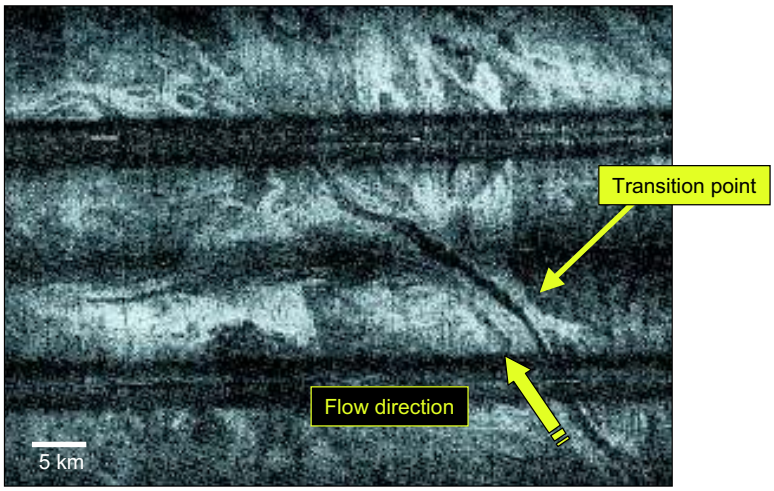

FIG. 120.—Leveed channel feeding frontal splay in the Bering Sea offshore Alaska (from Kenyon and Millington, 1995).

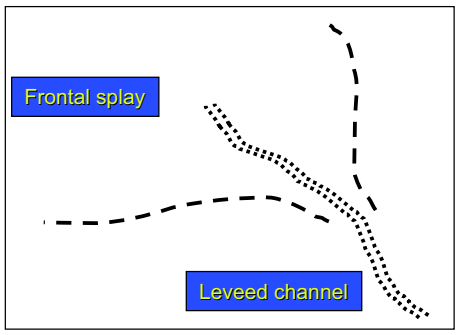

FIG. 121 (below).—Leveed channel feeding frontal splay on the mid-slope, eastern Gulf of Mexico. This 3D perspective view illustrates a reflection amplitude map draped onto the upper bounding surface of the channel–levee complex. Note that in the final stages of this channel-frontal splay complex a solitary leveed channel flows across the top of the frontal splay. Seismic data courtesy of VeritasDGC.

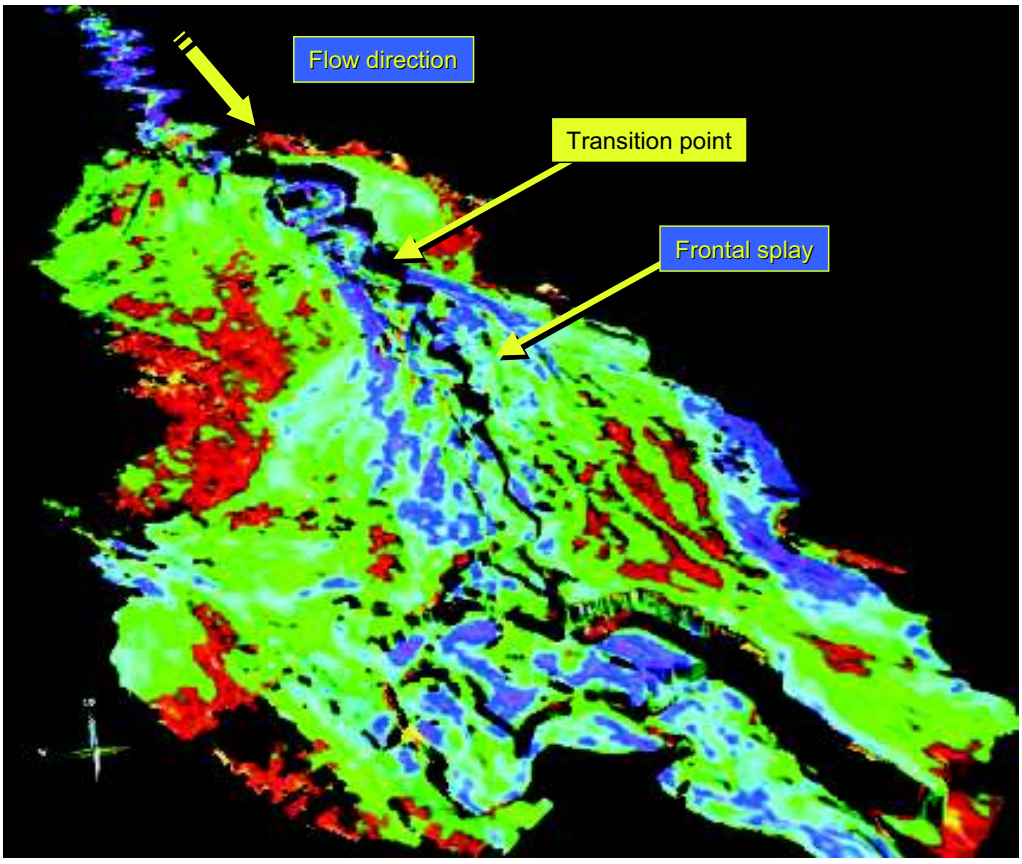

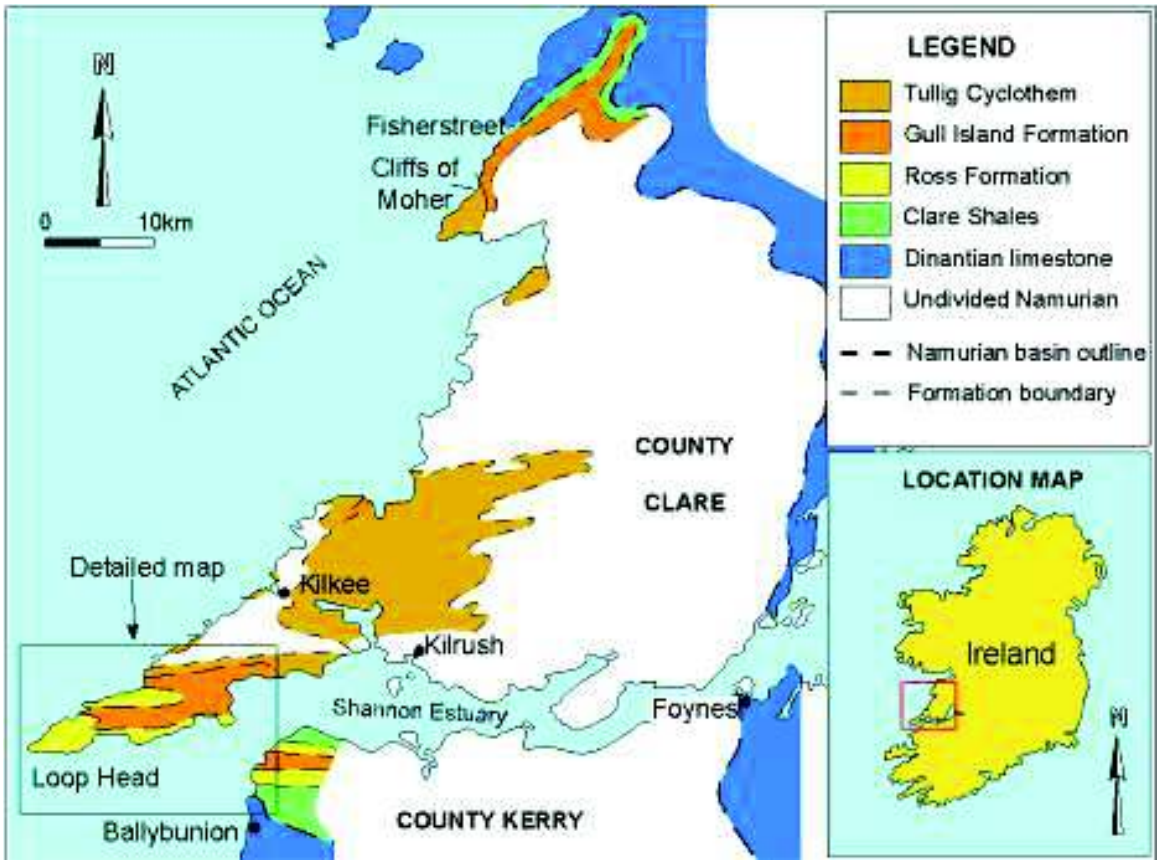

FIG. 122.—Location map for the Ross Sandstone of western Ireland. Rectangle shows location of detailed map in Figure 123 (after Lien et al., 2003).

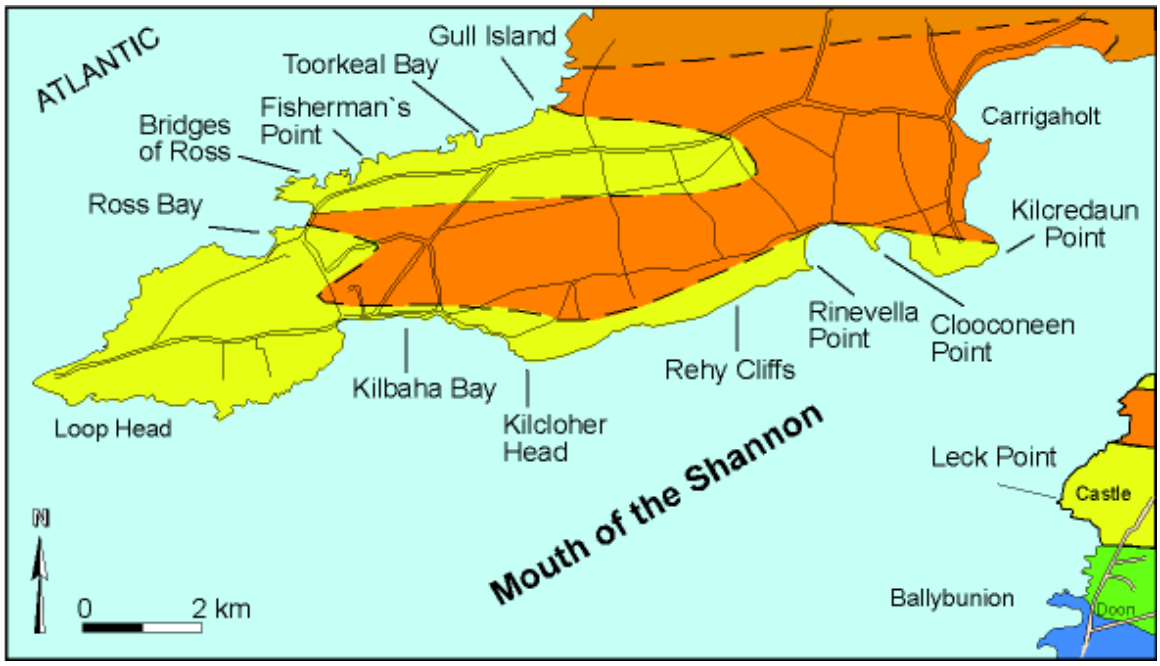

FIG. 123.—Detailed location map for the Ross Sandstone (yellow) and the overlying Gull Island Formation (brown), western Ireland (see Fig. 122) (after Lien et al., 2003).

FIG. 124.—Classical turbidites in the Lower Ross Sandstone. Note the bedding continuity and absence of any thickening- or thinning-upward successions. Cliff north of Ballybunion, about 10 m high.

FIG. 125.—Thickening-upward packages shown by yellow arrows in the upper Ross Sandstone, south side of Ross Bay. Note succession from mudstones into thin-bedded turbidites, with thicker-bedded amalgamated turbidites in the upper parts of the packages.

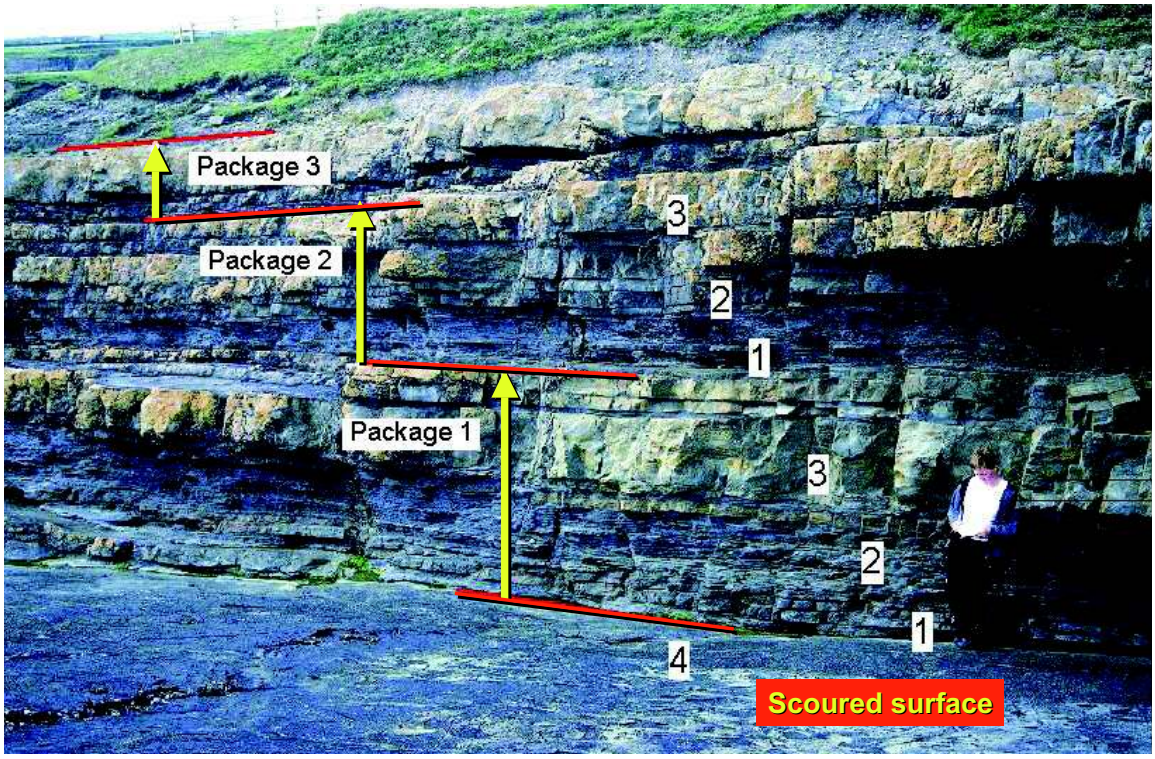

FIG. 126.—Thickening-upward packages at Kilbaha Bay. Note the mudstones at the base, overlain by thin-bedded turbidites, overlain in turn by amalgamated thick-bedded turbidites. The uppermost surface is scoured, but the scours are not visible in this picture.

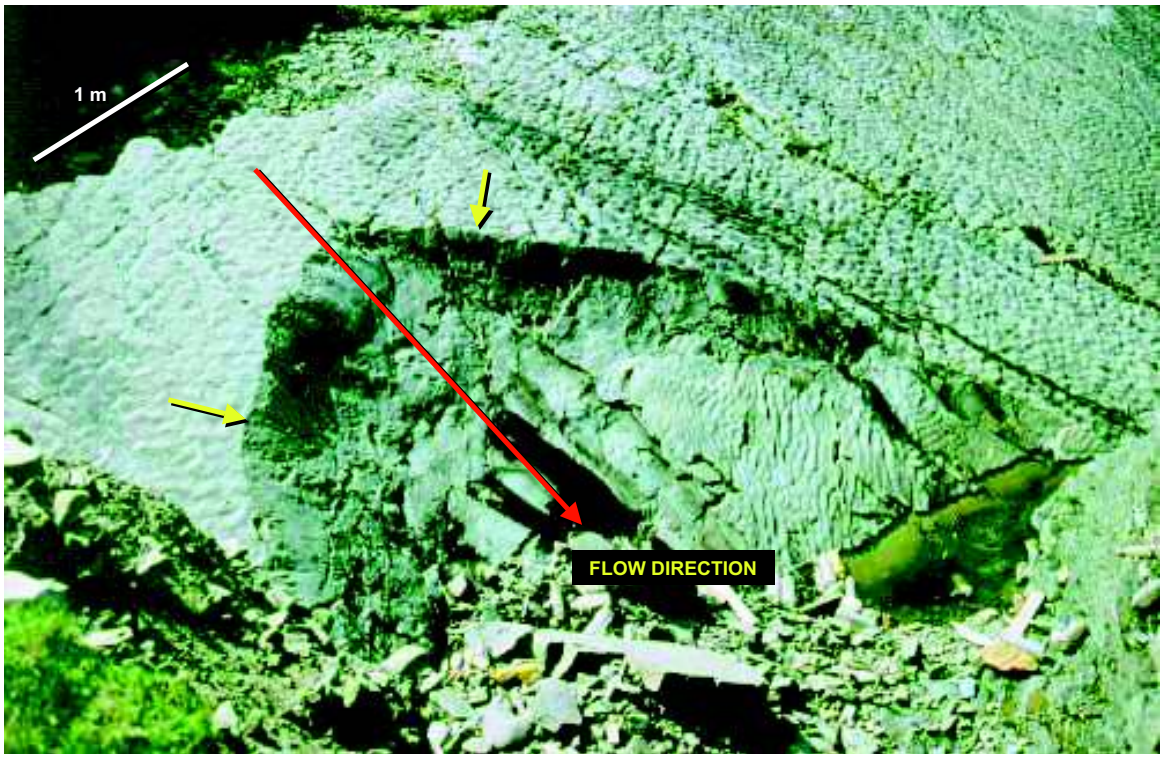

FIG. 127.—Giant flute at Ross Bay. The shape of the flute is shown by the yellow arrows, and the flow direction by the red arrow. The flute scours into amalgamated sandstones with a top surface covered in sinuous-crested ripples. The flute itself is partly filled with mudstones and thin-bedded turbidites, with one surface showing straighter-crested ripples. There are no ripples on the steeply dipping walls of the flute. Note the scale—the flute is nearly 2 m wide.

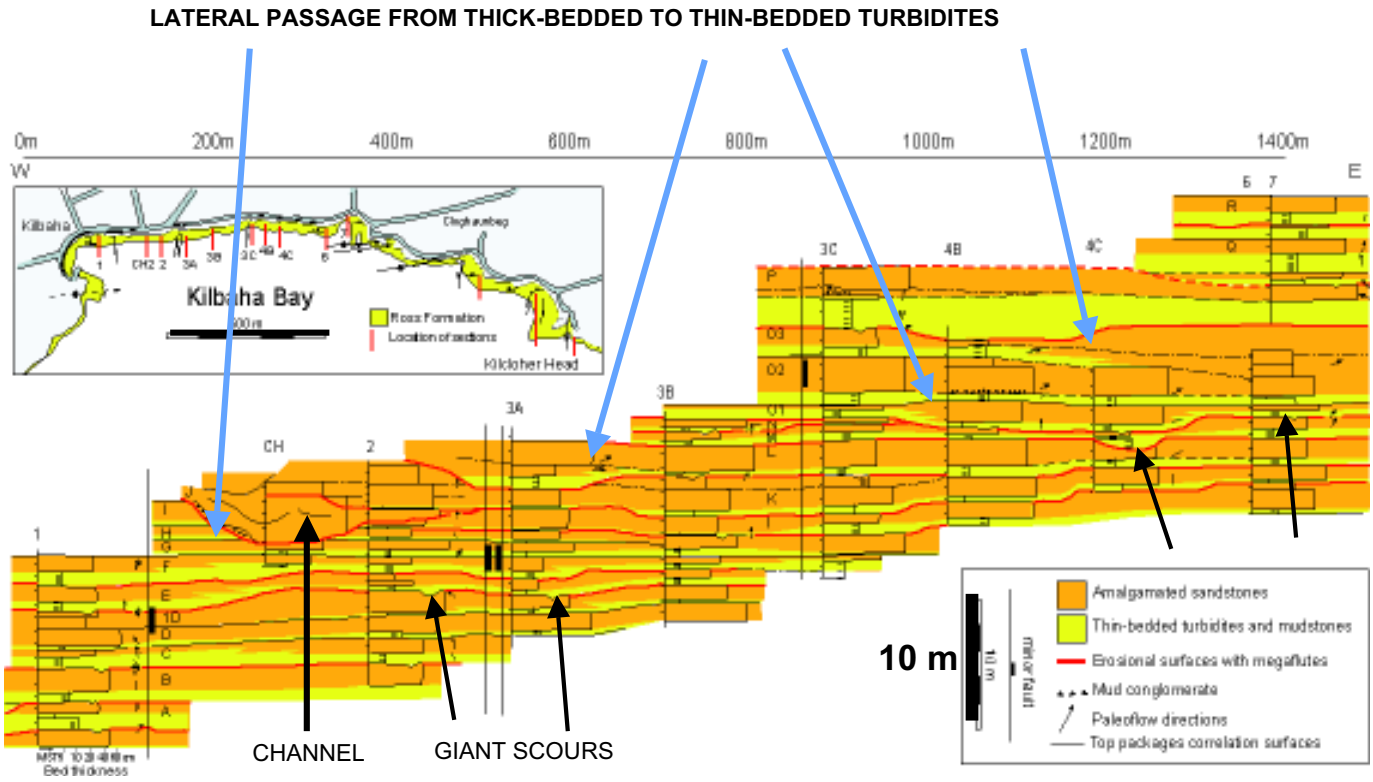

FIG. 128.—Cliff face at Kilbaha Bay. Beds can be walked out along the cliff and in the wave-cut platform. Mudstones and thin-bedded turbidites are yellow, and amalgamated sandstones orange. Note lateral passage from amalgamated turbidites into thin-bedded turbidites in several locations (blue arrows). Note also the giant scours (black arrows). The thick-bedded amalgamated turbidites that fill the channel also pass laterally into thinner beds.

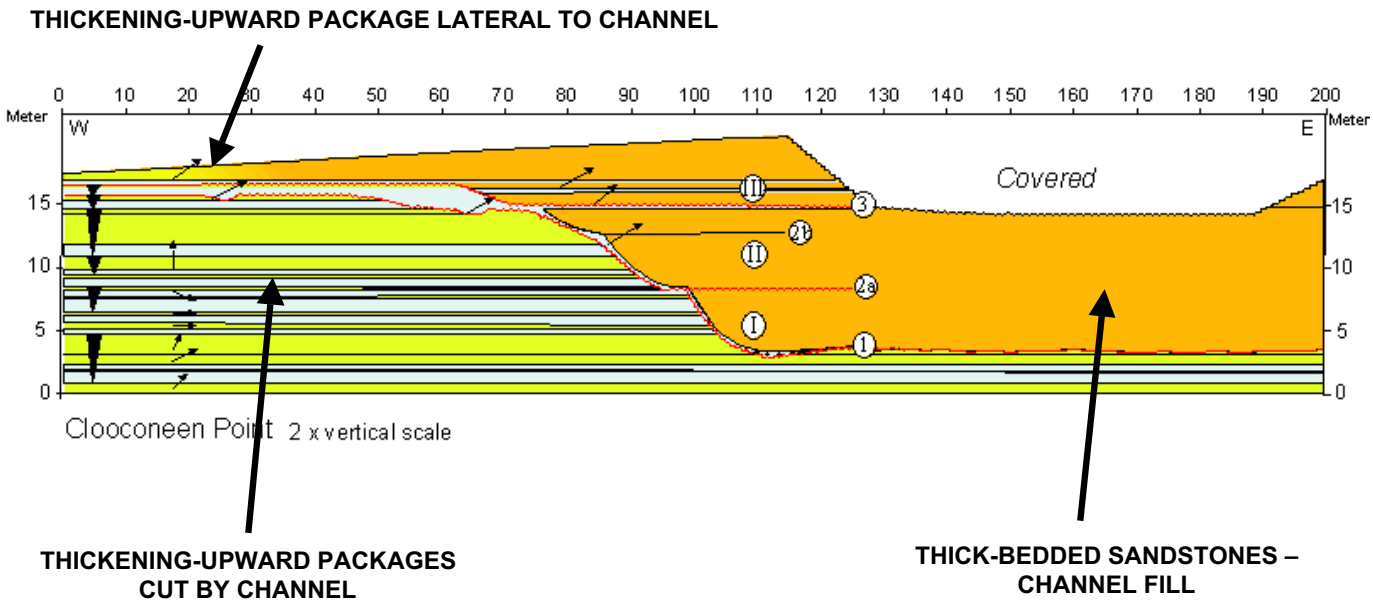

FIG. 129.—Diagram of channel at Cloonconeen Point. Exposure is almost 100 percent, but details of the channel wall are partly obscured by rock rubble and minor tectonics. Channel is filled with amalgamated structureless sandstones and cuts into adjacent thickening-upward packages. Note that the uppermost amalgamated sandstones of the channel fill can be walked out laterally into an overbank thickening-upward package.

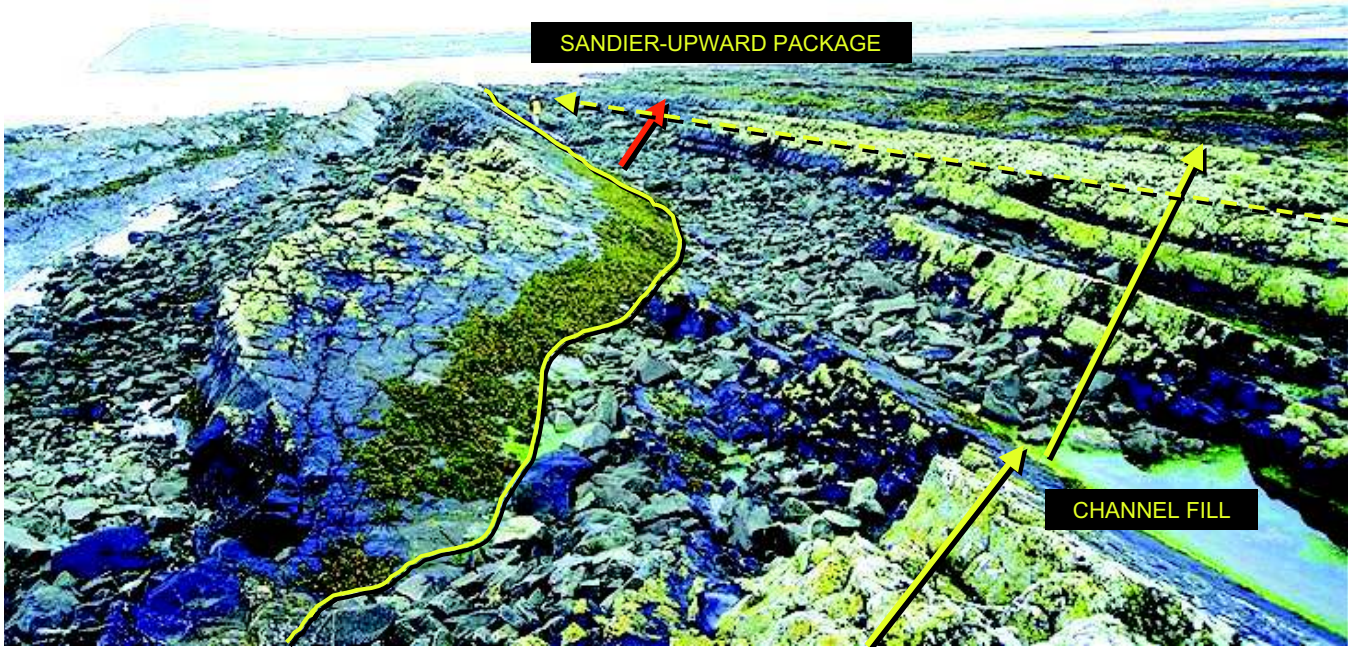

FIG. 130.—Channel margin at Cloonconeen point. Photographer is standing in the middle of the channel fill (two yellow arrows). The channel margin is outlined in yellow (see Fig. 129), and the lateral passage from thick amalgamated channel sandstones to a thickening-upward package (red arrow) is shown with a dotted yellow arrow. Person for scale at end of dotted yellow arrow.

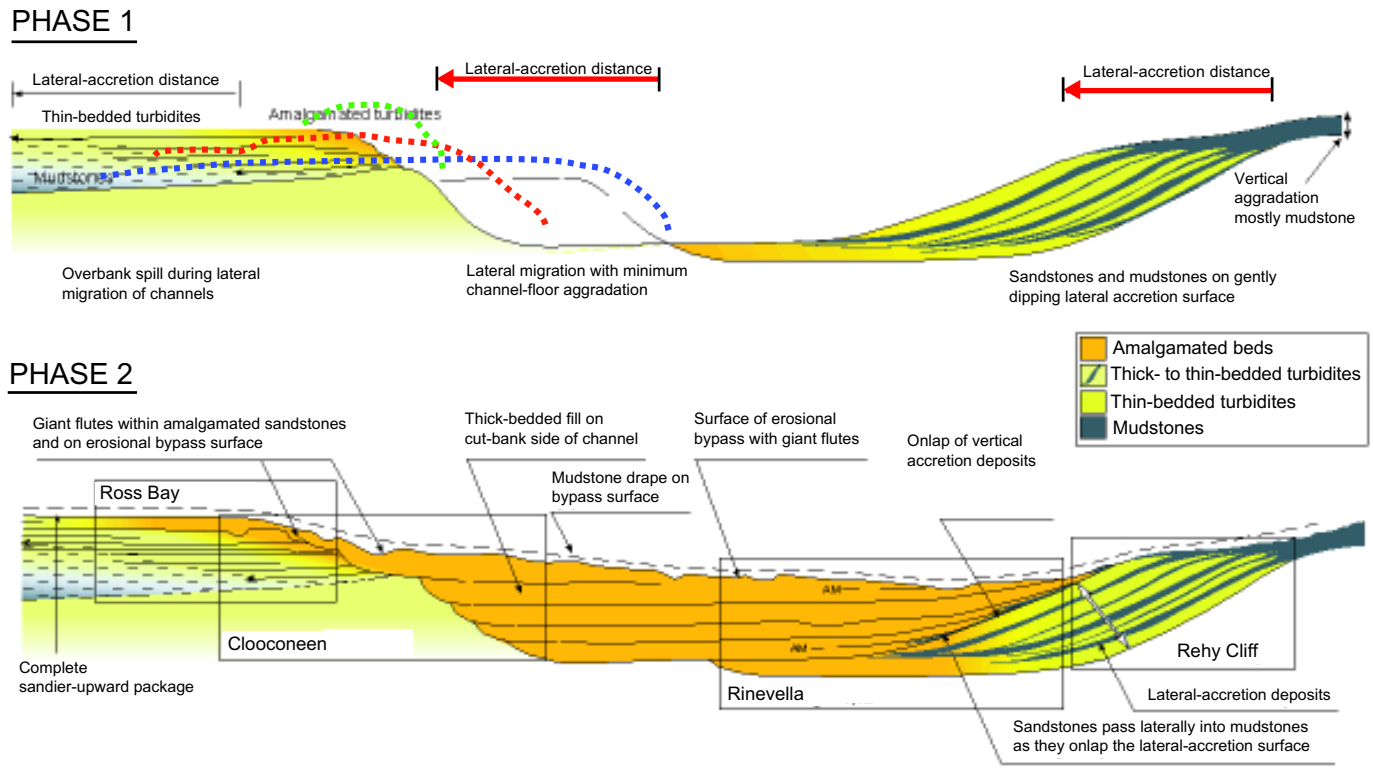

FIG. 131.—Composite diagram for the upper Ross Sandstone, showing the development of a channel. In phase 1, note the lateral shifting, with lateral accretion on one side, and a cut bank on the opposite side. Thickening-upward sequences form as the channel migrates, with mudstones deposited when the channel is far away (blue dotted line), thin-bedded turbidites as the channel approaches (red dotted line), and thick-bedded amalgamated turbidites when the channel is closest (green dotted line). As the channel migrates, the opposite bank may receive lateral accretion deposits. In phase 2, the main channel is filled with structureless amalgamated turbidites, probably resembling those of Figure 68.

The thickening-upward packages represented overbank spill, and the non-packaged turbidites represented deposition on a smooth basin floor far from any channels. The exact position of the channels and channel belts was not discussed. The model is shown in Figure 132, where three individual sinuous channels are shown diagrammatically within a sinuous channel belt. At the end of the sinuous channel belt, turbidity currents spread laterally to form the unchannelized lower Ross turbidites.

In the light of the seismic images presented here, particularly those that show channelization in the proximal parts of frontal splays, it is possible that the entire Ross Sandstone represents a frontal splay. The lower Ross would represent the smooth outer portion of the splay, with the overall thickening-upward succession resulting from gradual progradation of the splay. The upper Ross would then represent the proximal channelized part of the splay, with the non-packaged parts of the upper Ross being deposited on smoother parts of the splay.

Importance of the Ross Formation Case History.—

The importance of this case history is that it illustrates how a stratigraphic unit can first be subdivided into architectural elements—non-packaged turbidites, thickening-upward packages, channel fills, and slump–slide depositional units. The channels are the easiest individual element to interpret, and the interpretation of the thickening-upward packages follows from their detailed relationships to the channel fills. Reliance on earlier models that would suggest prograding depositional lobes would give an alternative (and probably incorrect) interpretation. The suggestion that the upper Ross might represent the proximal part

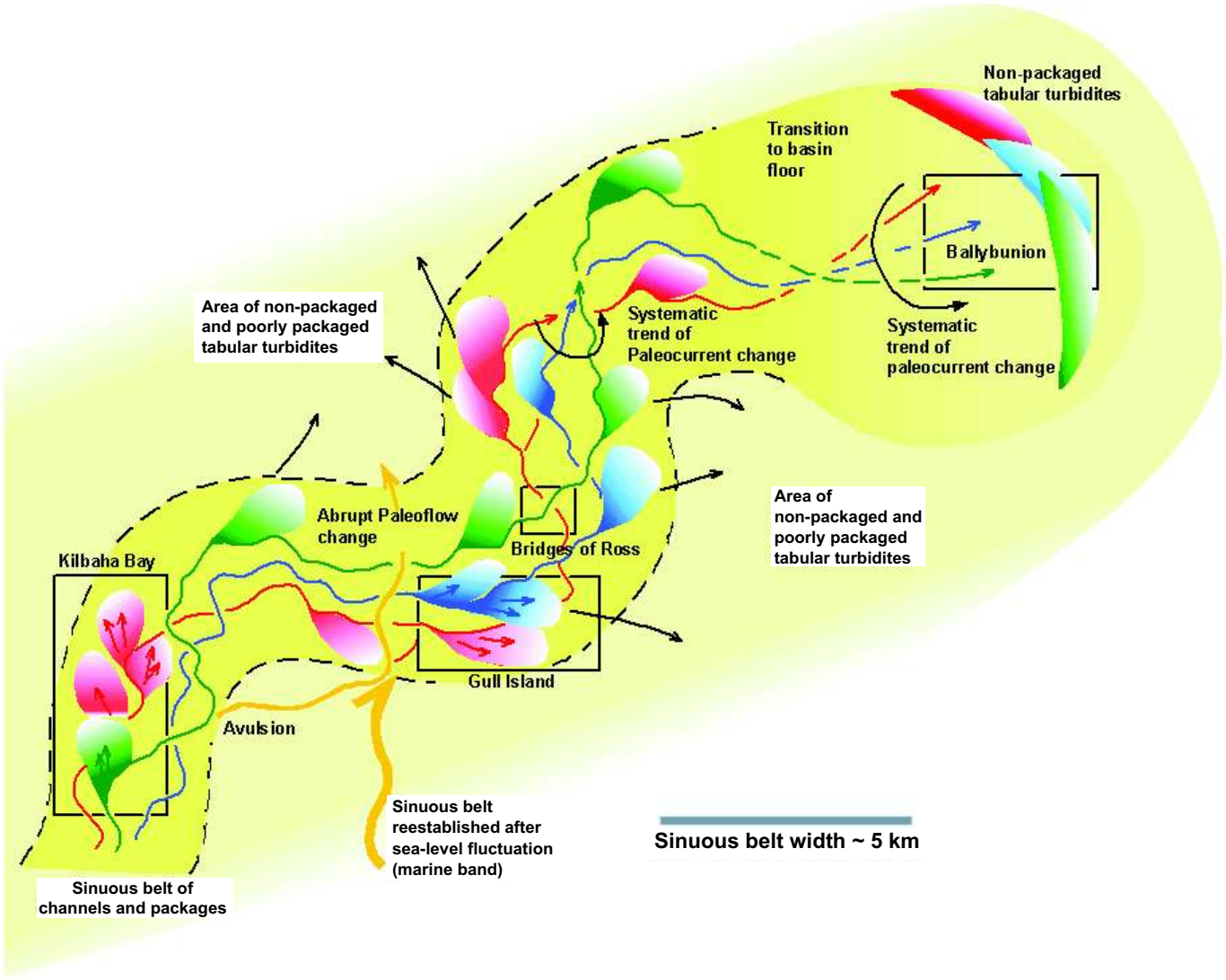

FIG. 132.—Overall interpretation of the Ross Sandstone. Individual sinuous channels in the upper Ross (shown as red, green and blue) are stacked into sinuous channel belts (yellow). At curves in the individual channel, overbank spill can create thickening-upward packages (red, green and blue "lobes"). Thus the sinuous channel belt consists of two main depositional elements—channel fills and overbank spills. At the downstream end, the channels lose their topography and feed a smooth basin plain (the lower Ross). The passage from lower to upper Ross implies progradation of the sinuous channel belts over the smooth basin plain.

of a frontal splay is based on stratigraphic context and comparison with 3-D seismic images. Thus an interpretation has been constructed that relies on defining architectural elements, defining their particular stratigraphic relationships, and comparing this construction with seismic images of the deep sea floor. In this way, we build our own model or interpretation without reliance on a preexisting model—the theme developed by Walker (this volume) in the introduction to this volume.

Debris-Flow Deposits—Mass-Transport Complexes

Various forms of debris-flow and mass-transport deposits comprise common depositional elements in many deep-sea environments (Fig. 133). These deposits can assume a variety of shapes and sizes. A characteristic that seems common to all is their highly erosional nature and their contorted, chaotic, and structureless internal architecture. Erosional relief at the bases of such deposits can exceed 250 m in some instances (Figs. 134, 135). Where clasts were embedded in the flow base, erosion of the substrate is marked by long, linear striations or grooves that tend to diverge in the downsystem direction (Figs. 21, 136–140). Clast sizes can range from cobbles to clasts larger than houses (Fig. 141). In some instances, small outcrop-scale scour can also be observed beneath mass-transport deposits (Fig. 142).

Large mass-transport deposits have been observed to originate at shelf edge (Fig. 143) as well as mid-slope locations (Fig. 144), where fault scarps as high as 54 m mark the point of slope failure. Smaller mass-transport deposits originating on the flanks of salt domes and mud volcanoes also have been observed, and on the flanks of turbidity-flow channel levees (Figs. 80, 86). Because in most instances mass transport originates in low-energy environments, the associated deposits of such processes tend to be mud-rich.

In plan view these deposits can be lobate or channelized (Figs. 145–148). In some instances mass-transport deposits can opportunistically use the channel of an earlier-formed turbidity-flow channel (Fig. 149). The seismic character in both planar horizontal or vertical section commonly is chaotic to contorted (Figs. 135, 150–153), though in some instances they can be characterized by large-scale convolute bedding (Fig. 154).

Where debris flows encounter obstructions or where flow velocities diminish abruptly, as is common near their termini, internal compressional structural features (i.e., low-angle thrust faults) can be common (Figs. 151,155, 156). On the basin floor, a commonly observed aspect of mass-transport deposits is an apparent large-scale channelization that is not so much related to erosion of a channel and subsequent fill as it is a consequence of "plowing" of the sea floor by a plug of debris analogous to the effect of a shovel pushing through a snow layer (Figs. 157, 158). In instances such as these it is possible to calculate the travel distance of the mass-transported debris (Fig. 159). Lateral compression caused by multiple phases of mass-transport events also has been observed (Figs. 152, 160).

The hallmark of the lithofacies of mass-transport deposits is its lack of organization. Commonly they comprise mud-supported conglomerates, though they can also occur as pure mudstone containing muddy rip-up clasts. In isolated instances they can also be relatively sand-rich (Jennette et al., 2000).

The upper bounding surfaces of mass-transport complexes can vary from smooth to highly rugose. In some instances this surface rugosity can exert an influence over subsequent turbidity -flow deposits (Fig. 161), whereas in other instances, because the short wavelength of the bathymetric lows, only ponding of mudstones seems to occur (Fig. 162).

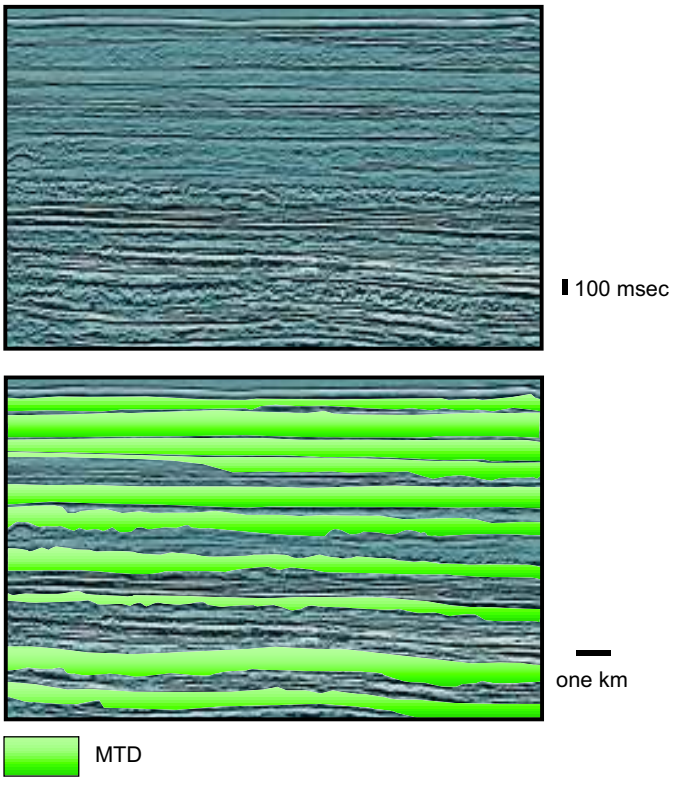

FIG. 133.—Seismic section from the eastern Gulf of Mexico illustrating the extensive nature of mass-transport deposits. At this location, the mass-transport deposits constitute approximately 45% of the total section shown. Seismic data courtesy of WesternGeco.

SEQUENCE STRATIGRAPHY

A typical deep-water depositional sequence on the basin floor has been proposed by Posamentier and Kolla (2003a) as consisting of basal debris-flow material, overlain by sand-rich frontal-splay deposits, in turn overlain by isolated leveed-channel deposits and finally by debris-flow deposits and a condensed section. This sequence is in part a distillation of the work of Weimer (1991), Piper et al. (1997), Pirmez et al. (1997), Manley and Flood (1998), Maslin et al. (1998), Beauboeuf and Friedmann (2000), Brami et al. (2000), and Winker and Booth (2000) (Fig. 163). It is relatively unlikely that each of these stratigraphic units would be observed at any given location; debris-flow deposits are most common on basin floors and within canyons, frontal splays are most common on basin floors, and leveed channels are common in both slope and basin-floor environments. In contrast, condensed sections are widespread and ubiquitous. Figure 74G shows a section of a deep-water depositional sequence, characterized by frontal-splay deposits overlying a condensed section (thin stratigraphic unit corresponding to the transgressive and high-stand systems tract of the preceding sequence). In this example, frontal-splay deposits gradually give way to an isolated leveed channel. We suggest that this transition from frontal splay to leveed channel during the waning phase of a deep-water depositional sequence occurs because of a progressive decrease in sand-to-mud ratio within the flows, which originate at the shelf-edge staging area. This diminished overall sand content results in a seaward shift of the transition point as discussed above.

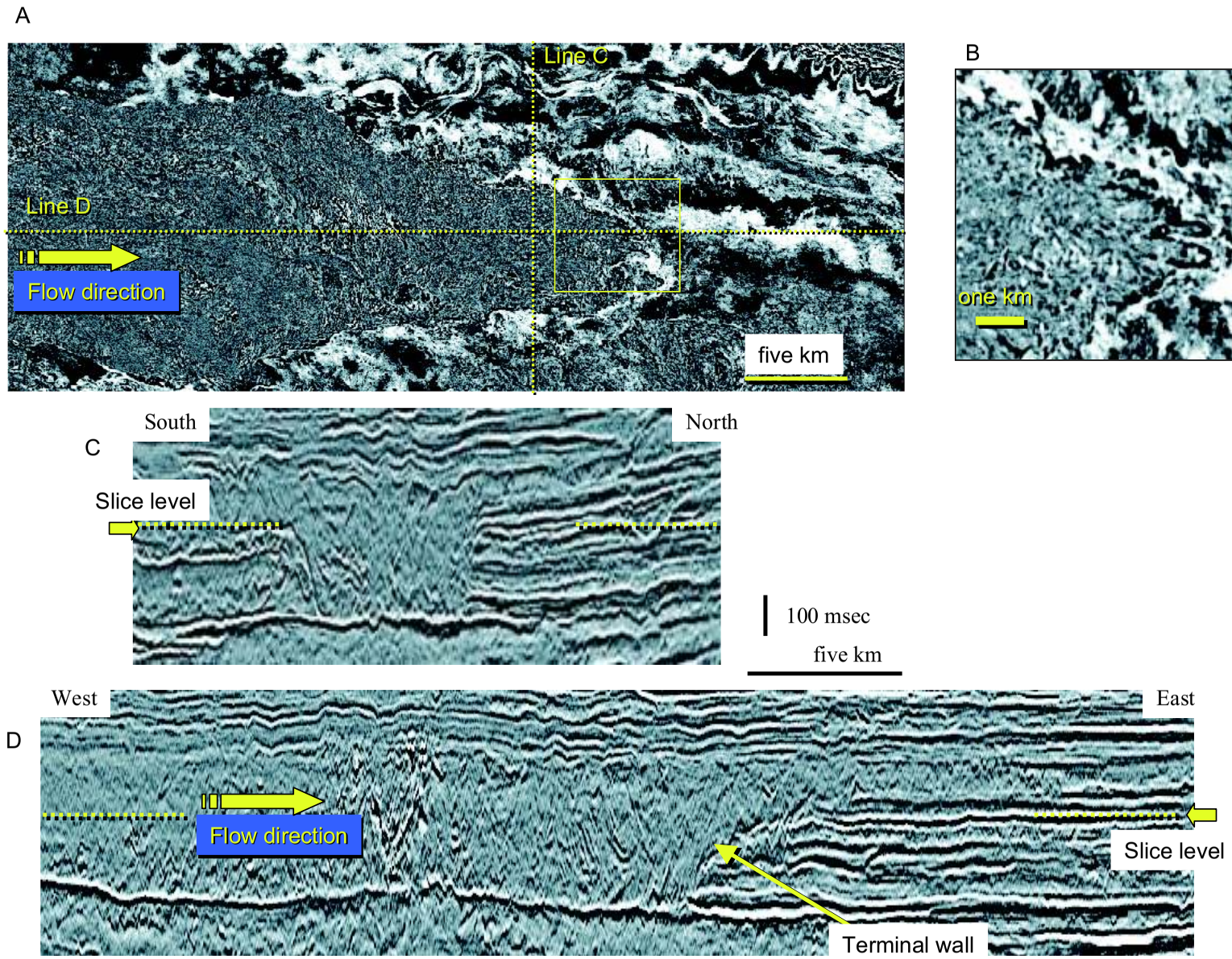

FIG. 134.—**A)** Mass-transport complex in the basin floor environment, eastern Gulf of Mexico, which lies within a broad, flat-floored channel **C)** that ends abruptly at a terminal wall **D)**. These sediments likely did not travel far but rather comprise a mass of material that was pushed from behind and slid to some degree along a decollement surface at the base (note the relatively flat base in section view (C and D). The complex rheology of this deposit is illustrated by the chaotic nature of the seismic reflections within the mass-transport complex as well as the tongues of sediments that extend beyond the terminal wall **B)**. The relief of the channel is approximately 240 m. Seismic data courtesy of WesternGeco.

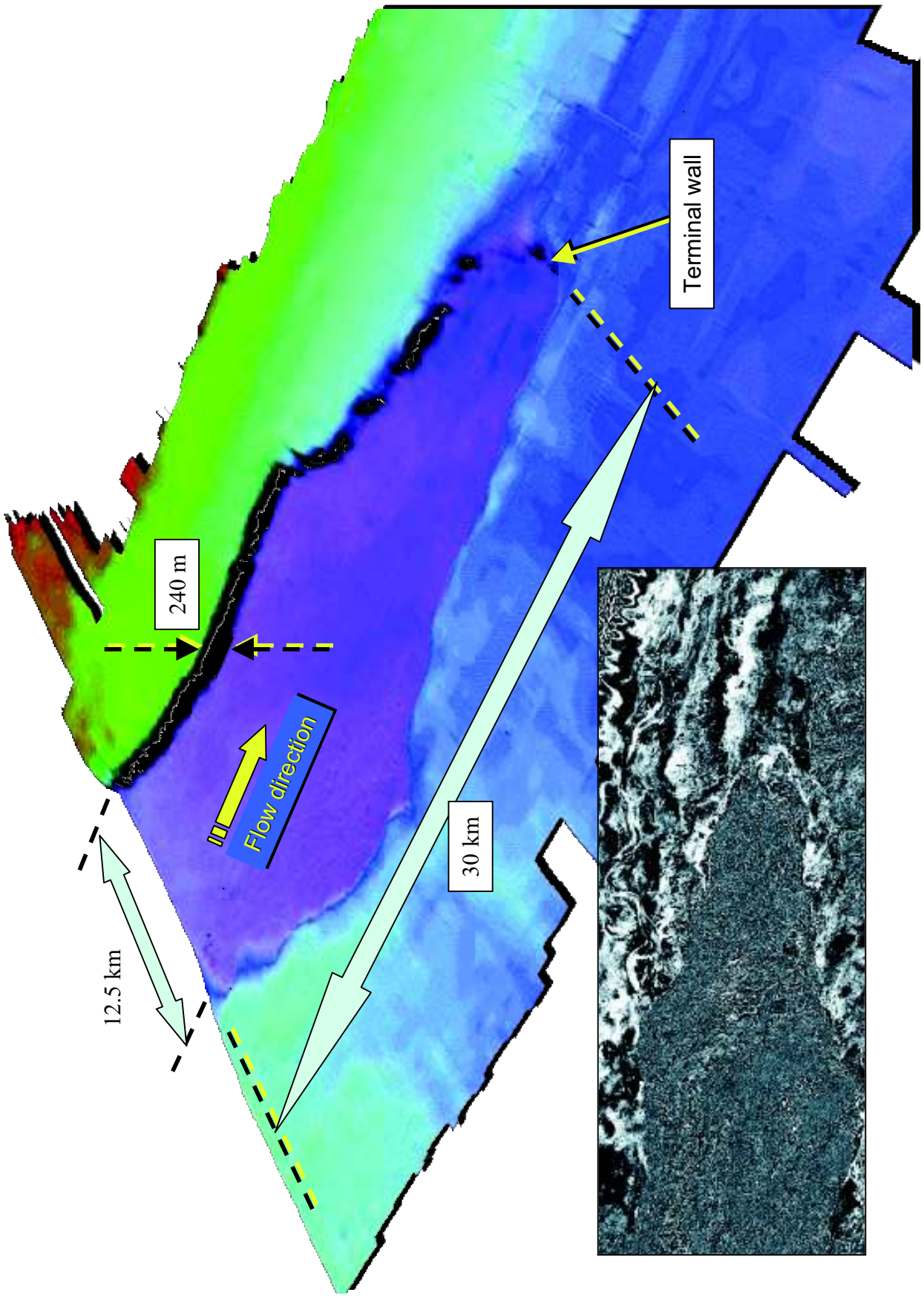

FIG. 135.—Perspective-view image of the base of the mass-transport complex shown in Figure 134. Seismic data courtesy of WesternGeco.

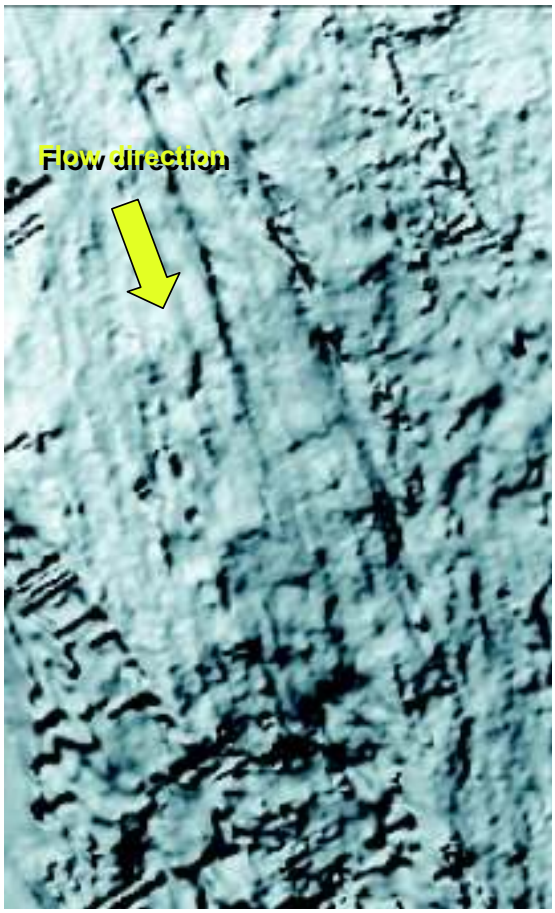

←

FIG. 136.—Grooves beneath mass-transport complex deposited in a continental-slope environment (image courtesy of D. Mosher).

FIG. 137 (below).—Grooves beneath mass-transport deposit at the base Paleocene, North Sea, in a basin-floor environment (after Wilson et al., 2005).

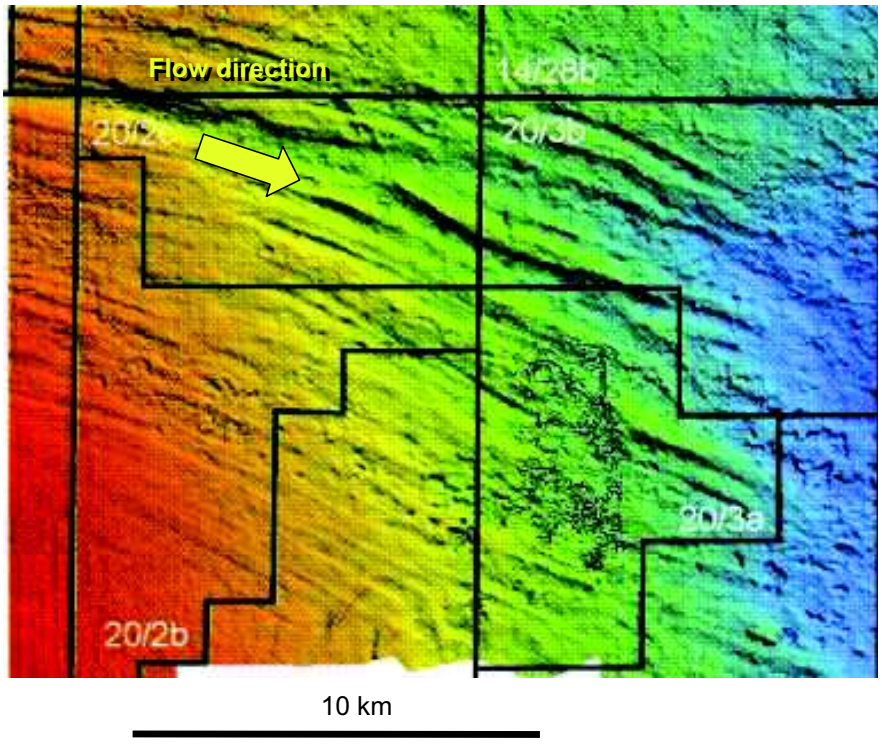

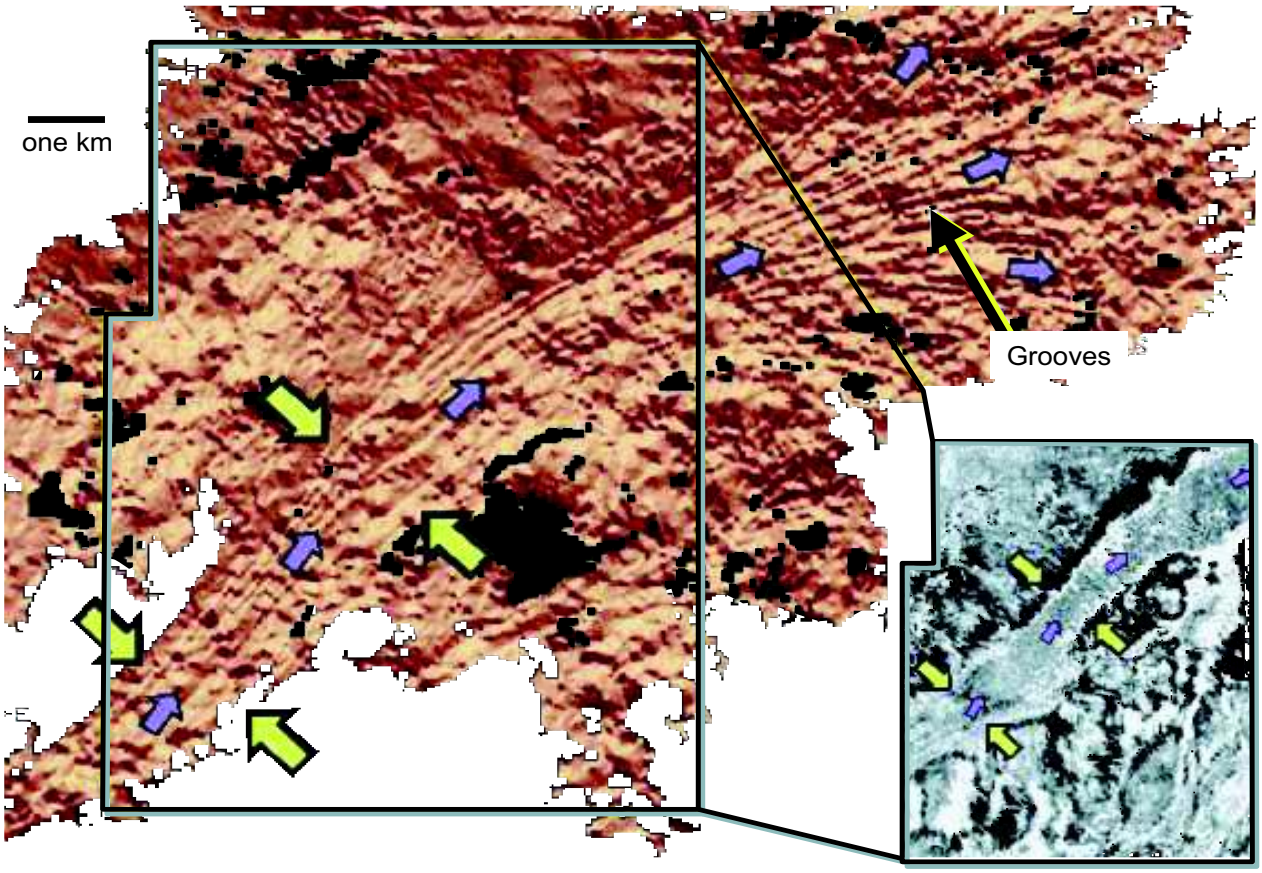

FIG. 138.—Dip-azimuth map of surface at the base of a channelized mass-transport deposit. Note the grooves that characterize this surface and the tendency for these grooves to diverge down-system. This suggests that internal deformation characteristic of flow rather than slide processes have occurred. Seismic data courtesy of WesternGeco.

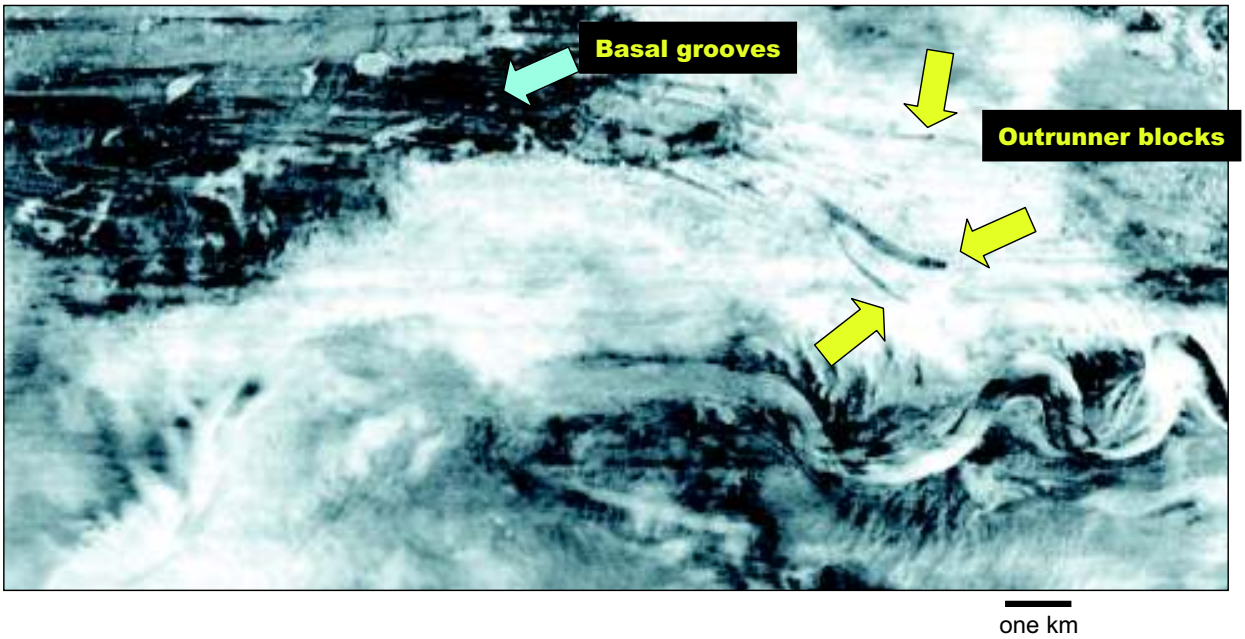

FIG. 139.—Grooves at the base of a mass-transport complex, basin floor, eastern Gulf of Mexico. Note the outrunner blocks (yellow arrows). Compare with Figure 154, a seismic slice through the middle of this mass-transport deposit. Seismic data courtesy of WesternGeco.

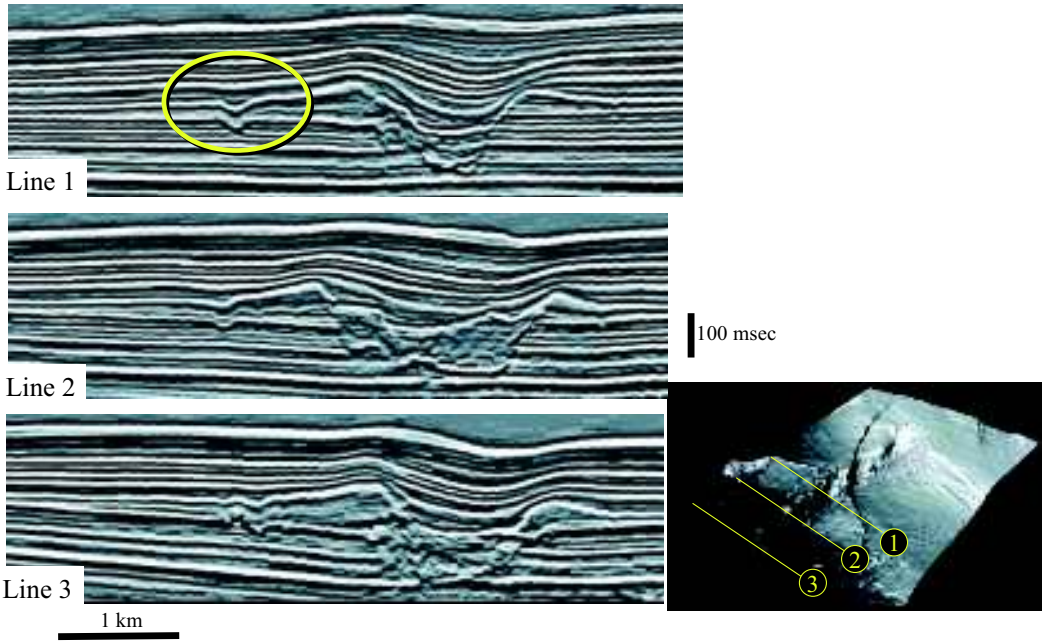

FIG. 140.—Linear grooves at base of levees of slope channel shown in Figure 43. The events responsible for eroding these grooves occurred just prior to levee construction, suggesting that these mass-transport events represent the earliest phases of a sea-level lowstand. Seismic data courtesy of VeritasDGC.

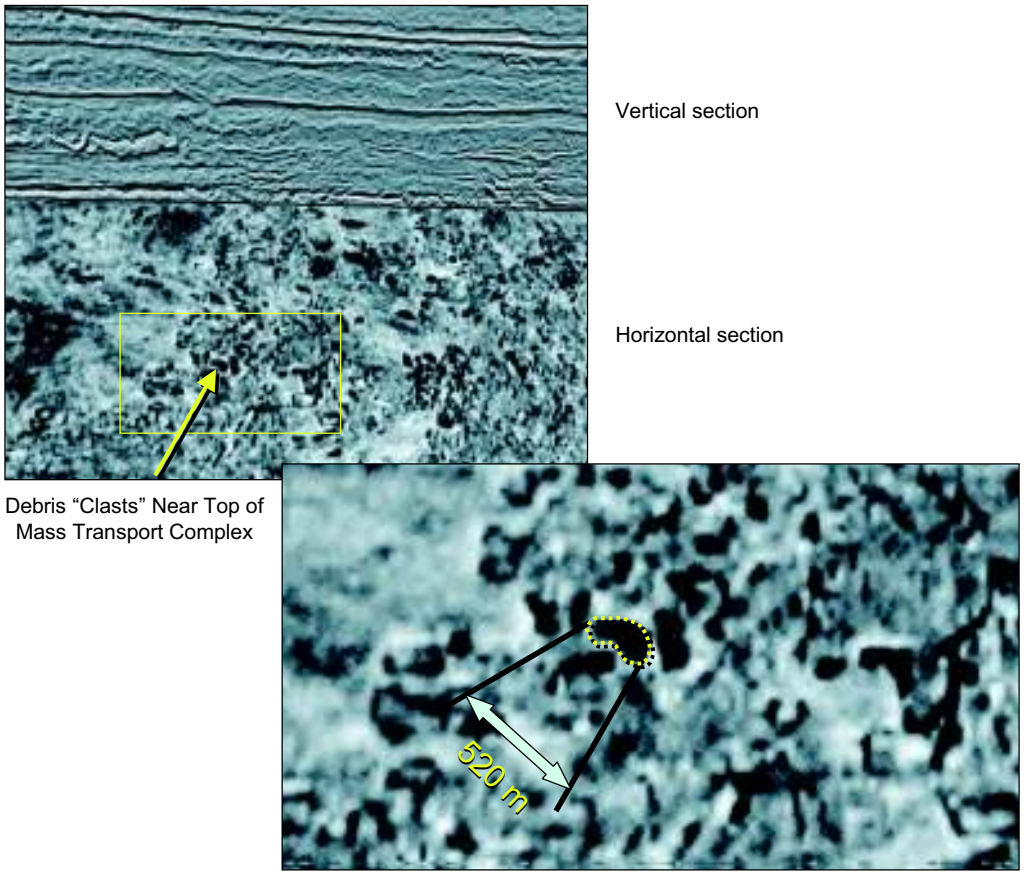

FIG. 141.—Seismic reflection time slice as well as section view through a mass-transport complex with a single megaclast over 500 m wide highlighted. This clast is observed to be rafted near the top of the mass transport complex.

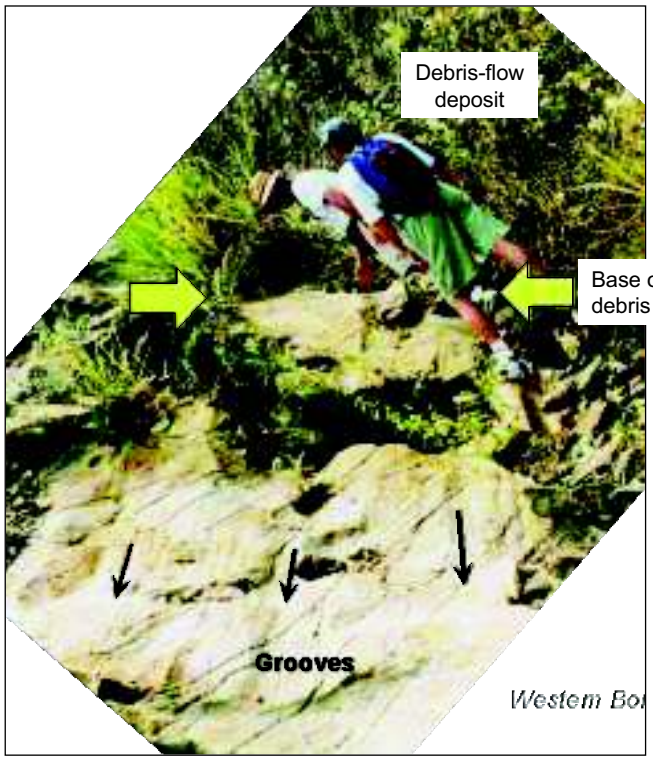

←

FIG. 142.—Small-scale grooves and striations on top of sandstone deposit at base of mass-transport complex, Borneo, Malaysia.

FIG. 143 (below).—Shelf-edge-detachment slump scars offshore Indonesia. These slump scars likely represent the point of detachment or staging area of sediments that traveled down the slope, possibly transforming from slump to slide to flow with increased distance from the shelf edge.

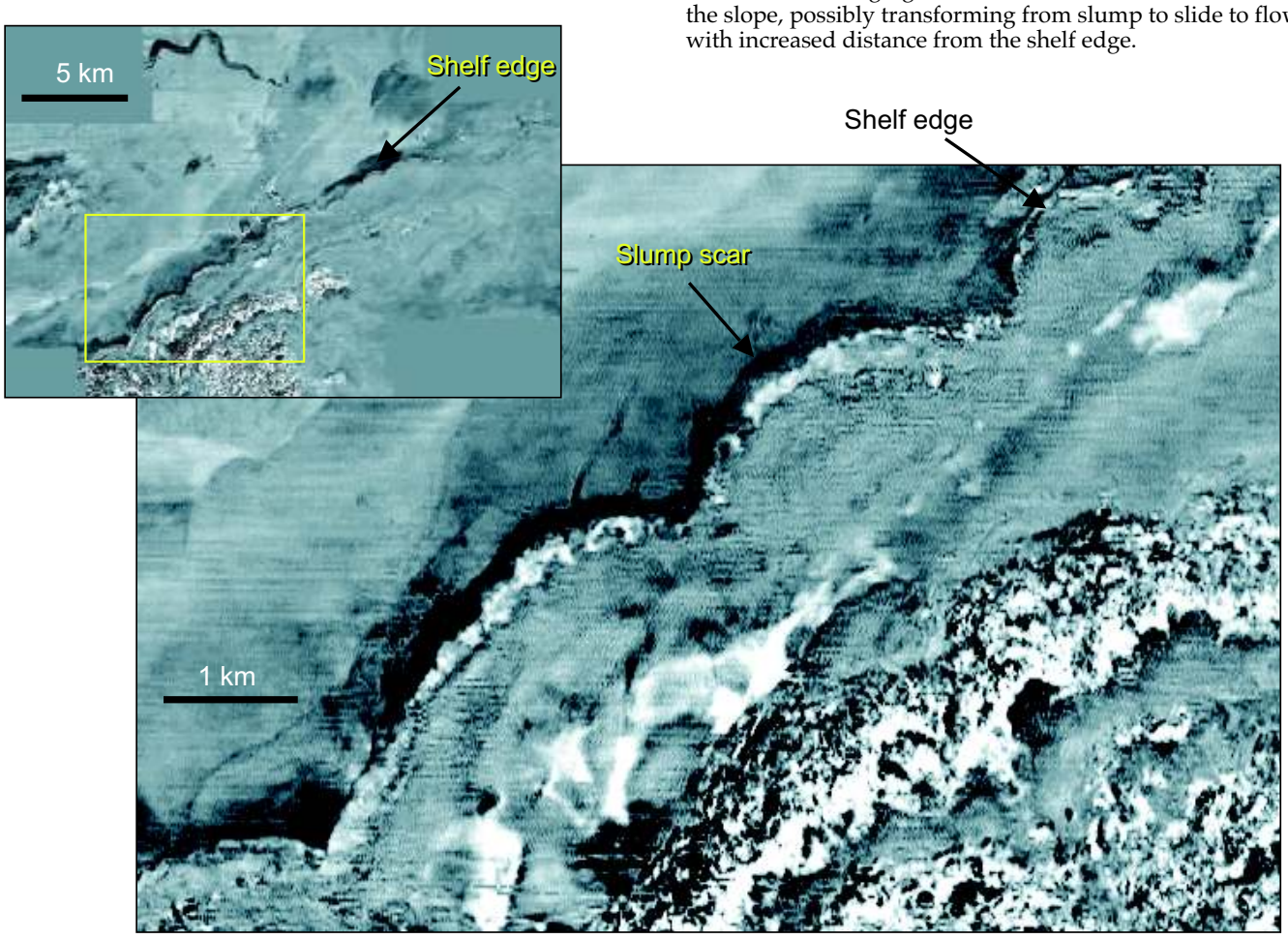

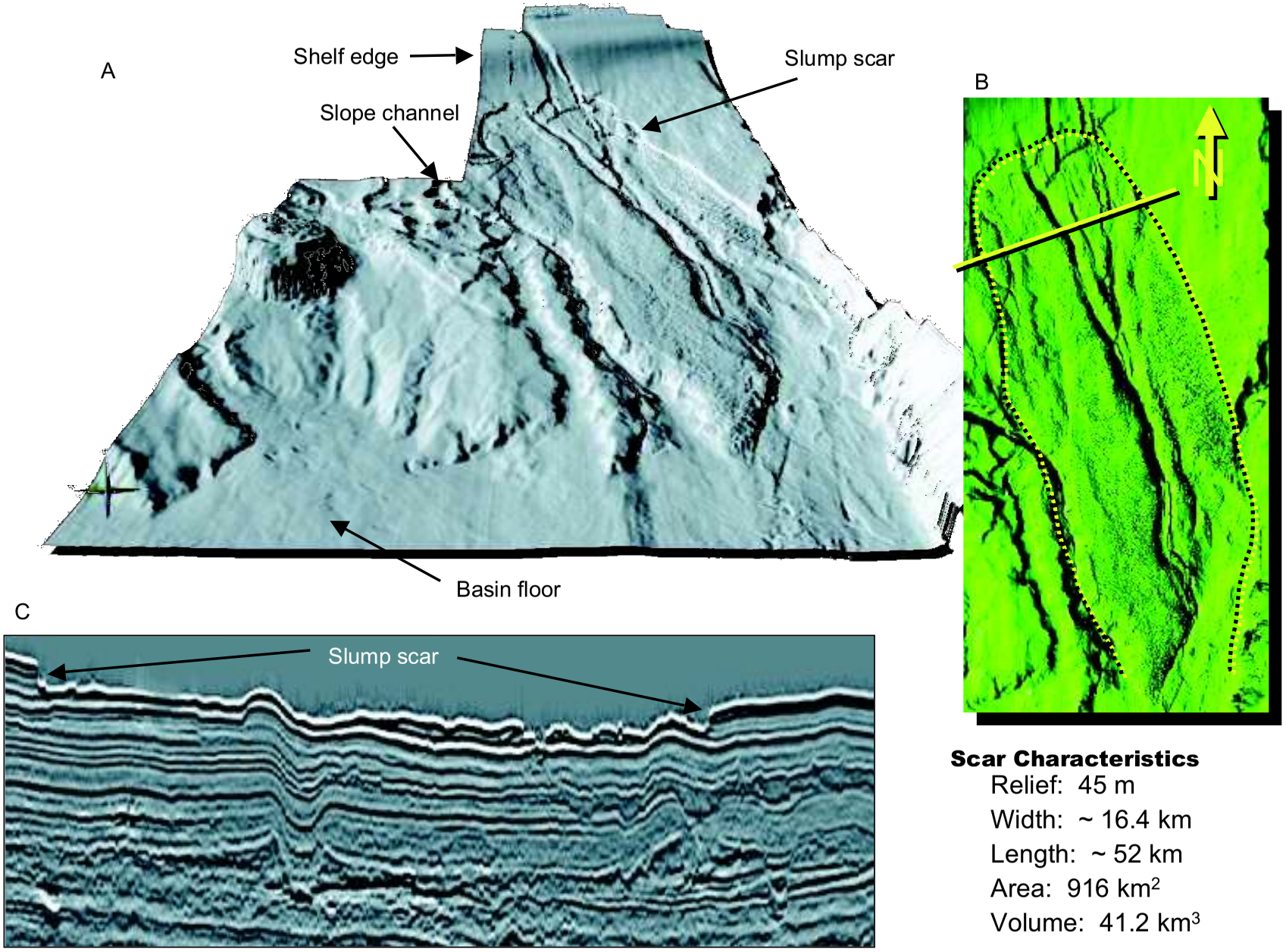

FIG. 144.—Perspective **A)**, dip-azimuth **B)**, and section **C)** views across the slope of the eastern Gulf of Mexico illustrating massive slump/slide scars and evacuation of massive amounts of material onto the basin floor to the south of this area. Seismic data courtesy of VeritasDGC.

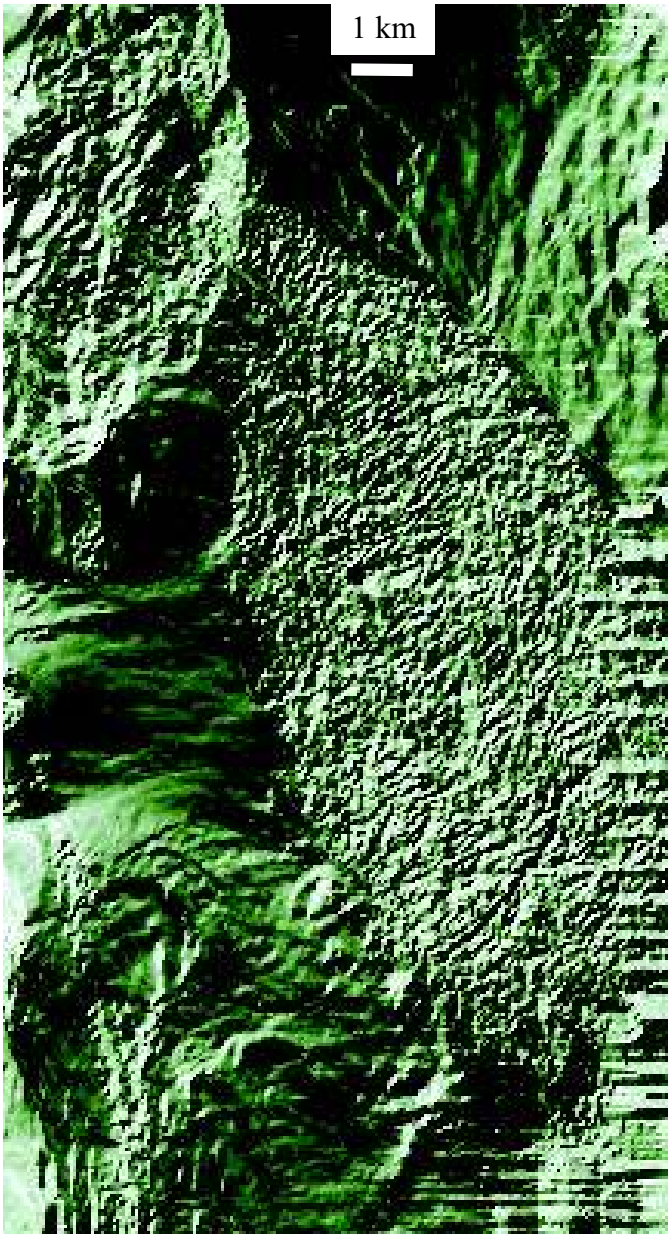

FIG. 145.—Debris flow off flank of submarine mud volcano.

The principal driver in deep-water sequence evolution is relative sea-level change—primarily the effect it has on characteristics of the staging area, including sand-to-mud ratio, sediment caliber, and depth of storm wave base. The stratigraphic, geomorphic, and sedimentologic expression of deep-water deposits is directly linked to the conditions at the shelf edge. It is there that sediments are delivered by rivers and other processes from hinterland areas. The locus of sedimentation, or depocenter, shifts seaward and landward as a direct result of sea-level fall or rise, respectively. During sea-level fall, forced regression occurs on the shelf (Posamentier et al., 1992) and depocenters shift rapidly toward the shelf edge. Even before the shoreline reaches the shelf edge, instability of the upper slope has been exacerbated both by lowered wave base and by unloading of a wedge of water (i.e., corresponding to the magnitude of sea-level fall). Another factor that may play a role in destabilizing the slope at this time is the shifting of oceanic currents that could accompany relative falls of sea level. Such instability can commonly result in mass failure in the mid- to upper-slope environment (Fig. 144) and subsequent deposition of a mass-transport complex on the slope and basin floor.

Ultimately, when river mouths are close enough to deliver sediments directly to the outer shelf or upper slope, deep-water turbidity currents become common across the slope and associated basin floor. During periods of relative sea-level fall, erosion by incising rivers results in increased sediment delivery to the shoreline, but more importantly increased sand-to-mud ratio of sediments delivered there. Whether the sediments are delivered directly from rivers by density underflow (i.e., hyperpycnal flow) or are initially deposited and then later remobilized as slumps transforming to slides and ultimately flows is not clear, and likely both occur. At these times of relative sea-level fall, relatively sand-rich flows tend to build relatively short leveed channels transitioning into relatively large frontal splays.

When relative sea-level rise resumes, initially stationary shorelines with aggrading coastal deltas and plains (Fig. 57) and then later transgressing shorelines result in a progressive decrease of sands available for transport to the deep-water environment. At these times coarser sands tend to be preferentially deposited behind the shoreline within incised valleys, back-barrier lagoons, and delta plains, producing gravity flows with potentially lower sand-to-mud ratio late in the relative sea-level lowstand and subsequent transgression. In response to this relative increase in mud content within flow events, levee construction becomes more efficient and leveed channels can extend significantly farther basinward. The transition point is observed to shift significantly farther seaward late in a sea-level cycle. This results in a juxtaposition of frontal splays overlain by solitary leveed channels corresponding to early and late lowstand systems tract times, respectively (Figs. 31, 74, 163, 164).

During subsequent periods of shoreline transgression, minimal amounts of river-supplied sediments reach the shelf edge and turbidite deposition largely ceases. Mass-transport deposition may continue at this time because of reequilibration of residual oversteepened, upper-slope deposits associated with lowstand shelf-edge delta deposition (Booth, 1979) or oversteepening of canyon walls associated with lowstand canyon or slope-channel cutting (Figs. 37, 165). A typical depositional sequence within a canyon is illustrated in Figs. 37 and 165. In most instances canyons are filled with relatively minor amounts of channelized turbidites (Figs. 37–39) and an overwhelming amount of mass-transport deposits that constitute the bulk of the canyon fill that forms during times when active turbidity flows have ceased (Fig. 165).

CONCLUSIONS

The complexity of deep-water deposits is apparent from the examples and discussions above. Large-scale, complex systems are particularly difficult to distill into simple models that can act as norms, predictors, and guides for future observations (Walker, this volume).

In the 1970s, little of this complexity was understood, and models such as those of Normark (1970, 1978), Mutti and Ricci Lucchi (1972), Mutti and Ghibaudo (1972), and Walker (1978) summarized observations from modern fans and ancient rocks, and combined such observations into models based on modern and ancient data (Walker, 1978). The models made little attempt to incorporate data from turbidity-current processes (laboratory

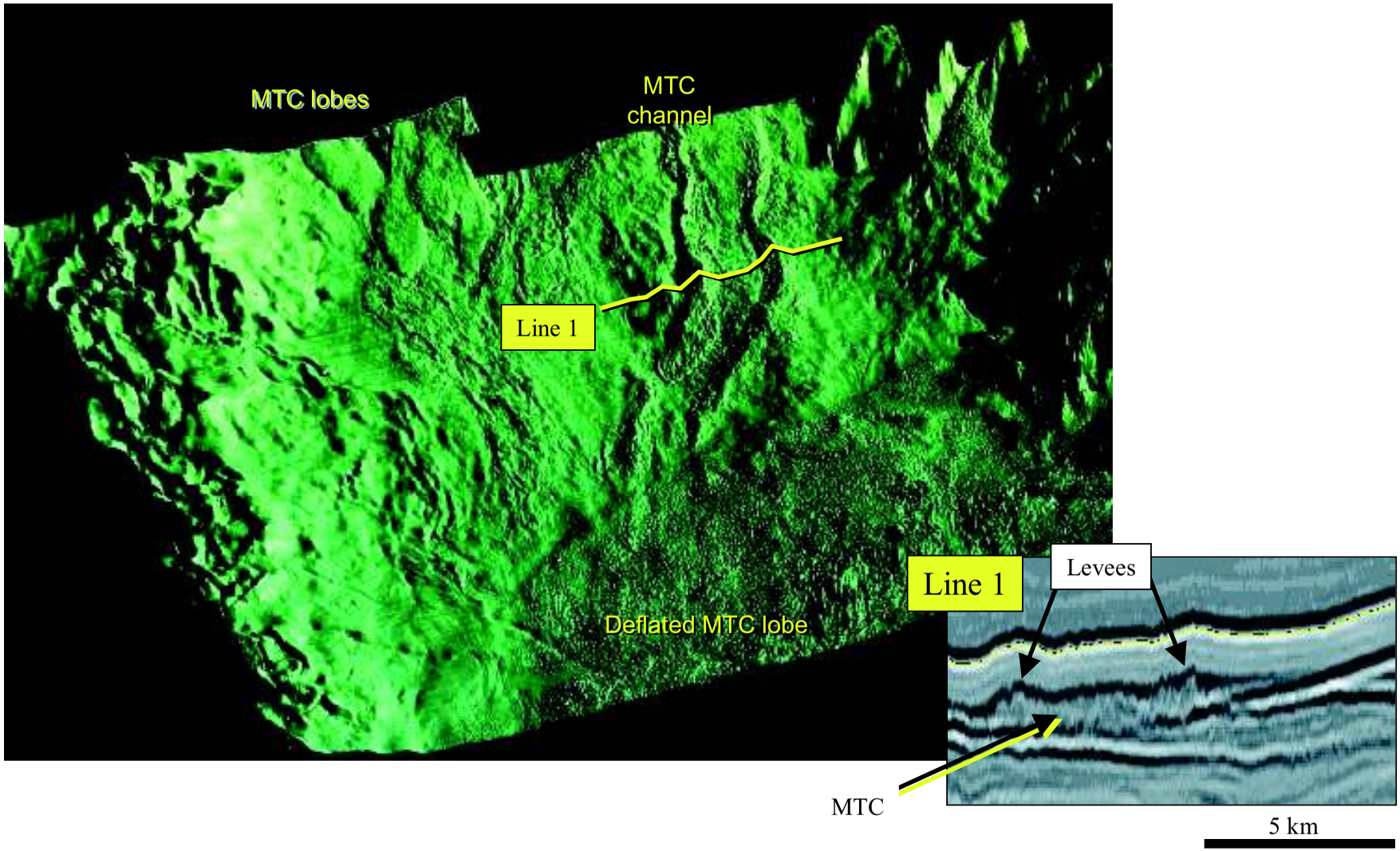

FIG. 146.—Seascape of the lower slope and basin floor, DeSoto Canyon area, eastern Gulf of Mexico. Note the varying types of mass-transport deposits, including a leveed mass-transport deposit, a lobate mass-transport deposit characterized by positive relief, and a flattened or deflated mass-transport deposit showing no positive relief and characterized only by a debris field. Seismic data courtesy of VeritasDGC.

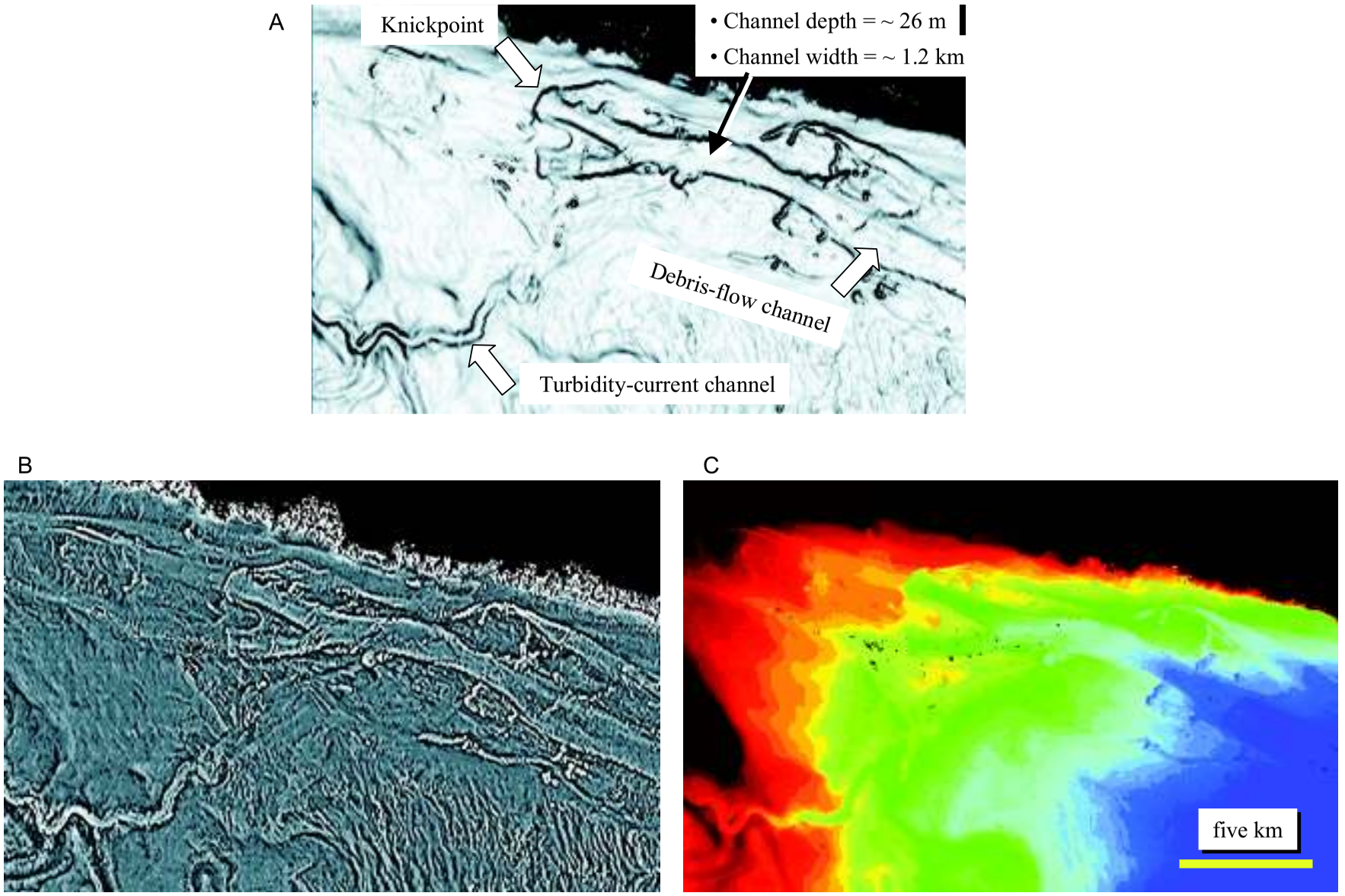

FIG. 147.—**A)** Dip-magnitude, **B)** curvature, and **C)** time-structure maps of a debris-flow channel. This channel is characterized by low sinuosity and the presence of a well-defined knickpoint at its head. Seismic data courtesy of WesternGeco.

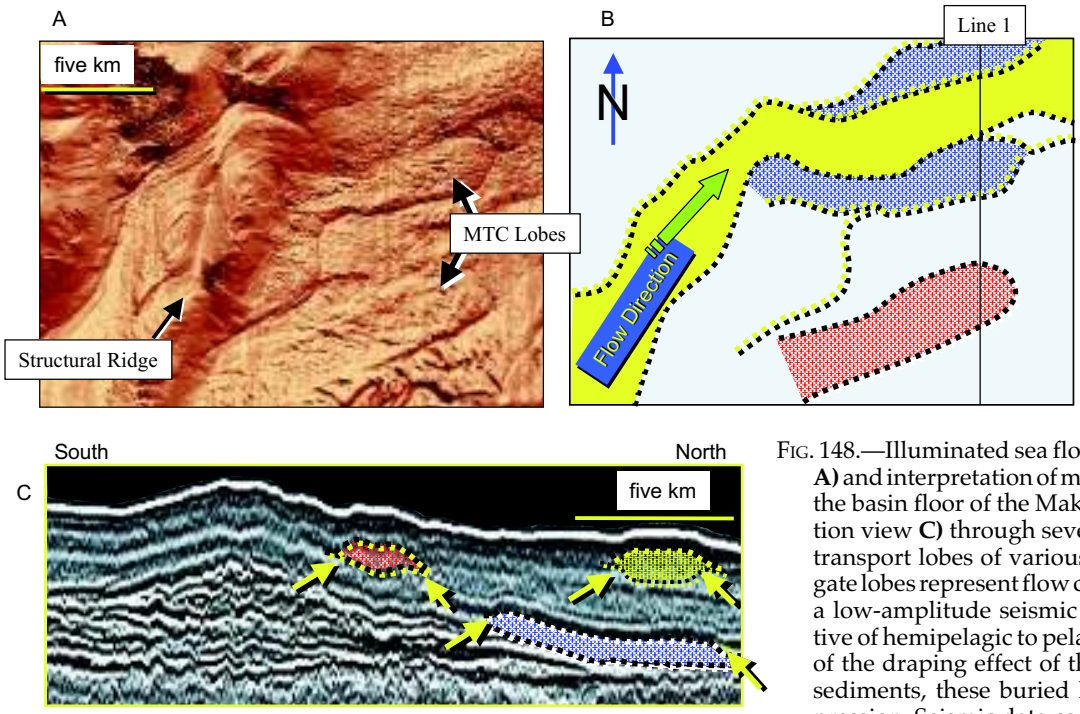

FIG. 148.—Illuminated sea floor based on 3D seismic data **A)** and interpretation of mass-transport deposits **B)** on the basin floor of the Makassar Strait, Indonesia. Section view **C)** through several shallowly buried mass-transport lobes of various age. Note that these elongate lobes represent flow complexes imbedded within a low-amplitude seismic reflection package suggestive of hemipelagic to pelagic sedimentation. Because of the draping effect of the hemipelagic and pelagic sediments, these buried lobes all have sea-floor expression. Seismic data courtesy of WesternGeco.

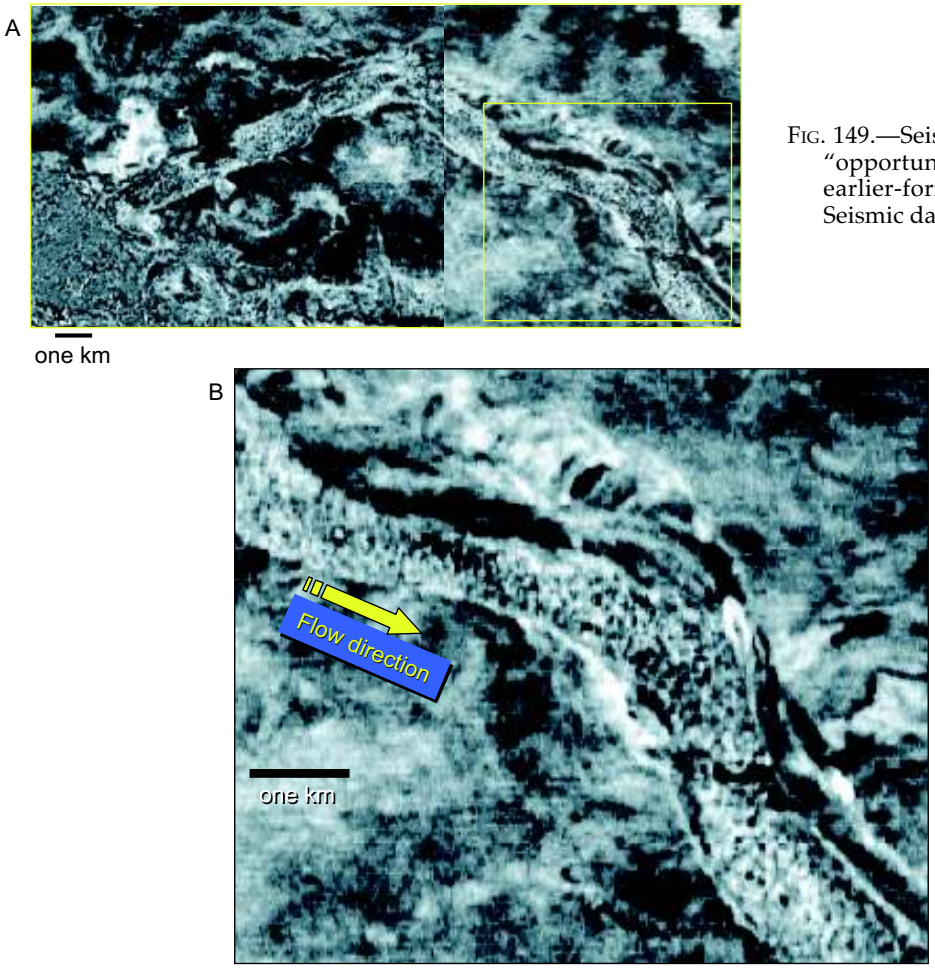

FIG. 149.—Seismic reflection horizon slice showing an "opportunistic" mass-transport deposit within an earlier-formed turbidity-current leveed channel. Seismic data courtesy of WesternGeco.

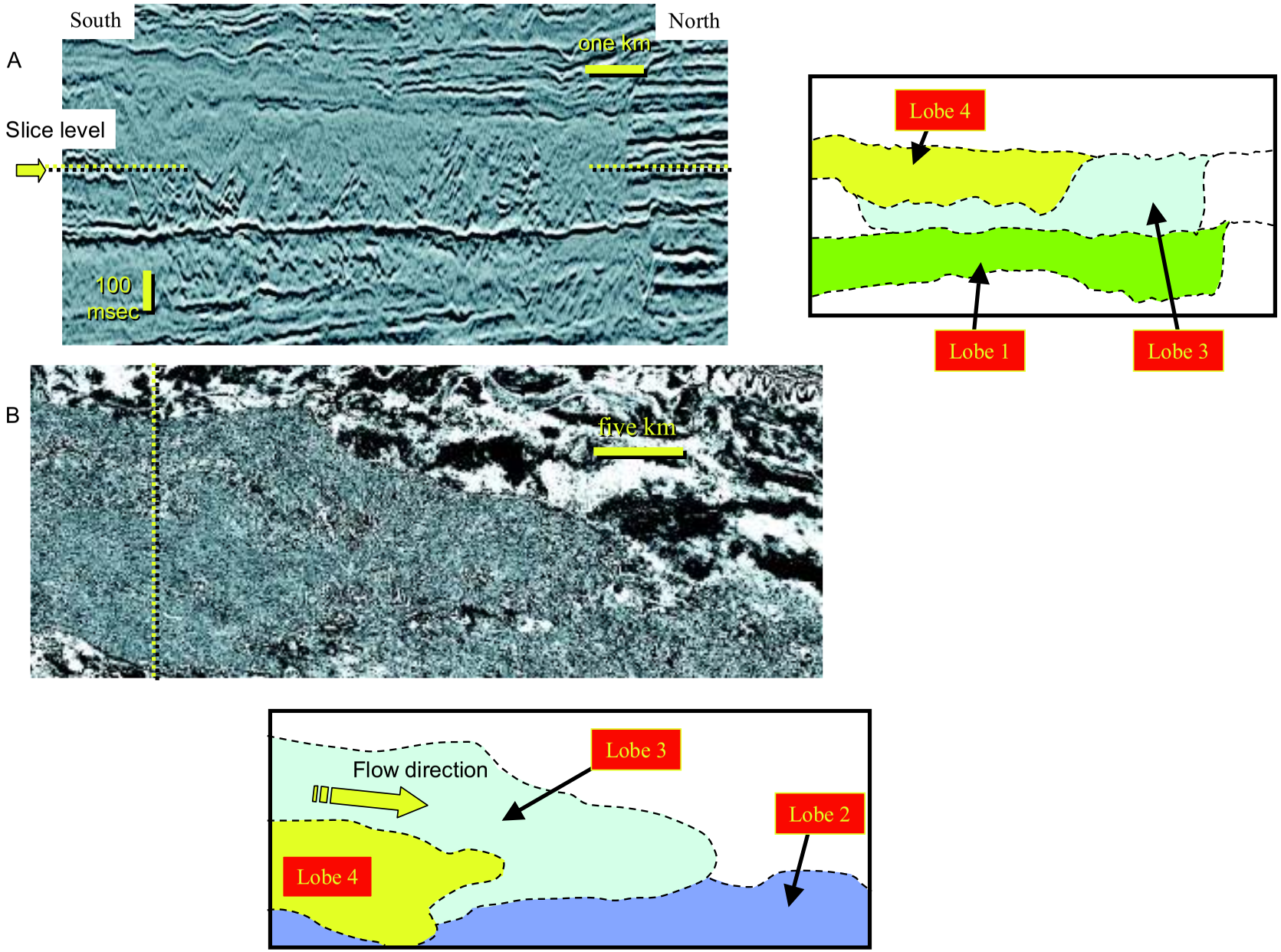

FIG. 150.—Seismic reflection cross-section **A)** and plan-view **B)** images illustrating a succession of amalgamating mass-transport deposits. Note the typical chaotic to transparent reflection character within these deposits, suggesting a severely disrupted and discontinuous stratigraphic architecture. Seismic data courtesy of WesternGeco.

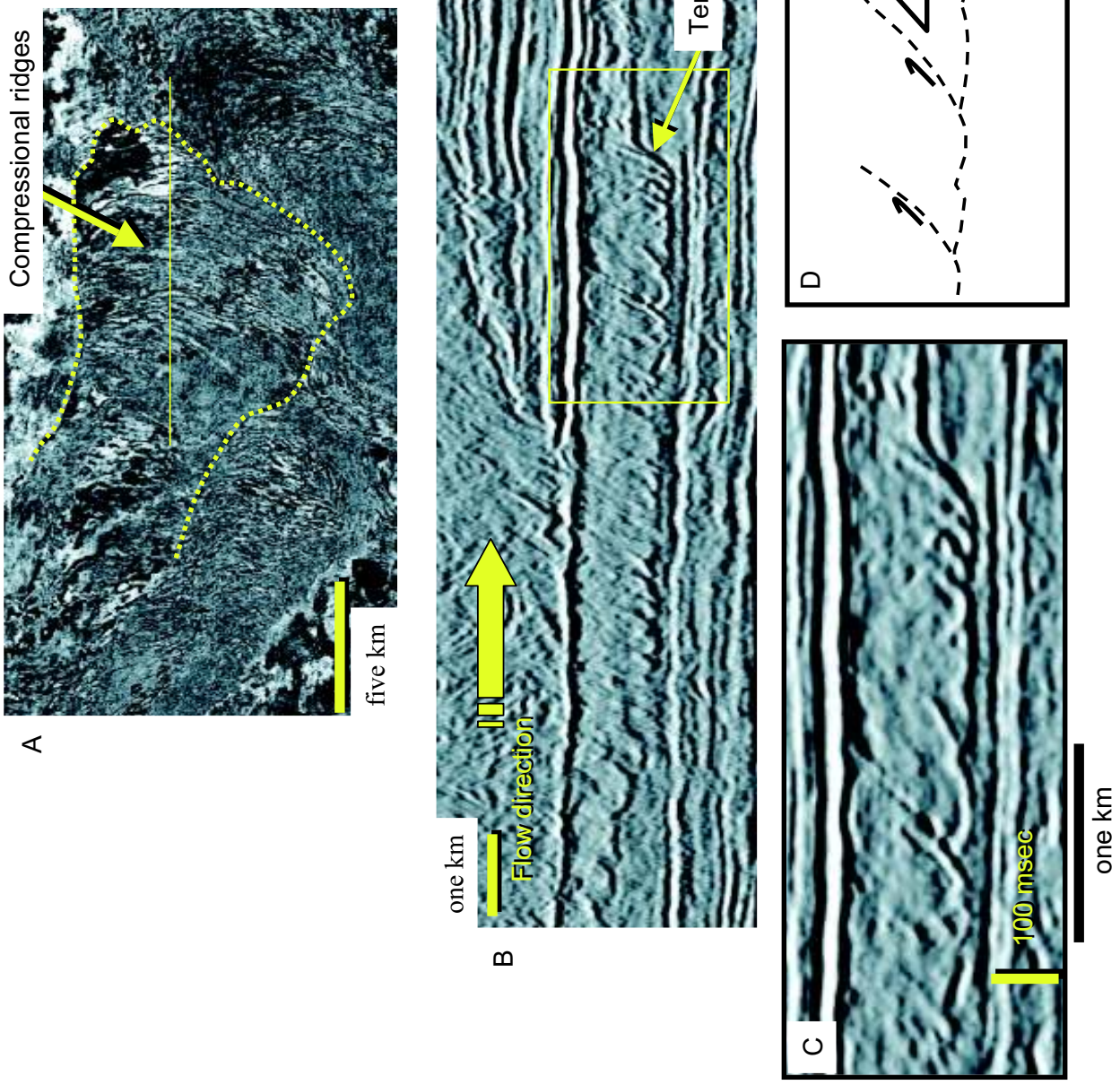

FIG. 151.—Seismic reflection plan view **A)** and section views **B–D)** through a mass-transport complex, Gulf of Mexico. The transverse lineaments are the plan-view expression of thrust faults caused by the mass flow abutting against the terminal wall. Thrust faults are measured at approximately a 15 degree dip. Seismic data courtesy of WesternGeco.

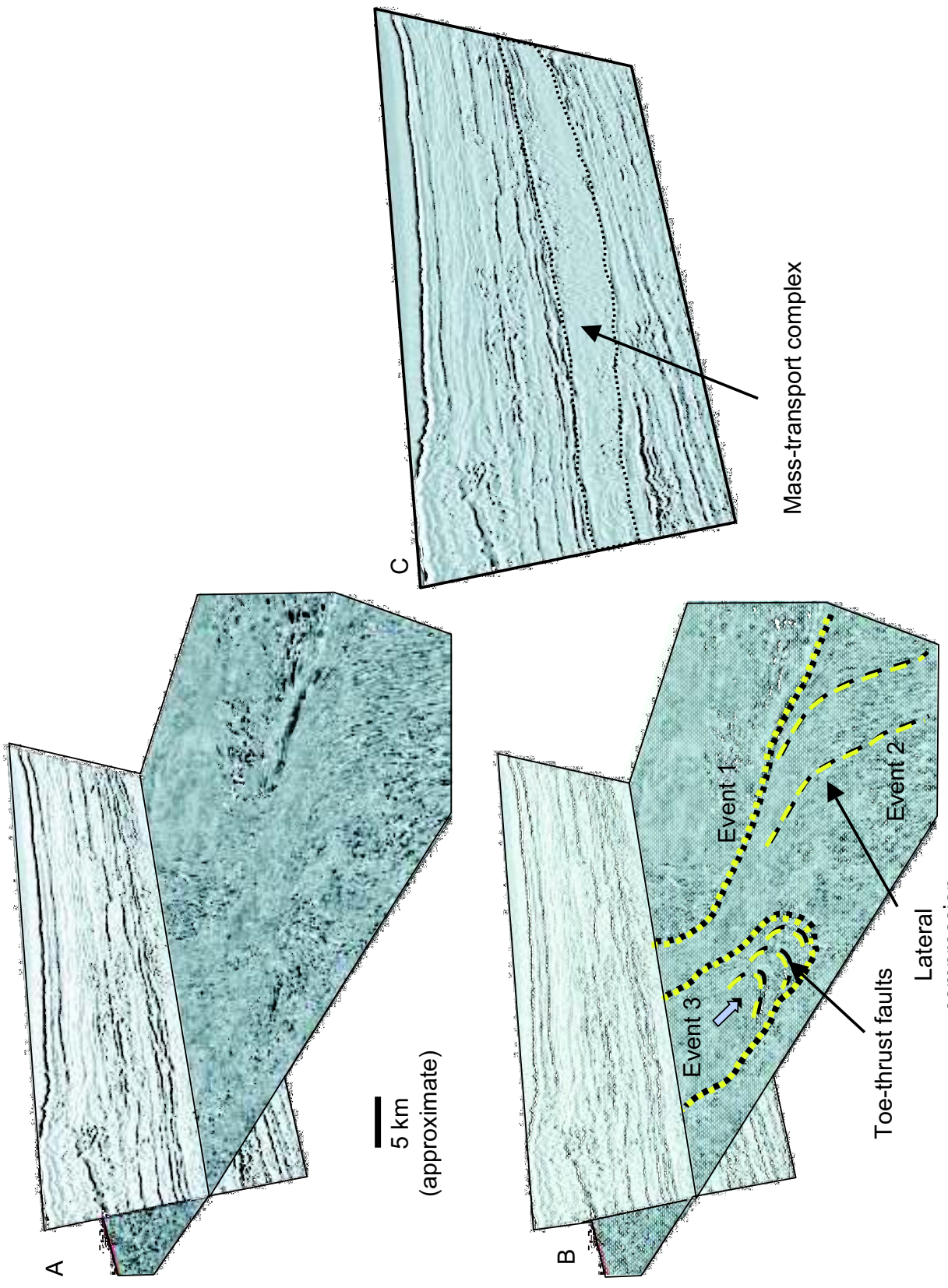

FIG. 152.—**A, B)** Oblique and **C)** section views through an amalgamated mass-transport complex. At least three event units can be recognized. Internal deformation in the form of compression-associated low-angle thrust faults can be observed within events 2 and 3 (B). Both toe thrusts as well as thrusts associated with lateral compression caused by later flows are seen. Seismic data courtesy of WesternGeco.

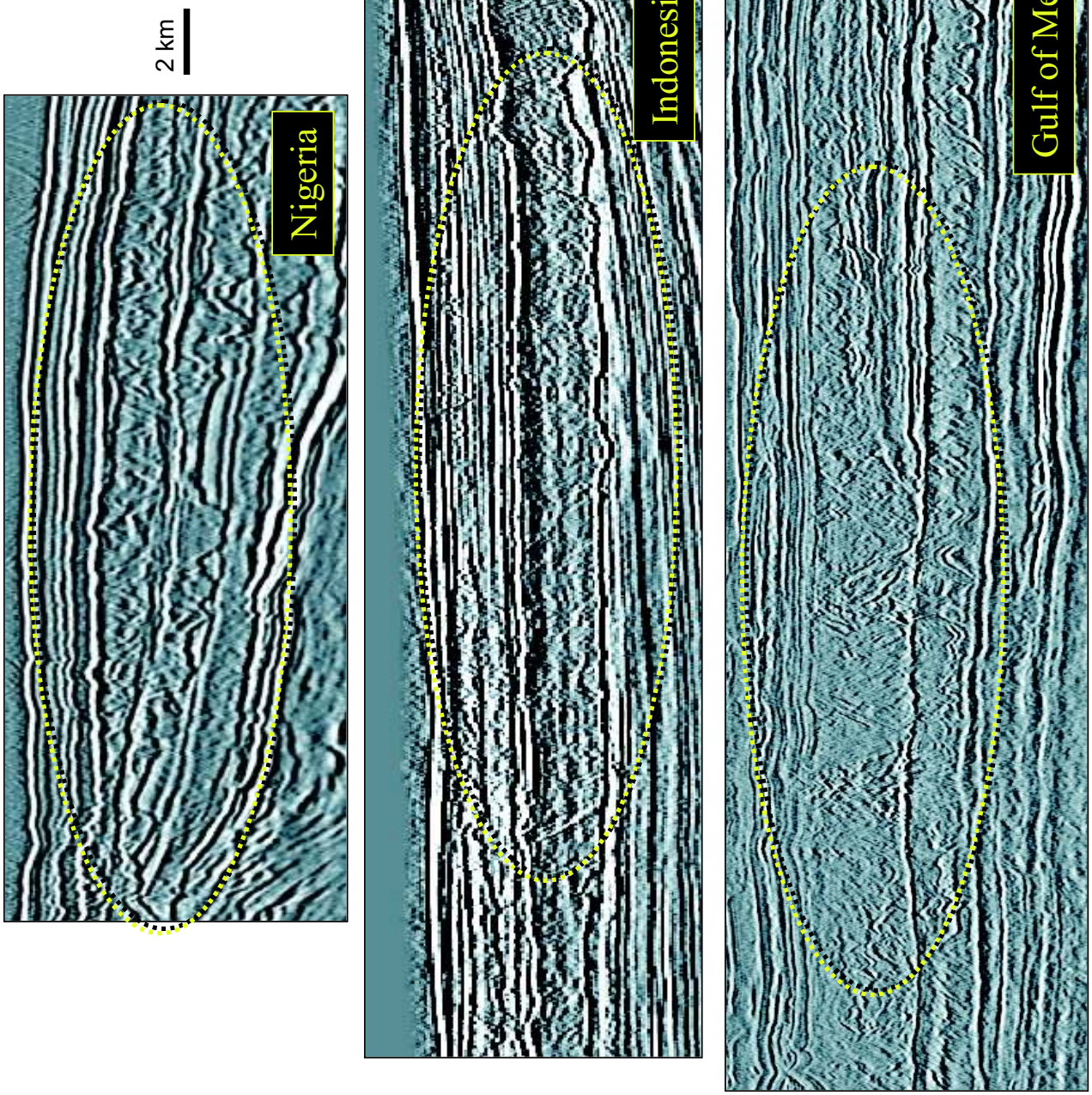

FIG. 153.—Cross-section view through three mass-transport deposits. Each is characterized by chaotic and contorted seismic facies pattern. Top line, seismic data courtesy of VeritasDGC. Middle and lower lines, seismic data courtesy of WesternGeco.

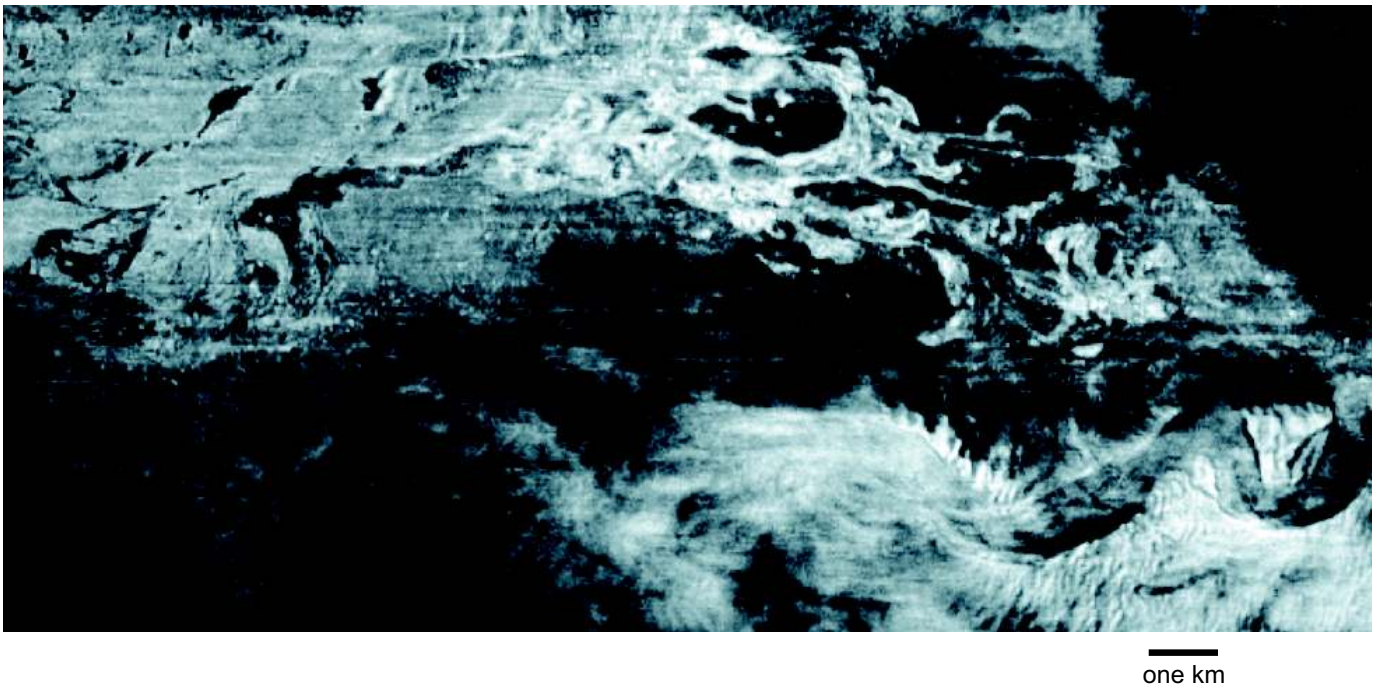

FIG. 154.—Seismic horizon slice through mass-transport deposit characterized by convolute bedding, basin floor of the eastern Gulf of Mexico. Compare with Figure 139, a seismic slice at the base of this mass-transport deposit. Seismic data courtesy of WesternGeco.

or modern ocean observations), and thus remained observational rather than process based. In retrospect, we note that the Walker (1978) model showed a very simplistic and commonly incorrect distribution of sand and mud on the fan, and also ignored the effects of different grain-size distributions, tectonic settings, and relative sea-level fluctuations.

Relative sea-level fluctuations were built into the models of Mutti (1985), Vail et al. (1977), and Posamentier and Vail (1985). This model essentially combined three aspects of older Mutti models into one evolving model, with sandy detached lobes forming during lowstands of relative sea level. During relative sea-level rise, the fan evolved into one where the channels were attached to smaller depositional lobes. At highstand, with a much reduced sediment supply, either condensed sections or finer-grained channels and levee formed, with little or no lobe formation.

The 1980s marked the time when geophysical observations became important, particularly side-scan sonar and shallow-penetration seismic profiles across fan surfaces. This information was very different in nature and scale from the rock observations and poorer-quality side-scan data from the 1970s. Because the data were so different—for example, data on the meandering channels from the Amazon Fan (Damuth et al., 1982a; Damuth et al., 1982b) and the data on channel, levee, and large-scale slump from the Rhône Fan (Droz and Bellaiche, 1985), it was difficult to combine older models with this new data—in fact, there are no published attempts to do so.

At around the same time, 3-D seismic data from Tertiary and Modern fans was becoming available to oil companies, but few of these studies made their way into the public literature until the 1990s. The seismic data revealed superb three-dimensional relationships between all of the depositional elements, but again it was difficult to relate seismic-scale data to outcrop data. With the advent of seismic geomorphology (Posamentier and Kolla, 2003a) the integration of such observations was made possible. Because the seismic data revealed so well the geometrical relationships between elements, it became possible to infer and better understand the processes that gave rise to the various depositional geometries—processes such as channel meandering and avulsion, and lobe development by crevassing, overbank spill, or flow expansion at the ends of channels.

Thus any attempts at modeling of turbidite systems must incorporate information of four different types and scales: processes (on the flume experimental scale as well as the scale of modern fans), 3-D seismic studies, observations of ancient rocks, and numerical models. There is still a rather incomplete linkage between these different sources of data, and we have tried to show how some of these linkages might be made. Our conclusions are based in fact as much as possible but are nevertheless somewhat process and conceptual in flavor. Future fan models will evolve as more work is done relating experimental studies to ancient rocks and relating the geometry of large outcrops to 3-D seismic data derived both from modern fans and Cretaceous–Tertiary turbidite systems. As the seismic studies evolve, so the large-scale processes of fan development will be better understood, and the future conceptual basis for modeling will be better established.

In this paper, we have integrated facies with depositional elements and then discussed modern and subsurface 3-D seismic examples to show how the depositional facies fit into the various depositional systems. Because in most instances ground truth is lacking in studies based on 3D seismic, we have integrated information from outcrop examples to help provide insights to assist in interpreting the 3-D seismic images (for example, the San Clemente and Ross outcrop examples help to calibrate the seismic images of meander loops; Figs. 51, 71, 72). Rather than create a model that would serve as a template, we have focused on first principles based largely on process sedimentology. In this way, we leave it to geoscientists to build their own models using depositional elements as building blocks in

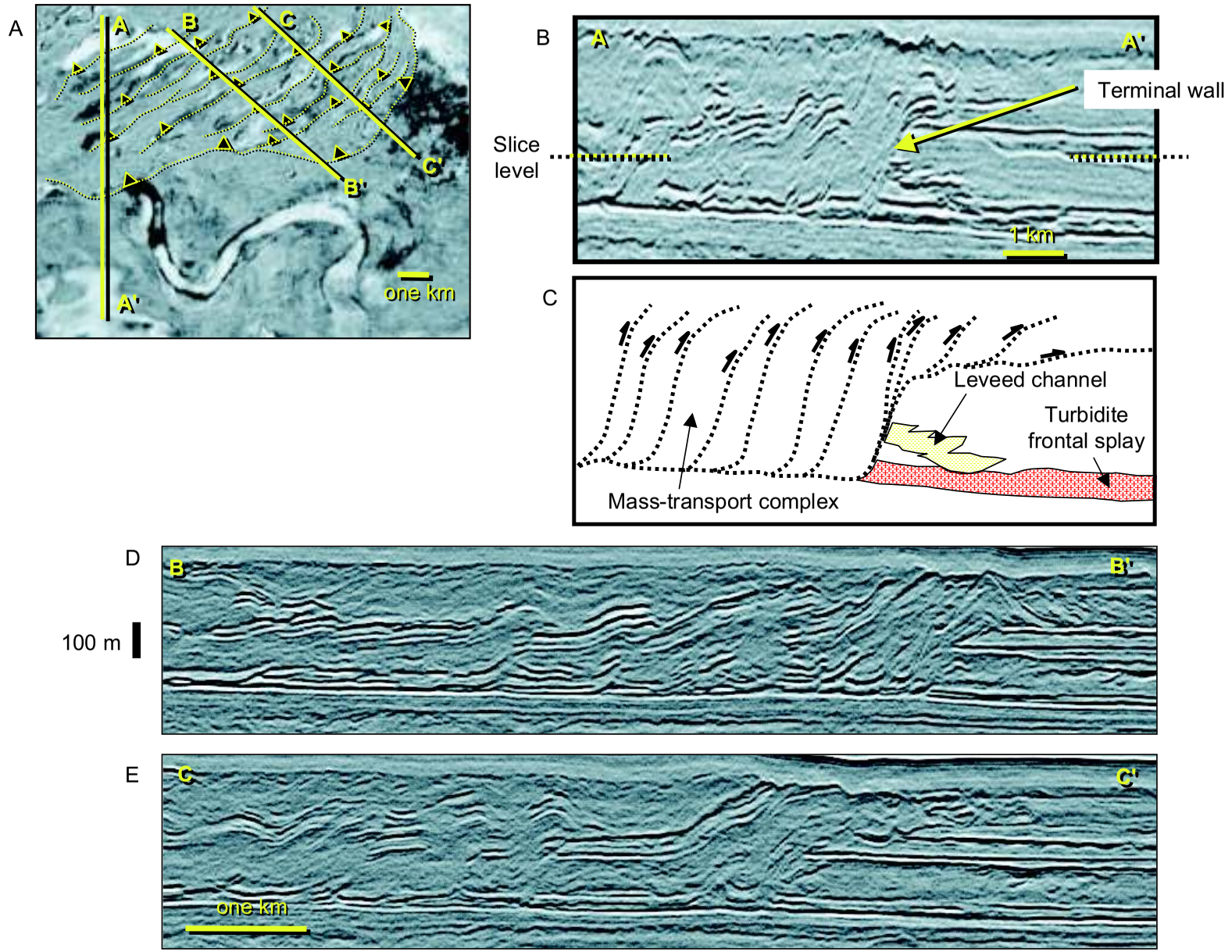

FIG. 155.—Example of the terminus of a mass-transport deposit, eastern Gulf of Mexico. This deposit shows evidence of having been transported across a decollement surface that likely was located within a condensed section at the base of a frontal-splay complex. In response to compression against a terminal wall, internal deformation in the form of thrust faulting occurred. The plan-view **A)** as well as the section views **B–E)** the clearly show the mass-transport unit entraining earlier-deposited, sand-prone leveed-channel and frontal-splay deposits. Seismic data courtesy of WesternGeco.

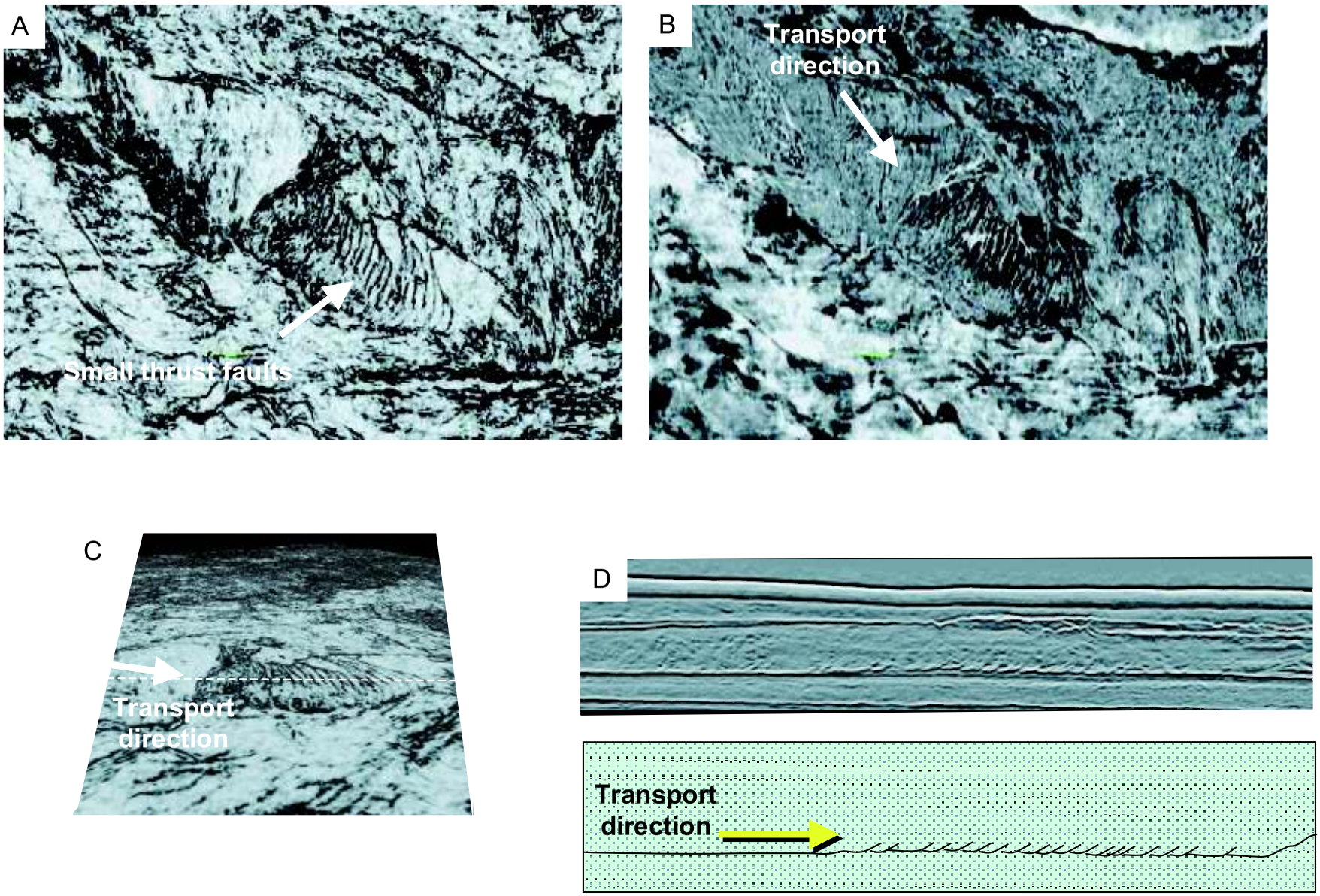

FIG. 156.—Seismic time slice in the coherence **A)** and amplitude **B)** domains illustrating the plan view and oblique view **C)** expression of thrust faults within mass-transport deposits. **D)** Seismic reflection profile across mass transport deposits characterized by low-angle thrust faults. Seismic data courtesy of WesternGeco.

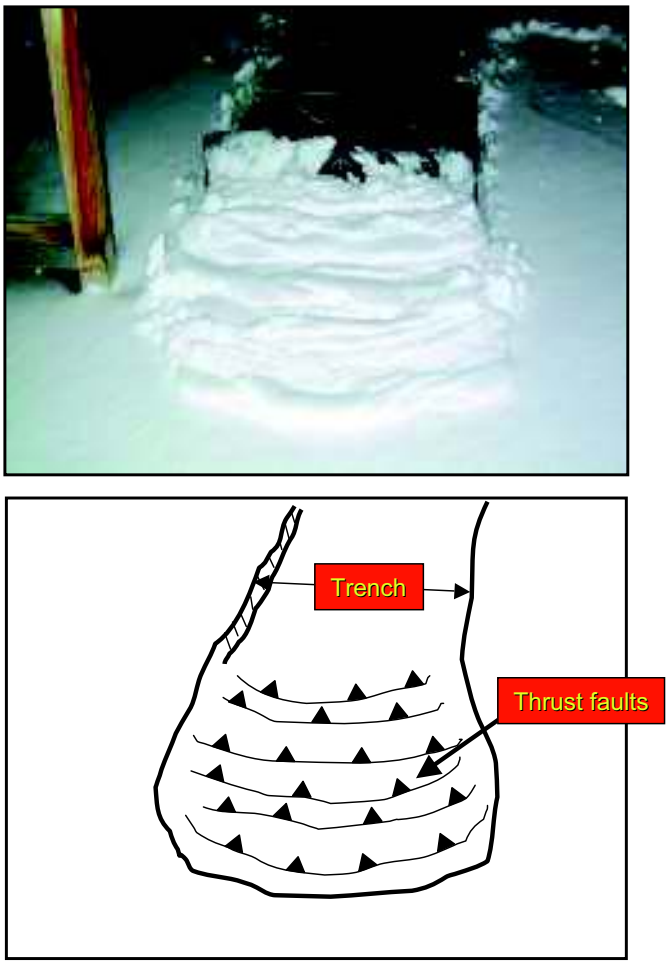

FIG. 157.—Small-scale analog for mass-transport deposits shown in Figures 134, 135, and 155. The snow shovel slides on a hard base, pushing snow before it. The semi-rigid snow pack deforms internally predominantly by low-angle thrust faulting as the mass slides on the underlying decollement surface and is compressed against the snow pack before it. The trench, which is formed in the wake of the shovel, is characterized by steep walls produced by shearing of the flowing mass.

space and time. On the basis of a sound understanding of local physiography, sediment flux, and sediment caliber, integrated with process sedimentology, predictive facies models can be constructed. Lateral as well as vertical facies successions can be predicted.

Sediment accumulates in staging areas, moves down canyons or slope channels, and ultimately travels onto the basin floor through leveed channels and frontal splays. Principal deep-water sand habitats include slope-channel complexes, basin-floor channel fills, crevasse splays and sediment waves in overbank settings, and frontal splays. Canyons also can be sites of confined leveed channel deposits, though the bulk of canyon fill commonly is mud prone. To a lesser extent, sand deposition also occurs within levees in response to repeated spillover across levee crests. Where slopes are characterized by high rugosity, such as areas underlain by mobile salt or complex toe-thrust ridges, deposition of a broad range of depositional elements can occur within relatively small areas. Intraslope basins can be characterized by the full range of sand habitats, insofar as they comprise, in microcosm, slope and basin-floor physiography. Figures 166–168 illustrate and summarize the various significant sand habitats on the basin floor. Figures 169 and 170 illustrate the significant sand habitats on the slope.

The role of grain-size distribution within a flow as well as in a succession of flows is critical to understanding the evolution of depositional elements, especially those on the basin floor. The more mud in the system, the farther seaward the leveed-channel depositional element extends. As flows travel seaward they are preferentially impoverished of their mud content through continual spillover of the upper parts of the flows into the overbank environment. At the point where the levees are low enough to allow sand from the higher-density, lower part of the flow to spill over the levees, the system morphology transitions from leveed channel to frontal splay. The frontal splays are commonly channelized in their proximal parts, but the channels are shallow and have small levees. Channel paths probably switch rapidly. In the distal parts of the frontal splays, flows become even less channelized and more sheet-like.

Mass-transport deposits, largely debrites, are common components of deep-water environments (Fig. 133). These deposits, which are largely mud prone, commonly originate in mid-slope to upper-slope environments. They commonly directly overlie erosional surfaces characterized by long grooves and striations. Near their termini as well as along their margins, they are characterized by internal compressive deformation in the form of imbricate thrust faults. Mass-transport complexes likely are characterized by complex rheology that reflects frequent transitions from turbulent to laminar to "plug" flow within a single flow event.

In summary, we urge caution in adopting overly simple facies models in deep-water environments. The deep water is a potentially complex depositional setting. The degree of complexity of the facies model desired should be dependent on the quality of data available and should be built upon depositional elements observed and inferred. However, as the geoscientist well knows, the devil is in the details!

ACKNOWLEDGMENTS

The authors acknowledge Anadarko Petroleum Corporation for permission to publish. Permission to publish seismic data from VeritasDGC, Western Geophysical, PGS Geophysical is gratefully acknowledged. We also wish to thank the various colleagues with whom we have had lengthy conversations about the world of deep-water sedimentation through the years. These include V. Kolla, P. Weimer, W. Normark, H. DeV. Wickens, B. Kneller, and W. Morris. This paper benefited from and was significantly improved thanks to the comprehensive reviews of Todd Greene and Octavian Catuneaunu.

REFERENCES

ABREU, V., SULLIVAN, M., PIRMEZ, C., AND MOHRIG, D., 2003, Lateral accretion packages (LAPs): an important reservoir element in deep water sinuous channels: Marine and Petroleum Geology, v. 20, p. 631–648.

BALLANCE, P.F., 1964, The sedimentology of the Waitemata Group in the Takapuna section, Auckland: New Zealand Journal of Geology and Geophysics, v. 7, p. 466–499.

BEAUBOEUF, R.T., AND FRIEDMANN, S.J., 2000, High-resolution seismic/sequence stratigraphic framework for the evolution of Pleistocene intra slope basins, Western Gulf of Mexico: depositional models and reservoir analogs, *in* Weimer, P., Slatt, R.M., Coleman, J., Rosen, N.C., Nelson, H., Bouma, A.H., Styzen, M.J., and Lawrence, D.T., eds.,

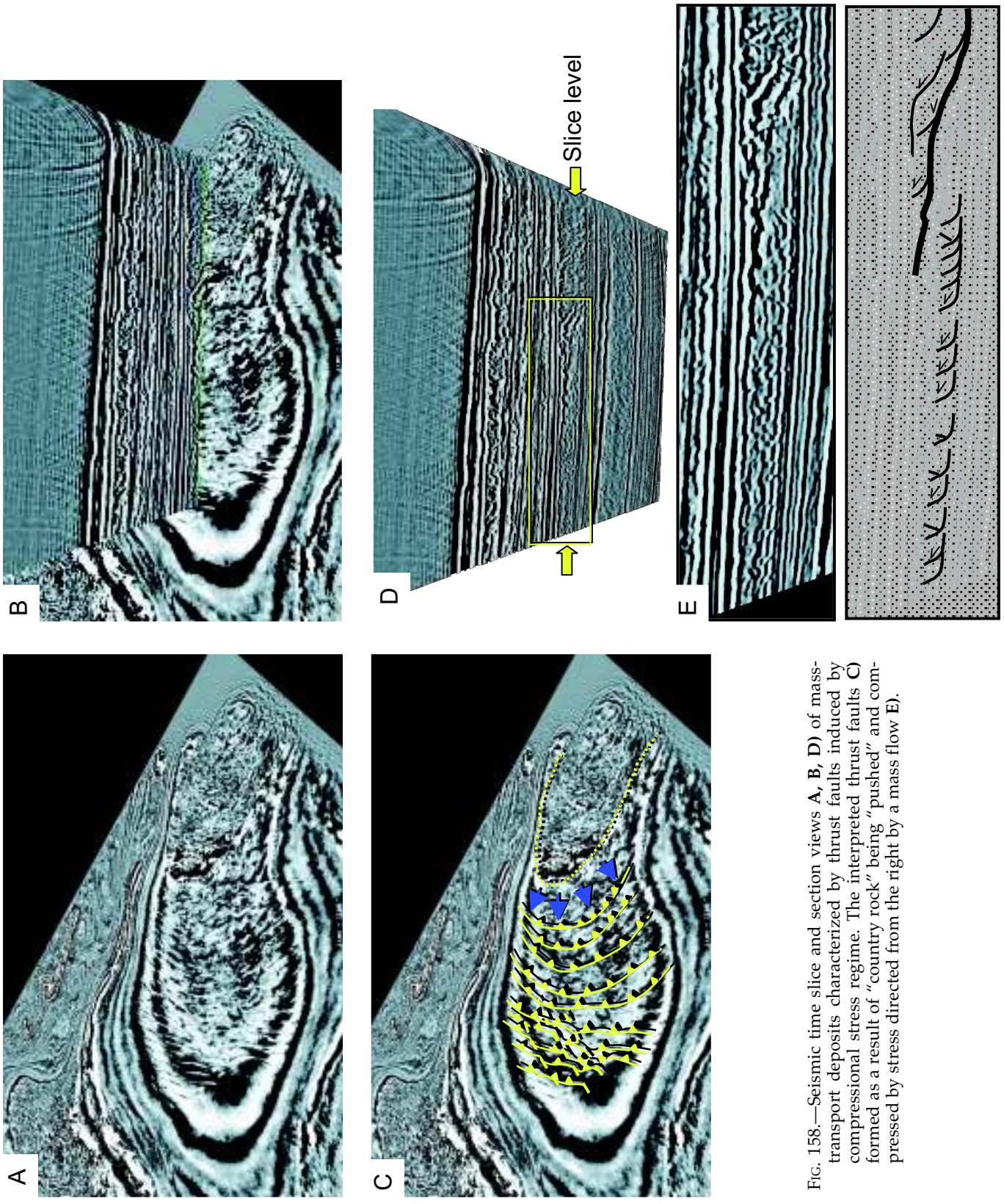

FIG. 158.—Seismic time slice and section views **A, B, D)** of mass-transport deposits characterized by thrust faults induced by compressional stress regime. The interpreted thrust faults **C)** formed as a result of "country rock" being "pushed" and compressed by stress directed from the right by a mass flow **E)**.

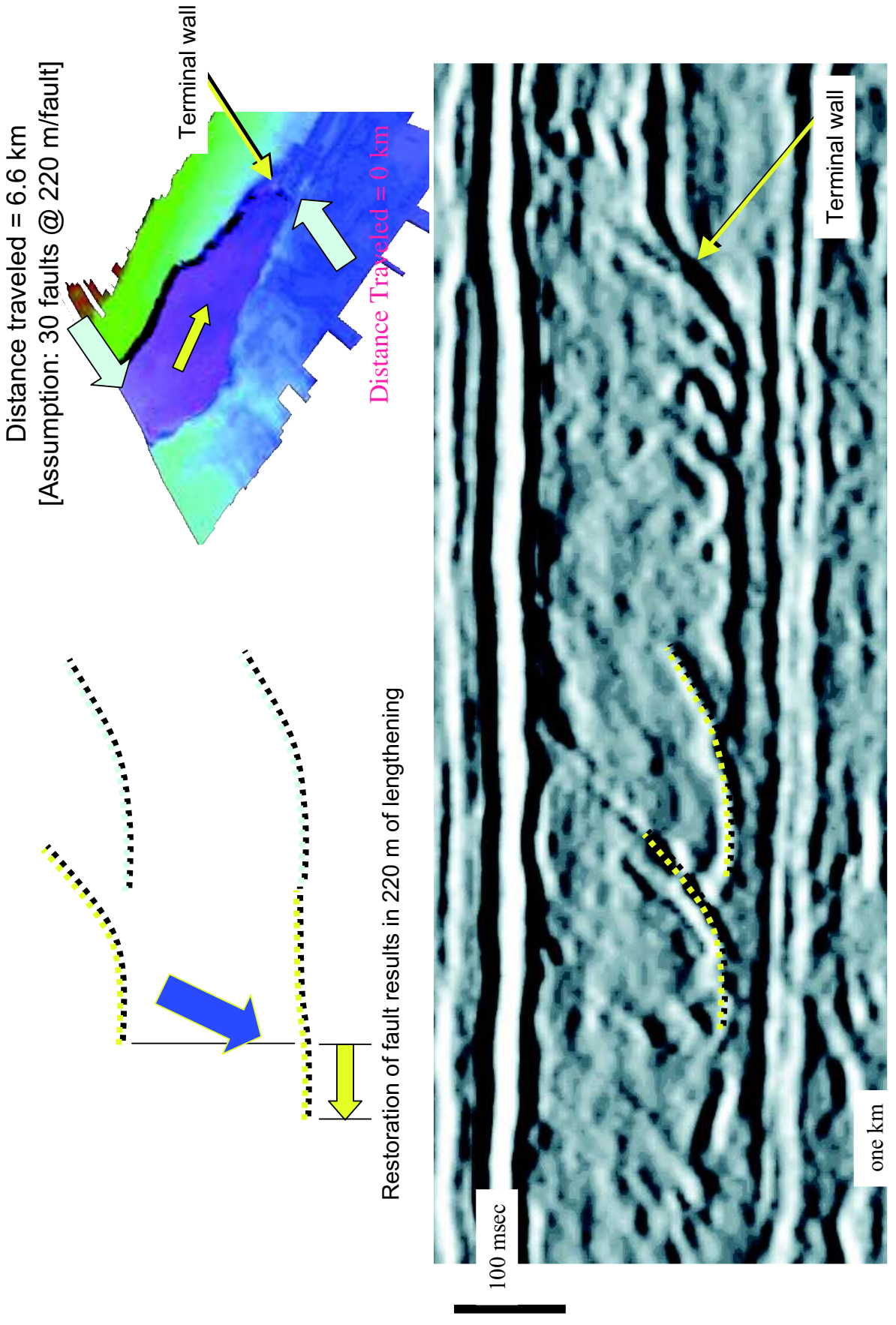

FIG. 159.—Seismic profile through mass-transport deposit shown in Figure 149. Approximate palinspastic reconstruction results in 220 m of lengthening for each thrust fault. With approximately 30 faults along an axial profile within the study area, restoration results in extension of approximately 6.6 km at the up-system limit of the deposit, whereas it can be assumed that the sediments near the terminal wall would have moved only minimally. Seismic data courtesy of WesternGeco.

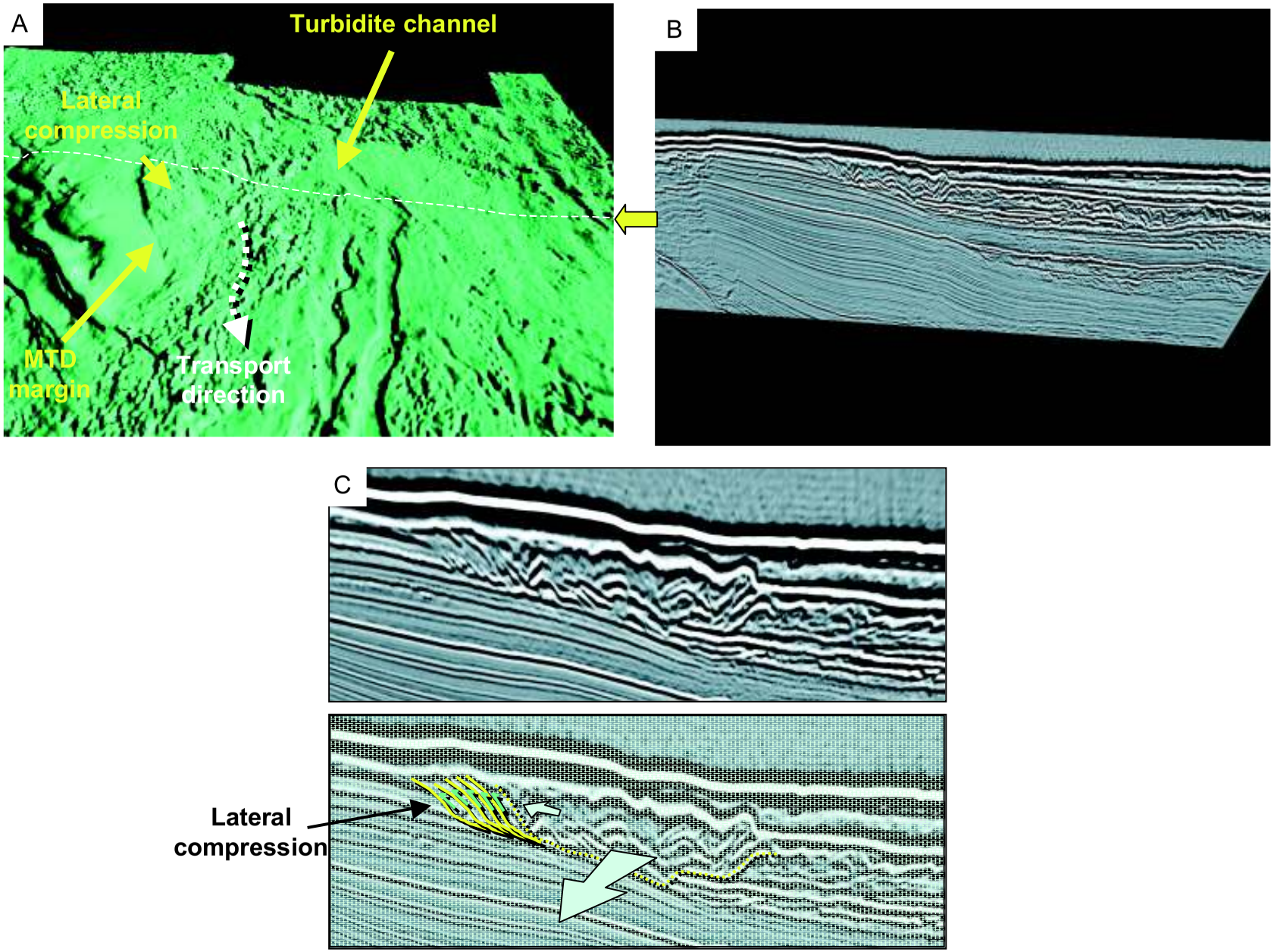

FIG. 160.—**A)** Illuminated horizon at the top of a mass-transport deposit illustrating a lateral compressional bulge. **B, C)** Seismic reflection profile illustrating lateral compression associated with a later phase of mass transport.

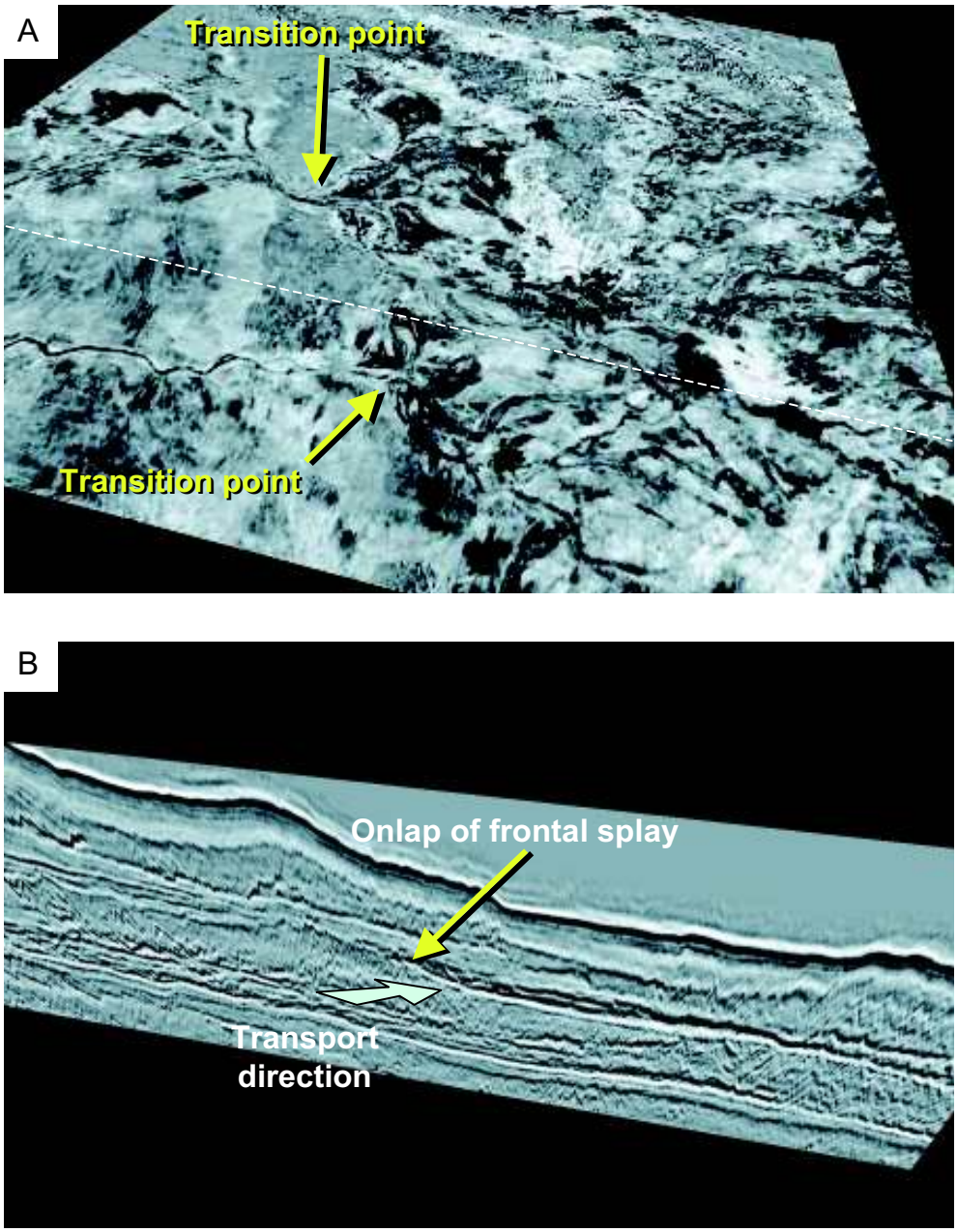

FIG. 161.—Influence on turbidites by rugosity atop mass-transport deposits. **A)** Seismic time slice that shows the transition point of a frontal splay, with extensive frontal-splay deposits seaward of that location. **B)** Seismic section that illustrates the onlap of frontal-splay deposits against a bathymetric high associated with the irregular top of a mass-transport complex. Seismic data courtesy of WesternGeco.

Deep-Water Reservoirs of the World: Gulf Coast Section SEPM, 20th Annual Research Conference, p. 40–60.

BOOTH, J.S., 1979, Recent history of mass-wasting on the upper continental slopes, northern Gulf of Mexico, as interpreted from the consolidation states of the sediment, *in* Doyle, L.J., and Pilkey, O.H., eds., Geology of Continental Slopes: SEPM, Special Publication 27, p. 153–165.

BOUMA, A.H., 1962, Sedimentology of Some Flysch Deposits; A Graphic Approach to Facies Interpretation: Amsterdam, Elsevier, 168 p.

BOUMA, A.H., NORMARK, W.R., AND BARNES, N.E., eds., 1985, Submarine Fans and Related Turbidite Systems: New York, Springer-Verlag, 351 p.

BRAMI, T.R., PIRMEZ, C., ARCHIE, C., HEERALAL, S., AND HOLMAN, K.L., 2000, Late Pleistocene deep-water stratigraphy and depositional processes, offshore Trinidad and Tobago, *in* Weimer, P., Slatt, R.M, Coleman, J., Rosen, N.C., Nelson, H., Bouma, A.H., Styzen, M.J., and Lawrence, D.T., eds., Deep-Water Reservoirs of the World: Gulf Coast Section SEPM Foundation, 20th Annual Research Conference, p. 104–115.

BRUHN, C.H.L., AND WALKER, R.G., 1995, High-resolution stratigraphy and sedimentary evolution of coarse-grained canyon-filling turbidites from the Upper Cretaceous transgressive megasequence, Campos Basin, Brazil: Journal of Sedimentary Research, v. B65, p. 426–442.

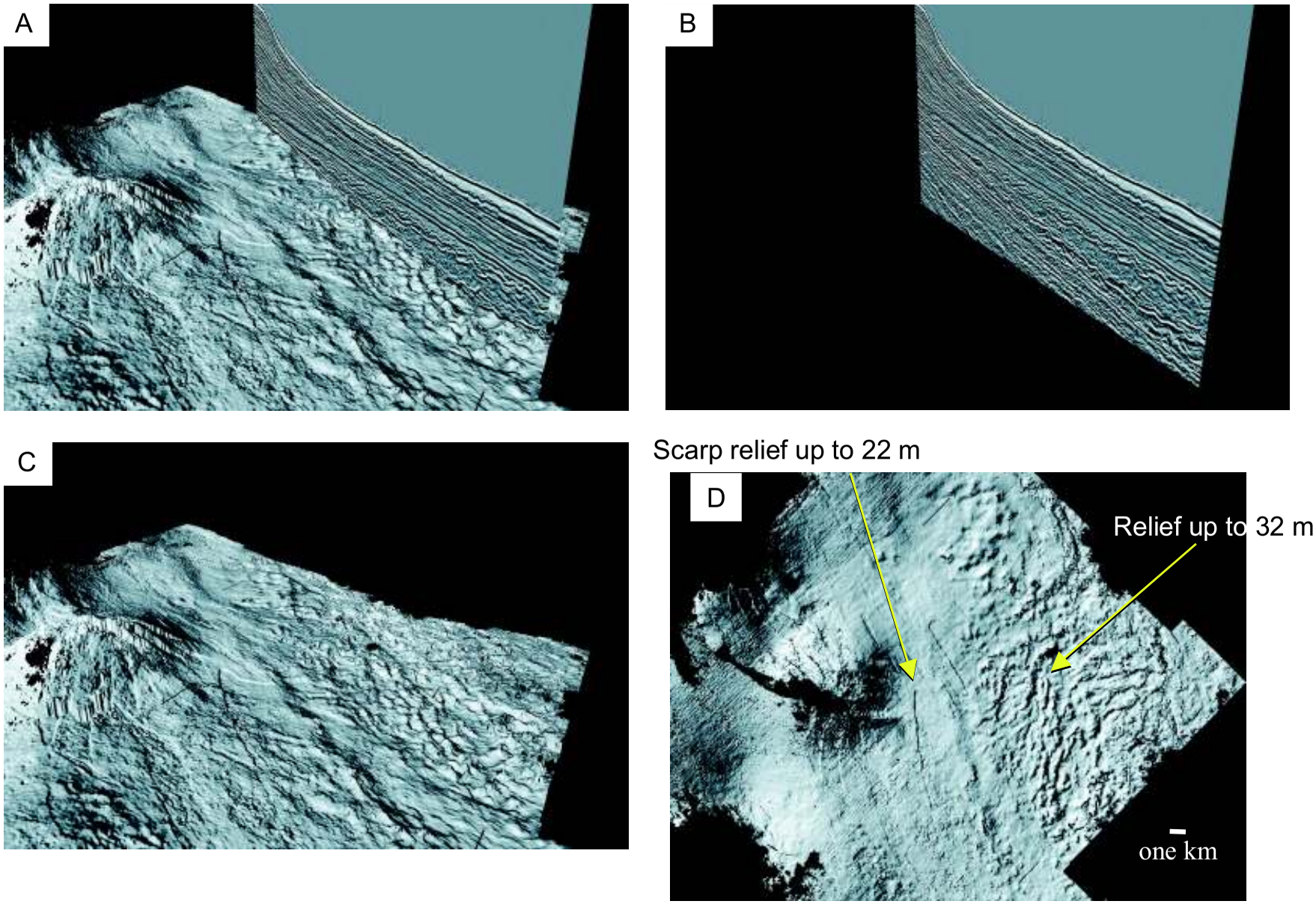

FIG. 162.—Rugose upper surface of a mass-transport deposit. Small-scale accommodation atop the mass-transport deposits shows no apparent influence on subsequent turbidite deposition.

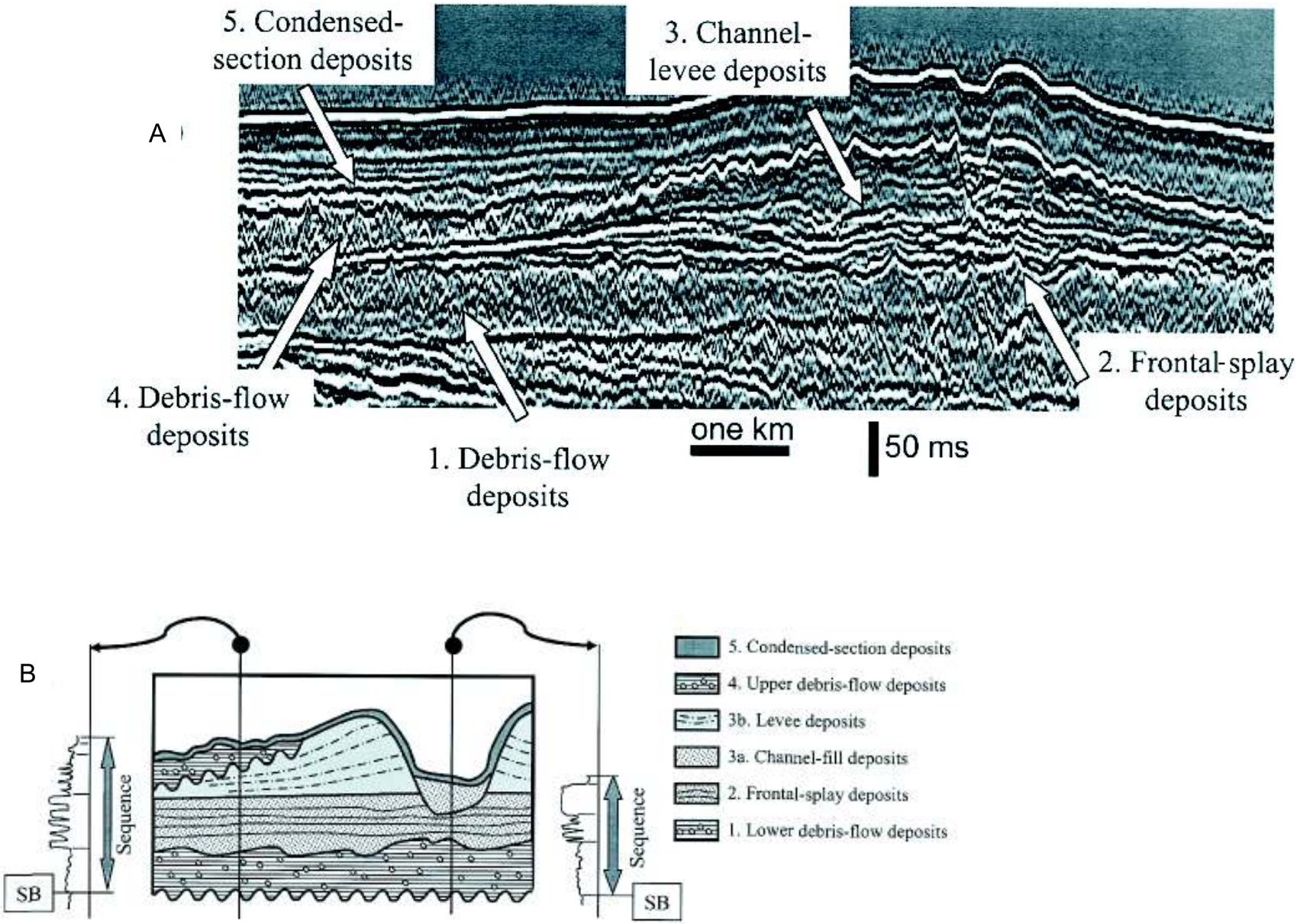

FIG. 163.—**A)** Seismic reflection profile across deep-water deposits on the basin floor of the Makassar Strait, Indonesia, illustrating a stratigraphic succession with mass-transport deposits at the base, overlain by frontal-splay deposits, leveed-channel deposits, a further mass-transport deposit and ultimately a condensed-section deposit. **B)** Idealized cross section and well logs through a deep-water depositional sequence (after Posamentier and Kolla, 2003a). Seismic data courtesy of WesternGeco.

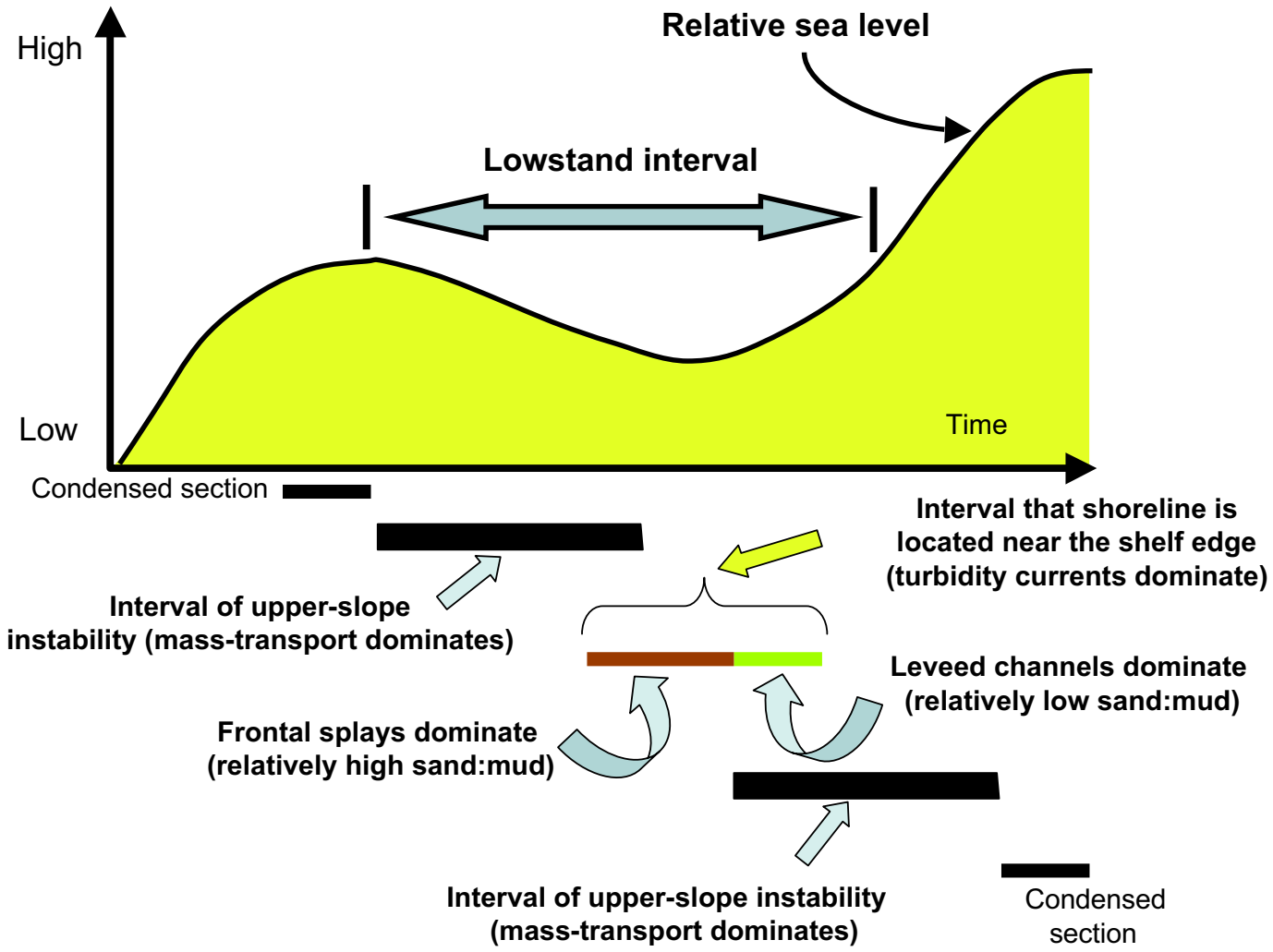

FIG. 164.—Schematic depiction of sediment transport events associated with relative sea-level change. As sea level begins its fall, lowered wave base results in slope disequilibrium conditions, which favor mass-transport events. Once sea level has lowered to the point where river mouths are in close proximity to the shelf edge, direct and indirect delivery of turbidites to the slope and basin floor is facilitated. During the early stages of this process, associated with the interval of relative sea-level fall, shelf valleys are incised and canyons can form. This results in sediment bypass of the shelf, which favors delivery of a relatively sand-prone sediment load to the deep water. During the late stages of sea-level lowstand, when sea level is slowly rising, sediments (preferentially coarse-grained sediment) tend to be trapped within earlier-formed incised valleys, resulting in muddier turbidites at that time. This progression favors an evolution from sand-rich frontal splays to mud-rich isolated leveed channels. Finally rapid sea-level rise again is associated with slope disequilibrium and deposition of mass-transport deposits. When sea level finally stabilizes, background deposition of hemipelagic and pelagic sediments dominates in the deep-water environment, forming a condensed section.

BRUHN, C.H.L., AND WALKER, R.G., 1997, Internal architecture and sedimentary evolution of coarse-grained turbidite channel–levee complexes, Early Eocene Regencia Canyon, Espirito Santo Basin, Brazil: Sedimentology, v. 44, p. 17–46.

CAMACHO, H., BUSBY, C.J., AND KNELLER, B., 2002, A new depositional model for the classical turbidite locality at San Clemente State Beach, California: American Association of Petroleum Geologists, Bulletin, v. 86, p. 1543–1560.

CAMPION, K.M., SPRAGUE, A.R., MOHRIG, D., LOVELL, R.W., DRZEWIECKI, P.A., SULLIVAN, M.D., ARDILL, J.A., JENSEN, G.N. AND SICKAFOOSE, D.K., 2000, Outcrop expression of confined channel complexes, *in* Weimer, P., Slatt, R.M, Coleman, J., Rosen, N.C., Nelson, H., Bouma, A.H., Styzen, M.J., and Lawrence, D.T., eds., Deep-Water Reservoirs of the World: Gulf Coast Section SEPM Foundation, 20th Annual Research Conference, p. 127–150.

CLIFTON, H.E., 1981, Submarine canyon deposits, Point Lobos, California, *in* Frizzel, E., ed., Upper Cretaceous and Paleocene Turbidites, Central California Coast: Pacific Section SEPM, Guidebook to Field Trip no. 6, p. 79–92.

CLIFTON, H.E., 1984, Sedimentation units in stratified resedimented conglomerate, Paleocene submarine canyon fill, Point Lobos, California, *in* Koster, E.H., and Steel, R.J., eds., Sedimentology of Gravels and Conglomerates: Canadian Society of Petroleum Geologists, Memoir 10, p. 429–-441.

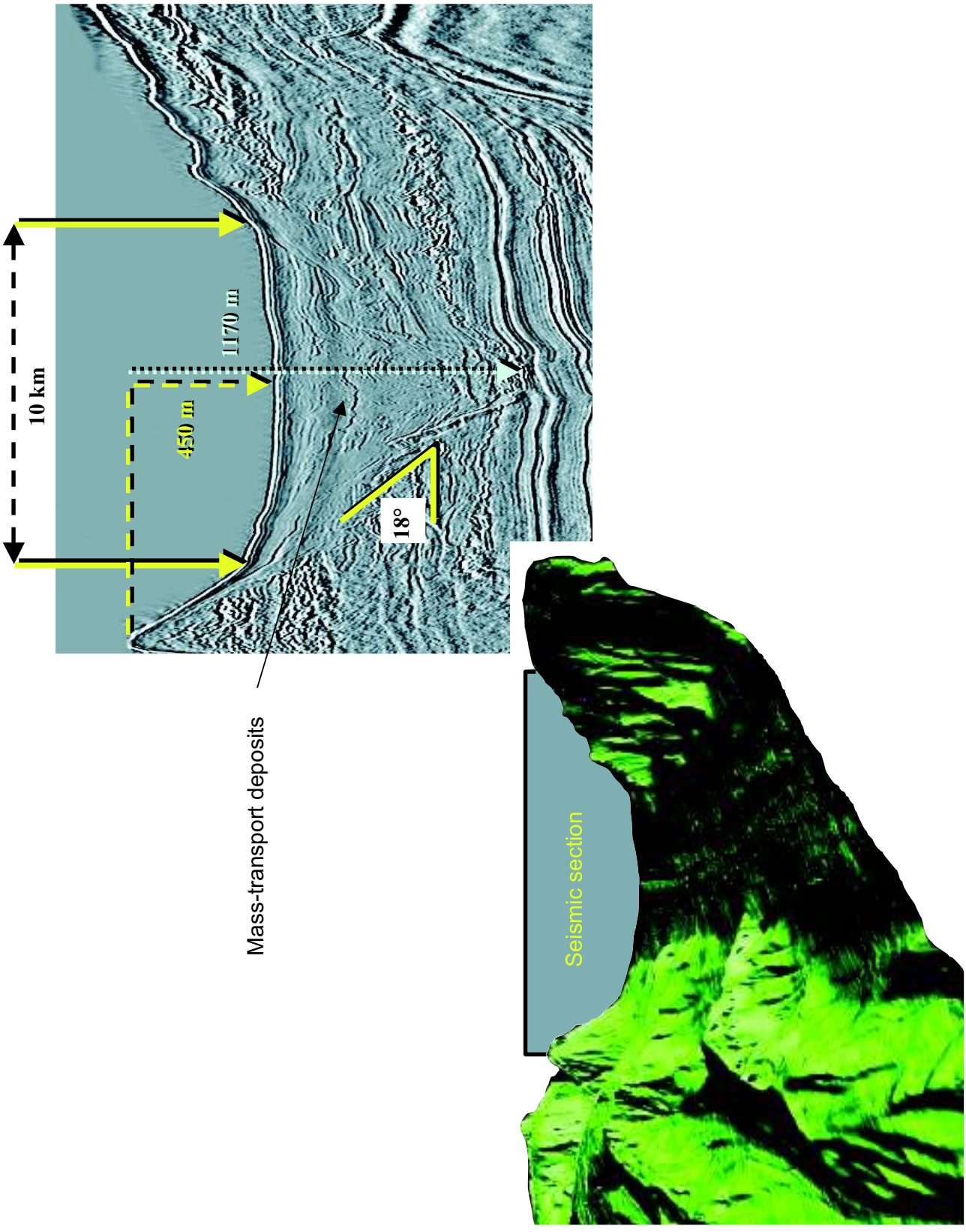

FIG. 165.—Seismic section across Mississippi canyon, along with perspective shaded relief. Seismic data proprietary to PGS Marine Geophysical NSA.

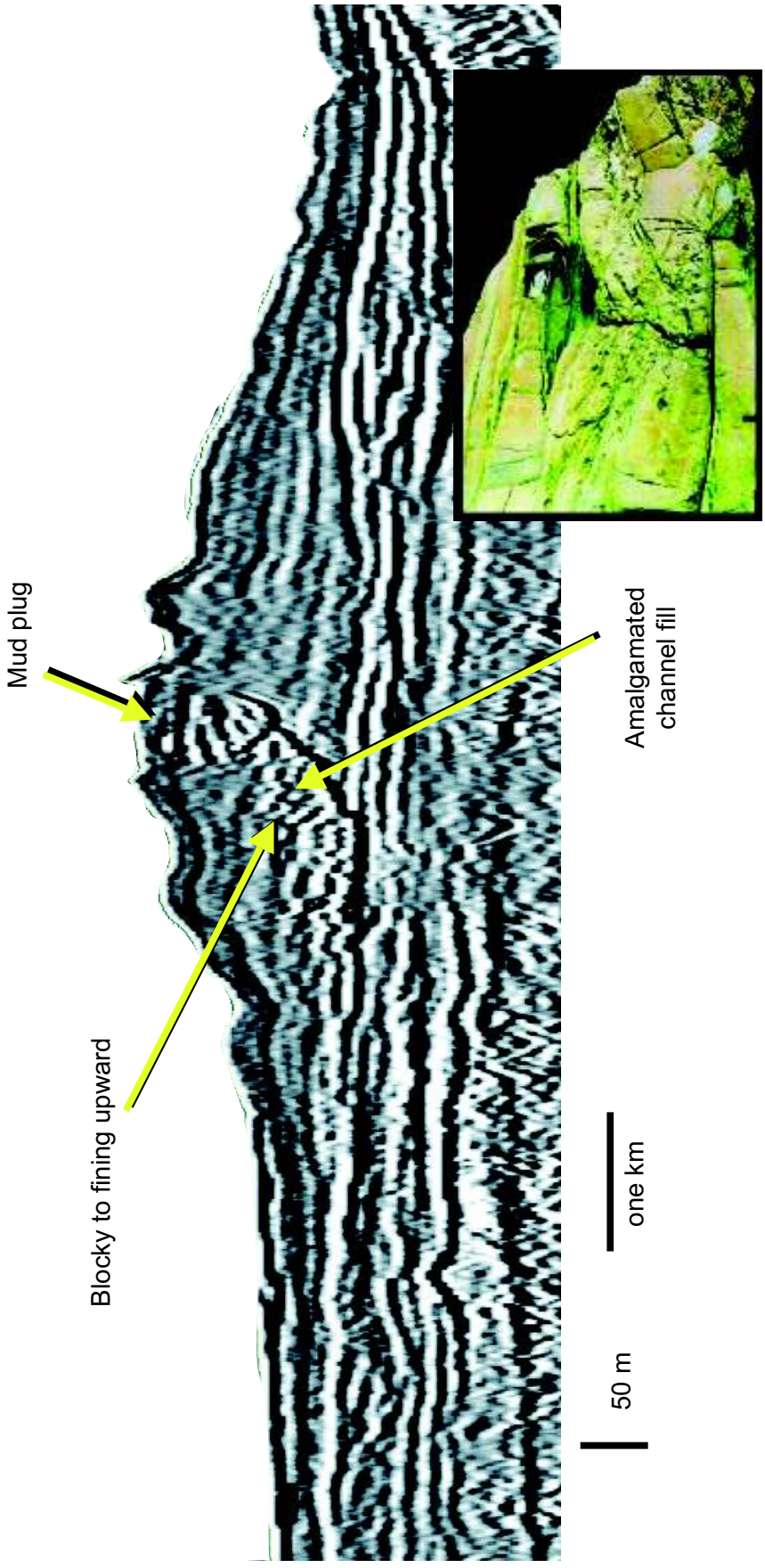

FIG. 166.—Basin-floor leveed-channel sand habitats—channel. Seismic data courtesy of WesternGeco.

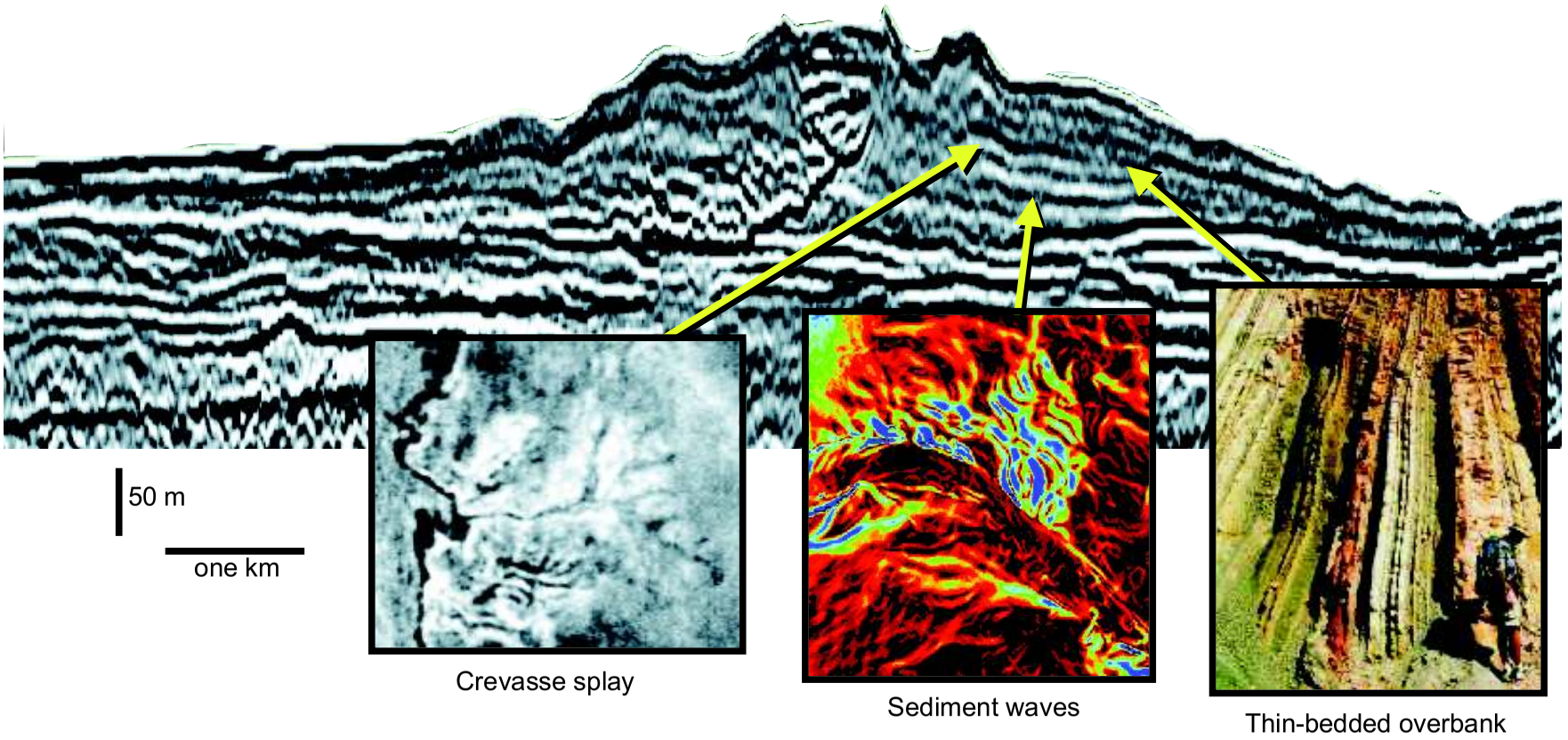

FIG. 167.—Basin-floor leveed-channel sand habitats—levee. Seismic data courtesy of WesternGeco.

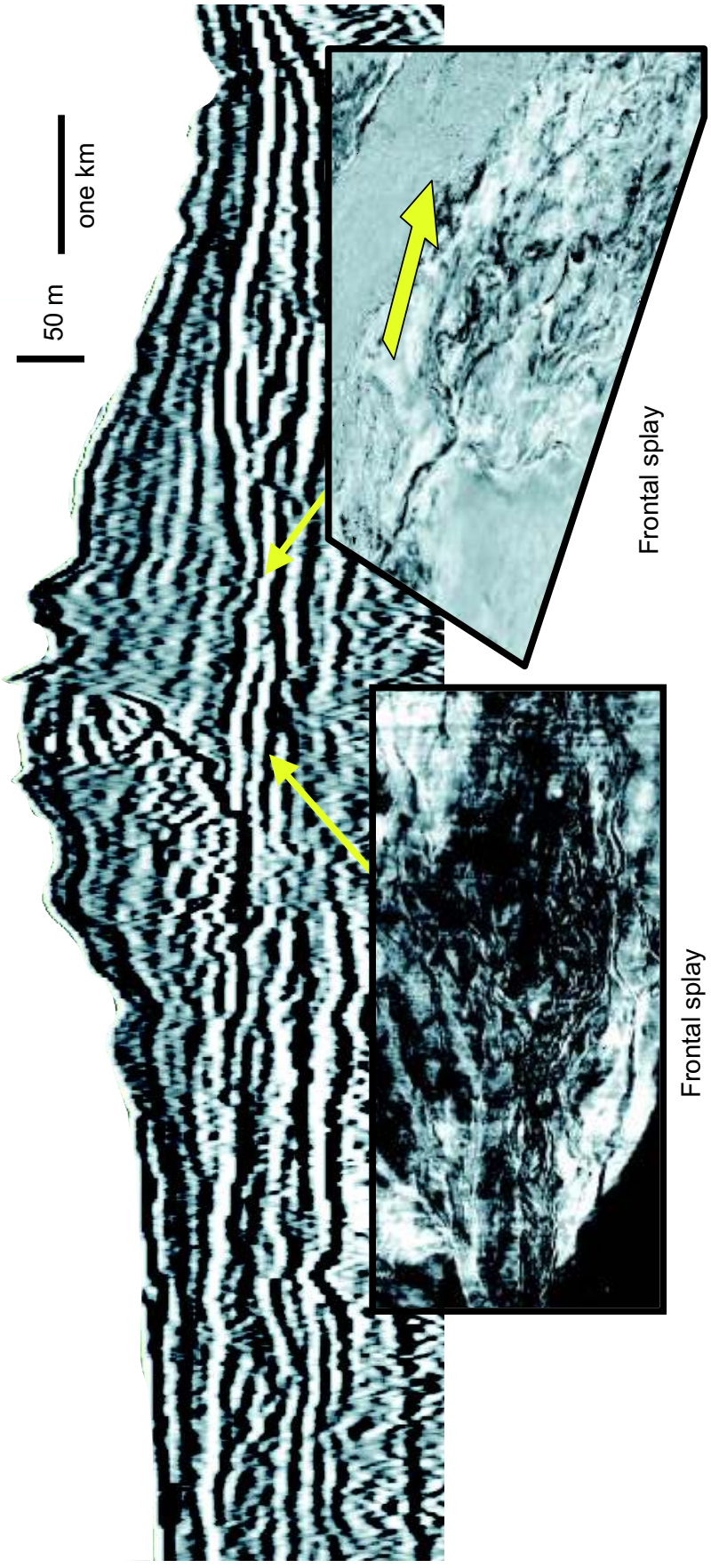

FIG. 168.—Basin-floor frontal-splay sand habitats. Seismic data courtesy of WesternGeco.

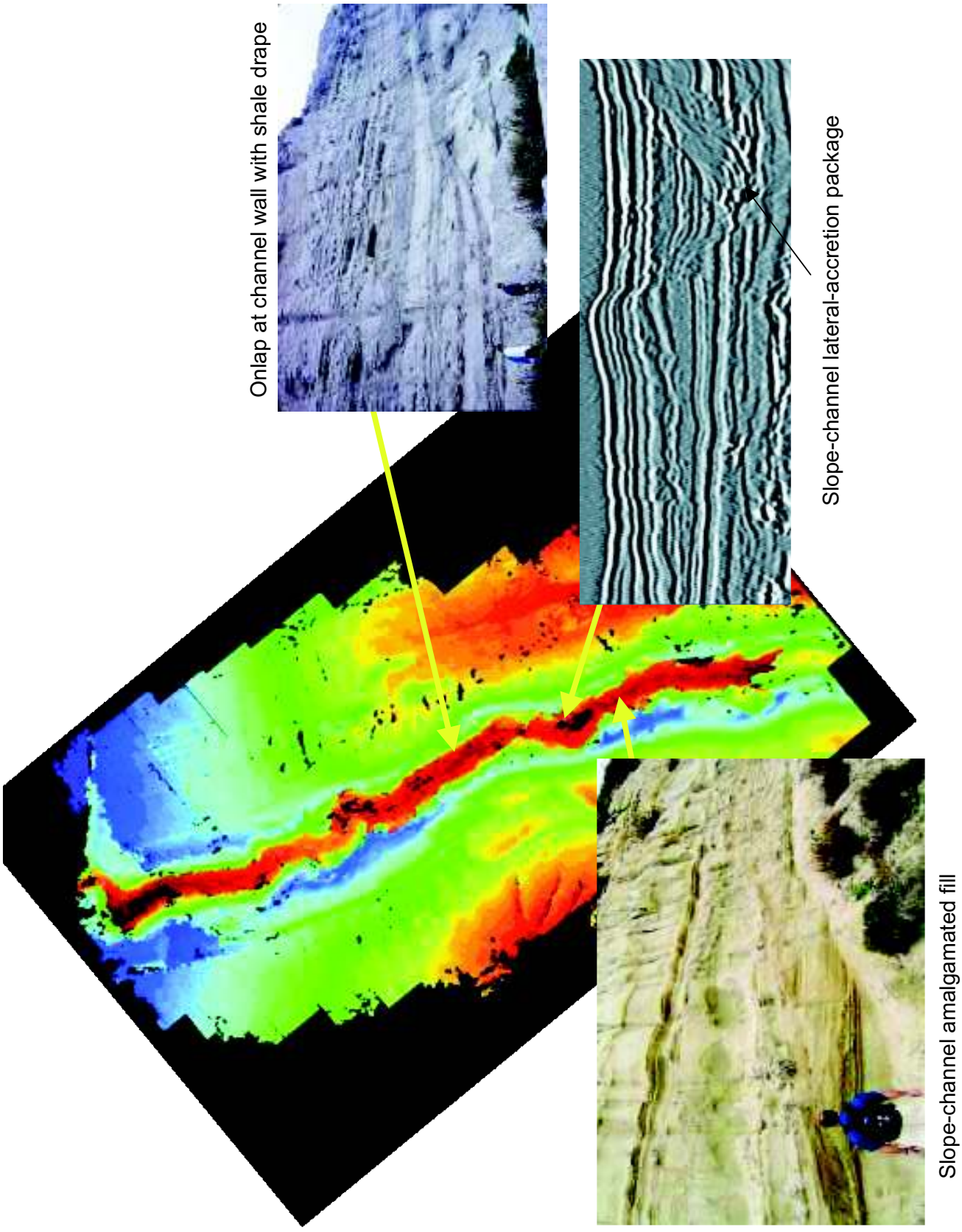

FIG. 169.—Slope-channel sand habitats. Seismic data courtesy of VeritasDGC.

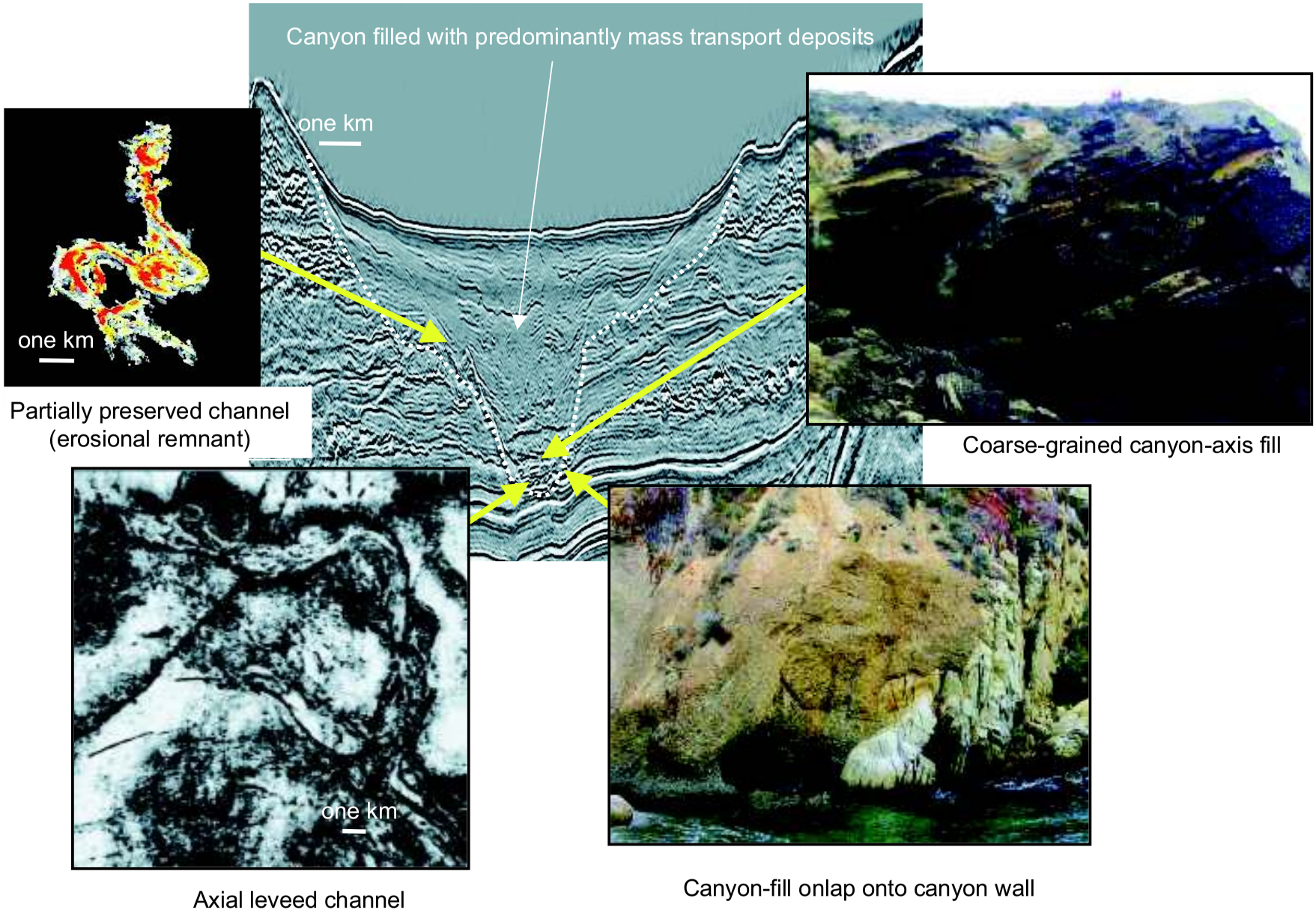

FIG. 170.—Slope-canyon sand habitats. Seismic data proprietary to PGS Marine Geophysical NSA.

CROWELL, J.C., 1957, Origin of pebbly mudstones: Geological Society of America, Bulletin, v. 68, p. 993–1009.

DAMUTH, J.E., KOWSMANN, R.O., FLOOD, R.D., BELDERSON, R.H., AND GORINI, M.A., 1983a, Age relationships of distributary channels on Amazon deep-sea fan: implications for fan growth pattern: Geology, v. 11, p. 470–473.

DAMUTH, J.E., KOLLA, V., FLOOD, R.D., KOWSMANN, R.O., GORINI, M.A., AND BELDERSON, R.H., 1983b, Distributary channel meandering and bifurcation patterns on the Amazon deep-sea fan as revealed by long-range side-scan sonar (GLORIA): Geology, v. 11, p. 94–98.

DROZ, L., AND BELLAICHE, G., 1985, Rhône deep-sea fan: morphostructure and growth pattern: American Association of Petroleum Geologists, Bulletin, v. 69, p. 460–479.

DZULYNSKI, S., KSIAZKIEWICZ, M., AND KUENEN, P.H., 1959, Turbidites in flysch of the Polish Carpathian Mountains: Geological Society of America, Bulletin, v. 70, p. 1089–1118.

ELMORE, R.D., PILKEY, O.H., CLEARY, W.J., AND CURRAN, H.A., 1979, Black Shell turbidite, Hatteras Abyssal Plain, western Atlantic Ocean: Geological Society of America, Bulletin, v. 90, p. 1165–1176.

GHIBAUDO, G., AND VANZ, V., 1987, Proposta di classificazione delle facies "torbiditiche" e di un metodo practico per la loro descrizione sul terreno: Giornale di Geologia, v. 49, p. 31/43.

GOODWIN, R.H., AND PRIOR, D.B., 1989, Geometry and depositional sequences of the Mississippi Canyon, Gulf of Mexico: Journal of Sedimentary Petrology, v. 59, p. 318–329.

GREGORY, M.R., 1966, Sedimentary features and penecontemporaneous slumping in the Waitemata Group, Whangaparaoa Peninsula, north Auckland, New Zealand: New Zealand Journal of Geology and Geophysics, v. 12, p. 248–282.

GRIGGS, G.B., AND KULM, L.D., 1970, Sedimentation in Cascadia deep-sea channel: Geological Society of America, Bulletin, v. 81, p. 1361–1384.

HACKBARTH, C.J., AND SHAW, R.D., 1994, Morphology and stratigraphy of a mid-Pleistocene turbidite leveed channel from seismic, core and log data, northeastern Gulf of Mexico, *in* Weimer, P., Bouma, A.H., and Perkins, B.F., eds., Submarine Fans and Turbidite Systems: Gulf Coast Section SEPM Foundation, 15th Annual Research Conference, p. 127–133.

HARMS, J.C., AND FAHNESTOCK, K., 1965, Stratification, flow phenomena and bed forms (with an example from the Rio Grande), *in* Middleton, G.V., ed., Primary Sedimentary Structures and Their Hydrodynamic Interpretation: SEPM , Special publication 12, p. 84–115.

HEEZEN, B.C., 1956, Corrientes de turbidez del Rio Magdalena: Sociedad Geográfica de Colombia, Boletín, v. 51/52, p. 135–143.

HEEZEN, B.C., MENZIES, R.J., SCHNEIDER, E.D., EWING W.M., AND GRANELLI, N.C.L., 1964, Congo submarine canyon: American Association of Petroleum Geologists, Bulletin, v. 48, p. 1126–1149.

HISCOTT, R.N., HALL, F.R., AND PIRMEZ, C., 1997, Turbidity-current overspill from the Amazon Channel: texture of the silt/sand load, paleoflow from anisotropy of magnetic susceptibility and implications for flow processes, *in* Flood, R.D., Piper, D.J.W., Klaus, A., and Peterson, L.C., eds., Proceedings of the Ocean Drilling Program: Scientific Results, v. 155, p. 53–78.

HURST, A., CARTWRIGHT, J.A., DURANTI, D., HUUSE, M., AND NELSON, M., 2005, Sand injectites: an emerging global play in deep-water clastic environments, *in* Doré, A.G., and Vining, B.A., eds., Petroleum Geology: Northwest Europe and Global Perspectives: Geological Society of London, Proceedings of the 6th Petroleum Geology Conference, p. 133–144.

JENNETTE, D.C., GARFIELD, T.R., MOHRIG, D.C., AND CAYLEY, G.T., 2000, The interaction of shelf accommodation, sediment supply and sealevel in controlling the facies, architecture and sequence stacking patterns of the Tay and Forties/Sele basin-floor fans, Central North Sea, *in* Weimer, P., Slatt, R.M, Coleman, J., Rosen, N.C., Nelson, H., Bouma, A.H., Styzen, M.J., and Lawrence, D.T., eds., Deep-Water Reservoirs of the World: Gulf Coast Section SEPM Foundation, 20th Annual Research Conference, p. 402–421.

KENYON, N.H., AND MILLINGTON, J., 1995, Contrasting deep-sea depositional systems in the Bering Sea, *in* Pickering, K.T., Hiscott, R.N., Kenyon, N.H., Ricci Lucchi, F., and Smith, R.D.A., eds., Atlas of Deep Water environments: London, Chapman & Hall, p. 196–202.

KNELLER, B.C., 1995, Beyond the turbidite paradigm: physical models for deposition of turbidites and their implications for reservoir prediction, *in* Hartley, A.J., and Prosser, D.J., eds., Characterisation of Deep Marine Clastic Systems: Geological Society of London, Special Publication 94, p. 31–49.

KOLLA, V., AND COUMES, F., 1987, Morphology, internal structure, seismic stratigraphy and sedimentation of Indus Fan: American Association of Petroleum Geologists, Bulletin, v. 71, p. 650–677.

KOLLA, V., BOURGES, P., URRUTY, J.M., AND SAFA, P., 2001, Evolution of deepwater Tertiary sinuous channels offshore, Angola (West Africa) and implications to reservoir architecture: American Association of Petroleum Geologists, Bulletin v. 85, p. 1373–1405.

KOMAR, P.D., 1971, Hydraulic jumps in turbidity currents: Geological Society America, Bulletin, v. 82, p. 1477–1488.

KUENEN, P.H., AND MIGLIORINI, C.I., 1950, Turbidity currents as a cause of graded bedding: Journal of Geology, v. 58, p. 91–127.

LIEN, T., WALKER, R.G., AND MARTINSEN, O.J., 2003, Turbidites in the Upper Carboniferous Ross Formation, western Ireland: reconstruction of a channel and spillover system: Sedimentology, v. 50, p. 113-148.

LINK, M.H., SQUIRES, R.L., AND COLBURN, I.P., 1984, Slope and deep-sea fan facies and paleogeography of Upper Cretaceous Chatsworth Formation, Simi Hills, California: American Association of Petroleum Geologists, Bulletin, v. 68, p. 850–873.

LOWE, D.R., 1975, Water escape structures in coarse-grained sediments: Sedimentology, v. 22, p. 157–204.

LOWE, D.R., 1979, Stratigraphy and sedimentology of the Pigeon point Formation, San Mateo County, California, *in* Nilsen, T.H., and Brabb, E.E., eds., Geology of the Santa Cruz Mountains, California: Geological Society of America, Cordilleran Section, Field Trip Guidebook, p. 17–29.

LOWE, D.R., 1982, Sediment gravity flows: II. Depositional models with special reference to the deposits of high-density turbidity currents: Journal of Sedimentary Petrology, v. 52, p. 279–297.

MANLEY, L., AND FLOOD, R.D., 1998, Cyclic sediment deposition within Amazon deep-sea fan: American Association of Petroleum Geologists, Bulletin, v. 72, p. 912–925.

MARTINSEN, O.J., LIEN, T., AND WALKER, R.G., 2000, Upper Carboniferous deep-water sediments, western Ireland: analogs to passive margin plays, *in* Weimer, P., Slatt, R.M., Coleman, J., Rosen, N.C., Nelson, H., Bouma, A.H., Styzen, M.J., and Lawrence, D.T., *eds*., Deep Water Reservoirs of the World: SEPM, Gulf Coast Section, 20th Annual Bob F. Perkins Research Conference, Houston, p. 533–555 (available only on CD).

MASLIN, M., MIKKELSEN, N., VILELA, C., AND HAQ, B.U., 1998, Sea-level and gas-hydrate–controlled catastrophic sediment failures of the Amazon fan: Geology, v. 26, p. 1107–1110.

MAYALL, M., AND STEWART, I., 2000, The architecture of turbidite slope channels, *in* Weimer, P., Slatt, R.M, Coleman, J., Rosen, N.C., Nelson, H., Bouma, A.H., Styzen, M.J., and Lawrence, D.T., eds., Deep-Water Reservoirs of the World: Gulf Coast Section SEPM Foundation, 20th Annual Research Conference, p. 578–586.

MIGEON, S., SAVOYE, B., AND FAUGERES, J.-C., 2000, Quaternary development of migrating sediment waves in the Var deep-sea fan: distribution, growth pattern and implication for levee evolution: Sedimentary Geology, v. 133, p. 265–293.

MOHRIG, D., WHIPPLE, K.X., HONDZO, M., ELLIS, C., AND PARKER, G., 1998, Hydroplaning of subaqueous debris flows: Geological Society of America, Bulletin, v. 110, p. 387–394.

MULDER, T., AND SYVITSKI, J.P.M., 1995, Turbidity currents generated at river mouths during exceptional discharges to the world oceans: Journal of Geology, v. 103, p. 285–299.

MULDER, T., SYVITSKI, J.P.M., AND SKENE, K.I., 1998, Modeling of erosion and deposition by turbidity currents generated at river mouths: Journal of Sedimentary Research, v. 68, p. 124–137.

MUTTI, E., 1985, Turbidite systems and their relations to depositional sequences, *in* ZUFFA, G.G., ed., Provenance of Arenites: NATO-ASI Series, Dordrecht, The Netherlands, Reidel, p. 65–93.

MUTTI, E., AND GHIBAUDO, G., 1972, Un esempio di torbiditi di conoide sottomarina esterna: le Arenario di San Salvatore (formazione di Bobbio, Miocene) nell'Appennino di Piacenza: Memorie dell'Accademia delle Scienze di Torino, Classe di Scienze Fisiche, Matematiche e Naturale, Serie 4a, no. 16, p. 1–41.

MUTTI, E., AND NORMARK, W.R., 1991, An integrated approach to the study of turbidite systems, *in* Weimer, P., and Link, M.H., eds., Seismic Facies and Sedimentary Processes of Submarine Fans and Turbidite Systems: New York, Springer-Verlag, p. 75–106.

MUTTI, E., AND RICCI LUCCHI, F., 1972, Le torbiditi dell'Appennino settentrionale: introduzioni all'analisi de facies: Società Geologica Italiana Memorie, v. 11, p. 161–199.

MUTTI, E., STEFFENS, G.S., PIRMEZ, C., ORLANDO, M., AND ROBERTS, D., EDS., 2003, Thematic set: Turbidites: models and problems: Marine and Petroleum Geology, v. 20, p. 523–933.

NELSON, C.H., GOLDFINGER, C., JOHNSON, J.E., AND DUNHILL, G., 2000, Variation of modern turbidite systems along the subduction zone margin of Cascadia Basin and implications for turbidite reservoir beds, *in* Weimer, P., Slatt, R.M., Coleman, J., Rosen, N.C., Nelson, H., Bouma, A.H., Styzen, M.J. and Lawrence, D.T., *eds*., Deep Water Reservoirs of the World: SEPM, Gulf Coast Section, 20th Annual Bob F. Perkins Research Conference, Houston, p. 714–738 (available only on CD).

NILSEN, T.H., 1980, Modern and ancient submarine fans: discussion of papers by R.G. Walker and W.R. Normark: American Association of Petroleum Geologists, Bulletin, v. 64, p. 1094–1101.

NORMARK, W.R., 1970, Growth patterns of deep-sea fans: American Association of Petroleum Geologists, Bulletin, v. 54, p. 2170–2195.

PEAKALL, J., MCCAFFREY, W.D., KNELLER, B.C., STELTING, C.E., MCHARGUE, T.R., AND SCHWELLER, W.J., 2000, A process model for the evolution of submarine fan channels: Implications for sedimentary architecture, *in* Bouma, A.H., and Stone, C.G., eds., Fine-Grained Turbidite Systems: American Association of Petroleum Geologists, Memoir 72 and SEPM, Special Publication 68, p. 73–88.

PICKERING, K.T., STOW, D., WATSON, M., AND HISCOTT, R.N., 1986, Deep-water facies, processes and models: a review and classification scheme for modern and ancient sediments: Earth-Science Reviews, v. 23, p. 75–174.

PILKEY, O.H., 1988, Basin plains: giant sedimentation events, *in* Clifton, H.E., ed., Sedimentologic Consequences of Convulsive Geological Events: Geological Society of America, Special Paper 229, p. 93–99.

PIPER, D.J.W., AND NORMARK, W.R., 1983, Turbidite depositional patterns and flow characteristics, Navy submarine fan, California borderland: Sedimentology, v. 30, p. 681–694.

PIPER, D.J., SHOR, A.N., AND HUGHES-CLARK, J.E., 1988, The "1929" Grand Banks earthquake, slump and turbidity current, *in* Clifton, H.E., ed., Sedimentological Consequences of Convulsive Geological Events: Geological Society of America, Special Paper 229, p. 77–92.

PIPER, D.J.W., PIRMEZ, C., MANLEY, P.L., LONG, D., FLOOD, R.D., NORMARK, W.R., AND SHOWERS, W., 1997, Mass-transport deposits of the Amazon Fan, *in* Flood, R.D., Piper, D.J.W., Klaus, A., and Peterson, L.C., eds., Proceedings of the Ocean Drilling Program, Scientific Results, v. 155, p. 109–146.

PIRMEZ, C., AND FLOOD, R.D., 1997, Morphology and structure of Amazon Channel, *in* Flood, R.D., Piper, D.J.W., Klaus, A., and Peterson, L.C., eds., Proceedings of the Ocean Drilling Program, Scientific Results, v. 155, p. 23–45.

PIRMEZ, C., HISCOTT, R.N., AND KRONEN, J.K., 1997, Sandy turbidite successions at the base of channel–levee systems of the Amazon Fan revealed by FMS logs and cores: unraveling the facies architecture of large submarine fans, *in* Flood, R.D., Piper, D.J.W., Klaus, A., and Peterson, L.C., eds., Proceedings of the Ocean Drilling Program, Scientific Results, v. 155, p. 7–22.

PLINT, A.G., AND NUMMEDAL, D., 1998, The falling stage systems tract: recognition and importance in sequence stratigraphic analysis, *in* Gawthorpe, R.L.G., and Hunt, E., eds., Sedimentary Responses to Forced Regression: Geological Society of London, Special Publication.

POSAMENTIER, H.W., 2003a, A linked shelf edge delta and slope channel turbidite system: 3D seismic case study from the eastern Gulf of Mexico, *in* Roberts, H.H., Rosen, N.C., Fillon, R.H., and Anderson, J.B., eds., Shelf Margin Deltas and Linked Down Slope Petroleum Systems: Global Significance and Future Exploration Potential: Gulf Coast Section of SEPM Foundation, Proceedings of the 23rd Annual Bob F. Perkins Research Conference, p. 115–134.

POSAMENTIER, H.W., 2003b, Depositional elements associated with a basin floor channel–levee system: case study from the Gulf of Mexico: Marine and Petroleum Geology, v. 20, p. 677–690.

POSAMENTIER, H.W., AND ALLEN, G.P., 1999, Siliciclastic Sequence Stratigraphy—Concepts and Applications: SEPM, Concepts in Sedimentology and Paleontology, no. 7, 210 p.

POSAMENTIER, H.W., ALLEN, G.P., JAMES, D.P., AND TESSON, M., 1992, Forced regressions in a sequence stratigraphic framework: concepts, examples, and exploration significance: American Association of Petroleum Geologists, Bulletin, v. 76, p. 1687–1709.

POSAMENTIER, H.W., ERSKINE, R.D., AND MITCHUM, R.M., JR., 1991, Models for submarine fan deposition within a sequence stratigraphic framework, *in* Weimer, P., and Link, M.H., eds., Seismic Facies and Sedimentary Processes of Submarine Fans and Turbidite Systems: New York, Springer-Verlag, p. 127–136.

POSAMENTIER, H.W., JERVEY, M.T., AND VAIL, P.R., 1988, Eustatic controls on clastic deposition I—conceptual framework, *in* Wilgus, C.K., Hastings, B.S., Kendall, C.G.St.C., Posamentier, H.W., Ross, C.A., and Van Wagoner, J.C., eds., Sea Level Changes: An Integrated Approach: SEPM, Special Publication 42, p. 109–124.

POSAMENTIER, H.W., AND KOLLA, V., 2003a, Seismic geomorphology and stratigraphy of depositional elements in deep-water settings: Journal of Sedimentary Research, v. 73, p. 367–388.

POSAMENTIER, H.W., AND KOLLA, V., 2003b, Anatomy of a deep-water channel avulsion—Example from the basin floor of the Desoto Canyon area, Gulf of Mexico (abstract): American Association of Petroleum Geologists, Annual Meeting, Abstracts Volume, p. A140.

POSAMENTIER, H.W., MEIZARWIN, WISMAN, P.S., AND PLAWMAN, T., 2000, Deep water depositional systems—Ultra-deep Makassar Strait, Indonesia, *in* Weimer, P., Slatt, R.M., Coleman, J., Rosen, N.C., Nelson, H., Bouma, A.H., Styzen, M.J., and Lawrence, D.T., eds., Deep-Water Reservoirs of the World: Gulf Coast Section SEPM Foundation, 20th Annual Research Conference, p. 806–816.

POSAMENTIER, H.W., AND VAIL, P.R., 1985, Eustatic controls on depositional stratal patterns: SEPM, Research Conference no. 6, Sea Level Changes—An Integrated Approach, October 20–23, 1985 (Abstract and Poster).

PRATHER, B.E., BOOTH, J.R., STEFFENS, G.S., AND CRAIG, P.A., 1998, Classification, lithologic calibration and stratigraphic succession of seismic facies of intraslope basins, deep-water Gulf of Mexico: American Association of Petroleum Geologists, Bulletin, v. 82, p. 701–728.

READING, H.G., AND RICHARDS, M., 1994, Turbidite system in deep-water basin margins classified by grain size and feeder system: American Association of Petroleum Geologists, Bulletin, v. 78, p. 792–822.

RUST, B.R., 1966, Late Cretaceous paleogeography near Wheeler Gorge, Ventura County, California: American Association of Petroleum Geologists, Bulletin, v. 50, p. 1389–1398.

SHANMUGAM, G., 1996, High-density turbidity currents: are they sandy debris flows?: Journal of Sedimentary Research, v. 66, p. 2–10.

SHANMUGAM, G., LEHTONEN, L.R., STRAUME, T., SYVERTSEN, S.E., HODGKINSON, R.J., AND SKIBELI, M., 1994, Slump and debris-flow dominated upper slope facies in the Cretaceous of the Norwegian and northern North Seas (61–67°N): implications for sand distribution: American Association of Petroleum Geologists, Bulletin, v. 78, p. 910–937.

SIKKIMA, W., AND WOJCIK, K.M., 2000, 3D visualization of turbidite systems, Lower Congo Basin, offshore Angola, *in* Weimer, P., Slatt, R.M., Coleman, J., Rosen, N.C., Nelson, H., Bouma, A.H., Styzen, M.J., and Lawrence, D.T., eds., Deep-Water Reservoirs of the World: Gulf Coast Section of SEPM Foundation, 20th Annual Research Conference, p. 928–939.

SURLYK, F., AND NOE-NYGAARD, N., 2003, A giant sand injection complex: the Upper Jurassic Hareelv Formation of East Greenland: Geologia Croatica, v. 56, p. 69–81.

UCHUPI, E., AND AUSTIN, J., 1979, The stratigraphy and structure of the Laurentian Cone region: Canadian Journal of Earth Sciences, v. 16, p. 1726–1752.

VAIL, P.R., MITCHUM, R.M., JR., AND THOMPSON, S., III, 1977, Seismic stratigraphy and global changes of sea level, part 3: relative changes of sea level from coastal onlap, *in* Payton, C.E., ed., Seismic Stratigraphy—Applications to Hydrocarbon Exploration: American Association of Petroleum Geologists, Memoir 26, p. 63–81.

VAN WAGONER, J.C., BEAUBOUEF, R.T., HOYAL, J.C.J.D., DUNN, P.A., ADAIR, N.L., ABREU, V., LI, D., WELLNER, R.W., AWWILLER, D.N., AND SUN, T., 2003, Energy dissipation and the fundamental shape of siliciclastic sedimentary bodies (abstract): American Association of Petroleum Geologists, Annual Meeting, Abstracts Volume, p. A175.

VAN WEERING, T.C.E., NIELSEN, T., KENYON, N.H., KATJA, A., AND KUIJPERS, A.H., 1998, Large submarine slides on the NE Faeroe continental margin, *in* Stoker, M.S., Evans, D., and Cramp, A., eds., Geological Processes on Continental Margins: Sedimentation, Mass-Wasting, and Stability: Geological Society of London, Special Publication 129: p. 5–27.

WALKER, R.G., 1965, The origin and significance of the internal sedimentary structures of turbidites: Yorkshire Geological Society, Proceedings, v. 35, p. 1–32.

WALKER, R.G., 1967, Turbidite sedimentary structures and their relationship to proximal and distal depositional environments: Journal of Sedimentary Petrology., v. 37, p. 25–43.

WALKER, R.G., 1973, Mopping up the turbidite mess, *in* Ginsburg, R.N., ed., Evolving Concepts in Sedimentology: Baltimore, The Johns Hopkins Press, p. 1–37.

WALKER, R.G., 1975a, Generalized facies models for resedimented conglomerates of turbidite association: Geological Society of America, Bulletin, v. 86, p. 737–748.

WALKER, R.G., 1975b, Nested submarine channels at San Clemente, California: Geological Society of America, Bulletin, v. 86, p. 915–924.

WALKER, R.G., 1978, Deep-water sandstone facies and ancient submarine fans: models for exploration and stratigraphic traps: American Association of Petroleum Geologists, Bulletin, v. 62, p. 932–966.

WALKER, R.G., 1985, Mudstones and thin-bedded turbidites associated with the Upper Cretaceous Wheeler Gorge conglomerates, California: a possible channel–levee complex: Journal of Sedimentary Petrology, v. 55, p. 279–290.

WALKER, R.G., 1992, Turbidites and submarine fans, *in* Walker, R.G., and James, N.P., eds., Facies Models; Response to Sea Level Change: Geological Association of Canada, p. 239–263.

WEIMER, P., 1989, Sequence stratigraphy of the Mississippi Fan (Plio-Pleistocene), Gulf of Mexico: Geo-Marine Letters, v. 9, p. 185–272.

WEIMER, P., 1991, Seismic facies, characteristics and variations in channel evolution, Mississippi Fan (Plio-Pleistocene), Gulf of Mexico, *in* Weimer, P., and Link, M.H., eds., Seismic Facies and Sedimentary Processes of Submarine Fans and Turbidite Systems: New York, Springer-Verlag, p. 323–347.

WEIMER, P., AND LINK, M.H., eds., 1991, Seismic Facies and Sedimentary Processes of Submarine Fans and Turbidite Systems: New York, Springer-Verlag, 447 p.

WEIMER, P., SLATT, R.M., COLEMAN, J., ROSEN, N.C., NELSON, H., BOUMA, A.H., STYZEN, M.J., AND LAURENCE, D.T., eds., 2000, Deep-Water Reservoirs of the World: SEPM, Gulf Coast Section, 20th Annual Bob F. Perkins Research Conference, Houston (available only on CD).

WILSON J., WALL, G., KLOOSTERMAN, H.J., CONEY, D., CAYLEY, G., WALKER, J., AND LINSKAILL, C., 2005, The discovery of Goldeneye: *in* Doré, A.G., and Vining, B.A., eds., Petroleum Geology: North-West Europe and Global Perspectives: 6th Petroleum Geology Conference, Proceedings, p. 199–216.

WINKER, C.D., AND BOOTH, J.R., 2000, Sedimentary dynamics of the salt-dominated continental slope, Gulf of Mexico: integration of observations from the sea floor, near-surface and deep subsurface, *in* Weimer, P., Slatt, R.M., Coleman, J., Rosen, N.C., Nelson, H., Bouma, A.H., Styzen, M.J., and Lawrence, D.T., eds., Deep-Water Reservoirs of the World: SEPM, Gulf Coast Section, 20th Annual Bob F. Perkins Research Conference, Houston, p. 1059–1086.